CRANFIELD UNIVERSITY

Ali Rabiee

Lightweight Design of Multi-Stitched Composite Crash Absorbers to Improve Specific Energy Absorption Capability under Quasi-Static and Impact Loading

School of Aerospace, Transport and Manufacturing
Aerospace Engineering

PhD
Academic Year: 2015 - 2018

Supervisor: Dr Hessam Ghasemnejad
May 2018

CRANFIELD UNIVERSITY

School of Aerospace, Transport and Manufacturing
Aerospace Engineering

PhD

Academic Year 2015 - 2018

Ali Rabiee

Lightweight Design of Multi-Stitched Composite Crash Absorbers to Improve Specific Energy Absorption Capability under Quasi-Static and Impact Loading

Supervisor: Dr Hessam Ghasemnejad
May 2018

This thesis is submitted in partial fulfilment of the requirements for the degree of PhD

ABSTRACT

A comprehensive numerical and experimental study was performed to investigate the energy absorbing capabilities of glass/epoxy and carbon/epoxy members that could serve as stanchions in the subfloor structure of aircraft or rotorcraft. Circular cross sections with chamfered-ends failure trigger mechanism were investigated under axial and off-axis loading conditions. The optimal configuration that resulted in the highest possible specific energy absorption (SEA) was identified, which was at axial loading. The parameters in off-axis loading conditions that affected energy absorption capability were identified. Several cases were experimentally studied to cancel off-axis (oblique) loading effect.

To increase interlaminar fracture toughness, stitching through the thickness was considered. Single, multi and pattern-stitching were studied to increase energy absorption capability of GFRP composite sections. The failure mechanisms, crushing process and force-displacement curve diagram of each case was studied to establish the effect of stitching on energy absorption capability. A correlation between stitching location and localised and global increase of energy absorption was established. It was identified, that the closer the stitching locations are, the higher the localised peak load becomes, and it influences the Mode-I crack propagation (main central crack) resistance, bending of fronds and friction, consequently, pattern-stitching resulted in a 15% increase in specific energy absorption capability (SEA) under quasi-static loading. Similarly, this stitching pattern resulted in a 14% increase in SEA using CFRP sections. Under impact loading, it was identified that pattern-stitching through the thickness resulted into 17% and 18% increase in SEA using GFRP and CFRP sections, respectively.

Finite element models were also developed to simulate the crushing behaviour of the CFRP and GFRP sections observed experimentally under axial, off-axis, quasi-static and impact loading conditions. A multi-layer modelling methodology was developed by determining the most effective element size, number of shells, formulation, contact definitions, delamination interface, material model, friction and trigger mechanism. This approach captured the failure process, predicted the SEA and sustained crush load quite accurately within 5% error. Stitching through

the thickness was modelled using an energy-based contact card to implement stitched and non-stitched Mode-I and Mode-II energy release rate parameters. This method accurately predicted stitched composite sections with 3% error compared with experimental data. Such modelling could thus support the future design of aircraft stitched and non-stitched stanchions within reasonable computer efficiency and accuracy.

Keywords:

LS-DYNA, Through-thickness stitching, Multi-stitches, Crack resistance, Oblique, Off-axis loading, Crashworthiness

ACKNOWLEDGEMENTS

I would like to express my sincere gratitude to Dr. Hessam Ghasemnejad, this dissertation would not have been possible without his constant support, guidance, and encouragement throughout my studies. Dr. Ghasemnejad has always been there as a great friend, and I appreciate his time, friendship and effort.

I am deeply grateful to engineering officers, Mr. Jim Hurley and Mr. Jim Watson for their technical advice and availability.

Most importantly of all, I would like to thank my family, Amir, Farah and Sepideh for always supporting me, encouraging me, and believing in me through all decisions I have had to make so far. Without them, I would not be the person I am today, I greatly appreciate their dedication and sacrifices they have made for me. I would like to thank all my friends for their help and support.

Last, but not the least, I would like to thank my special one, ‘Sizmin’ with her everything makes more sense, she is my best friend and I would like to thank her for everything over the years, that has undoubtedly helped me complete this dissertation, and complete my personal life.

TABLE OF CONTENTS

LIST OF FIGURES

LIST OF EQUATIONS

LIST OF TABLES

LIST OF ABBREVIATIONS

CFE	Crush force efficiency
CFRP	Carbon fibre reinforced plastic
GFRP	Glass fibre reinforced plastic
DCB	Double-cantilever beam
3ENF	Three-point-end-notched flexure
KE	Kinetic Energy
ρ	Density
A	Cross-sectional area
E	Young's modulus
F	Load
F_{max}	Initial maximum load
F_m	Mean load
P_L	Peak load
G_{12}	Shear modulus
G_{IC}	Mode-I interlaminar fracture toughness
G_{IIC}	Mode-II interlaminar fracture toughness
SEA	Specific energy absorption (kJ/kg)
t	Wall-thickness
D	Diameter
C	Circumference
L	Axial length
CCS	Circular cross section
RCCT	Radial corrugated cross section
RCSCT	Radial corrugated surrounded by circular composite tubes
CC	Conical Circular
V_R	Volume reduction
V_f	Fibre volume fraction
ν	Poisson's ratio
β	Weight factor
μ	Coefficient of friction
Δ	Displacement

δ	Post crushing displacement
m	Crushed specimen mass
V	Volume of crushed specimen
s	Cross-head distance
a, ALPH	Nonlinear shear stress parameter
X_t	Longitudinal tensile strength
X_c	Longitudinal compressive strength
Y_t	Transverse tensile strength
Y_c	Transverse compressive strength
DFAILC	Max strain for fibre compression
DFAILT	Max strain for fibre tension
DFAILM	Max strain for matrix straining in tension and compression
DFAILS	Max shear strain
EFS	Effective Failure Strain
σ_n	Normal stresses
σ_s	Shear stresses
σ_1	Longitudinal stress
σ_2	Transverse stress
σ_{12}	Transverse shear stress
σ_u	Ultimate tensile stress
σ_b	Flexural strength
τ_s, S_{12},Sc	Shear strength
NFLS	Normal failure strength
SFLS	Shear failure strength
SOFT	Softening reduction factor for material strength in crashfront elements
TFAIL	Time step size criterion for element deletion
PARAM	Critical normal separation of the surface
FE	Finite element
FEA	Finite element analysis
FEM	Finite element model
UD	Unidirectional
θ	Fibre orientation

Ph	Hertzian failure load
DTL	Delamination threshold load

1 Introduction

1.1 Motivation

Crashworthiness by definition means the ability of structural absorbers to protect occupants in a case of an impact by absorbing the applied energy. The energy absorption is obtained through controlled failure mechanisms and modes that enable a stable load pattern during energy absorption. To design composite absorbers, the overall energy absorbing capabilities are dependent upon number of factors including, structure geometry, material system, lay ups, and impact velocity. Composite materials can be tailored for a specific application and are getting more popular day by day for their outstanding characteristics including non-conductivity, low coefficient of thermal expansion, fatigue and corrosion resistance, and most importantly high stiffness-to-weight and strength-to-weight ratios. High-energy absorption of materials, reduces the overall damage to the main structure and it provides greater safety for the passengers by reducing the initial/post impact load. The challenge is to maximise the energy absorption and simultaneously have weight reduction, but without any negative effect to the safety, nor production and fabrication. Currently, thin-walled structures are being manufactured from FRP composites due to its capacity to withstand axial load through membrane as opposed to through bending.

Composite tubes are known to be outstanding where crashworthiness is concerned due to excellent energy absorption capabilities under axial loading. Although many studies have been carried on axial impact and compressions, based on different materials systems and geometrical shapes with development of different manufacturing techniques. The prediction of energy absorption behaviour of composites is not as easy and simple because of failure mechanism complexity that occurs. Structural failures of composites are due to a combination of fracture mechanisms that includes fibre fracture, matrix cracking, fibre matrix debonding and delamination.

Effect of crushing process is dependent on interlaminar fracture toughness. Researches have studied the crack propagation and stablished ways to control

failure within the laminate. Various methods are used to increase energy absorption capabilities by improving interlaminar fracture toughness such as stitching through the thickness resulted from knitting process that influences an increase in energy absorption capabilities without increasing the weight of the structure. Introducing stitching through the thickness to FRP composite sections results into higher specific energy absorption compared to non-stitched specimen when subjected to impact and the stitched specimen can collapse in a progressive and controlled manor.

In this thesis, the effect of energy absorption capability of stitched FRP composite sections compared with non-stitched sections are studied against their crashworthy behaviour and specific energy absorption capability. Using unidirectional CFRP and GFRP composite sections with symmetric lay-up sequence of $[-45/45/-45/45/0/90/0/90/0/90/0]_S$ and $[-45/45/0/90/0/90]_S$ respectively. This stacking sequence is balanced and symmetric, in this laminate lay-up, the coupling forces cancel out and the distortions are significantly reduced. The author investigated the influence of single and multi-located stitching through the thickness on energy absorption capabilities and fracture toughness Mode-I using GFRP cylindrical shells under quasi-static loading. As well as increasing energy absorption capabilities, the author also concentrated on the ability to control the force-crush distance curve by applying multi-located stitching. This research led to developing a pattern for UD composite sections and further investigations of energy absorption capabilities of multi-located stitched GFRP and CFRP showed 17% and 18% increase in specific energy absorption capability respectively, under impact loading compared to non-stitched section. Both GFRP and CFRP stitched specimens showed 15% and 14% increase in specific energy absorption capability, under quasi-static loading respectively.

1.2 Research objectives

1.2.1 Aim

To improve specific energy absorption capability of unidirectional composite crash absorbers. In order to maximise the Specific Energy Absorption (SEA), the sustained crush load must be increased. Hence, through-thickness stitching is introduced to increase delamination resistance which is directly linked to friction and bending of petals to improve local and global energy absorption and consequently improving SEA capability.

1.2.2 Objectives

The main objective is to improve energy absorption capabilities without increasing the weight of composite absorbers. This research investigates on the effect of stitching through the thickness on interlaminar fracture toughness and consequently its effect on the energy absorption capabilities in the case of a crashing event. Several objectives have been defined at the start of the research. These can be listed as:

- To study the crushing behaviour of composite crash absorbers, subjected to axial and off-axis loading.
- Identifying the parameters affecting energy absorption capability at off-axis loading and improving energy absorption by cancelling/reducing the off-axis effect.
- Develop a multi-stitching pattern to improve interlaminar fracture toughness, friction and fronds bending to improve specific energy absorption capability of composite crash absorbers under quasi-static and impact loading conditions.
- To develop a numerical model capable of predicting the crushing behaviour of composite crash absorbers under various loading conditions.

- Study how various parameters such as contact definition, material card, number of shells, friction, stiffness, mesh size, failure trigger mechanism, element formulation and delamination modelling effect specific energy absorption capability
- To develop a method to predict the crushing behaviour and energy absorption capability of multi-stitched composite crash absorbers.

1.3 Contribution to the research

- To study the behaviour of composite absorbers at axial and off-axis loadings
- To introduce single stitching and multi-stitching pattern on composite sections to obtain a stitching pattern to improve specific energy absorption capabilities.
- To investigate the effect of through-thickness stitching pattern developed on progressive crushing behaviour under quasi-static loading conditions
- To investigate the effect of the developed stitching pattern on composite sections under impact loadings.
- To develop a robust finite element model to simulate composite sections under various loadings
- To develop FE model to capture stitching pattern behaviour under static and impact loadings.

1.4 Thesis structure

This section presents a concise overview of the different chapters appearing in this thesis.

Chapter 2: *Literature Review*

This chapter consists of a survey covering general and specific factors affecting energy absorption capabilities in composite tubular structures. Progressive crushing behaviour of tubular structures are covered, and its failure collapse mechanisms are identified. The previous studies about fracture toughness and consequently energy absorption capability of composite sections are included, and the current status of the field is identified and factors influencing the performance are covered including material selection, laminate design, impact velocity, structural size and geometry, strain rate sensitivity. Relative FE models suitable for the case are covered. The aim is to identify the current status of the field. The missing link in the field is identified and a solution is proposed.

Chapter 3: *Experimental Studies of Axial and Off Axis Loading under Quasi-Static Loading*

This chapter experimentally investigates the effect of lateral inclination angle on energy absorption capability of impregnated GFRP composite sections. This chapter also focuses on the fabrication and testing setup of the proposed investigation. The factors effecting energy absorptions at off-axis loading conditions are identified and the energy absorption capability is improved at off-axis loading.

Chapter 4: *Experimental Studies of Single, Multi and Pattern-Stitched Composite Sections under Quasi-Static Loading*

This chapter mainly focuses on the energy absorption capability of stitched composite sections. The effect of through-thickness stitching location on energy absorption capability is studied and the failure mechanisms are identified in each case. Eight cases were proposed and studied in detail to establish the effect of

stitching on specific energy absorption (SEA) capability compared with non-stitched specimen.

Chapter 5: *Experimental Studies of Pattern-Stitched Composite Sections under Quasi-static and Impact Loading*

This chapter continues from chapter 4, to study the effect of pattern stitching on specific energy absorption capability. In this chapter impregnated CFRP with different geometry size is also subjected to pattern stitching to determine the effect of the proposed stitching pattern on another material. In this chapter the loading conditions are quasi-static and impact loading to establish a comparison of force-displacement curves, crushed morphologies, SEA and crushing process of stitched and non-stitched CFRP and GFRP composite sections.

Chapter 6: *Numerical Modelling Approach of Composite Structures under Progressive Failure*

In this chapter, the numerical modelling approach is covered. Different number of shells are compared in regard to force-displacement curves, trigger modelling, mesh sensitivity, element formulation, material model, stiffness and delamination resistance also were investigated in respect to computational costs, initial peaks, and mean crushing force and SEA values.

Chapter 7: *Numerical Study of Axial, Off-axis, Stitched and Non-Stitched Sections under Quasi-Static and Impact Loading*

In this chapter, a comparison of numerical studies with experimental studied were carried out. Stitched modelling techniques is covered in this section. A total of thirteen final simulations were compared with experimental studies, including axial and off-axis under quasi-static loading, stitched and non-stitched impregnated CFRP and GFRP under quasi-static loading, and stitched and non-stitched impregnated CFRP and GFRP under impact loading. The comparison included, force-displacement curves, SEA values, crushed morphologies and crushing process.

Chapter 8: *Summary, Conclusion and Recommendations*

This chapter presents the main findings of this work and discusses the accomplishment of the thesis and contribution to knowledge of this work are summarised. Different ways of possible future research concluded from this work are proposed.

2 Literature Review

2.1 Introduction

Axial crushing of metal tubes has been studied by the vast majority of researchers. Metal tubes have energy absorption mechanism of plastic deformation due to progressive folding formation [1]. Some researchers increased wall thickness to increase specific energy absorption [2,3], and furthermore for better energy absorption, foam filled aluminium and stainless-steel tubes were introduced [4]. Other researchers introduced metals in inner core of sacrificial cladding structures [5-7]. However, due to high expense of material, manufacturing and maintenance for metals and heavier sacrificial structure, these types of structures were found insufficient [8,9]. Alternatively, in terms of specific energy absorption and weight reduction, polymer composite materials are comparatively introduced to improve structural energy absorption capabilities as well as further weight reduction [10,11].

In passenger carrying applications such as aerospace and automotive where weight concerning application is an important factor, these improvements are no longer relevant due to fuel consumption. Consequently, fibre reinforced polymer (FRP) composites have been extensively studied due to weight to stiffness ratio in comparison with metals [12,13]. Researchers concluded that a well-engineered FRP composite structures would be an appropriate choice where energy absorption is concerned [14-16]. Composite materials such as carbon fibre reinforced polymer and glass fibre reinforced polymer encounter fractures in axial crushing to absorb energy unlike metals which absorbs energy by plastic deformation [17,18]. Savona CS [15] stated that majority of energy absorption are obtained through failure modes of Mode I and Mode II fracture, frond bending, fibre fracture and friction at crushed fronds [19].

One of the main factors that FRP composite materials are commonly used in high performance automotive and airframe substructures is having capabilities of high-energy absorption. The structural elements used in high performance automotive and aerospace applications are mainly from FRP composites, which are

economically beneficial due to weight reduction and lower fuel consumption. Furthermore, FRP composite materials provide enhanced level of structural vehicle crashworthiness that ensures high-energy absorption in sudden collision in a controlled progressive collapse. This is achieved by extensive and complex fracture mechanisms of FRP composites [17, 20-22].

FRP composite materials are known for being tailored to improve material properties based on specific applications with high specific strength and verification of fibre and matrix, and fibre orientations. This factor makes this type of materials more advanced compared to more conventional isotropic materials.

There are several ways to absorb impact energy. Deformation of solids is usually based on plastic flow, although appreciable amounts of energy can be absorbed by controlled brittle fracture mechanisms. Absorbers can also be reusable like a hydraulic damper; rechargeable with the energy absorbing component being replaced in a permanent container; or expandable, as in the collapse of a vehicle structure during a crash. Composite materials have a significant potential for kinetic energy absorption during a crash. The application of energy absorbers depends on the type of impact load. This can be distributed over the whole impact body, as in explosion loading, or it can be localised, with a small or pointed body hitting a large body. The large body may deform in an overall manner in the same way as if the load were distributed, or the small body may penetrate it locally.

Other studies [10,23,24] investigated the parameters that influence composite tubes crushing performance. Higher energy absorption is yielded by progressive crushing process that depends on mechanical properties, fibre orientation, laminate stacking sequence, fibre and resin volume fractions, and the geometry of the structure. However, different levels of the specific energy absorption for the same parameters can be achieved by only altering the geometry of composite structures [17]. Various dimensions affecting the energy absorption were studied [25,26] for square and circular composite tubes. It is concluded from experimental studies that the D/t ratio of these composite tubes significantly affects energy absorption capability. Thornton et al. [27,28] stated that circular cross sectional composite tubes perform better compared to square and rectangular cross

sectional composite tubes. Similar conclusion was also reported by Mamalis et al. [29,30] that circular cross sectional composite tubes demonstrated a better performance in energy absorption capability. Jimenez et al. [31] investigated ‘‘I” sectional tubes. Based on the study, square cross sectional composite tube absorbed 15% more energy compared to ‘‘I” section profile. Mamalis et al [32-34] studied conical shells on their specific energy absorption capabilities and concluded that specific energy absorption decreases by increase of semi-apical angle of the frusta. Many researchers [17, 24, 32-36] conducted experiments on energy absorption of composite tubes both circular and square cross sections. It was concluded that geometrical shape significantly influences the energy absorption capability of composite structures.

Farley and Jones [29,37] studied energy absorption capability of reducing the included angle of ‘near-elliptical’ carbon/epoxy tubes. The authors noted that as the included angle decreased the energy absorption capability increased. An improvement of 10% - 30% in specific energy absorption corresponded to include angle reduction from 180° to 90°. This investigation was carried out to determine how the geometrical variable of included angle affects tube crushing characteristics and energy absorption capability (see Figure 2-1). Elgalai et al. [38] studied carbon/epoxy and glass/epoxy composite tubes for their crush response under quasi-static axial loading.

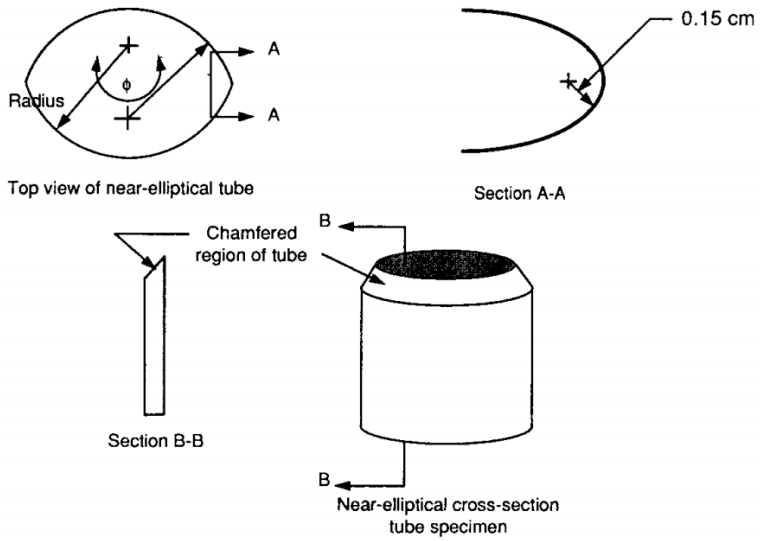

Figure 2-1 Near-elliptical cross-section tube specimen [37]

Energy absorption capability of composite tubes reported to be enhanced by corrugation. Zarei et al. [39] investigated and experimented on hexagonal box with vertical ribs for their energy absorption capabilities using woven fibre glass/polyamide plates with thermoforming welding method. Abdewi et al. [40] studied radial corrugated glass/epoxy composite tubes both at quasi-static axial and lateral crushing. The conclusion of these studies stated that radial corrugation significantly influences the energy absorption of composite tubes.

Extensive experimental investigations have been carried out on the effects of fibre orientations in composite fabrication on axial crushing behaviour. Carroll et al. and Mahdi et al [41-43] carried out an investigation on filament-wound glass fibre/epoxy with ply orientations of ±55° under quasi-static compression and reported that failure depends on rate of loading and stress ratio. Strength and stiffness were implied to be a function of loading direction and stress strain behaviour influenced the total energy absorption. It was also suggested that ply orientations of (±0) and (±90) of carbon/epoxy fibre can crush more progressively and absorb more energy in comparison with (±45) [7].

In axial crushing the aspect ratio of geometrical parameters were also studied. Mamalis et al. [19] studied the effect of L/w (length/inner width) ratio on axial crushing capability and concluded that as the aspect ratio of compressed tube increases, the peak load (F_{max}) decreases. Palanivelu et al. [44] showed that crushing state was influenced by aspect ratio of t/d or t/w (wall thickness/outer diameter or width) of 0.045 in different shape i.e. both geometries of square and round tubes, crushed progressively, although catastrophic crush in square tube was observed, however in aspect ratio of 0.083 both shapes were progressively crushed [45]. It is proven that progressive crushing for composite tubes of circular cross section can be obtained by t/D ratio of 0.015 - 0.25 whereas t/D ratio of less than 0.015 results into catastrophic failure [46].

The energy absorption capability of composite materials offers an exceptional combination of structural weight reduction and vehicle safety improvement with providing an equivalent or higher crash resistance compared to metallic structures. In automotive industry the basic occupant crash protection since

1950s has been used to optimise crash safety and ever since it became the priority of any car design requirement. The study of first structural design requirements in aeronautical industry were crash protection in military helicopters and light flexing aircraft that were in crash survival design guide forms [47]. In aerospace application the material structures considered are high performing materials including epoxy resins reinforced glass fibres, and increasingly, carbon and aramid fibres on hybrids composites. In automotive field reinforced polymers must meet a complex set of design requirements among other crash energy absorption management in front-end and side of the car structures [48-50].

This section, reviews the influence of various parameters on progressive crushing. Anisotropic materials are non-linear and by consideration of the parameters introduced, explained and evaluated in this section, a well-engineered composite structure can be tailored. This chapter evaluates a well-engineered composite structure, followed by different trigger mechanism. Moving on to different aspect of strain rate sensitivity and loading parameters, followed by extensive evaluation of failure mechanism and interlaminar fracture toughness. Simply, composite structure design, testing conditions, and failure mechanisms are extensively reviewed.

The following sections are structured initiating from introduction of crushing behaviour criteria and gradually moving on to factors effecting energy absorption capabilities and different failure modes. The chapter then reviews the effect of fibre and matrix on energy absorption capabilities followed by laminate design and geometry. These criteria are sensitive; a simple alteration can lead to change in material behaviour. Trigger mechanisms enable initiating a progressive failure and avoid local buckling. At this stage a detailed review of composite structures from tailoring and triggering is complete and testing begins. Different types of strain rate and loading conditions are introduced and evaluated, followed by different types of failure mechanisms. The effect of interlaminar fracture toughness on energy absorption is reviewed, this is accompanied by various fracture mechanism of intralaminar and interlaminar, which is a great evaluation of progressive failure modes that leads to high energy absorption capabilities of

composite structures. Through-thickness stitching is reviewed as a solution to increase delamination resistance, friction and bending, that consequently, increase specific energy absorption capabilities. Lastly, the different approaches towards finite element models are reviewed.

2.2 Valuation criteria for crushing behaviour

In the study of energy absorption capabilities of FRP composite materials, important variables such as manufacturing process and method, microstructures, specimen geometry, crush initiator and trigger mechanisms, and crushing rate are investigated. Specific energy absorption (SEA) performance is one of the most important parameters of specimens crushing material or collapsing of structural parts. SEA value is the relation between energy absorption compared to the absorber crushed mass or structure [21]. Consequently, it becomes critically important for lightweight designs. Study of energy absorption for energy management capabilities is another factor, which is the shape of the force-crush distance curve. Identification of one measure is used to mark and indicate the shape of the curve, which is known as crush-force efficiency (CFE). This value relates the average crush force (F_m) to the maximum force (F_{max}) of the crush characteristic.

Within the initiation phase the highest force normally occurs. Absorbers with rectangular shape of force-crush distance curve demonstrate a crush force efficiency of 100%. It is not optimum to have the maximum force to be substantially larger than the average crush force, due to energy management's goal of absorbing all the energy without conveying or transmitting large amount of force to the passengers.

Another parameter in energy absorption management is stroke efficiency (SE), which is the ratio of initial length of the absorber to the stroke at 'bottoming out' and high ratios specify high efficiency of material used.

2.3 Factors affecting energy absorption

In this section several variables related to energy absorption of composite thin-walled components are reviewed. In composite materials, design with constituent material properties and reach macro-mechanical properties by micromechanics analysis [21]. Regarding different applications of composite materials, their suitability is defined by impact properties and energy absorption properties and then usual design parameters. However, composite material constituent phases and the laminate layup is crucial in crashworthiness capability of composite structures as it effectively changes the mechanical property of the final product. Temperature is another important factor, which has considerable effects on material crashworthy response.

Quasi-static compression or impact loading is carried out in axial crushing. In static loading the crushing speed is within a range of 0.01 to 11 mm/s, normally a composite tube is compressed between two plates (crossheads) of one being hydraulic press. In dynamic impact loading a drop hammer or an impactor is used. To avoid buckling, specimen dimensions are determined based on the preliminary calculation [51]. Different shapes and geometries such as round, square, hexagon [44], cones [51], and plates [13] are used for instance. A typical thin-walled specimen length is within a range of 50-150 mm in length, 20-100 mm in outside diameter or width and wall thickness of 1-3 mm [238].

In crushing event, energy absorption capability is calculated to work out the specific energy dissipation rate. In composite crushing, the total work (W_T), indicates the energy absorption capability and is equal to the area under the load–displacement curve,

$$W_T = \int F\, ds \tag{2-1}$$

where F is the corresponding force on the structure and s is the cross-head distance.

Specific Energy Absorption (SEA) is energy absorption capability, which is calculated as per unit of the crushed specimen mass.

$$SEA = \frac{W_T}{m} = \frac{W_T}{\rho V} \quad \textbf{(2-2)}$$

where m is crushed mass, ρ is the material density, and V is the volume of crushed specimen.

Before material failure under buckling such as global buckling occurs, local buckling, fracture or yield or progressive crushing, the peak load is measured [52]. Further buckling failure can lead to either catastrophic or progressive failure [53] where it illustrated on load displacement curve, where the area under the curve represents the total energy absorption. In occurrence of progressive failure, a larger area under the curve is gained with a progressive constant load with increase of crushing displacement.

Catastrophic failure leads to a rapid load drop and a lower energy absorption. This is due to specimen crush being from fracture in mid-plane [54] or axial cracks [44]. Progressive failure results into higher energy absorption due to a combination of multi-failure modes initiated during crush such as local buckling, Mode-I, Mode-II, and Mode-III [55]. More energy absorption is obtained from Mode-I, Mode-II [56] due to main central crack resistance, bending and friction between ply laminates [13]. Fibre orientations influence the energy absorption in Mode-I interlaminar fracture [57]. In study of Mode-III although lower energy absorption is obtained of compressed tubes due to fracture in mid-plane and unstable collapse [19], this contradicts with another study that stated failure in Mode III is due to fibre fracture and matrix deformation that progressively extends through elliptical structure with ratio of 2, which resulted into higher specific energy absorption [55], this contradiction could be a result of geometry differences between the two studies.

2.3.1 Fibre and matrix

The vast majority of the literature on the crashworthiness of composites are focused on fibres of carbon, glass or aramid in a thermosetting resin, for example, epoxy. Farley [58], Thornton [59], Schmueser and Wickliffe [60] and Farley and Jones [61] all extensively experimented and compared energy absorption

capabilities of various specimens made of glass, carbon and aramid epoxy. Hybrid composites were investigated to combine different types of fibres into a single laminate to optimise the energy absorption characteristics [56]. Thornton and Edwards [62] stated that hybrids of glass-aramid and carbon-aramid cause an unstable folding collapse that would not have occurred if the specimens were composed of glass or carbon fibres alone. New fibre and matrix materials such as Dyneema PE fibre/carbon fibre hybrid [63] have been introduced to improve specific energy absorption capabilities. Most of these investigations have been carried out with thermosetting matrix materials, usually an epoxy. Other thermoplastic matrix materials such as polyester and polyether ether ketone (PEEK) have been used as matrix material [64,65].

Hamada et al. [65] conducted a study on the usage of a thermoplastic polyether ether ketone (PEEK) matrix with fibre carbon which concludes an outstandingly high specific energy absorption value of 180 kJ/kg. This value of energy absorption is even more than a double the value of carbon-epoxy. This is credited to PEEK matrix that has high crack growth resistance between the fibres, which prevents failure and results into stable progressive crushing [66].

2.3.2 Laminate design

In this section several variables related to energy absorption of composite thin-walled components are reviewed. In composite materials, design with constituent material properties and reach macro-mechanical properties by micromechanics analysis [21]. Regarding different applications of composite materials, their suitability is defined by impact properties and energy absorption properties and then usual design parameters.

However, composite material constituent phases and the laminate layup is crucial in crashworthiness capability of composite structures as it effectively changes the mechanical property of the final product. Temperature is another important factor, which has considerable effects on material crashworthy response. Various reports have been extensively concentrated on the effects of laminate design on energy absorption of composite structures. Thornton and Edwards [62] showed that in a stable collapse, a [±45/±45]n layup resulted into obtaining lower energy

absorption value than [0/90]n lay-ups. Furthermore, the specific energy absorption generally increases in [0/90] aramid-epoxy and glass-epoxy circular tubes for $45^o < \theta < 90^o$ with increasing of θ. Schmueser and Wickliffe [60] showed variations in specific energy absorption of carbon-epoxy, glass-epoxy and aramid-epoxy $[0_2/\pm\theta]$ specimens all generally increase with increasing θ. Mamalis et al. [67] worked on different materials with various thin-walled circular and square tubes, and reported specimens made out of a commercial glass fibre and vinylester composite material which consists of nine plies in the sequence of $[(90/0/2R_c)/(2R_c/0/90)/R_{c.75}]$, show better energy absorption behaviour than those made of a glass fibre composite material in which the glass fibres were in the form of chopped-strand mat with random fibre orientation in the plane of the mat. This layup sequence, refers to a laminate with fibres in the 0^o and 90^o direction, combined with layers of random mat reinforcement (R_c) which has two thicknesses, R_c and 0.75 R_c. Hamada et al. [64] reported that the better specific energy absorption for 0^o carbon/PEEK tubes was due to high fracture toughness of PEEK.

Woven composites introduce a different approach to the fabrication of thick composite sections for use in primary and secondary structural applications. Two mutually perpendicular sets of yarn, the warps and the wefts are used. The lengthwise direction yarns are called warp and the crosswise direction yarns are known as fill or weft (see Figure 2-2).

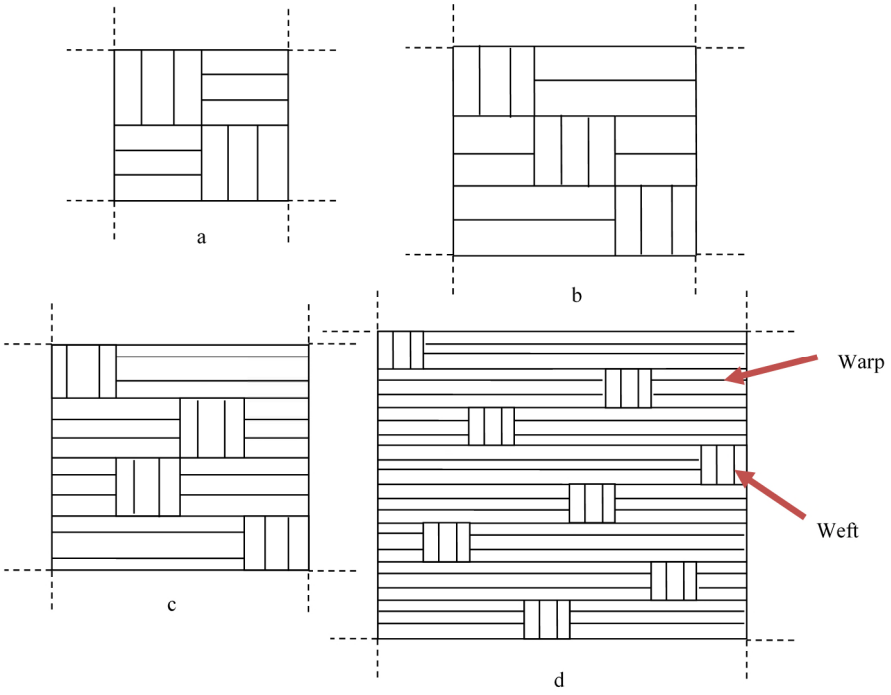

Figure 2-2 2D-Weave composites: (a) plain, (b) twill, (c) 4-harness, and (d) 8-harness. [57]

Warp and weft's interlacing pattern are known as weave. The fundamental two-dimensional weaves are plain, twill and satin, where it provides more balanced properties in the fabric plane than a unidirectional laminate [68-71]. The interlacing of fibre bundles in woven composites can often increase out-of-plane strength as in the case of three-dimensional woven fabrics. Woven fabrics are thicker than unidirectional lamina; therefore, fabrication of thick composites is less insensitive and less prone to assembly error.

The property improvements are achieved through in-plane stiffness and strength properties. The weave architecture influences the loss of in-plane stiffness and strength. This architecture is complex and therefore several parameters control the mechanical and thermal properties of woven composites. The classical laminate theory cannot be used to predict the mechanical properties of woven composite due to many specific factors including the density of the fibre bundles, the type of the weaving and the curvature that are essential to be considered [72]. Furthermore, the composite structure manufacturing is rather irregular in woven composite that can be eliminated in a non-woven laminate.

In brief, two approaches that are usually employed to study non-woven composite laminates are *micromechanics*, and *macromechanics*. In micromechanics study, the mechanical properties of laminate are studied in detail as (fibre, matrix and interface), while the macromechanics detects the material properties of laminate as a whole. Another approach, which is an intermediate of study, is called *mesomechanics*. This approach is provided to consider the mechanical properties of weave [73]. The major problem in the study of mesomechanics is the large variety of textile performs that are employed including weaves, braids, knits, mats, properties of weave stitched fabrics and two-dimensional or three dimensional.

2.3.3 Structural geometry

Extensive research was carried out based on the effect of various types of specimen geometry on the energy absorption capability by varying the shell geometric parameters such as wall thickness, t, axial length, L, mean diameter, D, or circumference, C [21]. Farley [74] reported the energy absorption capability of diameter to thickness, D/t, ratio for carbon-epoxy and aramid-epoxy circular tubes are a non-linear function. Furthermore, Farley reported that carbon-epoxy tubes are dependent on D/t for tubes with various internal diameters. Mamalis et al. [50] indicated that energy absorption of glass polyester circular tubes in static axial loading increases with increasing t/D. Thornton and Edwards [62] concluded that the energy absorption of square and rectangular cross-section tubes is less than circular ones. The primary reason for this energy absorption reduction is due to the corners and the edges response to stress concentration leading to the formation of splitting cracks.

Palanivelu et al. [44] investigated the axial crushing with cross-sectional shapes of square and hexagonal with t/D or t/W aspect ratio of 0.045 and reported catastrophic failure whereas the circular shape crushed progressively and uniformly. An increase in aspect ratio to 0.083 resulted into progressive crushing mode for square and hexagonal shapes. This increase also resulted into higher SEA value of 30.4 kJ/kg in circular shape compared with square 12.3 kJ/kg and hexagonal 16.4 kJ/kg. Abdewi et al. [75] studied composite tubes of circular cross

section (CCS) and radial corrugated cross section (RCCT) and concluded that circular cross section had lower peak loads and lower specific energy absorption compared with corrugated tubes. However, circular composite tubes with inner radial corrugated (RCSCT) failed to show any improvement in load carrying capacity [76].

Mahdi et al. investigated structures of glass/epoxy composite, and the elliptical ratio effect on the normalised SEA [55]. SEA equation was divided by cross-sectional area of the elliptical area to modify SEA. It was concluded that compared to circular tubes, ellipticity ratio of 2.0 has higher SEA and an increase of ellipticity ratio results into higher SEA.

Mahdi [77] also studied four different GFRP tubes with various cross-section properties under quasi-static crushing. The specimens included circular cross section, fuselage-shaped cross section and circular cross section with radial-geometrical reinforcement. The author concluded from the results that tubes with radial reinforcements had the highest values for peak load and an average crushing load, crush-load efficiency, absorbed energy, and specific-absorbed energy in comparison to other geometrical shapes.

In study of geometry, Mahdi et al. [78] studied conical shell angles effect on the crushing capability. It was concluded that better energy absorption of cylindrical structure was obtained with SEA value of 24 kJ/kg. Furthermore, an increase in cone vertex angle results into decrease of SEA, peak load (P_L) and volume reduction (V_R). Alkateb et al. [79] states that crushing behaviour was under influence of vertex angle within elliptical cone design. In more details, in elliptical cone vertex angle of 12°, an increase in vertex angle decreases crushing load.

Libo Yan [80] studied crashworthiness characteristics of natural flax fabric reinforced epoxy composite tubes under quasi-static uniaxial compressive load. The author concluded that short length and large number of composite plies results into large value of peak load and CFE. Increase in number of plies for specimens with the same inner diameter and length also increases crushing energy absorption capability significantly. Energy absorption capability of flax/epoxy composite tube is dependent on geometry of the tube and the

performance of composite tubes is superior to conventional metal energy absorbers.

Elfetori et al. [81] studied the effect of radial corrugation geometry on the crushing behaviour and energy absorption of circular composite tubes under quasi-static axial compression. The author based on experimental results concluded that structural geometry influences the crushing behaviour and radial corrugation geometry improves sliding mode of the structure. Radial corrugation geometry of circular composite tubes also improves energy absorption capability.

Perowansa [82] studied FRP pultruded composite square tubes under axial and oblique impact load. The author concluded that higher impact angle causes lower energy absorption capability. The impact angle and eccentricity of impact load plays an important role in determining the energy absorption capacity.

Palanivelu et al. [45,45] studied different geometrical structures, mainly on conical circular (CC) type made of glass fibre reinforced polyester composites shown in Figure 2-3. It was concluded from the work that HG-A and HG-B showed higher SEA value of 21.1 kJ/kg and 22.5 kJ/kg, respectively compared to HG-Y and HG-X that had SEA values of 13.0 kJ/kg and 6.96 kJ/kg, respectively. The failure mechanisms of HG-X and HG-Y were not catastrophic but due to lack of circumferential delamination. Palanivelu et al. [17,18] studied conical circular geometry of CC-Y and CC-X and concluded that CC-X showed lower SEA compared with CC-Y, with specific energy absorption value of 23.5 kJ/kg, and 28.8 kJ/kg, respectively.

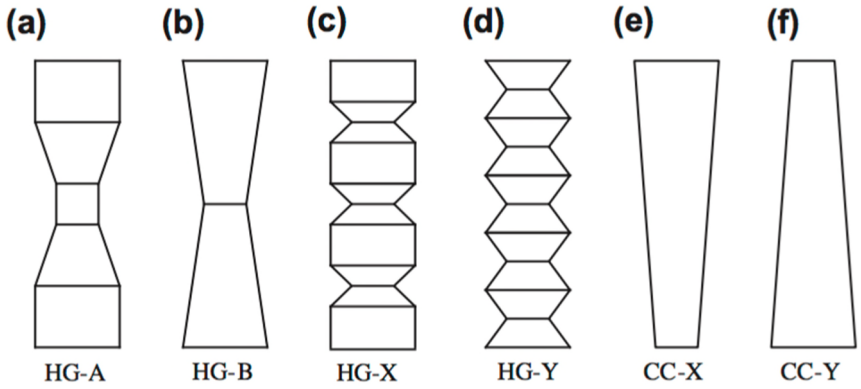

Figure 2-3 Types of hourglass (HG) and conical circular [44].

Mahdi et al. studied similar cone-tube-cone composite structure to HG-A as shown in Figure 2-2 [83]. It was stated by the author that specific energy absorption was under influence of tubular part height where normalised tubular height and high SEA value was shown in height/total height ratio between 0.06 and 0.11. In another study by the author HG-B cone-cone intersection composite with different vertex angle was studied [84]. It was concluded that more energy absorption was obtained from vertex angle of 20° and 25° compared to 10° and 15° vertex angle. In carbon and glass fibre comparison it is shown that using fibre as reinforcement enhances energy absorption capability due to enhancement in materials properties. Both materials showed similar trend in material behaviour, increasing vertex angle results into increase of SEA and crushing load.

Farley [74] conducted a study of the influence of specimen geometry on the energy absorption capability and scalability of composite materials by static crushing tests on graphite/epoxy and Kevlar/epoxy square cross section tubes. Czaplicki et al. [85] reported that significantly higher energy absorption of tulip-triggered specimens was observed compared to bevel triggered specimens of the same geometry and material. An external bevel or chamfer ground into one end of the specimen is one of the most common types of crush initiators [86]. Various types of crush initiator are shown in Figure 2-4.

In summary circular shapes geometry have outstanding performance compared to other geometry shapes tested. Moreover, compared to other shapes apart from radial corrugated circular, circular shapes geometry absorbs most of axial

crushing energy. In studies of geometry, highest resistance in the event of crushing was obtained from structure body parallel to the applied load. Lastly in axial crushing, increase of structure angle in any part of structural body affects the SEA.

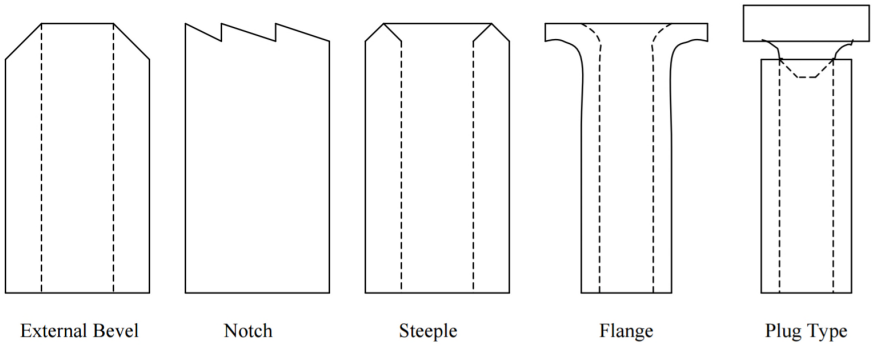

Figure 2-4 Various types of trigger mechanism [70].

2.3.4 Trigger mechanism

Triggering is a process that initiates failure and avoids load transfer to the whole structure by formation of stress concentration on edges of the profile geometry. Triggering mechanisms therefore prevent composite structures from crushing catastrophically. A suitable selection of triggering helps with progressive crushing, so the crush load is at maximum and the load is at a relevant constant value due to various fracture mechanisms such as splaying, fracture modes, etc.

Few studies [34-40,46] stated that more energy was obtained by fibre orientation along the axis of the tube compared to other orientations. Other researchers studied the performance of composite structures based on the effect of t/D ratio and size [87,88]. The conclusions of these studies were that the overall energy absorption capability of composite tubes determined by the fracture mechanisms that influenced by structure dimensions. To maximise energy absorption and decelerate crushing process, all the composite tubes during impact should exhibit axial cracking, fibre fracturing modes, delamination and bending [24]. Many researchers [23,25,26,34,89,90] studied edge chamfering and ‘‘I” sectional tubes to investigate its effects on the energy absorption capabilities [31,36].

Jimenez et al. [53] investigated the effect of triggered composites profile on energy absorption capabilities. Composite tubular type-B (bevel) with triggering angles of 30° and 60° (see Figure 2-5) reported to perform 25% difference in level of specific energy absorption. Type-B at 60° showed a peak load value of 74.7 kN which is the highest. Other investigations were reported on the effect of triggering of different cross-sectional shapes. It is reported that under quasi-static axial crushing the peak load is at maximum with edge triggering at 45° compared to 90° tulip triggering [45]. However, tulip triggering (type-T) showed higher specific energy absorption for all cross-section tubes tested than edge triggered. Palanivelu et al. [91] investigated the effect of edge trigger and tulip type triggering for round shape on specific energy absorption and reported an increase of 7-9% with edge trigger. However, opposite reaction was observed from square shapes. Tulip type triggering showed higher specific energy absorption of an increase of 16.5%. Energy absorption analysis on triggered effect was carried out using carbon and glass hybrid and non-hybrid composite braided rod [92]. It was concluded that progressive crushing was observed from conical triggered rod compared to non-tapered rod that leads to axial crack.

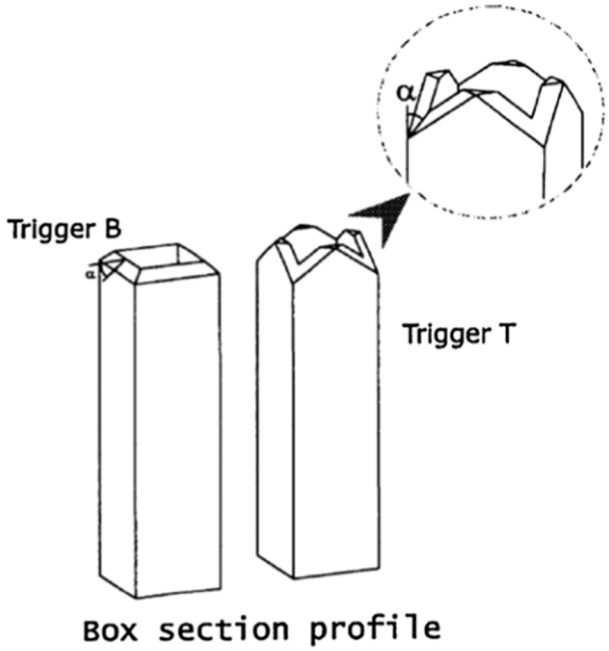

Figure 2-5 Types of triggering for composite sections, bevel (type-B), tulip (Type-T) [53].

2.3.5 Strain rate sensitivity

Extensive work of many researchers has been specifically focused to investigate the influence of strain rate on energy absorption of composite thin-walled structures. Farley [93] reported that matrix stiffness and failure strain are a function of strain-rate and the energy absorption of interlaminar crack growth (delamination) may be considered as a function of crushing speed. Later Farley reported that in $[0/\pm\theta]_2$ carbon-epoxy tubes, the energy absorption was not a function of crushing speed and found that the energy absorption in $[\pm\theta]_3$ carbon-epoxy specimen is a weak function of crushing speed with various crushing speed testing of 0.01 m/s to 12 m/s, which resulted into an increase in energy absorption of around 35%. Mamalis et al. [21] showed that the strain-rate affects the friction mechanisms developed between crushing surface and different new surfaces created after interlaminar crack growth.

2.3.5.1 Low impact velocity

FRP composite have mechanical property of orthotropic that results into complex damage modes including delamination and micro buckling. FRP composite have complex forms of damage mechanisms. At different stages of impact, matrix cracking, delamination and fibre breakage can occur and one or more being dominant [94].

In case of low velocity impact according to Cantwell and Morton [95] either of striking velocity that referred to velocities up to 10 m/s reconstructed by testing a falling weight impact, and according to Abrate [96] impact velocity test of less than 100 m/s or as suggested by Liu and Malvern [97] a low velocity impact, which is typically less than 11 m/s, takes place through sources such as debris from the runway hitting the fuselage during take-off or landing, ice from the propellers striking the fuselage, hail, and bird strikes. The impact object may cause internal damage that is often hard to detect and this can result in a severe reduction in the strength and stability of the structure, thus the effect of foreign objects impacting on composite material is a major problem. In metallic materials, the stress induced from low velocity impact due to ductile nature and high potential of energy absorption may not be considered threatening. However, in composite

materials at microscale level, low velocity impact may induce significant damages, resulting into reduction of strength and stiffness of the material [96,98–106].

Extensive research of FRP composites has been conducted at low velocity impact damage to study further the complex nature of damage mechanisms. Both properties of impactor and impacted material which influence the impact loading in FRP composites and could result into different failure modes [107-108]. Composite materials subjected to low velocity impact encounter failure modes of matrix mode, delamination mode, fibre mode and penetration [109]. Incipient impact energy, Fibre/matrix configuration, composite laminate thickness, impact velocity and impactor shape are essential parameters towards different types of failure modes. In composite materials, the interaction between failure modes affect energy dissipation properties and damage progress.

Low velocity impact in composite material has two critical threshold forces, Hertzian failure load and maximum impact load, with two critical threshold energies, penetration energy and perforation energy. Initial sign of significant damage in laminated composites subjected to low velocity impact is delamination. Delamination threshold load (DTL) is categorised as damage threshold known as Hertzian failure load (Ph) [110-111]. Delamination failure occurrence is due to lack of fibre contribution to overall strength in the thickness direction subjected to out of plane stresses generated by impact loading. Delamination propagates between plies due to bending of adjacent plies caused by out-of-plane low velocity impact.

Fibre fracture and laminate failure modes, which are the main damage mechanisms occur whist reaching maximum force threshold and develops up until the maximum energy level is reached [110,112,113]. However, at low impact energy, matrix cracking occurs although it does not degrade the mechanical properties, delamination significantly affect the laminates performance. Fibre damage, additionally, result into laminate failure (main failure) in laminates of composites.

Shyr and Pan [110] studied the effect of low velocity impact damage characteristics on various reinforced fabric structures with different laminate thicknesses. The study signifies the number of ply layers which determines the energy absorption capability. In thick laminates the dominating failure mode was fibre fracture whereas in thin structures delamination is more influential. The author concluded that the major threshold damage load was independent to incipient impact energy, but was dependent on laminates thickness. Similar conclusions were reached and stated by Belingardi and Vadori [112].

Yang and Cantwell [114] investigated experimentally the effect of varying key impact parameters on the damage initiation threshold of temperatures of 23 to 90 °C at low velocity impact tests on (0°, 90°) glass/epoxy laminated composites. The authors concluded that initial threshold damage showed a $t^{3/2}$ dependency, where t is thickness of the laminate, at both room and elevated temperatures.

Energy thresholds of penetration and perforation, which are among the main characteristic properties subjected to low velocity impact in FRP composites can be determined using energy profiling technique. A correlation between characteristic impact properties and major failure modes can be developed using energy profiling technique [115]. Quaresimin et al. [116] studied the effects of laminate thickness and stacking sequence on energy absorption capability under low velocity impact using woven carbon–epoxy composite laminates. The authors concluded that the damage initiation and delamination threshold load and the associated energy are controlled by the matrix, and they are not influenced by the stacking sequence and impact energy. Conversely, they depend on the laminate thickness. The maximum contact load was found to be independent on laminate stacking sequence, while it depends on the laminate thickness and slightly on the impact energy. The author noted that the absorbed energy was found to increase almost linearly with the impact energy and it was observed that the absorption capability of a laminate depends both on the laminate thickness and stacking sequence.

2.3.5.2 Loading conditions

In engineering applications generally, the loading classification are static, fatigue, high speed/rapid loading and impact. Impact is an important area of applied mechanics, which is strongly related to engineering practice, such as structural engineering, manufacturing engineering, aerospace engineering and material engineering. The study of impact is endless and has resulted in significant achievements both technically and economically [117-119].

For a period of short time the impact process involves relatively high contact forces acting over a small area. At the point of contact of two solids, local strains are generated that result in energy absorption [86]. The impact event may result in damage if energy absorption exceeds a threshold. A laminated composite facing a projectile strike may result in fracture processes involving delamination, matrix crack and fibre fracture. An impact event is defined as the action of one object hitting another or the force with which one object hits another.

The initial response of impact loading is to cause damage near the surface of the laminate. Although the inner layers are damaged as well and the material impact resistance changes locally as the projectile penetrates the laminate [120]. In the duration of the impact event it cannot be assumed that the contact force to be constant [121-122]. Furthermore, different projectile geometries were employed to reproduce real loading situation to measure the modifications of the composite reaction [123].

In quasi-static model testing, the impact response is a function of time and the composite model is expressed as a time dependent force that is represented by an equivalent mass with equivalent stiffness [124 - 125]. All forms of damage should be studied and considered due to the likelihood of the influence of the material residual mechanical properties, from each damage form.

2.4 Crashworthiness

The ability of a structure providing protection for occupants by absorbing the applied energy in a case of an impact is known as crashworthiness of a structure. Absorption of the impact energy enables reduction of the overall main body

structure damage and most importantly provides greater passenger safety. The two significant safety factors that can be considered in automotive and aerospace industries are crashworthiness and penetration resistance. Crashworthiness can be further defined as the absorption of impact energy by different modes and mechanisms that give moderate deterioration during energy absorption. On the other hand, the penetration resistance dealt with total energy absorption without allowing projectile or fragment penetration [43].

The crashworthiness of a material is expressed in terms of its specific energy absorption, (SEA) and interlaminar fracture toughness, which are characteristic to a specific material and design. SEA is defined as the energy absorbed per unit of specimen crushed mass [21].

2.4.1 Material performance requirement

Crashworthy materials have work done during an impact event to absorb the kinetic energy over a time frame that ensure the deceleration of for instance a car to be less than 20 g [189], beyond this point the passenger experiences severe and irreversible brain damage due to relative movements of various parts of the brain with the skull cavity. Considering a midsize vehicle mass of 1500 kg travelling at a velocity of 15.5 m/sec (35 mph). The kinetic energy can be determined by,

$$KE = \frac{1}{2}mv^2 \quad \textbf{(2-3)}$$

The kinetic energy is equal to 180,188 J, therefore, 180 kJ of work needs to be done on the crashworthy material. One can calculate the minimum safe time frame over which this work needs to be done to ensure the safety of the passengers using the basic equation of motion.

$$v = u - at \quad \textbf{(2-4)}$$

Where v is the final velocity of the car which is equal to zero since the car comes to rest, u is the initial impact speed and a is the maximum allowable deceleration which is equivalent to 20 g. The minimum time is calculated to 0.079 s. Therefore,

the minimum allowable rate of work decay to ensure passenger safety is equal to 180188/0.079 = 2,281 kJ/s. It is equally important to determine the rate of energy absorption to determine magnitude of energy absorption by the specimen. The specific energy absorption of carbon/PEEK composite is recorded to be 180 kJ/kg [35]. Therefore, to absorb the applied energy in this case, only 1 kg of the material (carbon/PEEK) is potentially required. This clearly shows the practicality of energy absorption capability of composite materials and only a reasonable amount of composite material is required to meet the necessary impact performance standards.

2.5 Test methodologies

Composite test tubes are subjected to two crushing test conditions of namely quasi-static and impact loading.

2.5.1 Quasi-static testing

In quasi-static testing conditions, the specimen is crushed at a constant speed, although this testing condition may not be a true simulation of a real crash scenario because in an actual crash condition, the structure is subjected to a decrease in crushing velocity from an initial impact velocity to rest. Some materials used in designing crashworthy structures are rate sensitive and their energy absorption capability is dependent on the subjected velocity. Quasi-static testing can be used to test materials to observe its behaviour at different conditions including failure mechanisms in composite structures but does not ensure satisfactory performance as crashworthy structures in real crashing event. The disadvantage is, it may not be a true simulation of an actual crash conditions since certain materials are strain rate sensitive. However, there are two main advantages as follows,

1. Simple setup and easy to control.
2. Can set a reference line on material behaviour/ failure mechanism and energy absorption characteristics.

Impact tests are very expensive due to their expensive equipment including high speed cameras to record the crushing process of the impact in slow motion as it

takes place in a split second. Hence quasi-static tests are used to study the failure mechanism in composites by selecting appropriate crushing velocity.

2.5.2 Impact testing

The crushing velocity decreases (decelerates) from the initial impact velocity to rest, as the specimen absorbs the energy. This is a true simulation of a crashing scenario, since it considers the stress rate sensitivity of materials. A drop tower can simulate a crashing event, a mass is dropped from a predetermined height with an initial velocity and is subjected to acceleration (9.81 m/s/s), the test specimen is then subjected to a total energy the dropped mass has gained through the process. Although the disadvantage is, the crushing process takes place in a fraction of a second and it is difficult to study the crushing process, unless expensive high-speed cameras are used.

2.6 Crushing modes and mechanism

Three main modes of brittle collapse are categorised as mode I, II and III which were studied on composite tubes in the series of static and dynamic axial compression tests, respectively [126]. According to Hull classification [17] Euler overall column buckling or progressive folding with hinge formation were not found for fibre-reinforced plastic (FRP) composite tubes. Energy absorption in most fibre-reinforced composites are through a combination of fracture and friction [127]. The two main failure mechanisms of composite tube are catastrophic and progressive failures (see Figure 2-6). A stable progressive crush is established by localised failure that initiates at one end of the specimen and progress through the specimen. To reach this failure mechanism, crush initiator is used for FRP tubes. During catastrophic failure the initial maximum force is very high and drops rapidly, therefore the average force is low.

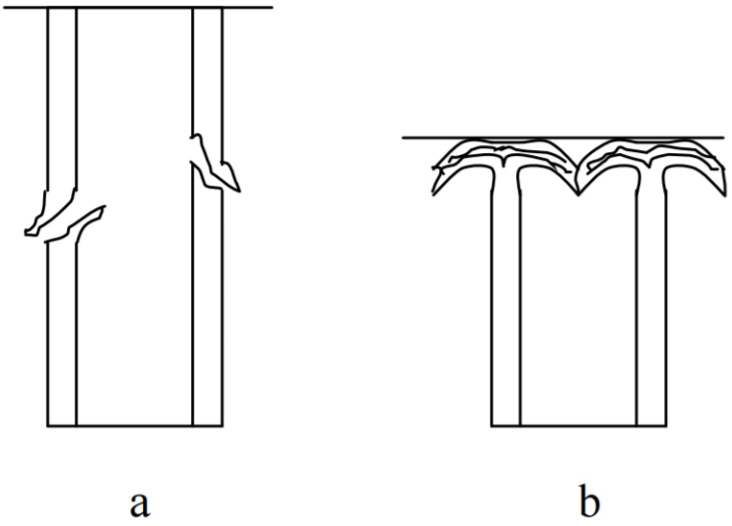

Figure 2-6 Typical collapse modes for composite tubes (a) catastrophic failure (b) progressive failure [127].

2.6.1 Failure mechanism

According to Mamalis et al. [126] in general the failure modes observed are greatly affected by the shell geometry, fibres arrangement, matrix and fibres properties of the composite material and the stacking sequences. Moreover, the macroscopic collapse modes in Figure 2-7 was classified by Mamalis et al. [126-128] from various geometries in extensive experimental treatment of axisymmetric tubes made of fibre-reinforced polymer matrix composite materials.

2.6.1.1 Progressive failure

Progressive failure can be achieved by applying a trigger at one end of the tube, this causes failure to initiate at a specific location within the structure by concentrating the applied stress. Progressive crushing of composite material with micro-fragmentation, associated with high crush energy, is designated as end crushing mode. Progressive failure mode is classified by the progressive end-crushing with splaying of the laminate tube starting at one end of the specimen. This causes the tube to form continuous fronds which spread outwards and inwards.

2.6.1.2 Catastrophic failure

The component's brittle fracture with little energy absorption resulting in catastrophic failure is designated either as transition mode of failure or mid-length collapse mode depending on the crack formation. Transition mode of failure is classified by a spiral or longitudinal crack propagation developed along the shell circumference. Mid-length collapse mode is classified by the circumferential fracturing formation of the specimens approximately equal to the mid-height of the shell into irregular shapes and described as mid-length collapse mode.

2.6.2 Progressive failure modes

Progressive failure modes are like crushing behaviour of thin-walled metal and plastic tubes, progressive folding and hinging have a very low energy absorbing capacity, which is introduced as progressive folding mode. Mamalis et al. [48-49] reported that the collapse modes can be categorised into two groups of stable and unstable collapse modes. Stable collapse modes have similar features as static loading whilst at the same geometries. According to Mamalis et al. [126] in some applications a failure could be considered by a very small deformation, and in others a total fracture or separation constitutes failure. In composite materials generally, the internal material failure initiates before any alteration in macroscopic appearance or behaviour. This indicates that failure takes place before any indication in macroscopic molecules.

Various fracture modes can be defined for a laminate composite. These modes are divided into intralaminar and interlaminar fracture modes. Intralaminar mode consists of longitudinal matrix fracture, transverse matrix fracture, fibre-matrix debonding and fibre fracture. Interlaminar mode is also referred to as delamination. Delamination is described as separation of layers from one another (see Figure 2-7). The fracture mechanisms depend upon the nature of the constituents including architecture of the layers, and mechanical loading mode [21].

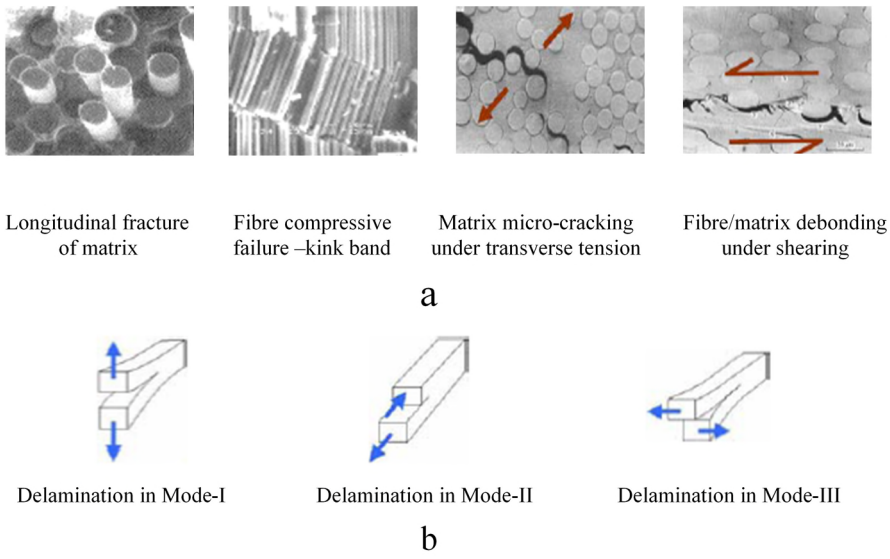

Figure 2-7 Fracture mechanisms observed in laminates (a) Intralaminar and (b) Interlaminar Failures [21].

Mamalis et al. [21] reported that the main micro fracture mechanism features of composite tubes are similar to that obtained for circular tubes. These micro fracture mechanisms are:

- An annular wedge of highly fragmented material, axially forced downwards through the shell wall;
- Ahead of the crush-zone an intrawall micro crack is developed at the apex of the annular wedge with approximately a propagation of the compression rate;
- Ply delamination in the crush zone causes two continuous fronds, mainly developed by the central bundle wedge that radially spreads inwards and outwards from the wall;
- Between the central crack and the shell wall edges a severely strained zone is formed showing a combined tensile-compressive type of deformation.

Farley and Jones [130] named and classified four main progressive crushing modes for composite tubular structures,

1. ***Transverse shearing or fragmentation mode***

Fragmentation mode or transverse shearing mode is characterised by the laminate wedge-shaped cross section with a single or multiple short interlaminar and longitudinal cracks from partial lamina bundles. The main energy absorption mechanism is fracturing of lamina bundles. When fragmentation occurs, the length of the longitudinal and interlaminar cracks are less than that of the lamina. Brittle fibre reinforcement tubes show this crushing mode. In this mechanism the energy absorption is controlled by the interlaminar crack propagation and laminar bundle fracture.

2. ***Lamina bending or splaying mode***

Lamina bending mode is characterised by parallel to fibre cracks shaped with long interlaminar fracture. This mechanism initiates the formation of inwards and outwards spreading continuous fronds. The energy absorption of lamina bending mode is controlled by inter/intra laminar fracture and friction. Brittle fibre reinforcement tubes show this crushing mode. Matrix crack growth is the main energy absorbing mechanism.

3. ***Brittle fracturing***

Brittle fracture is a combination of fragmentation and lamina bending modes. In composite tubes, the highest energy absorption ever observed is from the combination of brittle fracture crushing modes. Brittle fibre reinforced tubes show this crushing mode. The main energy absorption mechanism is fracturing of lamina bundles. The length of the interlaminar cracks are between 1 and 10 laminate thickness when brittle fracturing occurs [130].

4. ***Local buckling or progressive folding***

The local buckling crushing mode involves local buckle formation meaning plastic deformation of the material. The post-crushing integrity of ductile fibre-reinforced composites is a result of fibre and matrix plasticity, i.e. significant deformation without fracture and fibre splitting. Local buckling can exhibit from brittle fibre-reinforced composites when small interlaminar stresses relative to the strength

of the matrix is applied, or the matrix has a higher failure strain than the fibre, and when plastic deformation under high stress exhibited from the matrix.

Brittle fibre-reinforced composites exhibit the transverse shearing and lamina bending crushing modes, although ductile fibre-reinforced composite materials have similar mode behaviour as ductile metals in local buckling crushing see Figure 2-8.

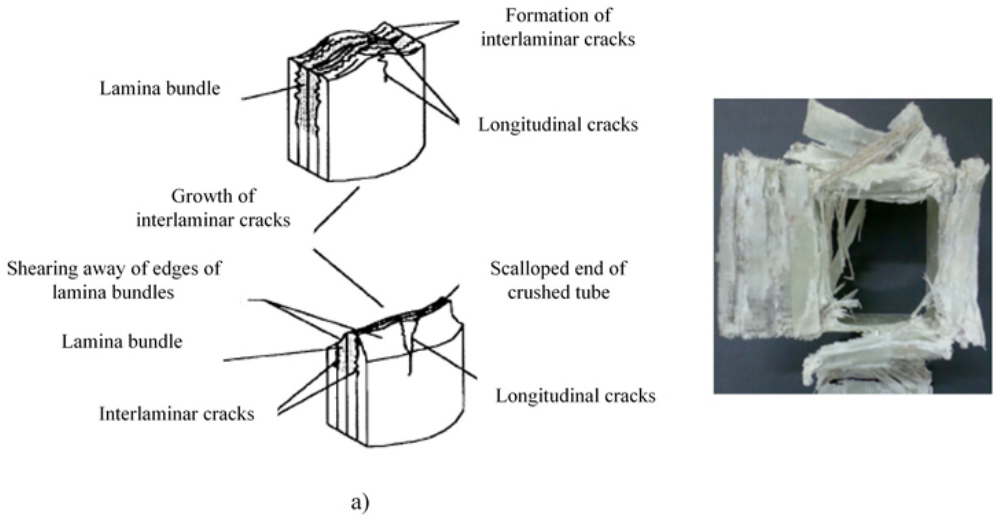

a)

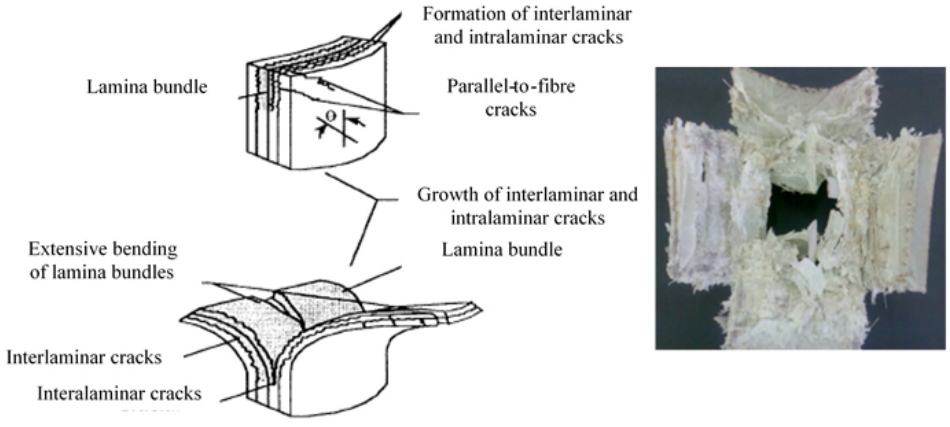

b)

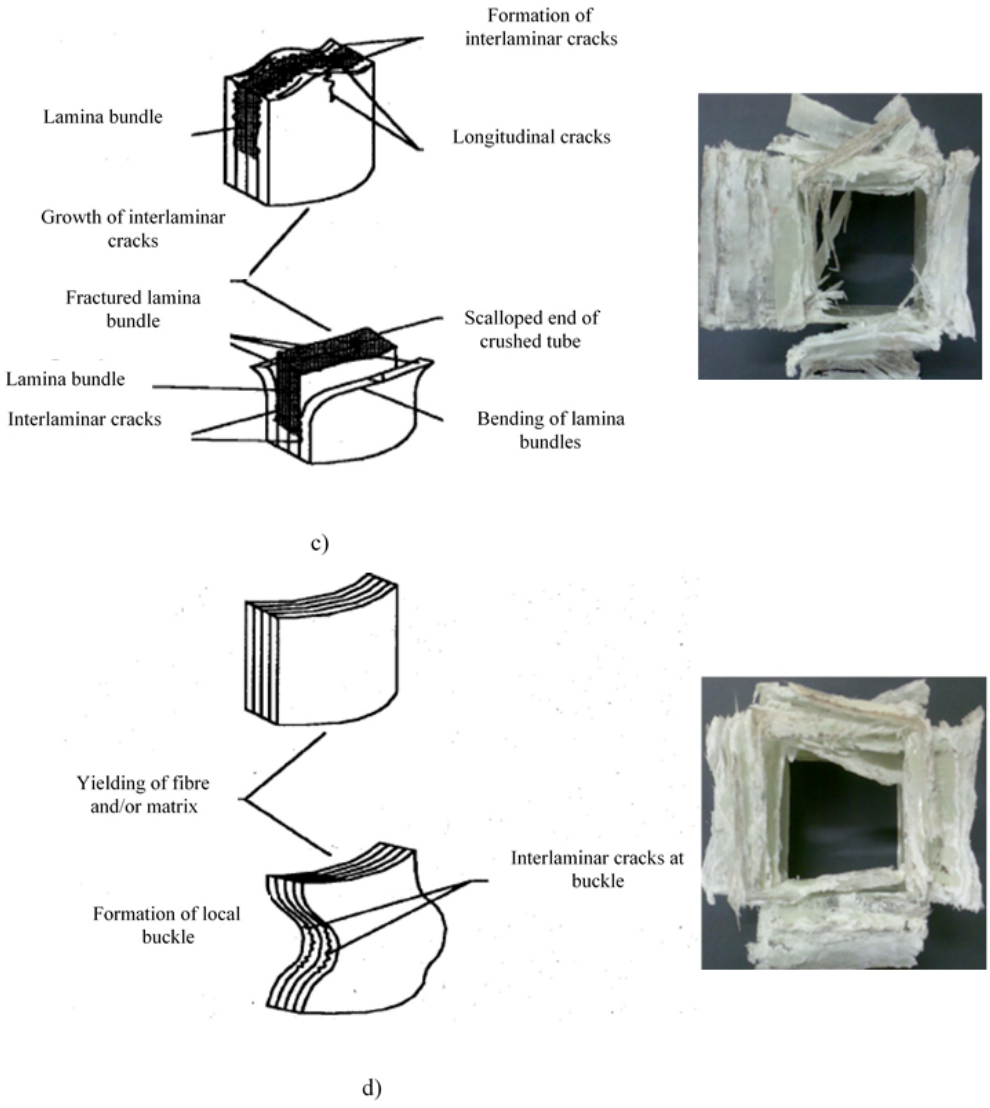

Figure 2-8 (a) Transverse shearing crushing mode, (b) Lamina bending crushing mode, (c) Brittle fracture crushing mode, (d) Local buckling crushing mode [131].

2.7 Off-axis crashworthy behaviour of FRP composite structures

Different types of crashworthy components were studied in the past two decades including material systems, various geometrical shapes and various fabrication methods were developed and axially tested [75-77]. In a real-life crashing event, the likelihood of having a non-axial collision is very high [144,136,225]. Quite recently few researches have concentrated on the energy absorption capabilities of elements such as box under two types of non-axial loadings. Non-axial loadings are divided into angled loading, and off-axis loading also referred to as oblique loading. Some studies can be found in the literature with complex loading conditions [29,41,75,90,128]. Since during an impact event, the thin-walled structures undergo severe collapse failure and in oblique loading conditions, it could suffer from drastic energy absorption reduction. In automotive applications for instance, the bumper system is expected to endure a load with impact angle of up to a 30^{o} to its longitudinal axis [206]. Therefore, maintaining high crashworthiness behaviour under different loading conditions is essential to be met whilst meeting the critical requirement of structural collapse [206,217-222].

Occurrence of off-axis loading is when the impact of an object is from a direction not along its longitudinal axis. Occurrence of angled loading is when the impact of an object is from being perpendicular to longitudinal axis. It is essential to undertake all the effects of collision in crashworthy composite structures on the capabilities of energy absorption. In off-axis crushing the formation of fracture mechanisms are different from axial crushing observations. During non-axial progressive collapse, an important role in dissipation of crushing energy is non-symmetrical crack propagation at the intrawall box and between fronds.

In practice, the above concern is mainly based on the fact that axial crushing always accompanies with high energy absorption capability through progressive crushing. However, according to previous studies on axial crushing behaviour and oblique loading [206,218,220,221], at oblique loading, the absorbers could experience an initial peak load followed by catastrophic failure which results into

low energy absorption. Extensive studies have concerned with this phenomenon [144,223,224].

Few researchers have investigated the effects of off-axis crushing on the energy absorption of composite materials and structures [133-135]. Czaplicki et al. [135] investigated on off-axis loading and angled loading crushing process of E-glass/polyester pultruded tubes. It was concluded that off-axis loading, and angled loading conditions dissipate energy in different friction mechanisms but both loading conditions observed a similar energy absorption tendency by increasing the inclination angle. It was also concluded that at 10° off-axis angle the mean crushing force increases in comparison to mean crushing force of axial crushing and a steady decrease with increase of angle of inclination. Song and Du [136] studied the energy absorption capabilities of off-axis loading of five different circular GFRP tubes with different off-axial crushing angles, varying from 5° to 25° with an increment of 5°. Three characteristic crushing stages were identified according to their extensive research, triggering stage (Tr), sustained crushing stage and toppling stage. In general, as the off-axis inclination angle increases the energy absorption decreases, caused by a change in two factors of toppling tendency and fracture pattern. They also concluded that 0º ply can prevent the circumferential cracks and therefore longitudinal resistance to delay the toppling stage (see Figures 2-9 and 2-10).

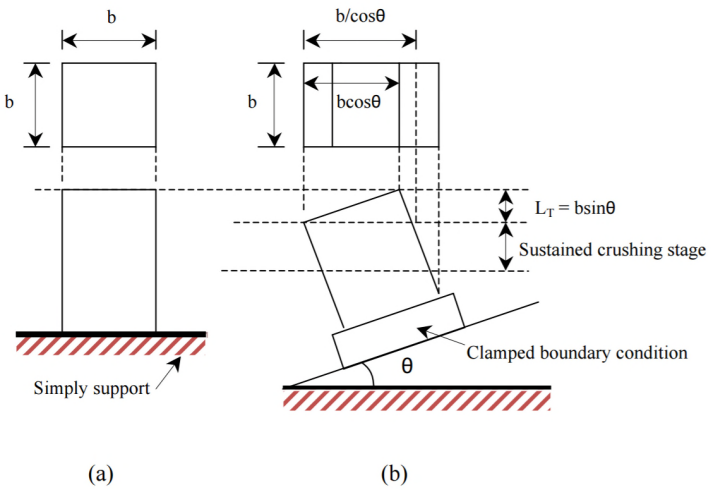

Figure 2-9 Comparison of axial and off-axis crushing process, a) axial crushing and b) off-axis crushing [143].

Czaplicki et al. [135] conducted experiments on the effect of fibre reinforcement type, structure type, fibres orientation in a layer and layers stacking sequence on the energy absorption capabilities of tubes and truncated cones. They also carried out an experimental investigation on the effect of wall-thickness and angled loading on specific energy absorption (SEA).

Ghasemnejad et al [56,144,15] experimentally investigated the axial and off-axis crashworthy behaviour of CFRP and GFRP composite box structures with inclination angles of 5º, 10º, 20º, and 30º under quasi-static loading. The authors concluded that at 10º off-axis loading the mean crushing force exceeds axial loading by 12%. This conflict with another study that the author [82] concluded that the energy absorbed in the square tube is decreased significantly when the impact angle is raised. Using fibre E-glass and polyester composite under oblique loading conditions.

Mamalis [29] investigated the crashworthy characteristics of composite structures by observing the brittle failure modes, such as progressive end-crushing, local tube-wall buckling and mid-length collapse, through a series of static and dynamic axial compressive tests. Greve et al. [227] conducted the impact tests and simulated the fragmentation process of braided carbon/epoxy composite tubes under axial and oblique loading conditions.

In recent studies, the crushing behaviour of composite structures subjected to axial and oblique loads have gained increasing attention [24,228-230]. Zhou et al. [231,232] for example investigated conventional square tubes and origami crash boxes under axial and off-axis loading and noted that origami crash box subjected to range of loading angles are potentially more desirable than conventional square tube. Sun and his co-authors [233-235] investigated the functionally-graded thin-walled structures crash characteristics under multiple loading angles using finite element analyses (FEA). Zarei [236] investigated on crashing response of simple and hybrid composite tubes with various numbers of GFRP overwrap.

Recent studies carried out by several researchers are noted that the dissipated internal energy is in relation to the geometry and material characteristics. A clear

overview of the various crushing parameters that effect the change in energy absorption of composite structures can be found in literature [90,205,206].

Following the current state-of-the-art, it can be concluded that in the case of off-axis loading conditions, the mechanical response varies with change of geometry. However, none of the reviewed articles studied the case of introducing integration of lay-up sequence and trigger mechanism to improve energy absorption capabilities. Assessing the crashworthiness of composite tubes subjected to off-axis loading is of particular interest in the aerospace industry because, in addition to the absorbers allocated axially there are off-axis positioned absorbers that can be improved for their energy absorption capabilities. In this chapter, glass/epoxy tubes were tested under quasi-static compression tests for their crushing behaviour. Five cases were also studied with combination of ply-orientation and flat trimming 45^{o} chamfer integration mechanisms to evaluate their effect on energy absorption capabilities. This improves mean crushing force and consequently increase specific energy absorption (SEA).

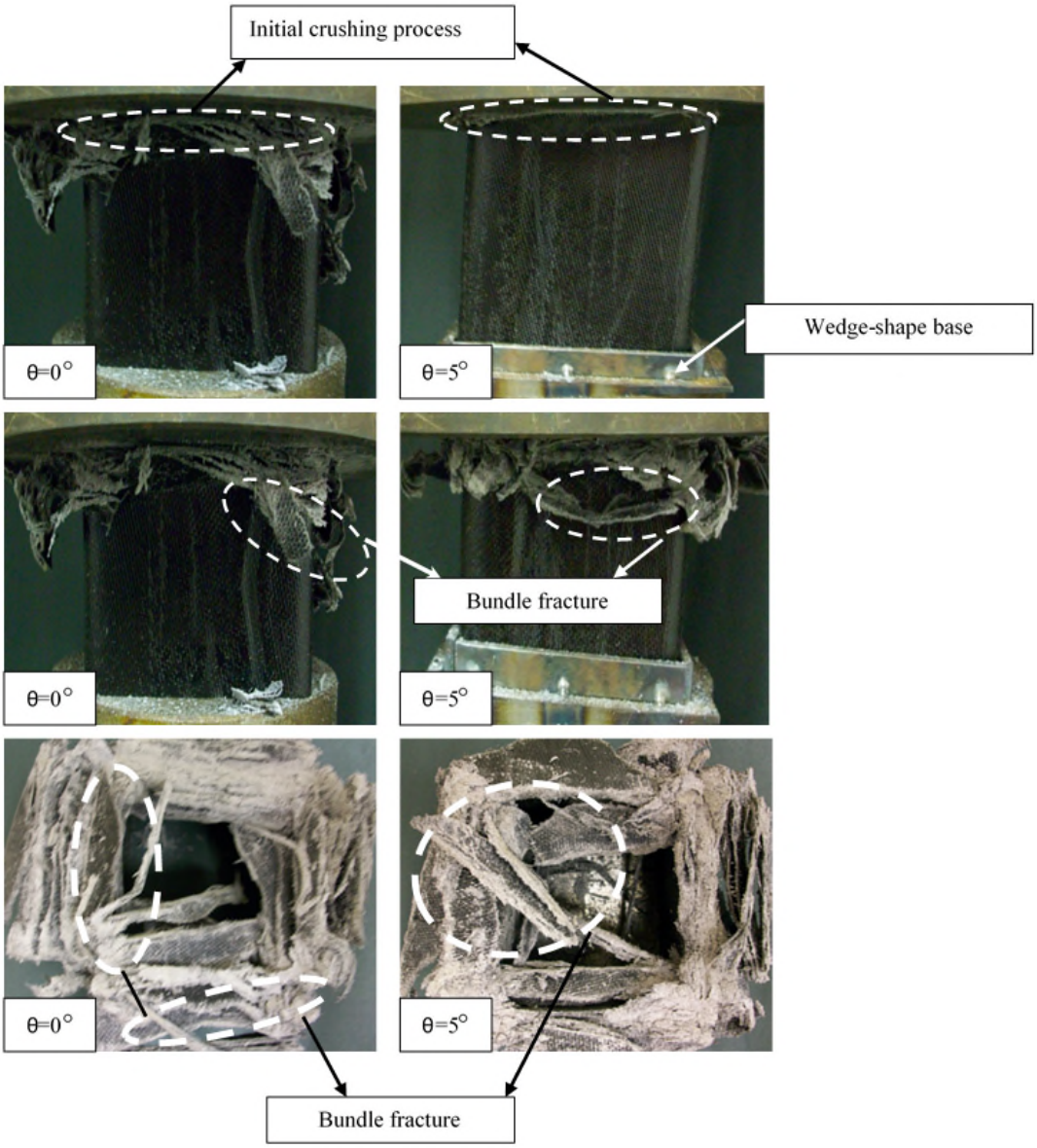

Figure 2-10 Various crushing stages of woven glass/epoxy composite box in axial crushing (θ =0) and off-axis loading at (θ =5°) [143].

2.8 Improvement of interlaminar fracture toughness

The energy absorption from interlaminar fracture toughness is accompanied by various fracture mechanisms of interlaminar failure. In the study of fracture toughness, delamination crack growth influences the energy absorption capability of composite structures. Progressive failure mode and energy absorption of composite structures, are affected mainly by various fracture mechanisms including fibre breakage and buckling, matrix cracking and crushing, debonding

at the fibre-matrix interface and especially plies delamination. Shear and tensile separation between fronds cause delamination. Energy absorption is the effect of these two crushing mechanisms that are due to interlaminar crack growth and fracturing of lamina bundles. The sources of energy absorption during progressive collapse are mainly from [136]:

- Frictional resistance between wedge and fronds and between fronds and platen: about 45% of total absorbed energy.
- Frond bending due to delamination between plies: about 40%.
- Intrawall crack propagation: about 12%.
- Axial splitting between fronds: about 3%.

2.8.1 Disadvantages of 2D fibres

High stiffness, fatigue life and strength are required in all engineering applications and composites are reinforced with continuous fibres rather than small particles or whiskers. A distinguishing feature of 2D laminate is that no fibres are aligned in the through the thickness or in the z-direction. The lack of through the thickness reinforcing fibres can be disadvantage in terms of mechanical performance, impact damage resistance and crashworthiness behaviour. Due to lack of reinforcement in the z-direction, the through the thickness mechanical properties are poor. The two-dimensional arrangements of fibres provide very little stiffness and strength in the through the thickness direction because these properties are determined by the low mechanical properties of the resin and fibre to resin interface [190]. In Figure 2-11, the through the thickness properties are often less than 10% of the in-plane properties and because of this reason 2D laminates are not suitable for structures supporting in z-direction or interlaminar shear load.

Impact damage can seriously degrade the in-plane mechanical properties under tension, compression, fatigue life and bending. The strength drops rapidly with increasing impact energy, and even a lightweight mass with low impact energy can cause a large reduction in strength of composite laminates. The low post-impact mechanical properties of 2D laminates is a major disadvantage, particularly when used in thin load-bearing structures to combat the problem of delamination damage, due to this, composites are often over-designed in

thickness and this leads to increase of cost, weight and volume of the composite and in some cases may provide only moderate improvements to impact damage resistance.

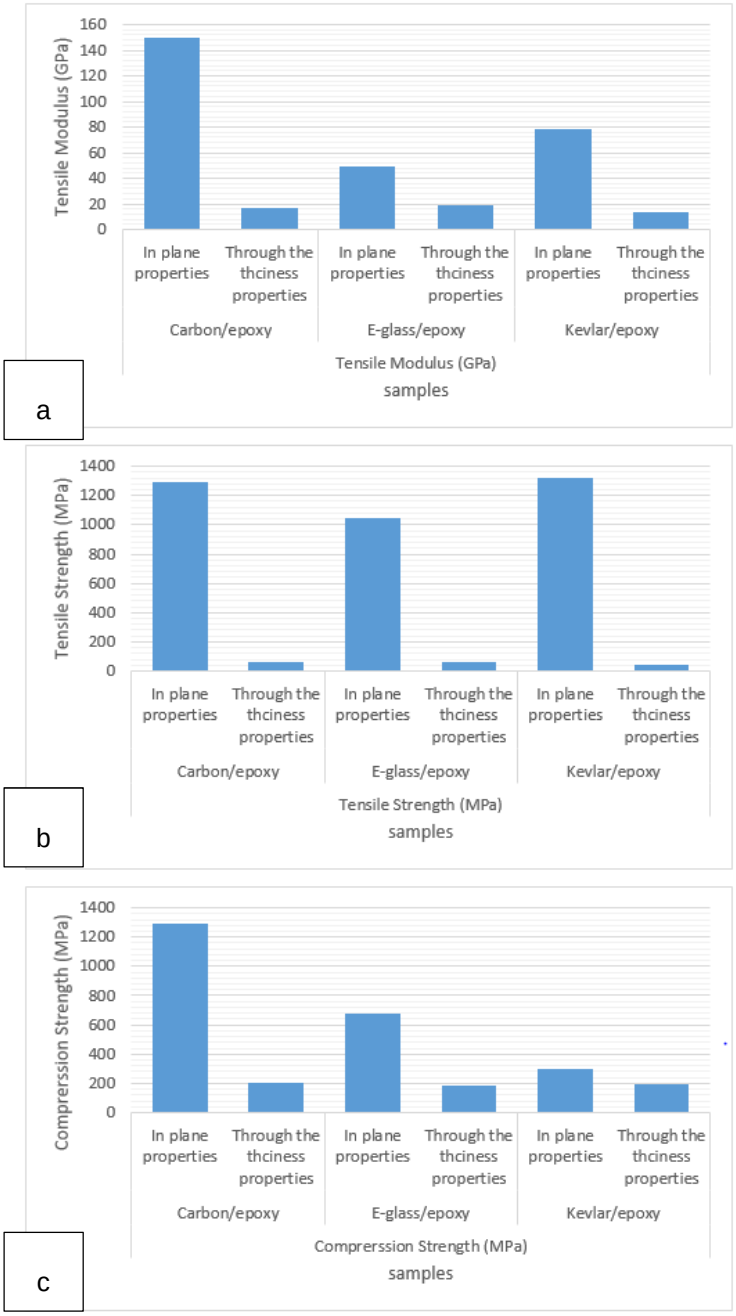

Figure 2-11 (a) Tensile modulus, (b) Tensile strength and (c) Compressive strength comparison of in-plane and through-thickness mechanical properties of some engineering composites [237].

2.8.2 Architecture of 3D fabric

Three-dimensional architecture is a type of advanced material which increases the mechanical properties and impact damage tolerance in the z-direction or through the thickness. There are five different types of 3D composite processing techniques due to high demands of space-craft, helicopters and aircrafts on FRP composites in load-bearing applications.

1. Weaving
2. Braiding
3. Knitting
4. Stitching
5. Z-pinning

2.8.2.1 Weaving

Weaving process is used in different applications and industries, such as aerospace, marine, civil and medical due to its flexibility characteristics. The ceramic-based composite consists of 3D woven carbon fibres and a silicon carbide matrix. This is used to reduce manufacturing costs, reduce of peeling stresses at the joints, improve of stress transfer and improve of aerodynamic performance. One of the influential material used in the industry due to simplified manufacturing assembly compared with conventional 2d laminate or aluminium alloy, nose cone in rockets for instance. Manufacturing of chamber as a single piece through this method and reduction of leakage problems associated with conventional 2d laminates is one of the main advantages of using 3D woven composites (see Figure 2-12). This process has been used for over 50 years.

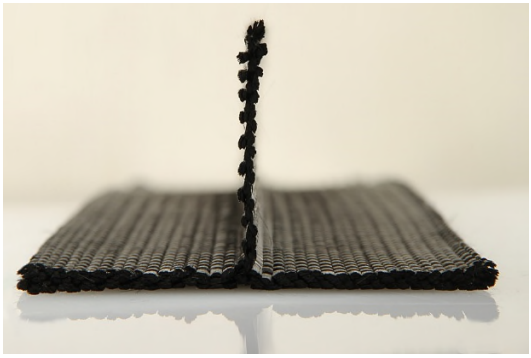

Figure 2-12 Multilayer woven fabric

2.8.2.2 Braiding

Braiding process is familiar to many field of engineering as standard 2D braided carbon and glass fabric has been used for a number of year in a variety of high technology items, such as lightweight bridge structures, aircraft propellers. This process has been around for two decades to produce high technology items such as advanced aircraft propellers and golf clubs. Multi-layer and thick material construction can be made from traditional 2D braiding, although the process of 2D and 3D braiding faces a variety of different techniques of manufacturing. A key benefit of using 3D braided over conventional 2D fabric braided is structural integrity, torsional stability and high levels of conformability. Aerospace applications for 3D braided included airframe spars, fuselage barrels, F-section fuselage frames, rocket engine nozzles and rib stiffened panels, although many applications are potentially suitable for ships, deck for lightweight military bridges, causeways, shafts and propellers. 3D braided composites are 50% lighter than similar components made from steel with the same performance such as crashworthiness properties and damage tolerance, this material is currently used in chassis and drive shafts.

2.8.2.3 Knitting

Knitting fabrics potentially enables manufacturers to produce specific types of composite structures, with excellent impact performance that makes them ideal for service conditions where damage tolerance or energy absorption is critical. Most 2D conventional knitted fabrics also contain a significant proportion of their strength in the thickness direction of the fabric. There is potential application for 3D knitted composites on aircraft such as wing panels, wing stringers, T-shaped connectors, jet engine vanes and I beam. And also, in automotive industry there is significant amount of room for knitted fabrics such as door members for automobiles, floor panels, bumper bars. Important advantages of 3D knitted composites over 2D conventional are high drape properties, high impact damage tolerance, although there are some drawbacks too, including costs and high density compared with UD pre-pregs.

2.8.2.4 Stitching

Stitching is the simplest and cheapest method to produce a 3D fabric architecture since 1980s which improves interlaminar fracture toughness. The stitching process in the z-direction is used for reinforcing composite through the thickness that improves impact damage tolerance and delamination resistance in comparison to 2D laminates. The stitching process takes place by inserting a needle, carrying the stitching thread, through a stack of composite layers to form a 3D structure (see Figure 2-13). Creating 3D architectures through stitching provides many benefits. Among those is the possibility to use the process with traditional 2D woven, braided, knit, etc. This allows for a great degree of flexibility in the fabric layup; using different material layers, as well as different yarn directions. Also, stitching can be placed only in the areas that require reinforcement in the z-direction.

Many studies were carried on the performance of stitched composite and there are conflicting conclusions. Depending on the purpose of the stitched laminate the final product result may vary. Some scientist concluded that stitching can be utilised in composites joints rather than co-curing and bonding techniques. This method eliminates the need of mechanical fasteners such as, bolts, screws, and rivets therefore, reduces weight and possibly production costs of the component by 50%. This method is cost-effective, and it improves tensile and compression properties. Although conflicting performance on material properties exists.

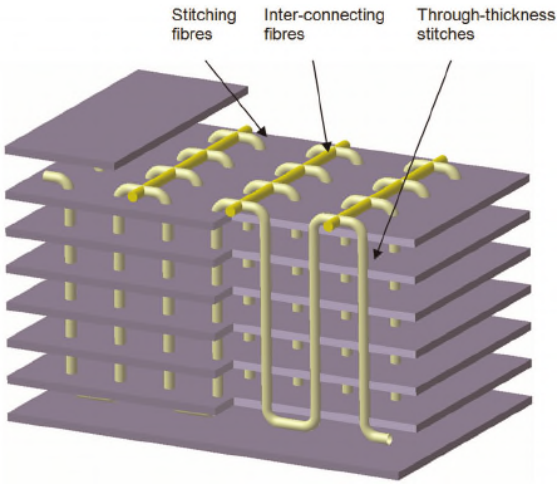

Figure 2-13 Through the thickness stitching of a composite laminate

2.8.2.5 Z-pinning

Z-pinning is used as an alternative method to through-thickness stitching. The process uses pre-cured reinforcement fibres, which are embedded in a thermoplastic foam and placed on top of the pre-preg or dry fabric. The thermoplastic foam collapses during the curing process, and the pressure pushes the z-pins into the component. The crimping in z-pinning are low compared with other methods and low fibre damage is observed while still maintaining the control over the reinforcement locations.

2.8.3 Delamination

Composite are wildly used in different industries due to their high in-plane tensile and compression strength. In most cases however, their through-thickness properties are very low (see Figure 2-10), in comparison to their in-plane properties. Therefore, the through thickness stresses may result into delamination initiation, and this factor increases by geometry characteristics of free edges, holes, ply drops and etc. or matrix crack may also be a consequence of fabrication problems, or impact damage. The brittle nature of FRP composite accompanying other forms of energy absorption mechanism such as lamina bending, fibre breakage, matrix cracking, matrix crushing, buckling, debonding at the fibre-matrix interface and ply delimitation that is a cause of shear and tensile separation between fronds. Delamination growth therefore is studied to establish and identify a threshold level to understand the mechanical behaviour of FRP composites. Delamination is one of the major life limiting failure mechanism in laminated composite subjected to service loads [54,113]. Initiating from interlaminar fracture such as delamination is considered as crack propagation and after delamination onset, the consequent propagation is not controlled by the through-thickness strength any more but the interlaminar fracture toughness [147,156].

2.8.4 Effect of stitching through the thickness on interlaminar fracture toughness

Warrior et al. [138] studied the influence of thermoplastic resin additives, toughened resins, stitching through-thickness, thermoplastic interleaving on the

interlaminar fracture toughness (G_{IC}), SEA for continuous filament random mat (CoFRM) and 0/90 non-crimp fabric (NCF) E-glass reinforced polyester composite tubes. It was concluded that the above factors increase G_{IC}, but toughened resin and through-thickness stitching improves SEA value. In general, a tougher matrix results into a higher G_{IC} in composites, this is beneficial in crashworthiness design [139]. Cauchi Savona et al. [140] studied the relation of glass fibre reinforced plastic composite plates between sustained crushing stress with their Mode-I and Mode-II fracture toughness properties. It was concluded that materials with low Mode-I and Mode-II fracture toughness, yield low crushing energies. Solaimurugan et al. [141-142] studied the effect of stitching, fibres orientation and stacking sequence on G_{IC}, SEA, and progressively crushing of glass/polyester composite cylindrical shells under axial compression. It was concluded that placing axial fibres close to outer surface tube cause formation of more petals and a stable crushing process, whereas placing axial fibres close to inner surface tube led to higher energy absorption. Moreover, circumferential delamination increases energy absorption for higher values of Mode-I fracture toughness. Also reported stitching causes higher energy absorption of cylindrical tube due to increase in Mode-I interlaminar fracture toughness.

Ghasemnejad et al. [143] studied the energy absorption of GFRP composite box affected by Mode-I interlaminar fracture toughness. It was concluded that during progressive collapse, a significant amount of energy absorption is attained by frond bending following the growth of a main central intra-wall crack due to delamination in the side-wall. The main central intra-wall cracks are Mode-I interlaminar crack propagation. Also concluded that engineering the laminate design for composite box improves energy absorption capability due to improving interlaminar fracture toughness. For different lay-ups the variation of specific energy absorption (SEA) with interlaminar fracture toughness is non-linear.

Hadavinia and Ghasemnejad [57] investigated the energy absorption of laminated CFRP composite box by the effect of Mode-I and Mode-II interlaminar fracture toughness. In combination of lamina bending/brittle fracture crushing mode according to their results, crack propagation development in Mode-I and

Mode-II causes higher crushing energy absorption relative to combination of local buckling/transverse shearing crushing mode that consists of only Mode-II interlaminar crack propagation. Ghasemnejad and Hadavinia [143] studied the off-axis crashworthy behaviour of woven GFRP composite box structures. They concluded that two fracture mechanisms of bundle fracture and crack propagation delamination in Mode-II for all composite boxes at various off-axis loading was observed. In Mixed-Mode I/II due to crack propagation and more resistance and friction at side of composite box that initially contacted the crushing platen, at off-axis loading of 10° the amount of SEA was maximum compared to other off-axis crushing load. Ghasemnejad et al. [56] have conducted more detailed study of hybrid composite box structures (carbon/glass epoxy) crashworthy behaviour affected by delamination failure. It was concluded that the hybrid laminate designs have higher fracture toughness in Mode-I and Mode-II. Hybrid composite box structure have shown a great increase in energy absorption capabilities in crushing process. Most recently, author [144] studied the effects of delamination failure of stitched composite box structures, where the specimen's crashworthy behaviour and performances were compared and studied against simple non-stitched specimens, under the same geometry and condition. A combination of unidirectional CFRP and GFRP composite materials with lay up of $[C_{90}/G_0]_7$ were used to laminate the composite boxes. The laminate design obtained the highest energy absorption capability within the previous study of authors. Delamination study in Mode-I was carried out using the same lay-up to study the effect of crack growth of delamination on energy absorption of natural stitched composite box structures. Using double cantilever beam (DCB) standard test for delamination studies. It was concluded stitching significantly increased interlaminar fracture toughness and consequently energy absorbing capability of composite materials and structures (see Figure 2-14).

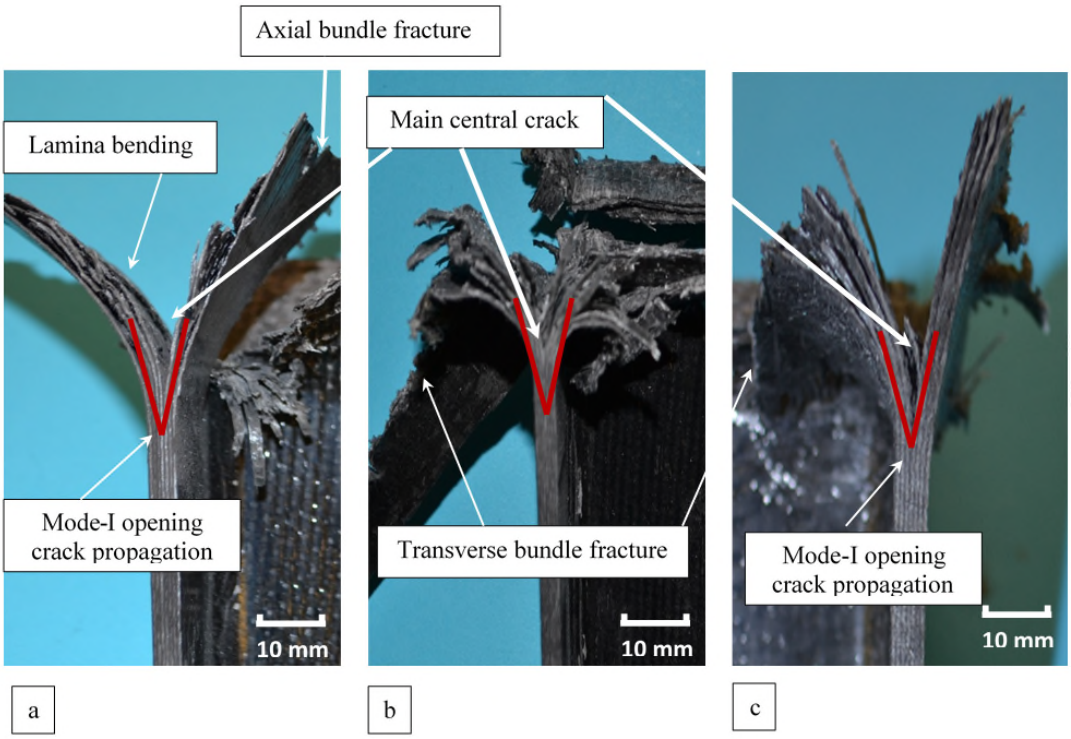

Figure 2-14 Mode-I interlaminar crack propagation at the central intra-wall, a) lamina bending crushing mode for non-stitched, brittle fracture mode for b) stitched-10mm and c) stitched-20mm composite crush box [144].

The structural integrity of stitched-composite absorbers depends on the stitching pattern used [146]. This through the thickness reinforcement has shown enormous improvement in Mode-I delamination resistance whilst stabilising Mode-II crack growth using continuous fibre [147,148, 212]. A similar conclusion was obtained by Solaimurugan and Velmurugan [142,149], that studied composite cylindrical shells with various stacking sequence, fibre orientation and stitching on progressive crushing of glass/polyester under axial compression. It has been noted that stitching improves energy absorption capabilities through Mode-I interlaminar fracture toughness. Allocation of axial fibre in outer surface results into stable crushing due to development of more petals, whereas axial fibres allocated in inner surface caused higher energy absorption. Circumferential delamination improves energy absorption capabilities by increasing Mode-I fracture toughness. Cauchi-Savona et al. [148] investigated the influence of

stitching through the thickness on fracture toughness using carbon and glass NCFs laminates under dynamic loading and noted that selecting an optimised stitched configuration causes 30% improvement in the energy absorption. Similarly, Korkiakoski et al. [150] performed an experimental study on the stitched NCF GFRP box structure and concluded that stitching affects damage progression and fatigue life. Zhao et al. [151] noted that, the significance of increase in interlaminar fracture toughness and energy absorption capabilities in thin-walled structures was obtained from the results by using stitching through the thickness. McGregor et al. conducted an experiment on the influence of increased plies on dynamic SEA testing which showed 39-53% increase using triaxially braided tubes of rectangular, circular and square cross-sections under both static and dynamic loadings [210]. Similarly, Wang et al. studied the effect of fibre orientations and wall-thickness on energy absorption capabilities using G827/5224 composite tubes under static and dynamic loadings. It was concluded that the fibre orientation and wall thickness have significant influence on energy absorption performance due to formation of thick delamination bundles and high bending resistance [128,211].

2.9 Finite element modelling of composite tubular structures

Two classes of Finite Element methods are available; either the Implicit or Explicit method [152]. Implicit method is widely available and used in a broad range of solving problems, including nonlinear stress analysis and static. The Explicit method is widely used in highly non-linear stress analysis and dynamic with contact dominated problems. Car crash for instance or metal stamping simulations are applications well suited for Explicit method.

Due to high cost of conducting experimental studies, there is a need for reliable computational models capable of predicting the crushing response of composite structures. There have been various attempts to develop explicit finite element models (FEM), with different degrees of precision, for circular tubes [153-157], square tubes [155-164], angle-stiffeners [159], C-channels [159] and hat-stiffeners [165]. The classification of structural FEM can be divided into two groups. The first group is the micro-mechanical one [166–171]. In this group the

finite element models try to simulate the composite crushing phenomenon through a detailed modelling of its micromechanical behaviour. A very fine solid mesh is developed to accurately capture the micro-mechanics matrix crack propagation phenomenon. The computational effort demanded by this kind of model is very high, making it impractical for engineering crash analysis. This approach is used mainly to perform simulations concerning the delamination phenomenon, in which the growth behaviour of a single crack is studied in a very detailed way [158]. The second group is the macro-mechanical one [154, 172-179, 184]. This type of model provide a macro-mechanical description of the material collapse. It is much more computational effective, and consequently it is a suitable choice for engineering crash analysis. However, it is not able to model precisely all the main collapse modes that occur simultaneously during a crush event.

The FE modelling of composite structures can be either shell or solid elements. Solid element models require more computation time and are less-widely used compared with shell elements in axial crushing of composite structures as mentioned above. A single layer [168,172,173,175] or multiple layers [154,176,184] of shell elements can be used to model a laminate, in the single-layer model, this can be modelled as a single layer of shell elements with each ply being represented by a through the thickness integration point also referred to as integration point in the thickness direction. This kind of model is not able to model the interlaminar collapse modes showed by composites under crushing in an accurate way. However, it is useful, if detailed representation of the failure physics is not the main concentration but only load and energy level predictions are required. The main advantages are its simplicity and computational effectiveness, so for that point they are highly suitable for practical engineering crash analysis. On the other hand, they have a notable lower robustness due to large amount of parameter calibration required to obtain acceptable global results, for a given test configuration [158].

Deleo, et al. [159] used this configuration for C-channel, angle-stiffeners and hollow square tube modelling technique. In multi-layer configuration model, the

laminate is modelled by multiple shell elements, with each layer representing either a single ply or a group of plies, and the layers are glued together using an automatic contact definition (Surface to Surface).

In recent studies, the single-layer configuration model has been used to simulate the behaviour of various composite structures, in the case of for instance thin-walled square sections. This method is capable of accurately capturing the local buckling and unstable collapse, however due to the complex failure mechanism of composite structures, this method was ineffective to depict the progressive failure process [155]. Precise input of key material properties and numerical parameters in the material model (e.g., eleven parameters in MAT 54), and defining a contact card between the test specimen and the impactor and applying an all degrees of freedom constraint on the end of the test specimen, the single-layer model was able to yield good correlation with experimental load-displacement graph for cross-sections studied in [159]. However, this configuration as mentioned above is not appropriate for failure mechanisms and crushing behaviour, as these are mostly neglected.

The multi-layer modelling technique can be utilised for better capturing of failure process of the tubes undergoing progressive crushing [154-158]. However, in multi-layer model, the correlation with the experimental load-displacement was not always satisfactory. The composite hollow tube was modelled in LS-DYNA using MAT 54 to analysis its crushing behaviour. The FEA results were satisfactory and agreed with the experimental load-displacement graphs, however, instead of brittle failure mechanism observed in experimental, a significant local buckling of the tube was observed in FEA.

A finite element model developed by [155], was able to accurately predict the peak load of thin-walled square CFRP tube, although the specific energy absorption was underestimated by 33%. In the FEA simulation the crushed elements were deleted instead of forming debris that were observed in the experiment. One of the parameters that contributed to the energy absorption, was the debris wedged formation between the fronds of the tube’s wall which was neglected in the simulation. The author noted that, this parameter alone affected

the SEA value in a significant way. In [156,157] the FEM was developed to capture the crushing behaviour of hollow circular and square tubes and compared with the experimental observations. It was noted by the authors that the model was not able to reproduce the axial matrix splits observed experimentally. This resulted into different load–displacement curves, deformation, and failure behaviour when compared with the experiment. Several parameters that influenced the crushing behaviour of square hollow tubes were analysed in [158]. The parameters were, element size, number of shell layers, coefficient of friction and interlaminar material properties. The author noted that by increasing the number of shells the main collapse mode was unchanged. The influence of the friction coefficient between the tube and the machine plate and the element dimension was also studied. The element size was coarse mesh (7 mm) and fine mesh (4 mm). The static friction coefficient values were 0.1, 0.2 and 0.3 and dynamic friction coefficient was kept constant at 0.65, base on literature. The increase of the friction coefficient from 0.1 to 0.3 and the use of finer mesh did not change significantly the crush zone morphology, in the sense that all the three tubes collapsed in the same way. For all the three values of friction the load-displacement curves have almost the same shape. In this sense, the effect of the friction variation was like a scaling of the magnitude of the load curves. The model with bigger elements shows a magnitude of force oscillation higher than the one showed by refined model, however the average force value is the same.

McGregor, et al. [161] combined series of experimental investigations and examined their effect in finite element analysis and concluded proportional failure mechanisms leading to SEA is a result of dominated energy absorption mechanisms of approximately 60% material damage and 30% friction with 10% related to contact parameter [180]. Although a detailed examination on the material behaviour is essential to reach a load adapted lightweight design. Axial finite element modelling of composite structures has different modelling methods. Various approaches were developed to obtain ideal force/displacement curve that are aligned with experimental data. One approach includes a hybrid mesh of shell and solid elements to capture ideal load/displacement curves [181]. This method is used for modelling of crack propagation with finite cohesion elements

[184] that consists of shell element representing the material and a solid element to represent delamination failure. Alternatively, material 54 of LS-DYNA is used to predict crushing behaviour and idealised force-displacement graph [182]. One strategy is SOFT parameter implemented in LS-DYNA to map pre-damaged and consequently create a progressive crash front of a CFRP square tubes or composite sections [143], the author concluded that Mat_Composite_Damage of LS-DYNA for GFRP box structures was found to be in accordance to experimental results when it was modelled as double shell configuration. Some similar conclusions were obtained by other researchers that using multi-shell configuration can predict energy absorption and maximum force under crushing [183,184]. Many studies focused on the contact parameter [180], crack propagation modelling with de-cohesion elements [185] or user defined material model which requires extensive experimental investigations [186].

In [187-188], the effect of failure trigger mechanisms on the energy absorption capability of CFRP tubes under axial compression is experimentally and numerically investigated. The conventional approach to introduce a failure mechanism is to apply a 45^{o} chamfer on one end and the failure could initiate progressively. Alternatively, an attachment of crush-cap can be utilised to initiate the progressive crushing. Two different types of crush-caps were studied, each causing the crushed material to fold either inward or splay outward. The effect of the corner radius of the crush-caps on the peak load, SEA, and crush behaviour was investigated. The author noted that the chamfer failure trigger was most effective at reducing the initial peak load while maintaining a high-sustained crush load and high specific energy absorption (SEA). The inward-folding failure trigger approach was not as effective at reducing the initial peak load but was more effective than using a chamfer for maintaining a high-sustained crush load and SEA. However, the modelling technique of the simulation, which was based on multi-shell configuration with failure trigger showed a high level of correlation with the experimental results for both the chamfer and combined failure trigger cases. The simulation was able to predict key deformation characteristics observed during the experimental crushing process the formation and progression of matrix splits, and the direction of splaying of plies.

In modelling approach, it is necessary to develop models that are simple enough to be employed in practical analysis situations but at the same time capable to provide results with a suitable level of accuracy. At the same time, the approach shall be numerically robust and practical in model build phase.

The primary focus of this study is to develop a 'multi-layer' finite element modelling methodology that can capture the crushing behaviour of CFRP and GFRP circular tubes with a failure trigger mechanism. The finite element modelling further investigates the effect of stitching pattern developed in chapter 4 and implementing that into FEM.

2.10 Summary of the literature review

Composite material is providing opportunities to reduce component weight and improve crashworthiness of aerospace and automotive structures and sub-structures and components. The parameters that influence energy absorption capability are, loading conditions, geometry shape and size, lay-up sequence, triggering mechanism, curing techniques.

Structural geometry of composite materials influences the energy absorption capability, the cylindrical shape is suitable for higher energy absorption due to no corners nor stress concentration. The geometry size of the composite sections should be from 50-150 mm in length and 20-100 mm in outside diameter with wall thickness of 1-3 mm [238]. The lay-up sequence is another factor that influence energy absorption capability. Quasi-isotropic laminate design provides closer to isotropic material behaviour in in-plane conditions. A typical quasi-isotropic laminate design includes 0/$\pm$45/90 and in some cases 0/$\pm$60. The loading conditions at quasi-static, should be around 1 to 11 mm/s and in dynamic impact an impactor is used with impact velocity of less than 100 m/s is suggested. The curing techniques should be based on manufacturer's guidelines. To obtain progressive crushing behaviour trigger mechanism is applied to one end of the composite section, 45^{o} bevelled trigger or 45^{o} chamfer trigger provide better crushing initiation.

Starting from interlaminar fracture toughness, delamination is considered as crack propagation and after delamination onset, the consequent propagation is not controlled by the through-thickness strength any more but the interlaminar fracture toughness. To improve crack propagation in laminates, the fracture toughness needs to be improved and consequently the energy absorption capability is improved, hence the objective of this research. However, friction and bending mostly contribute towards specific energy absorption capability, higher the delamination resistance, higher the friction and bending and consequently improving SEA.

In the current study of fracture toughness and energy absorption capability of stitched composite crash absorbers, the missing link is the effect of through-thickness stitching on specific energy absorption in respect to stitching location. This has been studied in the past, in singular format, 10 mm, 20 mm and 30 mm using natural flax yarns [145,147] and its effect on energy absorption. Although crack propagation resistance in most cases did not improve and a significant load drop was observed, which resulted in a lower energy absorption capability than non-stitched composite sections. However, the effect of multi-stitching and pattern stitching on UD pre-pregs have not being investigated in respect to adoption of stitching locations. The effect of single, multi and pattern stitching as one study to establish its effect on SEA is missing from the current field. This missing study led to conflict ideas around the subject of stitching through the thickness with negative perspective. Identifying the capability of though-thickness stitching can be beneficial towards better performing composites. Two decades ago, Boeing studied the subject of through-thickness stitching with sceptical approach and conclusions [191], the work was carried out on reinforcement of composite wings at the time. Many researches work on tensile and compression properties of laminated composites and the results vary. Some researchers suggest tensile strength improved by stitching and this conflicts with other studies. The main cause of this might be that, there is more than one variable for the study, such as constant resin and thickness, hence pre-pregs are more suitable for the sake of this study although higher fibre damage might be caused by insertion of the needle to penetrate the laminate, but this minimises the

variables to one, which creates an opportunity to concentrate on the effect of stitching on energy absorption capability. One of the main advantages of the composite material is that it can be tailored for a specific task and purpose. Through-thickness stitching is beneficial in energy absorption capability if a correct study can establish its benefits. Hence, the main aim of this study is to establish a relationship of stitching location with specific energy absorption capability and to control the force-displacement curve.

To concentrate on one parameter at a time, and to identify the effect of through thickness stitching on energy absorption, only one variable should be considered per case. In off axis loading condition, the only variable is the lateral inclination angle and all other parameters mentioned in chapter 2 that could potentially alter or influence energy absorption capability is kept constant. In stitched composite section the only variable is the stitching location or in final pattern stitched sections the only variable is the loading conditions, quasi-static and impact loading.

To determine crashworthiness of the material, the specific energy absorption is considered. This value evaluates the crushed mass of the specimen with the energy it absorbed. This leads to identifying the ability of the material with its load bearing capabilities, which leads to determination of any improvements made to the composite sections whilst being at different loading conditions or being subjected to through-thickness stitching.

Accurate prediction of deformed fibre architecture of the final component is vital in respect to energy absorption capability if a virtual design process is used to optimise composite components, that is considered a necessary process if the time taken for the design and costs are to be industrially acceptable. The current study consists of multi-shell configuration, and delamination modelling to capture an accurate enough model to predict energy absorption capability.

In many studies this is eliminated and replaced by friction between each shell acting as the delamination between the plies [143]. Although different contact definitions can be used to predict the delamination effect. Most cases reviewed in this study captured an acceptable load-displacement curve, which is the main

concentration of this study. However, to minimise modelling costs and experimental costs, a model should be developed to capture an acceptable load-displacement curve, energy absorption capability and SEA. There are currently no stitching techniques available in pre-pregs material, many studies concentrated on non-crimp fabric style materials and developed separate tow and stitch providing a simple method representing true fabric architecture and deformation mechanism. However, it is now becoming reasonable to consider modelling the crushing behaviour of stitched structures using contact definition techniques within acceptable timescale, therefore, this is the primary FE modelling aim of this project.

3 Experimental Studies of Axial and Off axis Loading under Quasi-Static Loading

3.1 Introduction

This chapter presents experimental investigation on the laminate tailoring of composite tubular structures to improve crashworthiness performance at off-axis loading. Various angles of 5^o, 10^o, 20^o and 30^o degrees were selected for the study of off-axis loading. The results indicate that by increasing the lateral inclination angle the mean crushing force and consequently energy absorption capability of all tested sections decreased. From design perspective it is necessary to investigate the parameters effecting this phenomenon. The effect of lay-up sequence and trigger mechanism of composite sections under quasi-static loading were investigated with an objective to improve mean crush force in 10^o off-axis loading. Five cases were studied with combinations of ply-orientation and flat trimming with 45^o chamfer. This method was applied at 10^o off-axis loading and the results showed significant improvement in energy absorption capability of composite sections.

Following the current state-of-the-art, it can be concluded that in the case of off-axis loading conditions, the mechanical response varies with change of geometry. However, none of the reviewed articles studied the case of introducing tailoring of lay-up sequence and trigger mechanism to improve energy absorption capabilities. Assessing the crashworthiness of composite tubes subjected to off-axis loading is of particular interest in the aerospace industry because, in addition to the absorbers allocated axially there are off-axis positioned absorbers that can be improved for their energy absorption capabilities. In this chapter, glass/epoxy tubes were tested under quasi-static compression tests for their crushing behaviour. Five cases were also studied with combination of ply-orientation and flat trimming 45^o chamfer integration mechanisms to evaluate their effect on energy absorption capabilities. This improves mean crushing force and consequently increase specific energy absorption (SEA).

3.2 Experimental method

3.2.1 Specimen fabrication and material

In this study, the composite sections were fabricated from glass/epoxy 7781/E722 (ρ = 2250 kg/m^3) with a symmetric twelve-ply laminate design of [-45/45/0/90/0/90]$_S$ using hand lay-up techniques. Each GFRP layer has a thickness of 0.25 mm after curing. The composite sections were 80 mm × 80 mm with the total wall thickness of 3 mm in size (see Figure 3-1). Four to six specimens were tested in each case of study to find the mean deviation of the experimental results. In this research, the main study is oriented around identifying the effect of off-axis loading and ways to improve crashworthiness at off-axis loading. Therefore, one of the lateral inclined angle was chosen which is at 10^o to carryout further study. This off-axis angle was chosen because when applying flat trimming, the remaining length of the specimen at off axis angles of 20^o and 30^o will only be 40 mm and 30 mm, which is not enough for 50 mm crushing distance. Therefore, 10^o off-axis was chosen to study the parameters affecting energy absorption capability at off-axis loading.

At simplified off-axis loading configuration compared with axial loading, two major differences can be identified, lay-up sequence and engagement of the cross-sectional area of the specimen with the crushing plate. Therefore, the stacking sequence was adopted and the top end of the specimen was flattened to study their crashworthiness and crushing behaviour under quasi-static loading compared with axial crushing behaviour. The tailored stacking sequence of [-55/35/-10/80/-10/80]$_S$ was adopted and used to cancel the 10^o off axis effect.

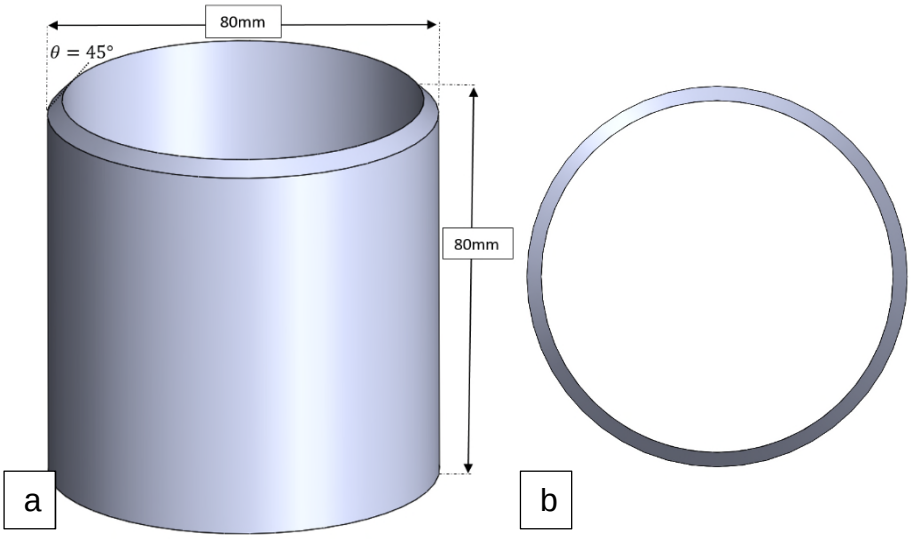

Figure 3-1 composite crush tube specimen

The steel mould base with a dimension of 74 mm outer diameter and 80 mm in height was used to facilitate easy attachment of the first layer, although to simulate a lubricant between the laminate and the mould, a thin polymer film was used (see Figure 3-2). This enabled better shaping of the first ply to the mould and ease of removal after curing. Each ply was stacked according to the lay-up sequence one at a time. Pre-pregs have two protective layers covering each ply, one side is glassy and white, and the other side depending on the material, GFRP or CFRP for instance, is a thin plastic easy peel either green or blue. The glassy white layer is removed and placed slowly onto the rigid steel mould covered with a non-stick polymer film. Using a roller to shape the ply evenly and to minimise any formation of air-pockets. At each stage of adding plies or stacking the plies, a 15 minute of debulcking is required. Placing the rigid steel mould into a vacuum bag connected to a composite vacuum pump to pressurise the ply onto the mould, this is known as debulcking or degassing. This minimises air bubbles/pockets formation between each ply and this increases the laminate bonding. Then, the next ply is stacked, once the thin-plastic of the first layer is removed, this layer is kept minimising any contamination whilst being rolled, degassed and kept at cleanroom. Once all the plies are stacked, it goes through a debulcking of 30 minutes under vacuum pressure. Then seal-wrapped onto the mould to minimise any available air gaps using a thin polymer film, because during the curing process a phenomenon takes place that effects the material property, this is

known as ‘resin escape’. This weakens the final product and ideally must be eliminated. Sealing the uncured laminate enables minimal room for the pre-preg epoxy to escape to, thus increasing the resin intact within the structure.

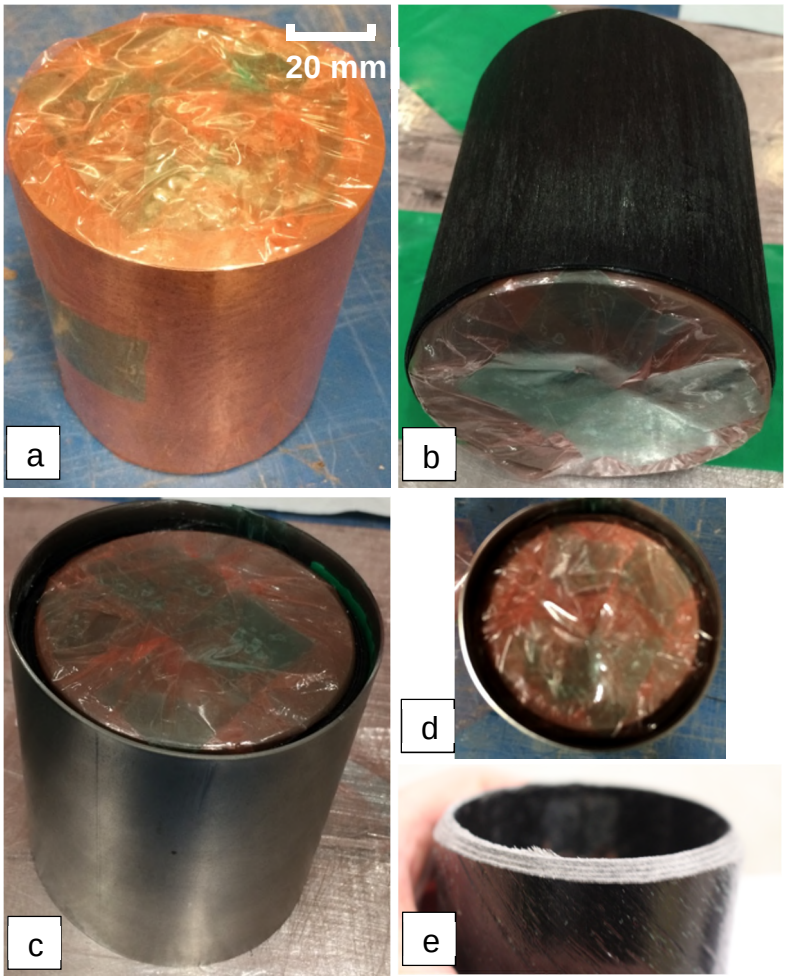

Figure 3-2 lay-up of composite crush tube and preparing for curing a) mould sealed with thin-polymer film, b) lay-up process, c) mould sleeve d) mould and laminate being fully sealed by polymer film and pressurised with the mould sleeve e) 45º chamfering (trigger).

To increase the pressure acting on the uncured laminate during the curing process for better bonding and elimination of delamination, a mould sleeve with the same outer diameter as the laminate is utilised which is 80 mm in inner diameter, and to keeping a constant laminate thickness of 3 mm. This also improves laminate surface finish. The assembled moulds containing the sealed laminates was then placed on a thick aluminium plate, covered top to bottom with

two sheets of ‘breather cloth’ which eliminates air pockets formation by allowing air circulation and placed inside of a heat resistant polymer bag (see Figure 3-3). A suction valve was inserted into the bag connected to a vacuum pump. The bag was open on either sides and was fully sealed with double-sided epoxy tape. Vacuuming applies more pressure onto the laminates and extracts the air inside of the bag, forcing the plies to cure in high pressure tightly together (see Figure 3-4). Using a pressure gauge, the pressure inside the bag was monitored. The effect of pressuring the mould using vacuum is forcing the plies of prepreg to merge together, allowing good adhesion evenly and minimises trapped air that could may cause delamination. The curing and post-curing process was based on manufacture’s guidelines. At each curing session two moulds were being processed in the same bag.

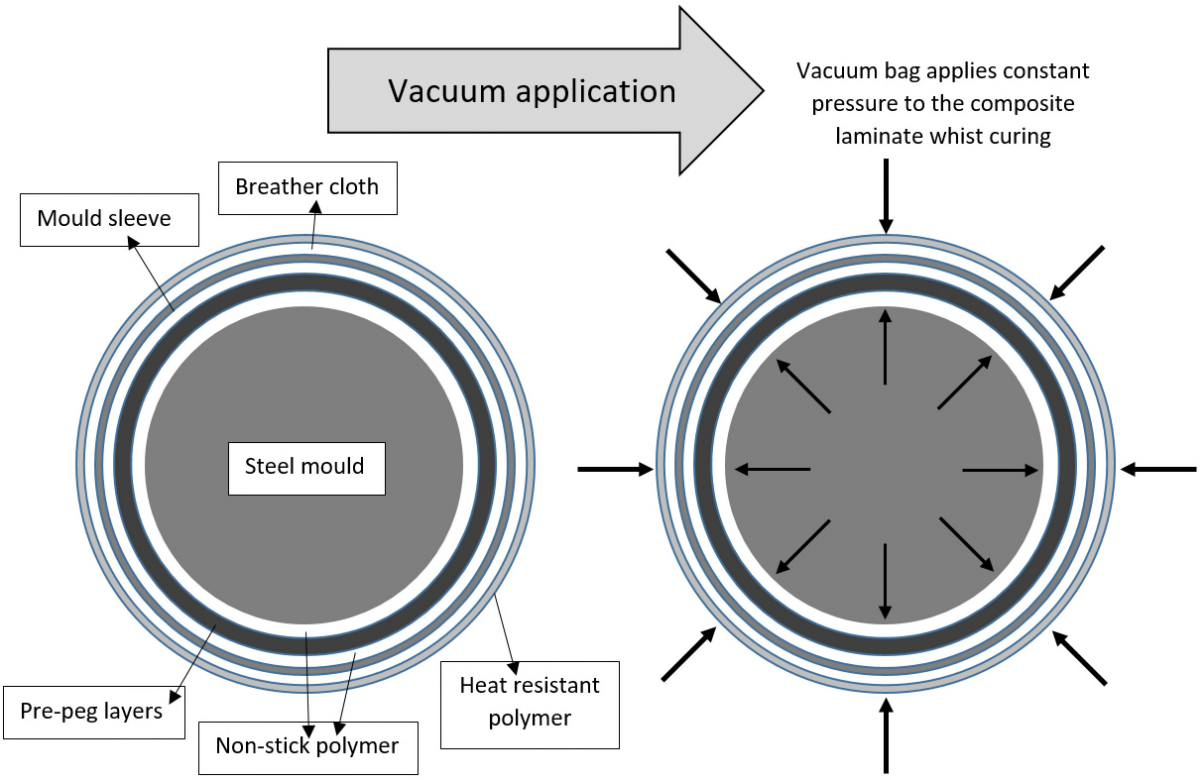

Figure 3-3 schematic of vacuum application

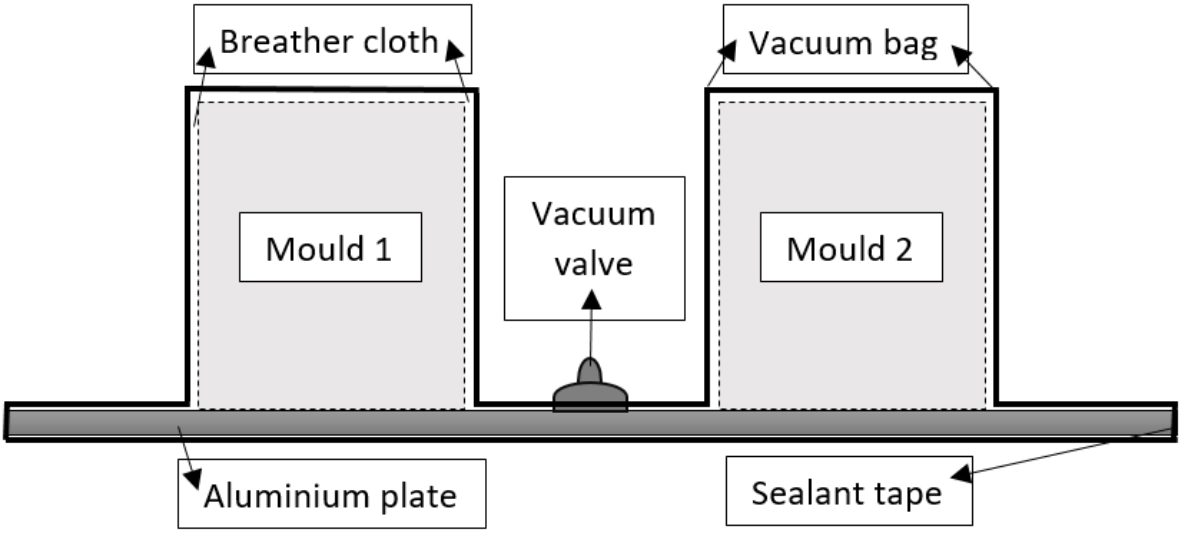

Figure 3-4 sectioned composite crush tube inside the heat resistant polymer for curing.

After curing, the composite tubes were removed from the mould and were subjected to post-curing. Then a trigger mechanism at one end of the tubes were applied to initiate the progressive crushing. A 45^{o} chamfer was applied onto the tube using a lathe machine acting as the trigger. The other end was flattened to remove the excessive pre-preg resin formation.

The main concentration of this research is the force/displacement curve to evaluate the energy absorption capability in each case. All parameters were kept constant in this research including geometry, strain rate, loading conditions and only the lay-up sequence and trigger mechanisms varied depending on the case of study to obtain its effect on the energy absorption capability.

3.2.2 Crashworthiness aspect of energy absorption

Energy absorption capability is determined from analysis of the following two.

1. Initial peak crush load: this can be obtained directly from the load-displacement curve.
2. Mean crush load: this is obtained by averaging the values in post-crush displacement region.

The force-displacement curve extracted from a quasi-static crushing test is the primary data and the main concentration of energy absorption capability. In Figure 3-5, a typical force-displacement curve is illustrated, where the three main stages are shown to analyse the curve. The first stage is pre-crushing region, this shows the initiation of the material failure response. The second stage is the post-crushing region, this is the material behaviour after reaching a load peak followed by a large displacement. The failure in this region spreads across the entire specimen, which is characterised by the mean crushing load, which is the average crush load response of the material in this region. The third stage is the compaction region, in this region the load increases rapidly until the end of the test. From the force-displacement curve the crashworthy behaviour of the material is analysed. This is crucial when comparing different structures and composite materials regarding their load-carrying capacity and energy absorption capability.

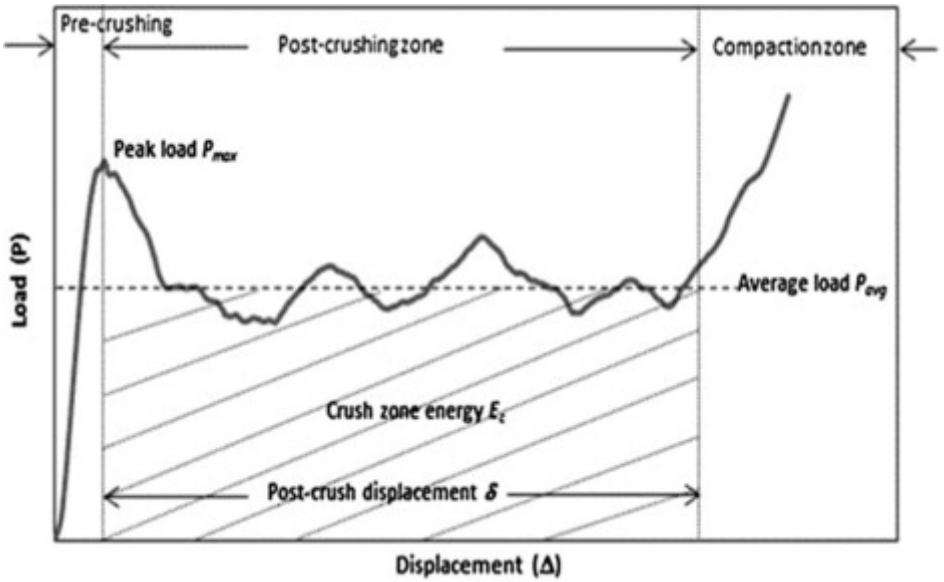

Figure 3-5 Typical force- displacement curve

The following parameters are critical when analysing crashworthiness characteristic of load-displacement curves.

- Peak load P_{max}, is the maximum initial load also expressed as F_{max}

- Crush zone energy E, is the absorbed energy determined by the area under the force-displacement curve, in the post-crushing zone (see Figure 3-5)
- Post crush displacement (δ), is the total crushing displacement excluding pre-crushing and compactionzone
- Displacement (Δ), is the total crushing displacement, including pre-crushing and compactionzone.
- Specific energy absorption (SEA), is the absorbed energy per unit mass of the crushed specimen.
- Crush force efficiency (CFE), is the ratio of the mean crushing load to peak load.
- Stroke efficiency (SE), is the post-crush displacement (δ), to the total specimen's length, L.
- Maximum compressive strength (δ_{max}), is the peak load to cross sectional area, A.

3.2.3 Calculation of Specific Energy Absorption

Specific energy absorption is one of the most important crashworthiness parameter. This parameter determines the energy absorption capability of each specimen regarding their crushed mass, meaning that the absorbed energy per unit of the crushed specimen mass. Referring to equation 2-1 and 2-2, as shown the SEA is a function of total work (W_T) that represents the energy absorption capability which is equal to the area under the load–displacement curve and crushed specimen mass. Total work done (equation 2-1) is a function of integration of mean crushing load multiplied by the stroke displacement. Specific Energy Absorption (SEA) is energy absorption capability, which is calculated as energy per unit crushed mass absorbed.

3.3 Experimental setup

A hydraulic press consists of a moving cross head which is mounted to two 500 kN screw jacks, and two large “I” beams attached to two large end blocks. The screw jacks are mounted on the bottom block and are driven by a double output, dual reduction worm gear powered with a 1492-watt AC motor. The cross head translates vertically with four precision profile rails which are mounted on the web of the vertical “I” beams.

The quasi-static testing was conducted using a hydraulic press with load cell capacity of 500 kN with crushing rate of 2 mm/second. All specimens were placed at the centre of the stroke for equal load distributions (see Figure 3-6). The stroke displacement for all specimens were kept the same at 50 mm. The profile of load-displacement consists of load cell and stroke displacement and were recorded automatically for each test.

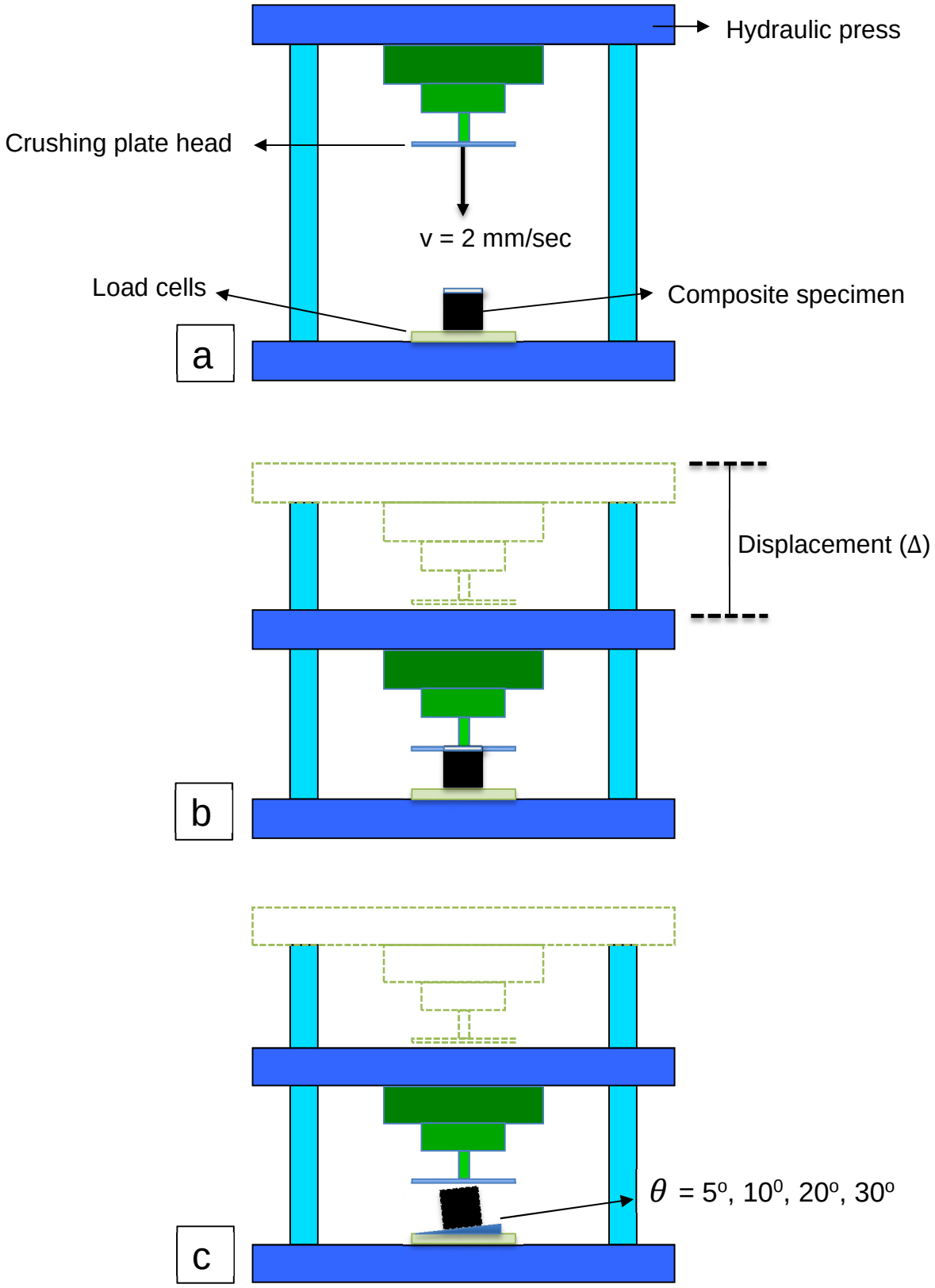

Figure 3-6 Axial and off-axis quasi-static setup

3.3.1 Clamped fixture

Boundary condition effects crushing performance of composite crush specimen and needs to be considered before initiating experimental investigation. Hong-Wei [12] and Ghafari-Namini [145] studied the influence of fixed conditions on the strength of the composite tubular structures. The authors noted that the position effect at the end-caps results into high stress concentration. This regional stress concentration at the end of the specimen may result into catastrophic failures as most catastrophic failures occur close to this region. Hence the boundary conditions in off-axis crushing must be considered. To securely place the crush specimen in an angle that could sustain the load, a high-density clamp fixture was designed. Four steel wedged shaped bases were manufactured at different angles of 5^{o}, 10^{o}, 20^{o}, 30^{o}. These off-axis angles were selected based on literature [144,145, 237] to study the effect of lateral inclination angle on energy absorption capability of composite tubular structures. The chosen off-axis angles as Ghafari-Namini stated [145, 237] provides the study of the correlation between lateral inclination angle and energy absorption without studying every single angle, and the gap between the lateral angles can be observed and studied on the force displacement graph.

This clamp fixture provided a constant boundary condition and prevented the specimen from defeating. The outer diameter of these fixtures are 100 mm x 100 mm with various thicknesses depending on the angle of inclination. The inner dimensions were 80 mm by 80 mm (see Figure 3-7). To prevent the toppling of specimen during crushing, the clamped-set with dimensions 10 mm was welded at each side of the fixture. In Figure 3-7, the geometry of the fixtures are presented in part a, and followed by the 5, 10, 20 and 30 degrees in d, e, f and g.

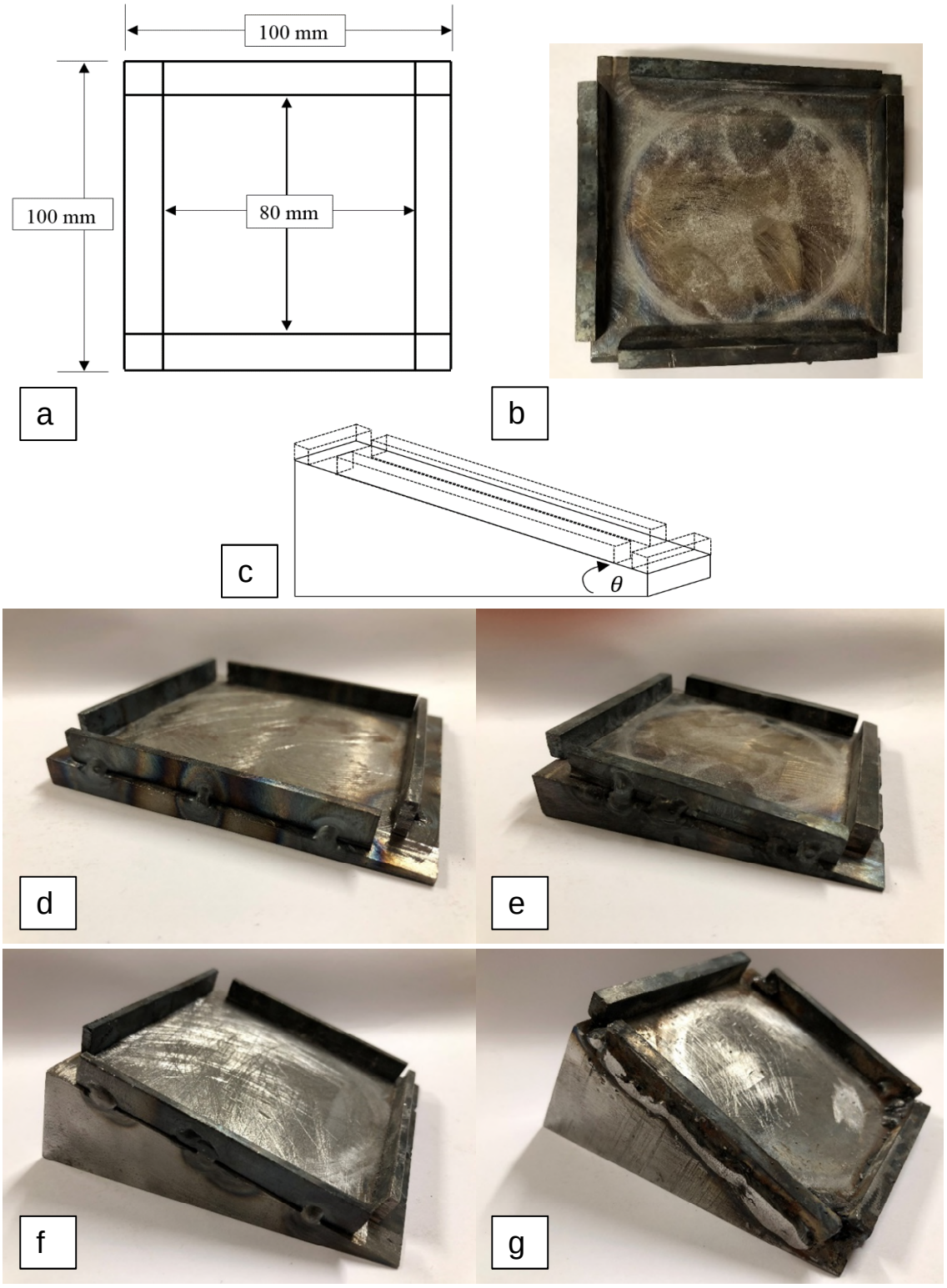

Figure 3-7 Wedge-shaped base for off-axis crushing. a) fixture geometry measurement, b) birds eye view of the fixtures, c) isometric view, d) 5 degrees, e) 10 degrees, f) 20 degrees, g) 30 degrees.

3.4 Progressive crushing process

Progressive crushing is dependent on triggering the specimen to initiate the crushing. Progressive failure is distinguished by an increase in load after the initial peak, and it is still capable of sustaining a significant compression load. In progressive crushing failure mode, high-energy absorption is obtained, which is thus the main goal of crashworthy structures, it is also important to analyse the associated failure mechanisms. Within the initial contact of the cross head with the specimen, local failure occurs and interlaminar cracks are formed. The length of these cracks along with lamina bundle fracture determines the failure modes taken place during crushing. These failure modes are transverse shearing and lamina bending or a combination of the two. Progressive crushing is categorised with fragmentation mode, lamina bending mode and a combination of fragmentation mode and lamina bending mode referred to as brittle fracture mode [130].

1. Fragmentation mode: is characterised by a wedge-shape laminate cross-section with one or multiple short interlaminar and longitudinal cracks.
2. Lamina bending mode: is characterised by a long interlaminar and cracks in parallel to the fibre, causing continuous in and out fronds formation.
3. Brittle fracture mode: is characterised by a combination of fragmentation mode and lamina bending mode. In composite tubes the highest energy absorption ever observed is from the combination of brittle fracture crushing mode.

3.5 Results and discussion

3.5.1 Crushing behaviour of composite sections under axial and off-axis loading

In this section, the effect of lateral inclination angle is experimentally investigated. Various angles of 5°, 10°, 20° and 30° were selected for off-axis loading. Four to six specimens were tested in each case of study, in Figure 3-8, five cases were axially tested under quasi-static loading and the mean deviation of the result is plotted. The various crushing stages is shown in Figure 3-9. The results indicated that as the lateral incline angle increases the mean crush force and energy absorption decreases (see Figure 3-12). Axial loading compared with off-axis loading has better energy absorption capability with mean crush force of 100 kN. The experimental morphologies and intra-walls (see Figure 3-10 and 3-11 respectively) of axial and off-axis angle 5^{o} illustrated bundle fracture and close to brittle failure mechanism which is a combination of lamina bending and transverse shearing modes. Off-axis angle 10^{o} showed transverse shearing mode characterised by wedge-shaped laminate cross section with multiple short interlaminar fractures and axial cracks. Off-axis angles of 20^{o} and 30^{o} showed catastrophic failure mechanism with unsymmetrical damaged area. This change results into minimising the energy absorption capability of the absorber.

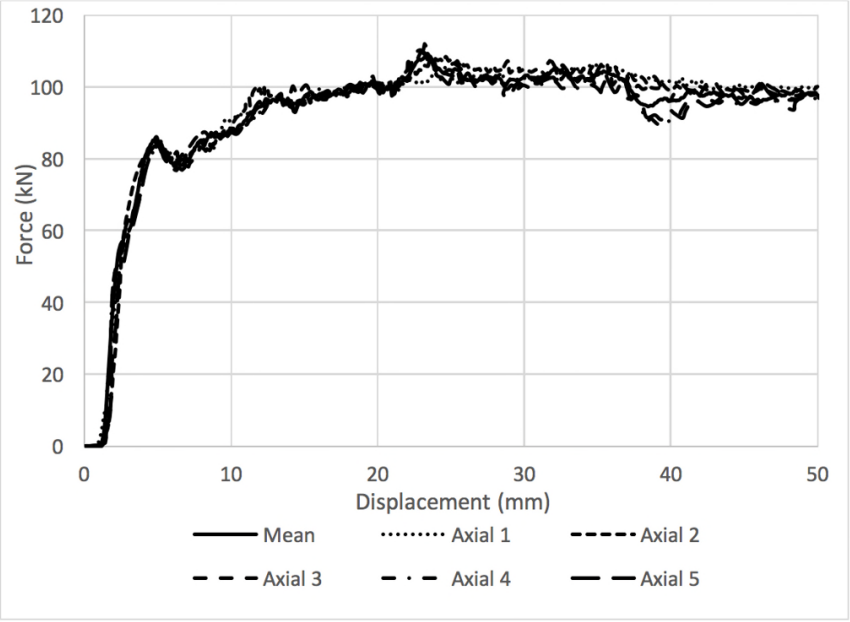

Figure 3-8 Five axial repeat tests with mean deviation

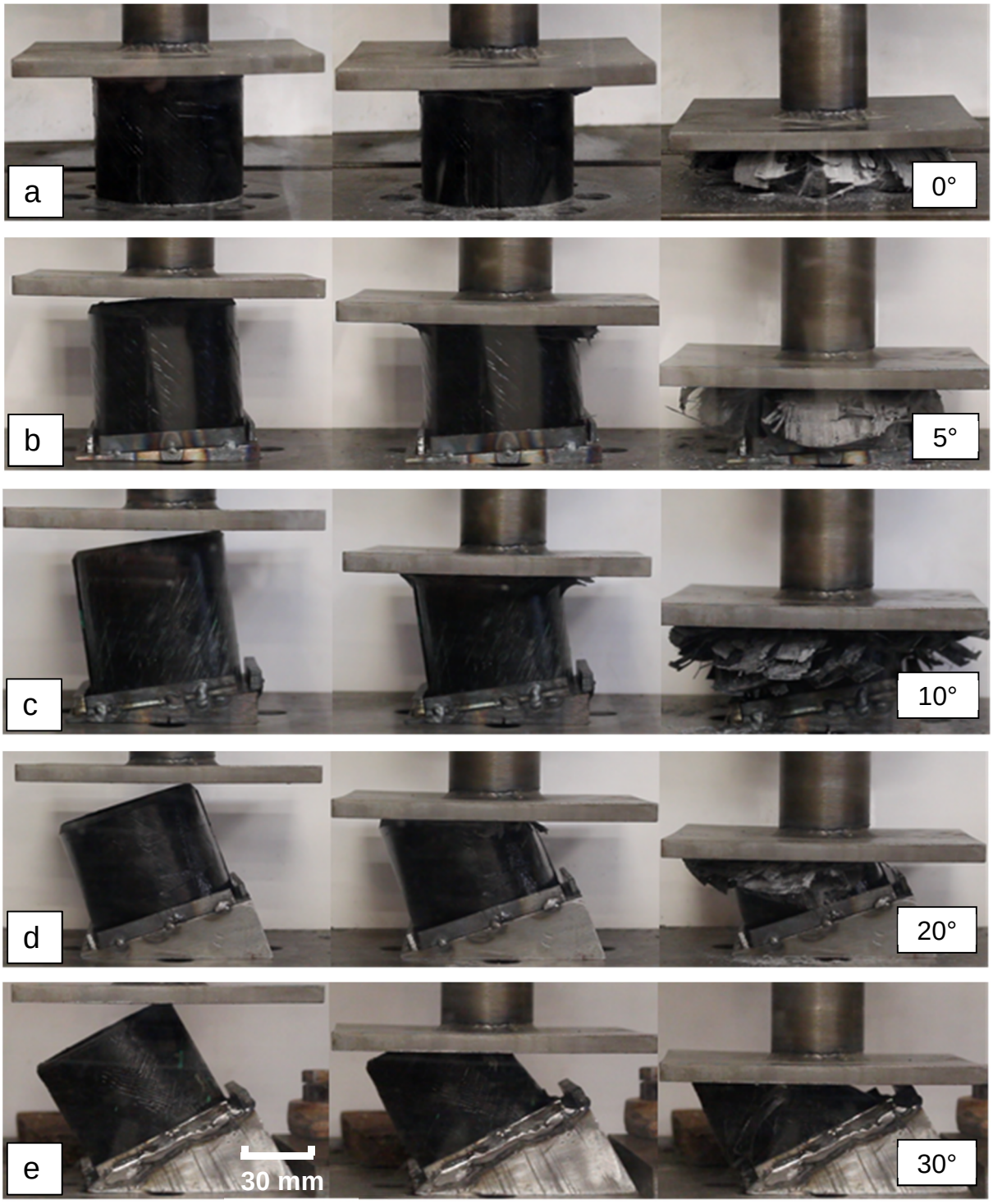

Figure 3-9 Various stages of high speed crushing a) axial, b) 5°, c) 10°, d) 20° and e) 30°.

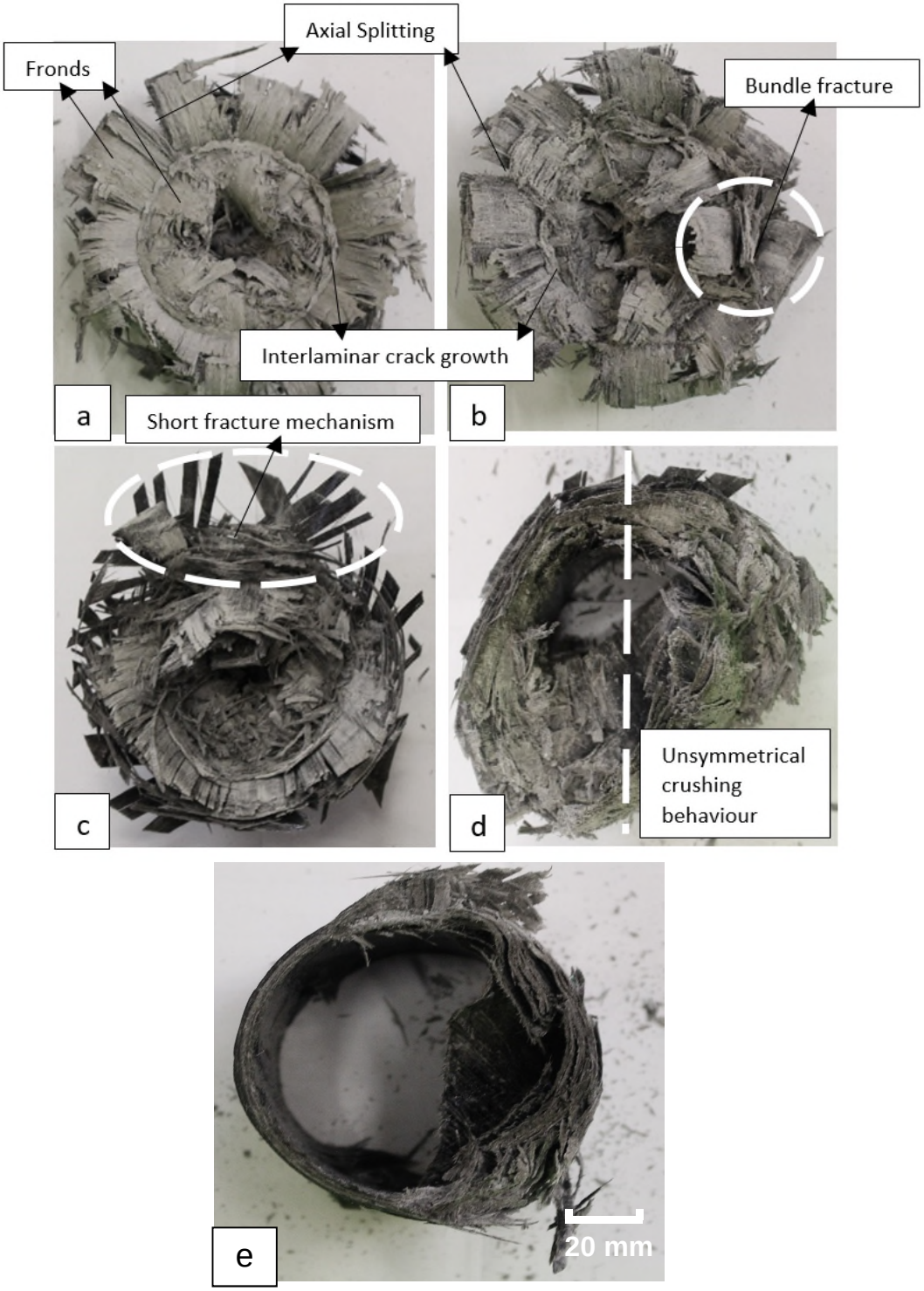

Figure 3-10 Plane view of crushed axial and off-axis specimens a) axial with brittle fracture crushing mode, b) 5° with brittle fracture mode c)10° with transverse shearing mode d) 20° with catastrophic failure e) 30° with catastrophic failure

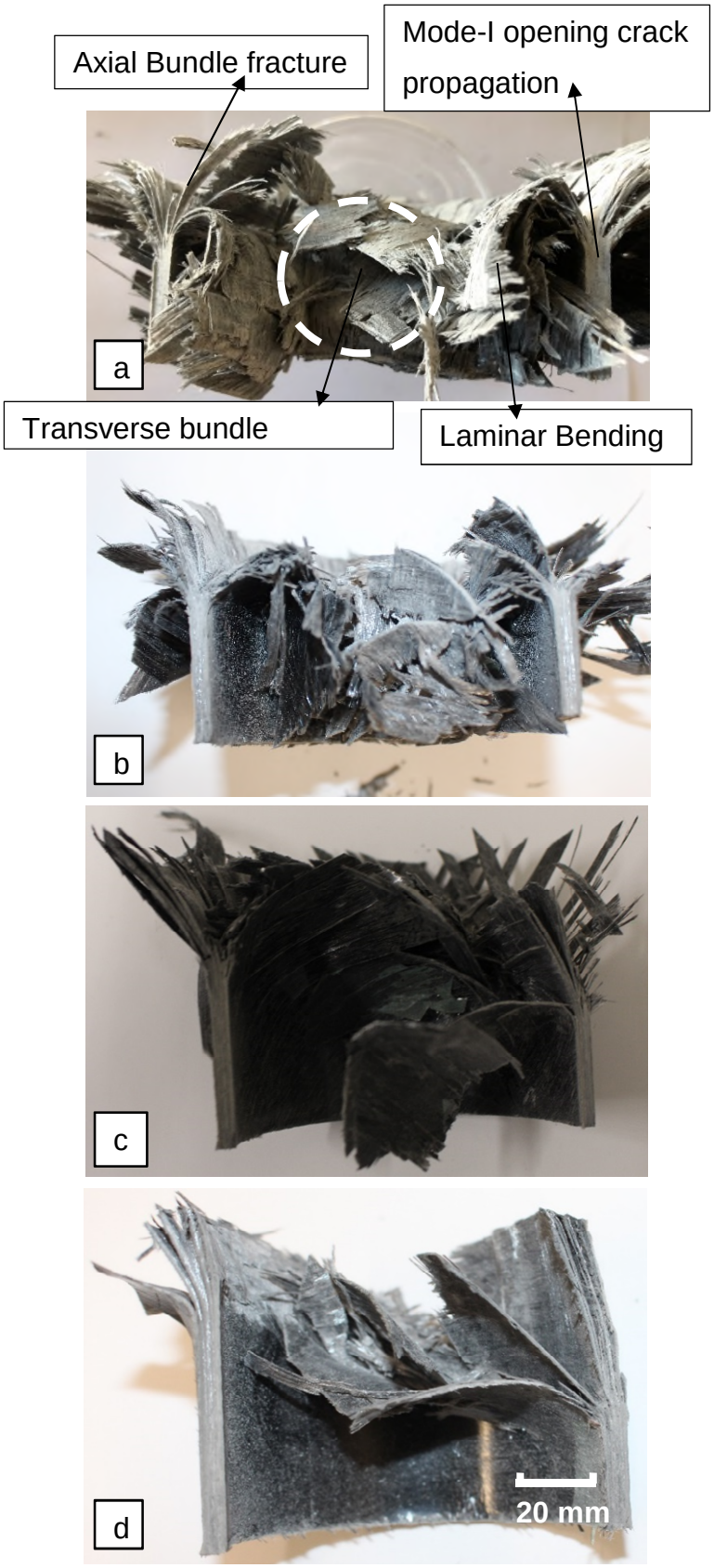

Figure 3-11 Crack Propagation at central intra-wall a) axial b) 5º c) 10º d) 20º

Mean Force:

Axial) 98 kN **5º)** 84 kN **10º)** 62 kN **20º)** 43 kN **30º)** 28 kN

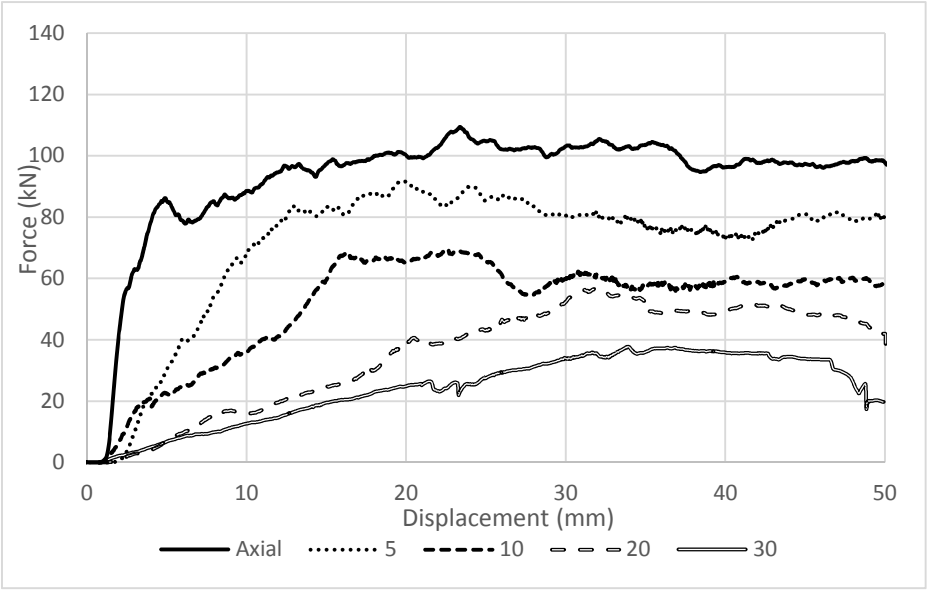

Figure 3-12 Force-displacement of axial and off-axis angles of 5°, 10°, 20° and 30°.

3.5.2 Axial crushing and improvement of off-axis loading

According to various positions of composite absorbers in aircraft and automotive structures, composite specimens were tested under axial and off-axis conditions at various off-axis angles. An off-axis study was carried out to increase energy absorption capabilities towards axial loading (see Figures 3-13 and 3-14). Case (a) is axial, case (b) is 10º off-axis, case (c) is 10º off-axis with flat 45º chamfer trimming and case (d) is like case (b) with integrated lay-up sequence. The original lay-up sequence (used in case a to c) was $[-45/45/0/90/0/90]_S$ which was changed to $[-55/35/-10/80/-10/80]_S$ to cancel the off-axis effect. This lay-up sequence creates a similar lay-up condition at axial in 10º off-axis. Case (e) is like case (c) with integrated lay-up sequence and also subjected to flat 45º chamfer trimming. Case (e) and (a) create a similar loading conditions with the difference of case (e) which is being considered as off-axis loading condition.

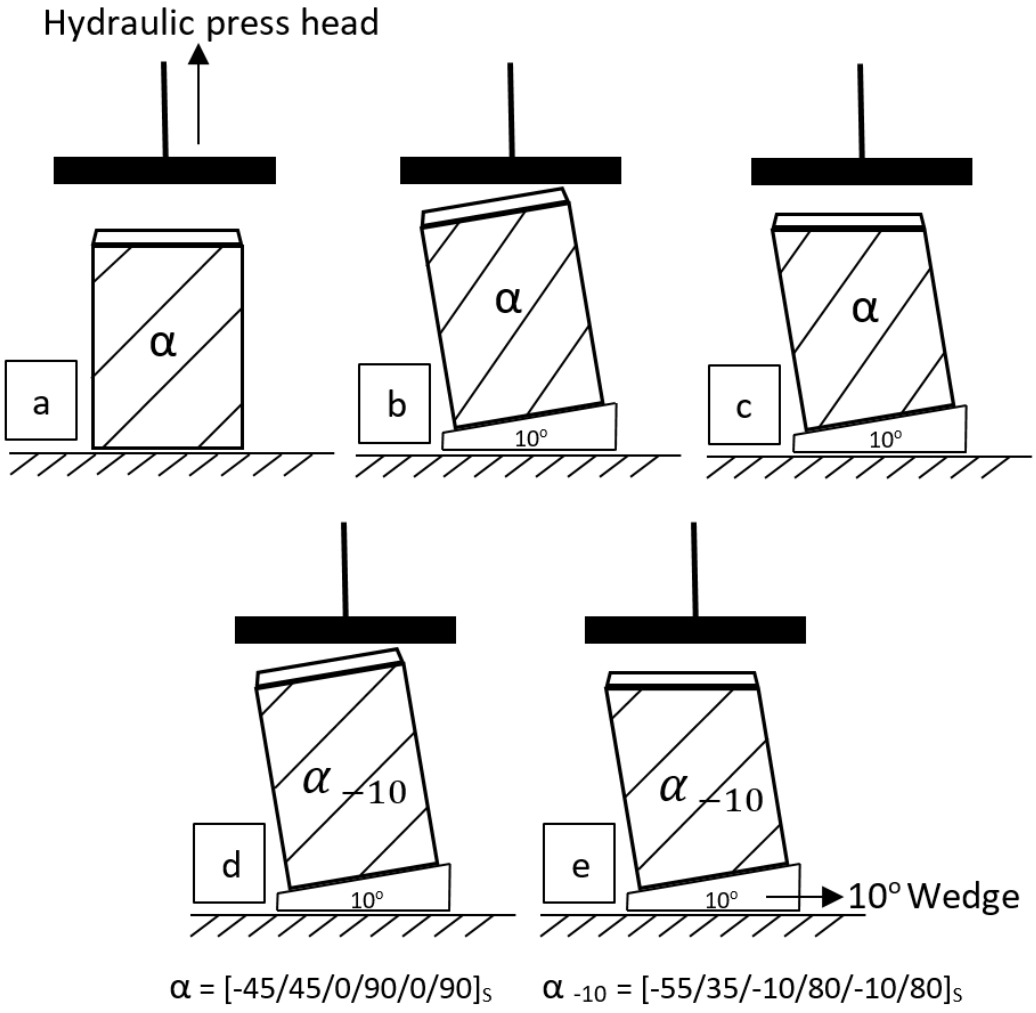

Figure 3-13 Off-axis loading integration of axial loading case study of a) axial b) off-axis at 10° c) 45° flat chamfer d) tailored lay-up sequence and e) 45° flat chamfer with tailored lay-up sequence.

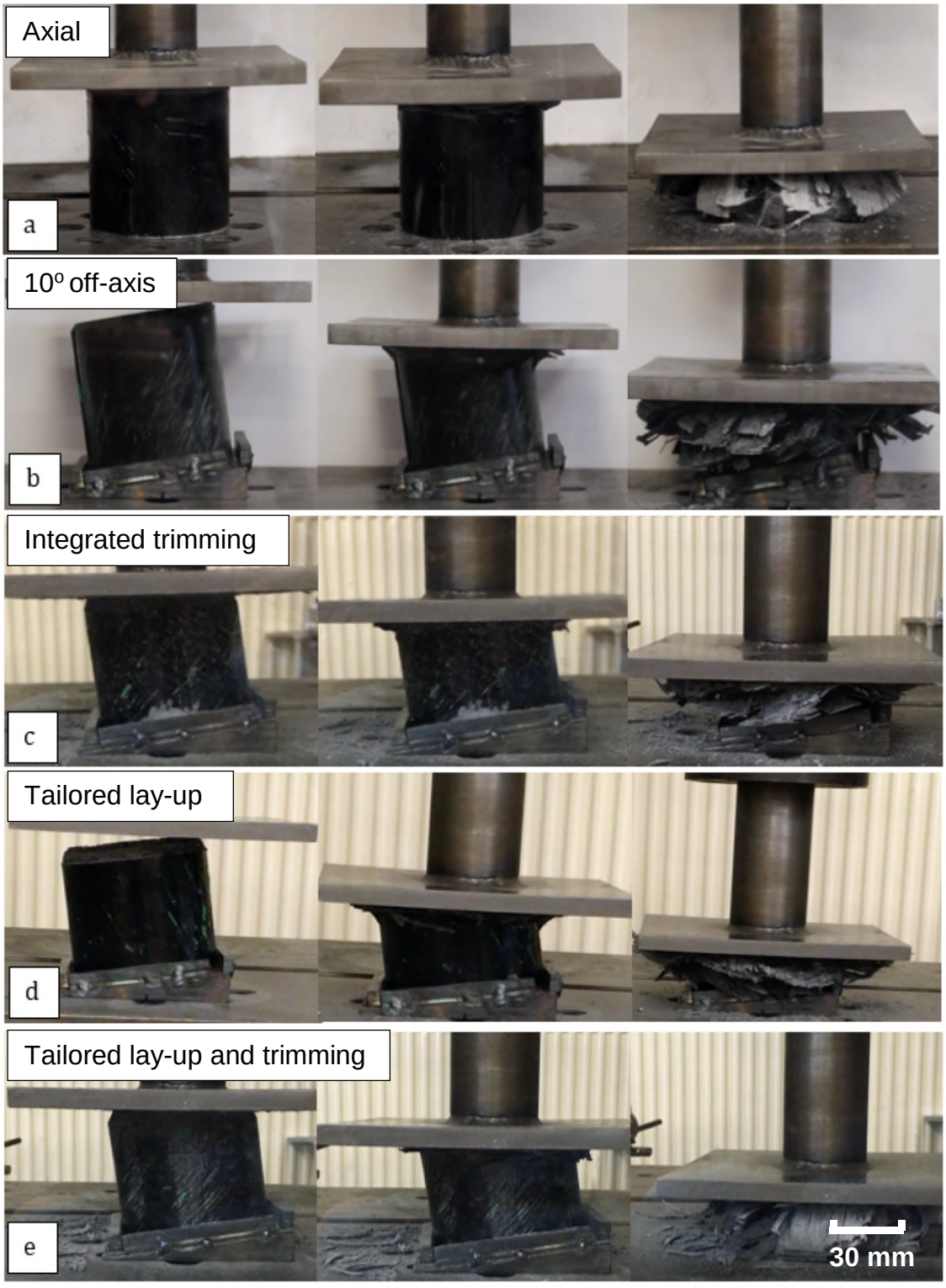

Figure 3-14 Various crushing stages of cases a) axial b) off-axis at 10º c) 45º flat chamfer d) tailored lay-up sequence and e) 45º flat chamfer with tailored lay-up sequence.

The crushing failure modes in case (a) and (b) were already mentioned as axial and 10^{o} off-axis angles (see Figure 3-13). Observing Figure 3-15, the morphologies demonstrate the failure mechanisms in each tested case. In case of (c), bundle fractures were observed with axial splitting, but the failure mechanism was based on brittle fracture. Case (d) like case (b) showed multiple short fracture mechanisms through brittle fracture failure. A transverse shearing is observed in both cases of (c) and (d). Case (e) is however the main aim of this study which has shown a similar behaviour towards case (a) followed by the hypothesis. The failure mechanism of case (e) consists of brittle fracture with lamina bending combinations. Axial splitting and bundle fractures were also observed in case (a) and (e). The force-displacement curve (see Figure 3-16) shows a trend of better energy absorption from the initial crushing process in cases of (a), (c) and (e) where flat 45^{o} chamfer trimming was utilised. Cases of (c) and (e) had similar testing conditions with a variable of lay-up sequence. Integrated lay-up sequence has shown slightly better energy absorption capabilities at off-axis loading in comparison with non-integrated layup design. The trimming mechanisms utilised in cases (a), (c) and (e) had shown better energy absorption capabilities compared to (b) and (d). Cases (a) and (e) both showed a similar trend as both have similar conditions of lay-up and triggering mechanisms. This has clearly indicated the similarity of their failure mechanisms. Both cases eliminate transverse shearing failure mode which is a common failure fracture mode in off-axis loading conditions.

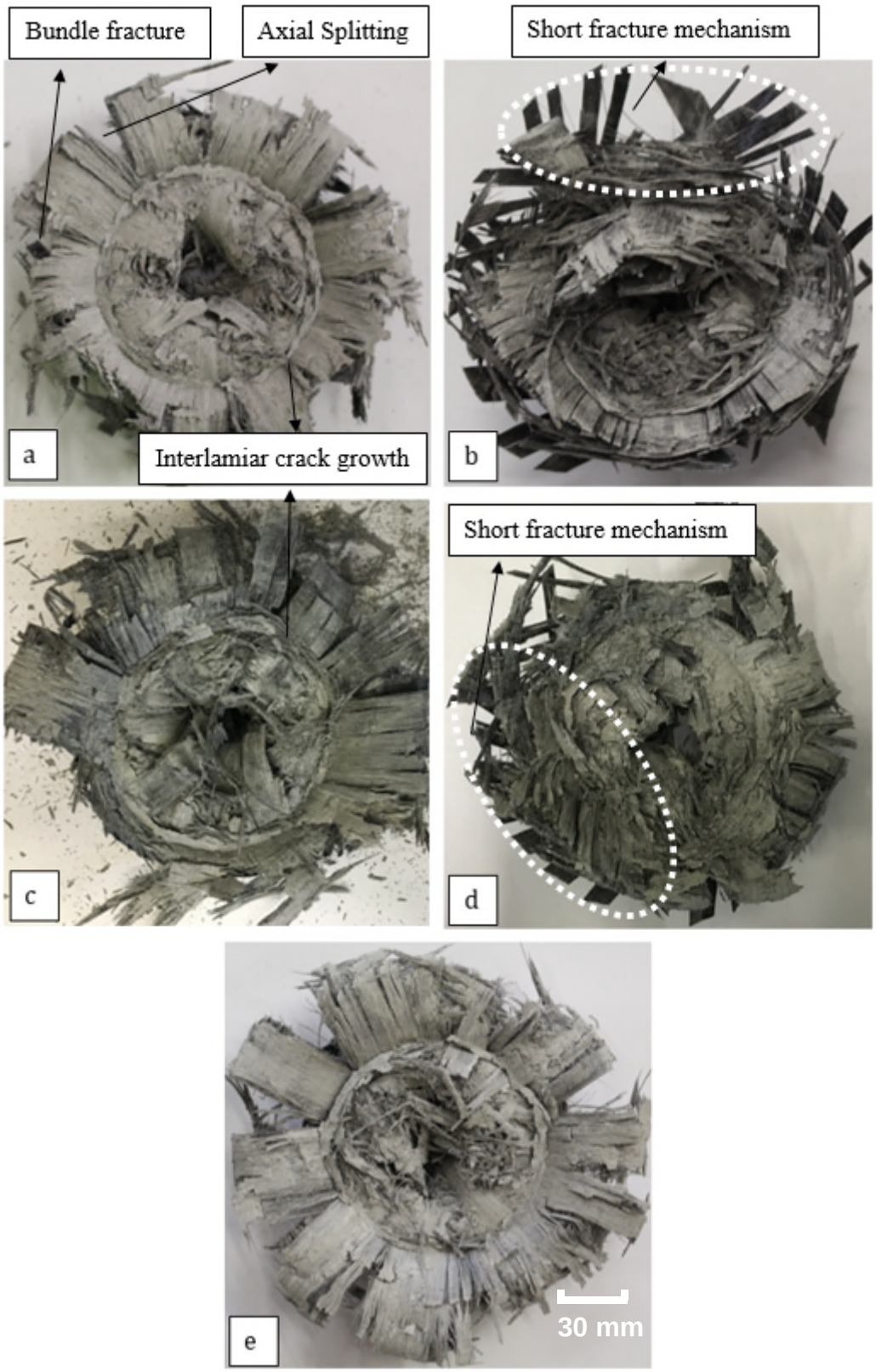

Figure 3-15 Plane view of crushed axial and off-axis specimens a) axial b) off-axis at 10^{o} c) 45^{o} flat chamfer d) tailored lay-up sequence and e) 45^{o} flat chamfer with tailored lay-up sequence

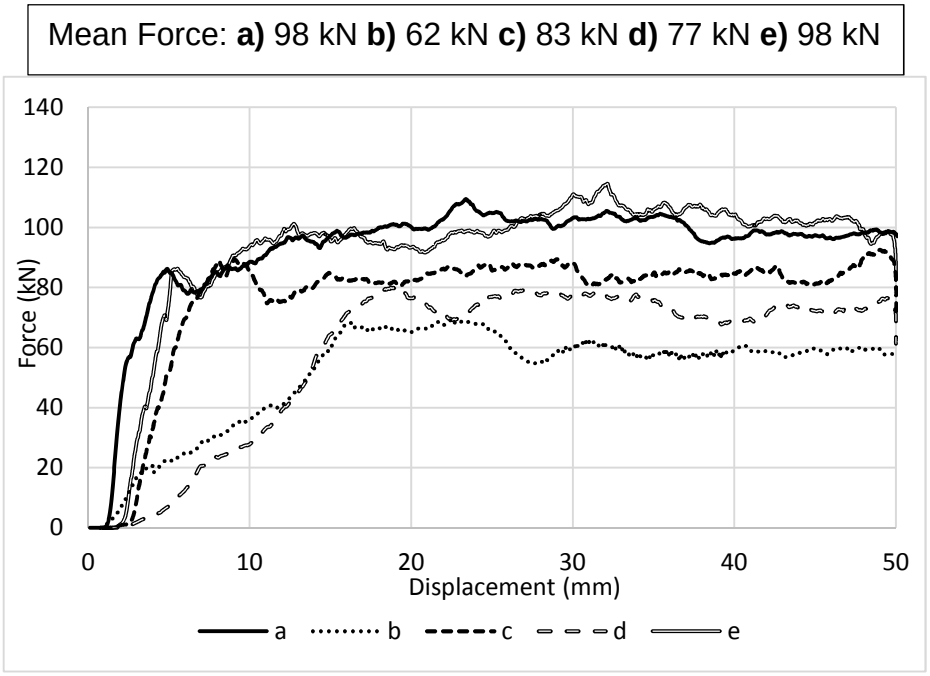

Figure 3-16 Force-displacement of axial and off-axis integration comparison a) axial b) off-axis at 10º c) 45º flat chamfer d) tailored lay-up sequence and e) 45º flat chamfer with tailored lay-up sequence.

3.5.3 Specific energy absorption (SEA) of axial, off-axis and tailored off-axis specimen

As the lateral inclination angle increases the specific energy absorption decreases, (see Figure 3-17). The specimens subjected to axial loading reached an SEA of about 64 kJ/kg, the 5º specimens reached SEA of about 54 kJ/kg, 10º specimens reached SEA of about 40 kJ/kg, this trend is followed by 28 kJ/kg and 18 kJ/kg for 20º and 30º off-axis loading conditions respectively. This research focuses on improving energy absorption capability at off-axis loading by tailoring the ply-orientations and 45º flat chamfering acting as the trigger to increase specific energy absorption capability. The integrated/tailoring off-axis at 10º showed higher SEA value than all other off-axis angles.

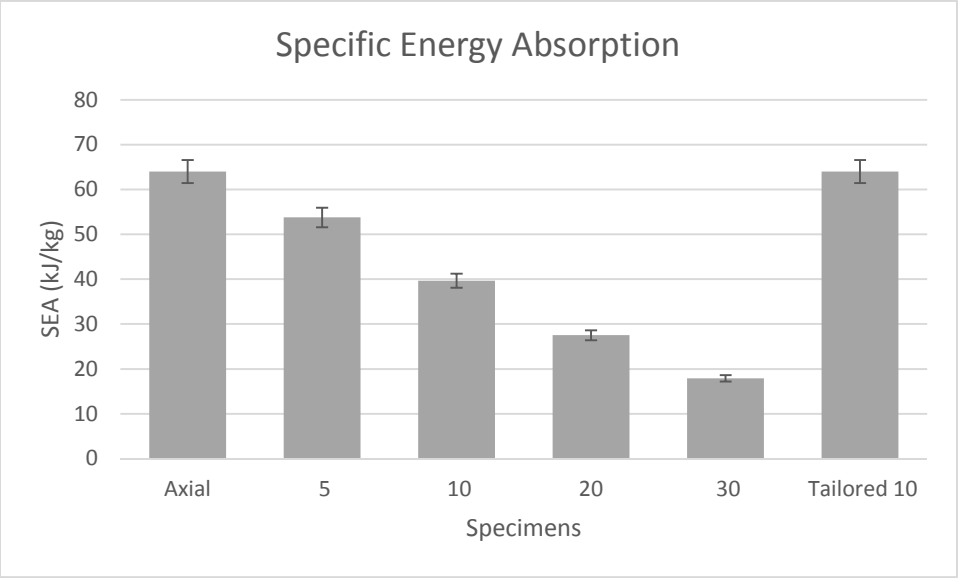

Figure 3-17 Specific energy absorption (SEA) of axial and off-axis comparison

3.6 Conclusion

In the present study, the crashworthiness of composite tubular structures was experimentally investigated under axial and oblique loading. The results have shown that, as the lateral incline angle increases the energy absorption decreases and catastrophic failures were observed at off-axis angles of above 20^{o}. This conflicts with various previous studies, it was noted from the researches that at 10^{o} off-axis angle higher energy absorption was observed [17,144]. This is due to the geometry differences, in previous studies box structures were used and, in this chapter, circular tube structures were subjected to investigation.

From a design perspective, the second part focused on improvement of mean crush force and consequently increase of energy absorption capabilities in off-axis loading. It was shown that tailoring ply-orientation can result into increase of mean crush force from 60 kN to 72 kN and consequently increasing energy absorption in 10^{o} off-axis angle. All specimens which were subjected to flat trimming integration showed higher energy absorption in comparison with the original ones. The combination of ply-orientation and flat trimming integration showed a similar trend as axial loading at 10^{o} off-axis loading with both mean crush force of close to 100 kN. This study helps to increase energy absorption

capabilities at various configurations. The present study has established sufficient information on the effect of various oblique angles on energy absorption capability and improving crashworthiness behaviours by integrating ply-orientation and altering the trigger mechanism to increase specific energy absorption capability.

4 Experimental Studies of Single, Multi and Pattern-Stitched Composite Sections under Quasi-Static Loading

4.1 Introduction

The present chapter experimentally investigates the progressive energy absorption of fibre-reinforced polymer (FRP) composite tubular structures under quasi-static loading conditions. Various multi-stitched locations are studied to find a correlation between single and multi-locations of stitches and energy absorption capabilities of composite absorbers. The through-thickness reinforcements are applied into locations of 10 mm, 20 mm, 30 mm, 10-20 mm, 10-30 mm, 20-30 mm, 10-20-30 mm and 10-15-20-25-30-35 mm from top of the composite tube sections (see Figure 4-2). It is shown that multi-stitched locations can cause several increases of crushing load and consequently increase of energy absorption of composite tube absorbers. The pattern-stitched design has shown 15% increase in specific energy absorption than non-stitched specimen. The idea would be expanded into other designs which are followed by increase of stitched locations and reduction of the distance between stitches to improve the mean force with a smooth and progressive pattern of crushing load.

In all previous researches several variables related to the energy absorption of composite thin-walled structural components have been investigated. Apart from all these parameters, multi-location stitching is another factor which significantly influences the energy absorption of composite tubular structures under high speed loading. This chapter experimentally aims to study the relation between locations of stitches and energy absorption capabilities of composite absorbers.

4.2 Valuation criteria for crushing behaviour

There are many important variables which must be considered in the study of energy absorption capabilities. These were mentioned in detail in previous chapters of 2 and 3. These include material properties; manufacturing method; microstructure; geometry of specimen, including any crush initiator used; and rate of crushing speed. One of the most important parameters is the specific energy

absorption (SEA) performance of collapsing or crushing specimens. This value is defined as the energy absorbed per unit crushed mass of material. In this case, it is an important criterion for lightweight designs. Another important factor in the study of energy management capability, is the shape of the force-crush distance curve. Catastrophic and progressive failures are two main failure mechanisms of composite tube structures. A progressive crushing is initiated at one end of the specimen using a bevelled trigger mechanism and then, it progresses through the specimen without significant damage, the initial force is very high and stays high throughout the crushing process, therefore the mean force is high. For a catastrophic failure the initial maximum force is high and drops rapidly, therefore the average force is low.

4.3 Fabrication of single-stitching, multi-stitching and pattern-stitching and status of the field

In this work, all composite sections were fabricated from glass/epoxy 7781/E722 material (ρ = 2250 kg/m^3) using hand lay-up techniques with a symmetric twelve-ply laminate of $[-45/45/0/90/0/90]_S$. Each GFRP layer has a thickness of 0.25 mm after curing. The composite sections were 80 mm × 80 mm with total wall thickness of 3 mm (see Figure 3-1). The quasi-static testing was conducted using a hydraulic press with load cell capacity of 500 kN with crushing rate of 2 mm/second. All specimens were placed at the centre of the stroke for equal load distributions (see Figure 3-6). The stroke displacement for all specimens were kept the same at 50 mm. The profile of load-displacement consists of load cell and stroke displacement and were recorded automatically for each test. For a detailed fabrication of the GFRP composite sections, please refer to chapter 3.

All composite sections were stitched by Kevlar fibre yarns (with 1.1 mm in diameter) to reinforce the structural properties of the composite sections through the thickness (see Figures 4-1c and 4-2). To apply fibre yarn stitching onto the composite sections at different locations, a needle was used with a diameter of 1.1 mm at the thickest point. Four to six specimens were tested in each case of study to find the mean deviation of the experimental results. The crushing stroke and total length of the specimens were chosen based on the literature and

capacity of the testing machine with maximum crush distance of 50 mm. In this research, the concentration was oriented on the specific energy absorption capability and force displacement diagrams. However, the composite specimen crushed morphologies were investigated to analyse the effect of through-thickness stitching on the failure mechanisms. From the force-displacement curve, the crashworthy behaviour of the material is analysed through load-carrying capacity and energy absorption capability of each individual case. Since there are various factors such as geometry, layup, strain rate and loading direction affecting failure mechanisms of FRP composite absorbers, all parameters or variables affecting energy absorption were kept constant, to only study the effect of stitching on the specific energy absorption capabilities of the composite absorbers.

Figure 4-1 a) Composite crushing tube, b) bevelled trigger mechanism, and c) stitching technique

The through the thickness reinforcement took place by inserting a needle (1.1 in diameter) through the uncured laminated composite by hand to penetrate the laminate. The stitching was approximately 6 mm apart using Kevlar yarn fibres (1.1 mm in diameter). Each line of stitching was marked and carefully followed to cover the circumference of the composite tube. Each line of stitching took approximately 40 stitches. To be able to apply stitching onto the uncured laminates and since the stacking and the laminate sticks onto the rigid mould, a thin polymer film was taped together onto the base mould, which allowed a lubricant for the laminate. Since the needle penetrates the laminate, the uncured

laminate was lifted upwards to allow the needle to go through. This allowed the uncured laminate to move on the longitudinal axis of the rigid mould with a bit of a force. In comparison with the non-stitched specimen, the mould was sealed wrapped with two layers of thin polymer films, and similarly, the stitched specimens had two layers of thin polymer films, to have the same thickness, one sealed the mould similar to the non-stitched specimen and the other provided lubrication for the uncured laminate (not attached to the rigid mould). This technique provided the same conditions and kept the circumference constant for both non-stitched and stitched specimens.

In the current study of multi-stitch locations on composite absorbers, there is lack of experimental and numerical studies on the effect of stitching through the thickness on force-displacement curve in respect to the stitching location and their effect on specific energy absorption of UD composite absorbers. The current study is designed to find the correlation between stitching locations and energy absorption capabilities, through studying the force-displacement curves of each case, their failure mechanisms and SEA values. This enables to create a database and analyse the effect of single and multi-stitching through the thickness on specific energy absorption. Single and multi-stitched locations on the crushing behaviour of composite absorbers under axial high-speed load is therefore investigated.

All GFRP composite tubes were stitched at different locations according to the design in Figure 4-2. The chosen cases for single-stitched locations are 10 mm, 20 mm and 30 mm from the top of the specimens, followed by multi-stitched locations with 10 and 20 mm (10-20), 10 and 30 mm (10-30), 20 and 30 mm (20-30) from the top of the specimens were studied. In pattern stitching, the chosen locations were, 10, 20 and 30 mm (10-20-30) followed by 10, 15, 20, 25, 30 and 35 mm (10-15-20-25-30-35), from the top of the specimens were studied to investigate their effect on energy absorption capabilities. The chamfer end of the composite section was subjected to z-directional through thickness stitching according to the design in Figure 4-2.

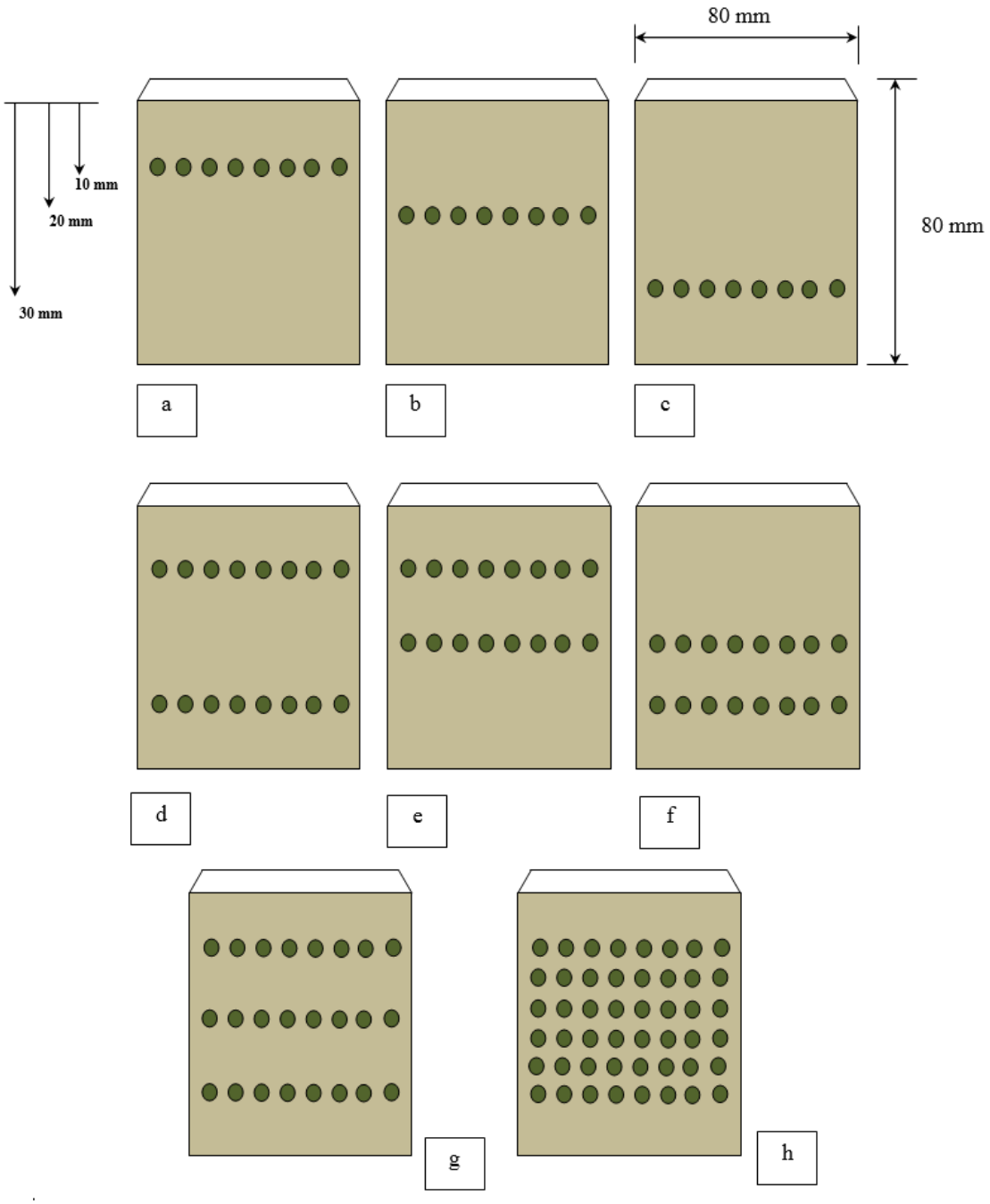

Figure 4-2 Various designs of single and multi-location stitches within composite section structure. a) 10 mm, b) 20 mm, c) 30 mm, d) 10-30 mm, e) 10-20 mm, f) 20-30 mm, g) 10-20-30 mm, h) 10-15-20-25-30-35 mm

4.4 Results and discussions

4.4.1 Crushing of single stitched tubes

The progressive crushing was initiated for all tested specimens at the beginning of the process. This behaviour was shown after extensive microcracking collapse and rapid rise of load in force displacement diagrams. The main central crack in the middle of the wall of all tubes behave as mode-I interlaminar crack propagation which has been extensively studied in the previous researches of authors [56-144] and many others. This main crack initiates progressive growth until it reaches to the stitched area. Here, there is a significant change in the force-displacement diagram which is followed by a rapid increase and then a quick drop to the lower level of the load. This change can cause increase of crushing load and consequently increase of specific energy absorption. This phenomenon was consistently observed for all single stitched composite tubes. Various crushing stages of single stitched location is shown is Figure 4-3.

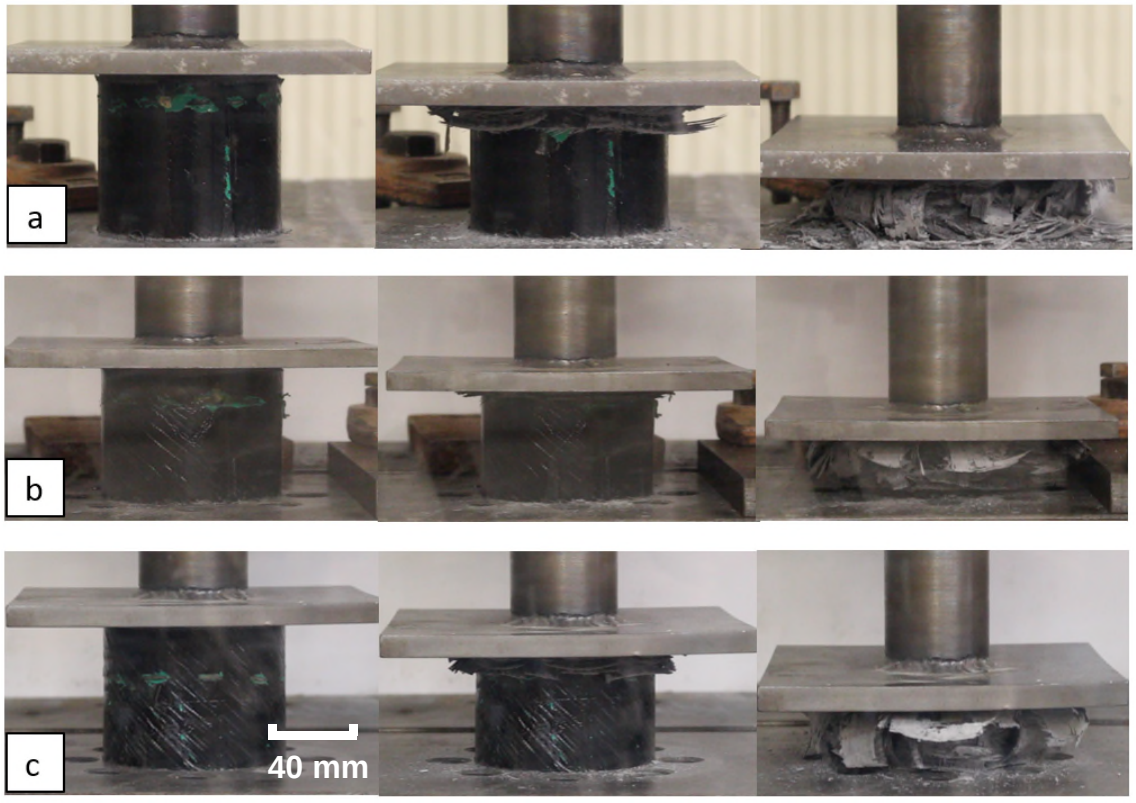

Figure 4-3 Various crushing stages of single stitched composite sections, a) 10 mm, b) 20 mm, c) 30 mm

Four to six specimens were tested as mentioned, an example is shown in Figure 4-4, which shows all five 10 mm single stitched tested specimen and the mean deviation.

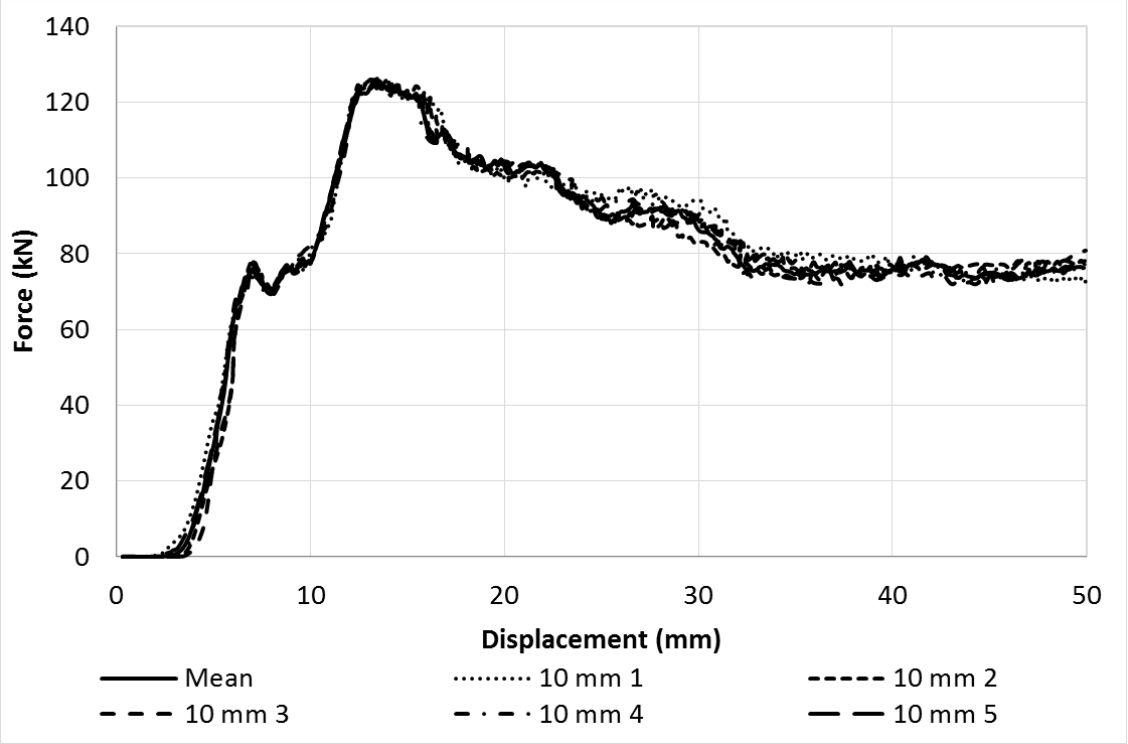

Figure 4-4 Five 10 mm stitched specimen repeat tests with mean deviation

The mean force (F_m) did not increase for single stitch of 20 mm in comparison with 30 mm stitch location, which was around 105 kN (see Figures 4-5 and 4-6 a). The observed crushing mode for these composite tubes was lamina bending which was shaped with long interlaminar, and parallel to fibre cracks. This mechanism causes fronds formation which spread inwards and outwards. In Figure 4-5, the morphologies of the crushed single stitched composite sections are shown. The difference between single stitched and non-stitched specimen (see figure 4-12 c) is higher axial cracks along the petals (inner and outer fronds) and higher fragmentations failures. Figure 4-12 is fully annotated based on the failure mechanisms occurred, which can be beneficial to analyse the crushed morphologies in this chapter.

In Figure 4-6 a, the comparison of all single stitched specimens with non-stitched specimen is shown. More specifically, Figure 4-6 b, represents non-stitched

specimen compared with 10 mm stitched specimen, it can be noted that a sudden localised load increase has occurred with a peak of 124 kN, followed by a slow drop in load due to local buckling and fragmentation with normalisation at 32 mm displacement. The mean crush force has dropped by 9 kN in total compared with non-stitched specimen.

Figure 4-6 c, represents non-stitched specimen compared with 20 mm stitched specimen. A sudden curved shaped increase in load is observed with a peak of 117 kN once reaching the stitching point with lower normalisation value than non-stitched specimen. The mean crush force dropped by 5 kN in total.

Figure 4-6 d, represents non-stitched specimen compared with 30 mm stitched specimen. A sudden drop is observed before reaching the stitching point, this is due to rapid interlaminar crack growth, followed by a sudden increase in load with a peak of 115 kN. Higher normalisation value is observed with the stitched specimen with a mean normalisation difference of 5 kN to non-stitched specimen. The mean crush force has increased by 3 kN in total.

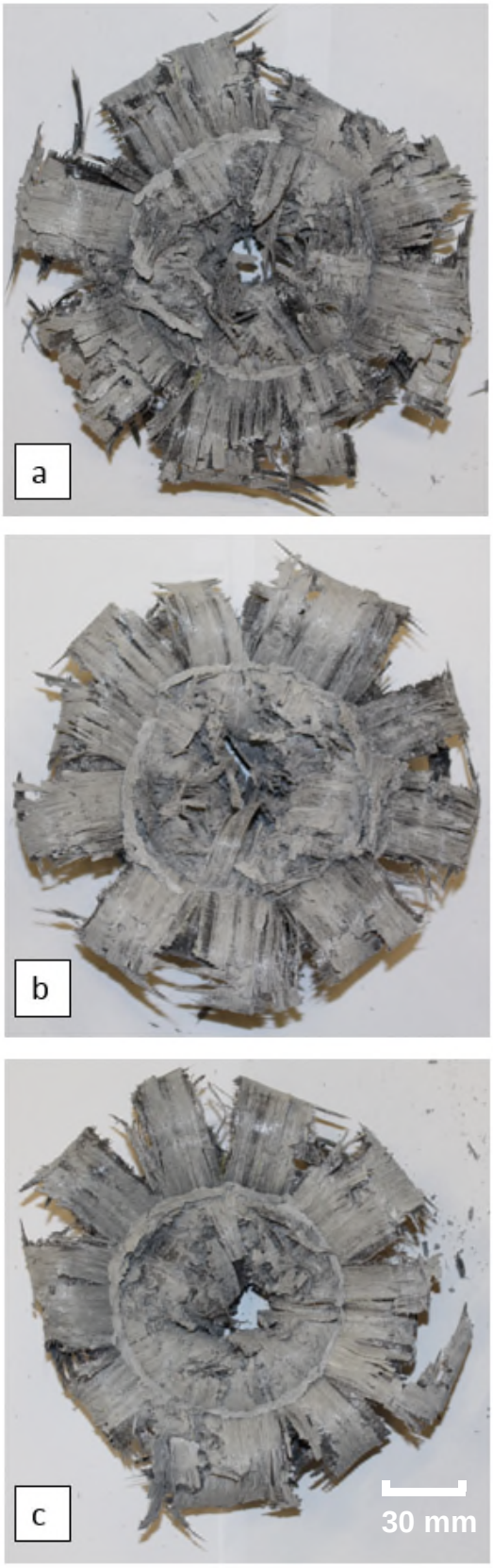

Figure 4-5 Plane view of crushed single stitched composite sections, a) 10 mm, b) 20 mm, c) 30 mm

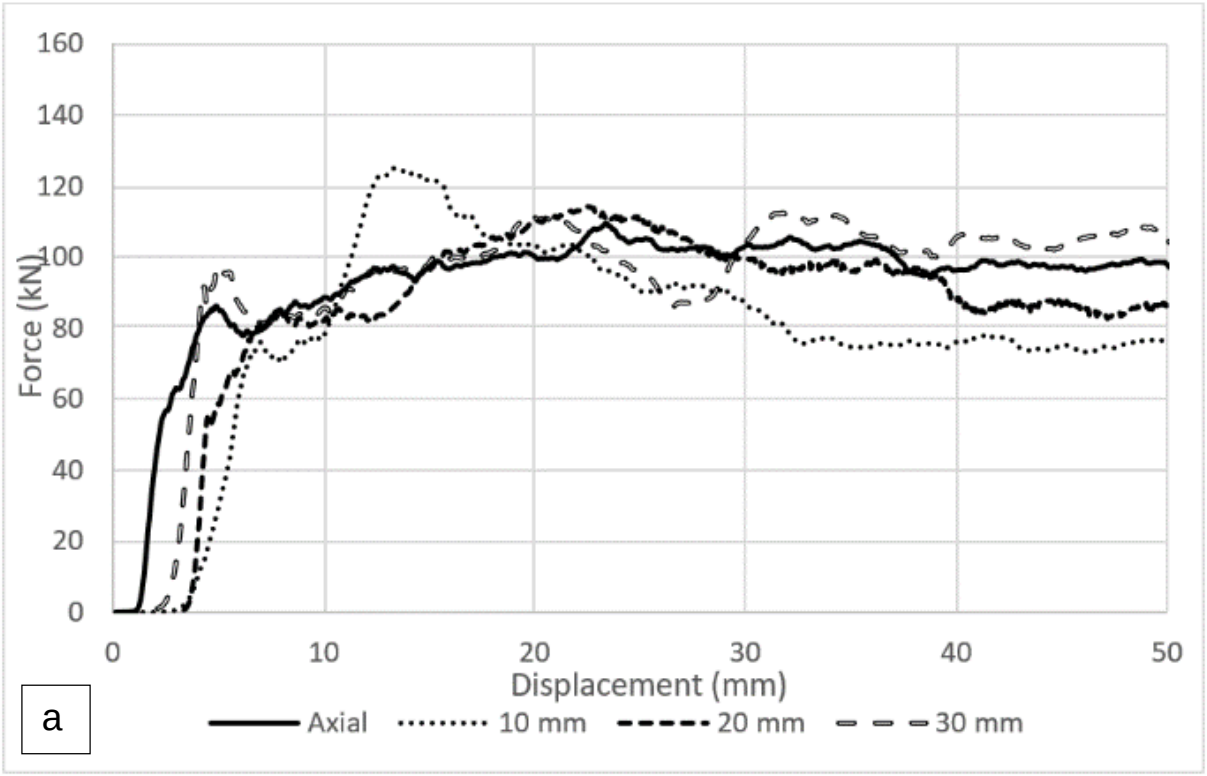
160
140
120
100
80
60
40
20
0
Force (kN)
0
10
20
30
40
50
Displacement (mm)
a
Axial
10 mm
20 mm
30 mm

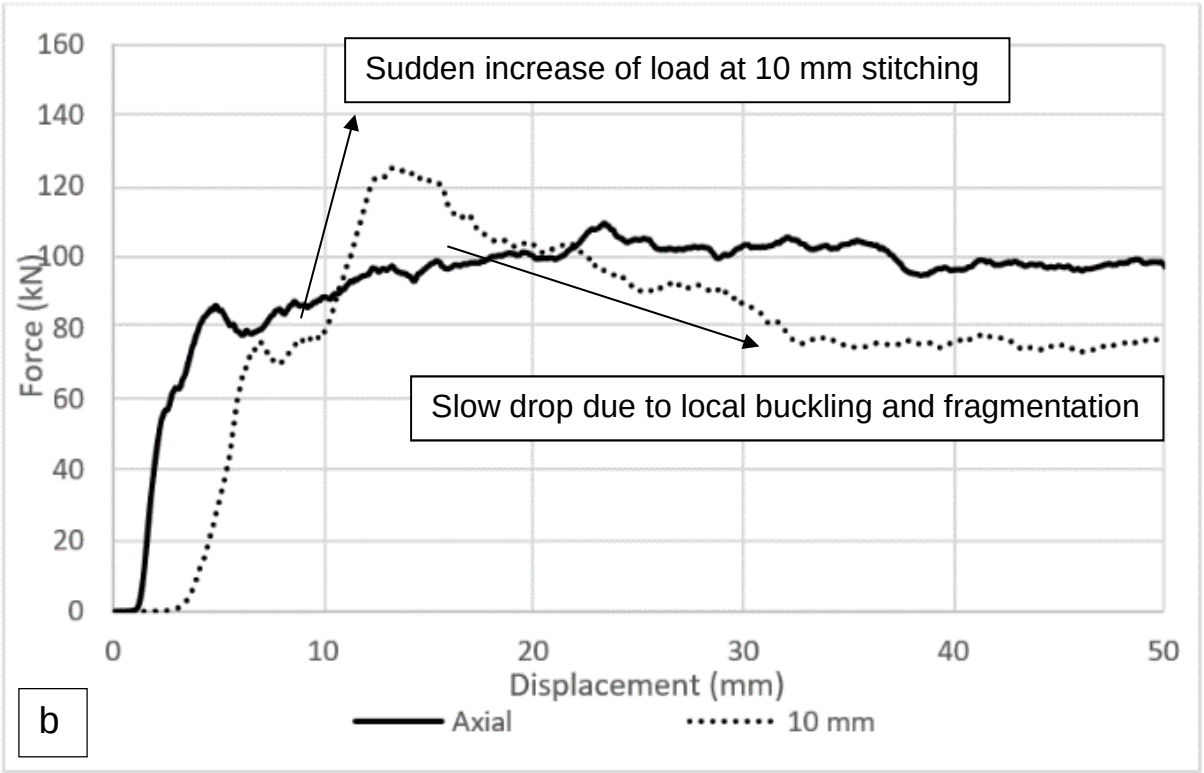
Sudden increase of load at 10 mm stitching
Slow drop due to local buckling and fragmentation
160
140
120
100
80
60
40
20
0
Force (kN)
0
10
20
30
40
50
Displacement (mm)
b
Axial
10 mm

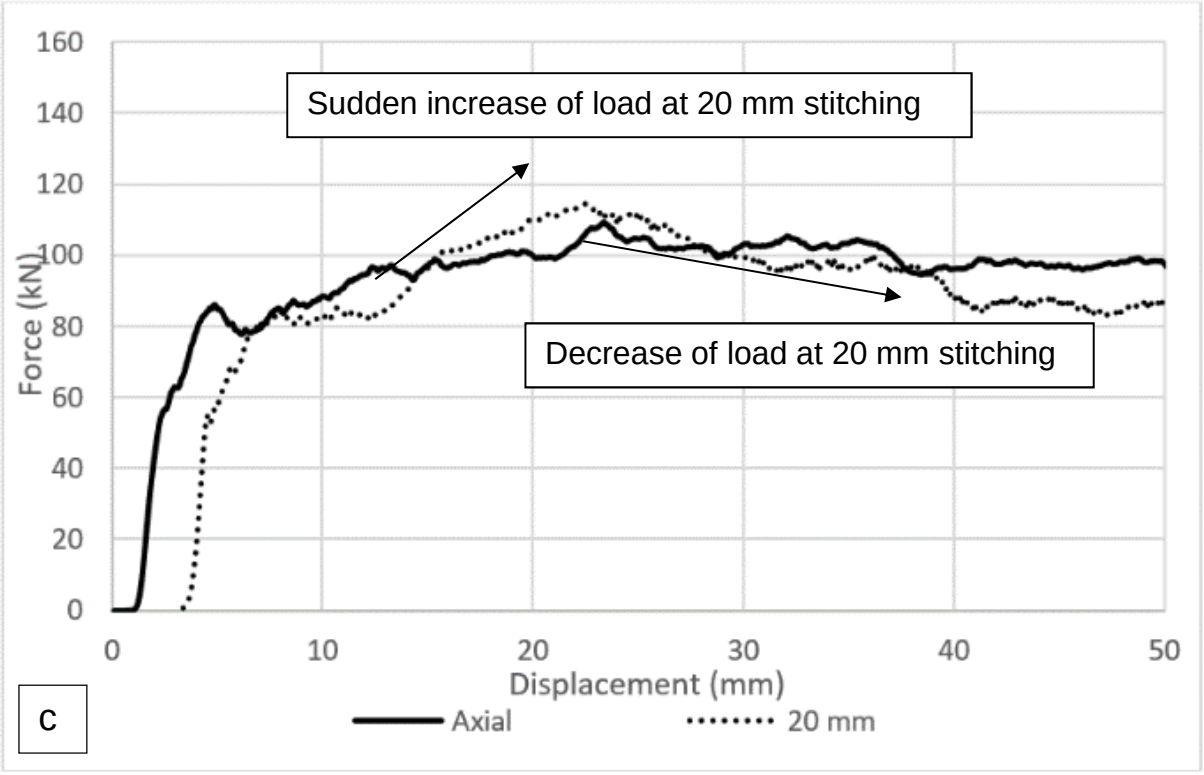

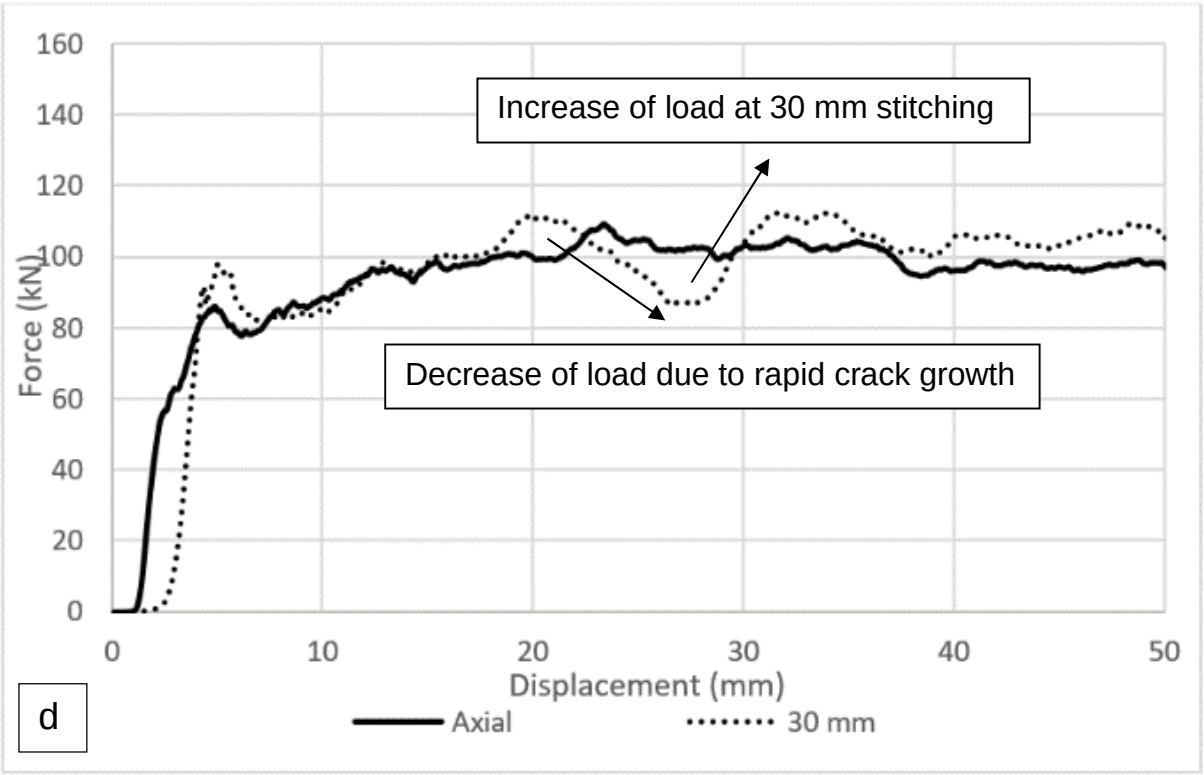

Figure 4-6 Force-displacement curve of single stitched composite sections, a) comparison of non-stitched (axial), 10 mm, 20 mm and 30 mm, b) non-stitched (axial) and 10 mm, c) non-stitched (axial) and 20 mm, d) non-stitched (axial) and 30 mm

The results 20 mm single stitching has been compared with previous similar work [145] which was carried out on single stitched composite box structures. These results clearly show that cylindrical tubular structures have significantly absorbed higher energy in comparison with box absorbers (see Figure 4-7). The difference in non-stitched mean crush force is 23 kN and stitched mean crush force is 19 kN. In both studies, Kevlar fibre yarn was used for reinforcing the structure.

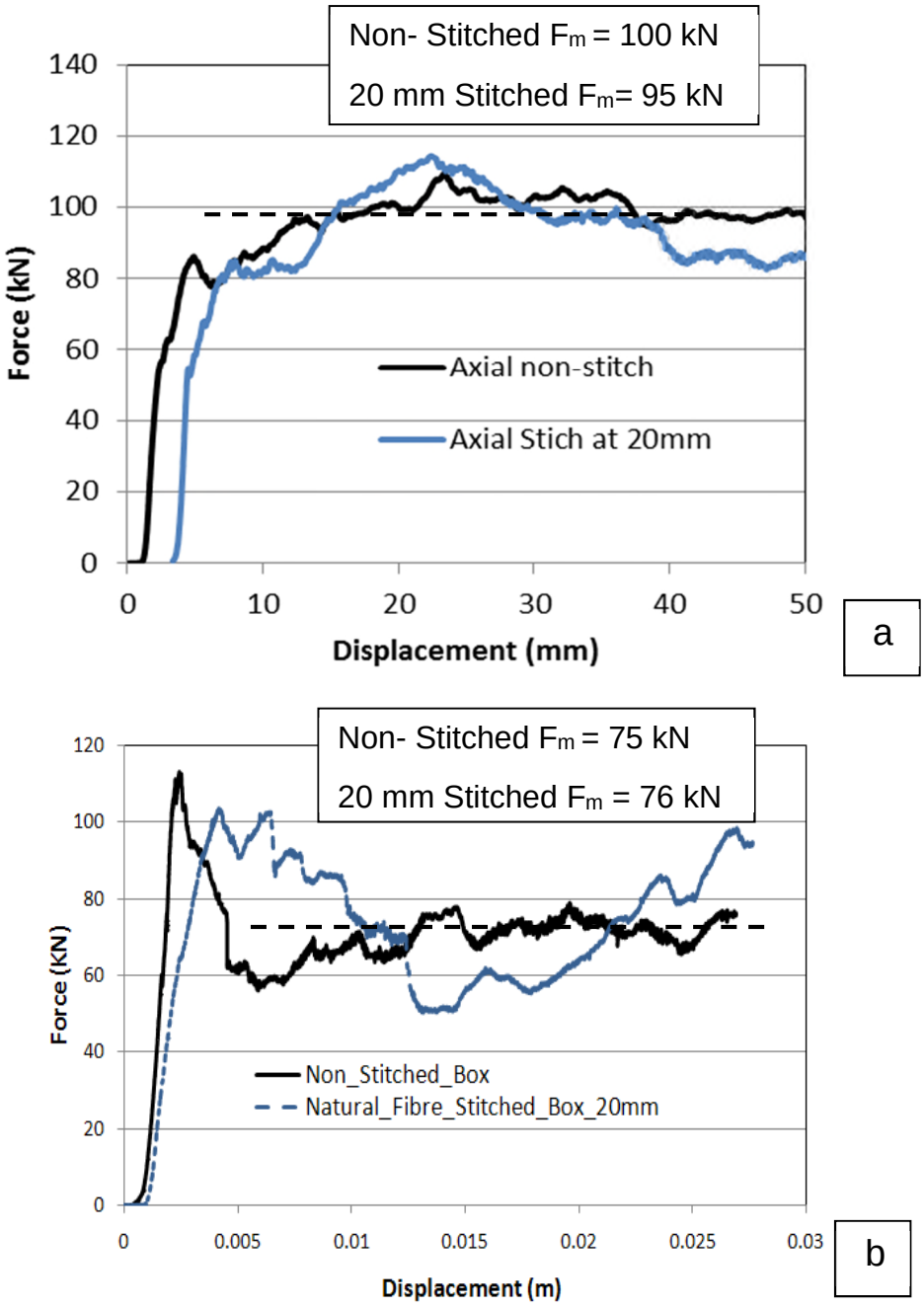

Figure 4-7 Comparison between force-displacement of composite absorbers a) circular-tube (Fm = 98 kN) and b) box structure (Fm = 75 kN) absorbers [145].

4.4.2 Crushing of multi-stitched tubes

A different scenario was observed in multi-stitched composite tubes which showed two rapid increases within the force-displacement graphs. Both, two increases can improve the mean crushing force and energy absorption of composite absorbers. However, this behaviour can vary in different cases, since high speed rate can overcome the resistance of through the thickness reinforcement and consequently causes minor effect on crushing process (see figure 4-8). Figure 4-9 shows the crushed view of the multi-stitched specimens with no significant difference in the crushing process of non-stitched and single stitched specimens, however, as the number of stitching location increases, the fragmentation and bundle fracture mechanisms increases. The force-displacement diagrams of non-stitched and multi-stitched tubes are shown in Figures 4-10 a.

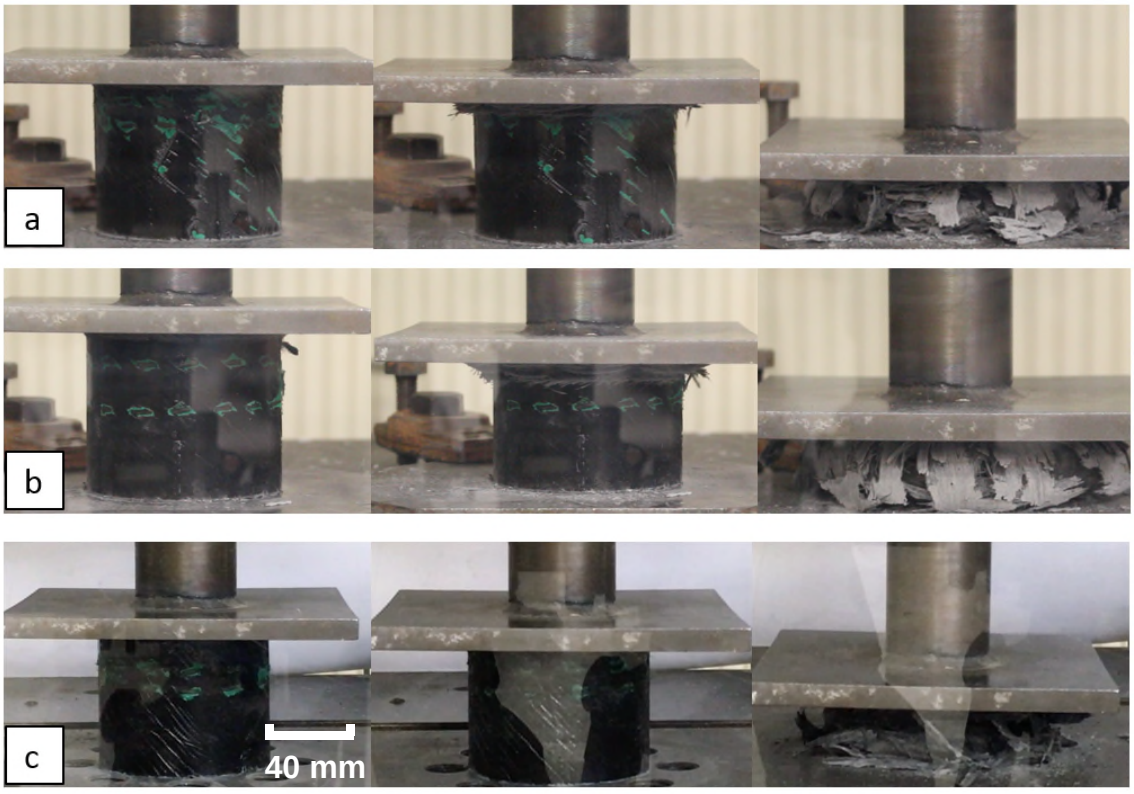

Figure 4-8 various crushing stages of multi-stitched composite sections, a) 10-20 mm, b) 10-30 mm, c) 20-30 mm.

Introducing stitching at two different locations along the length of the specimen can only be analysed for its load carrying capability, through analysing force-displacement curves and specific energy absorption (see Figure 4-10 a). Figure 4-10 b, represents non-stitched specimen compared with 10-20 mm stitched specimen. A sudden increase in load at 10 mm reaching a peak value of 118 kN and a slow increase at 20 mm is observed. The overall normalisation of the stitched curve is around 78 kN after passing the stitched points. The mean crush force has decreased by 14 kN in total compared with non-stitched specimen. Similar behaviour is observed in multi-stitched locations of 10-30 mm (see Figure 4-10 c), two sudden peaks are observed with highest peak of 123 kN, although the mean crush force has decreased by 11 kN in total, which is higher value than 10-20 mm case.

Figure 4-10 d represents non-stitched specimen compared with 20-30 mm multi-stitched specimen. A curved shaped increase in load is observed followed by a slow drop in load after passing the stitching points, with lower normalisation value than non-stitched specimen. The mean crush force has dropped by 5 kN. This case has shown better performance than other multi-stitched cases due to its steady behaviour and among other cases, it has higher mean crushing force values.

In comparison of the non-stitched specimen compared with single and multi-stitched specimens, it can be noted that composite tubes subjected to 10 mm stitching, a sudden peak is observed which indicates a high increase in load followed by a sudden drop in load, whereas, composite tubes subjected to 30 mm stitching, the absorber has better normalisation once passing the stitching point, although the peak at this location is also lower than 10 mm stitching. In 30 mm single-stitching location, the mean crush force improved by 3 kN compared with non-stitched specimen. Introducing another stitching location after the first stitching point enables better control of the drop in load. This increases interlaminar fracture toughness and consequently increases the mean crush force.

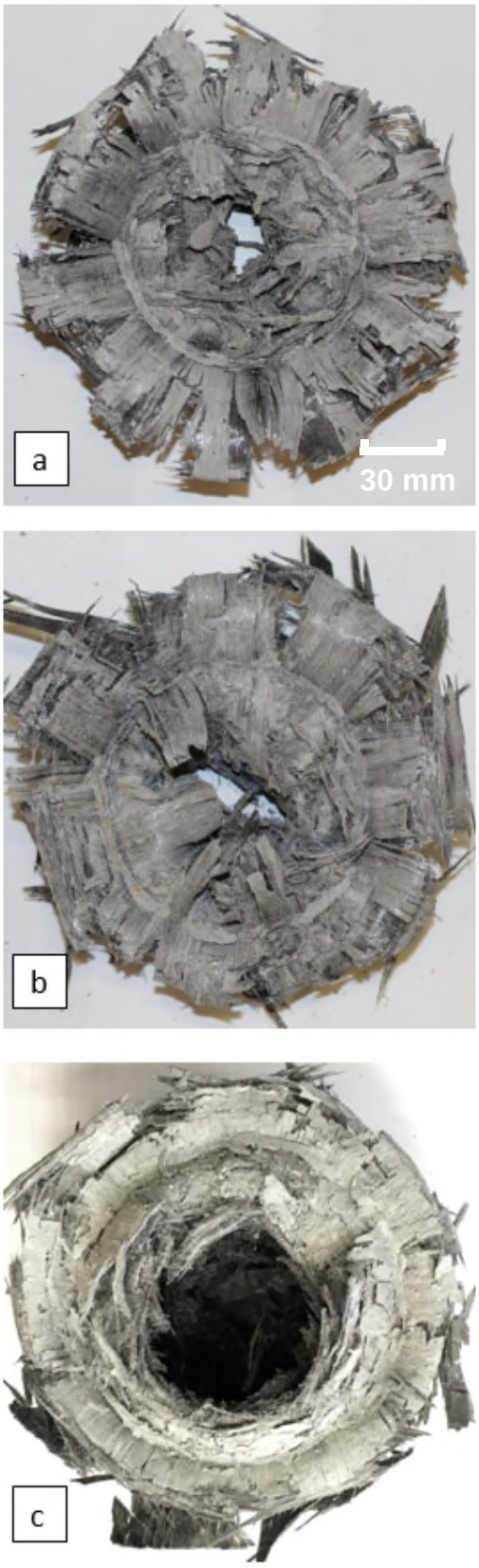

Figure 4-9 plane view of crushed multi-stitched composite sections, a) 10-20 mm, b) 10-30 mm, c) 20-30 mm.

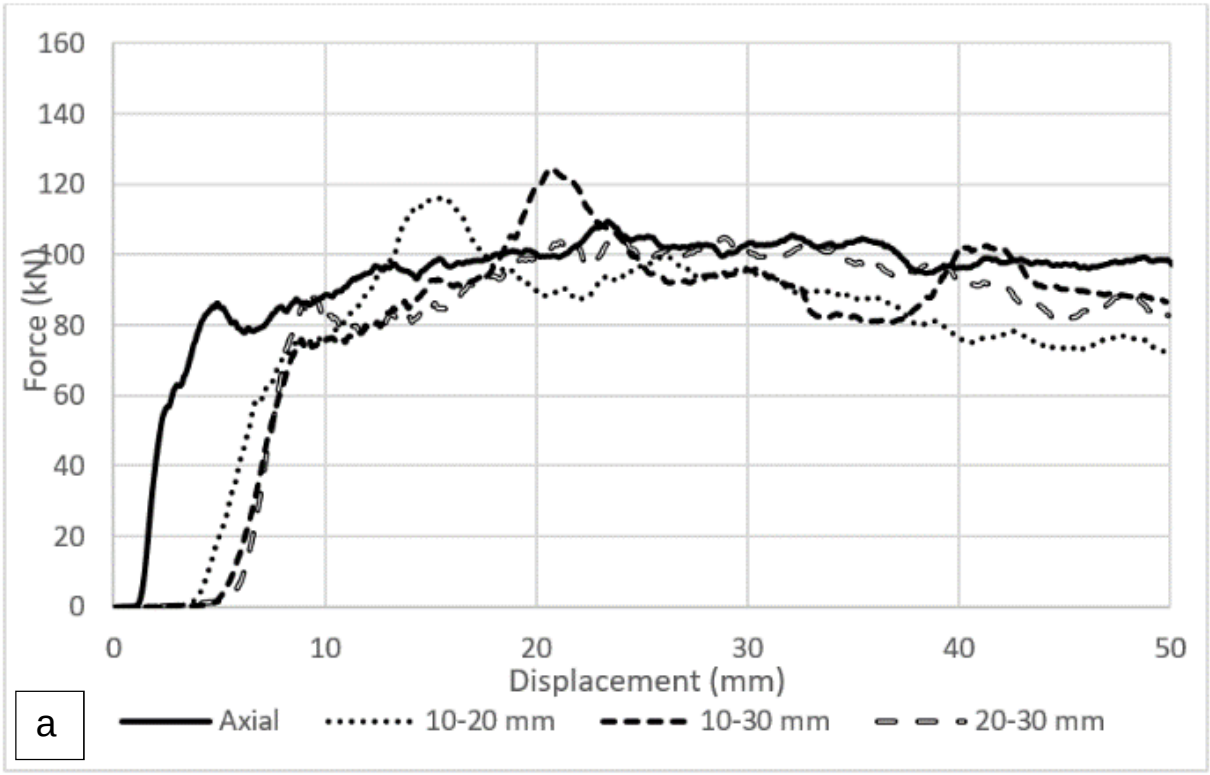
160
140
120
100
80
60
40
20
0
Force (kN)
0
10
20
30
40
50
Displacement (mm)
a
Axial
10-20 mm
10-30 mm
20-30 mm

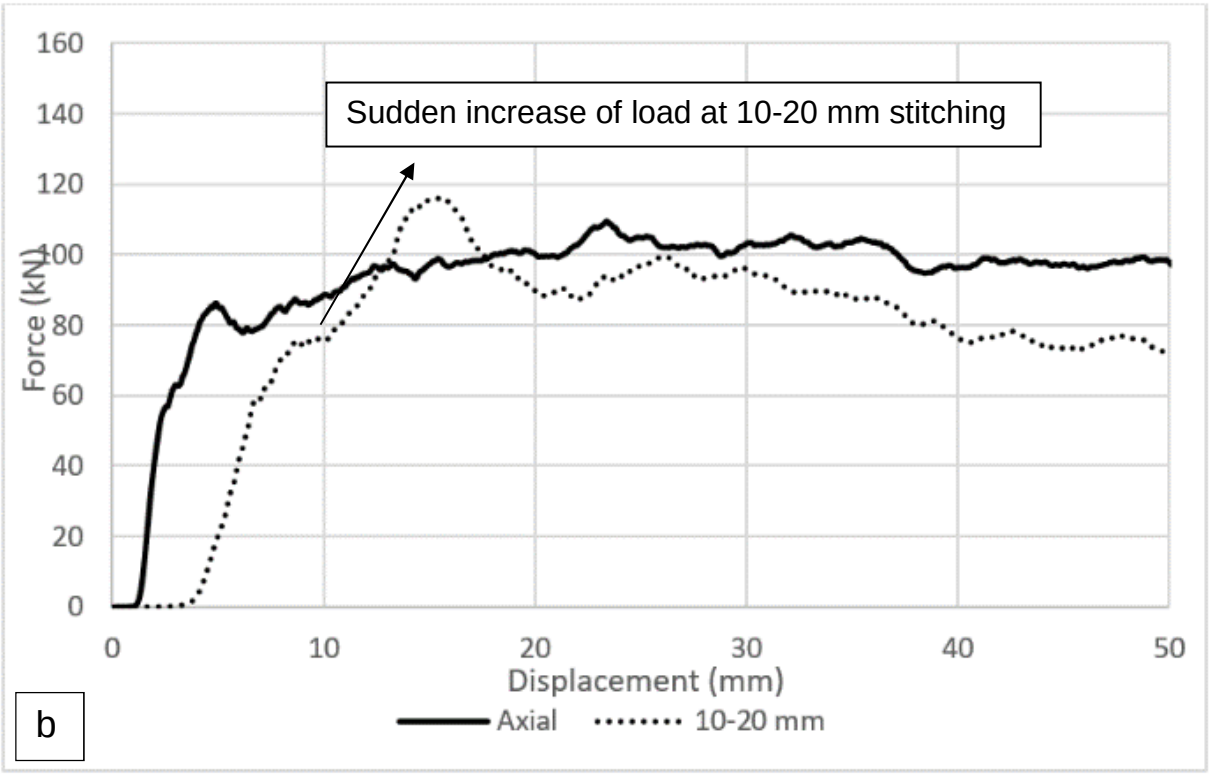
Sudden increase of load at 10-20 mm stitching
160
140
120
100
80
60
40
20
0
Force (kN)
0
10
20
30
40
50
Displacement (mm)
b
Axial
10-20 mm

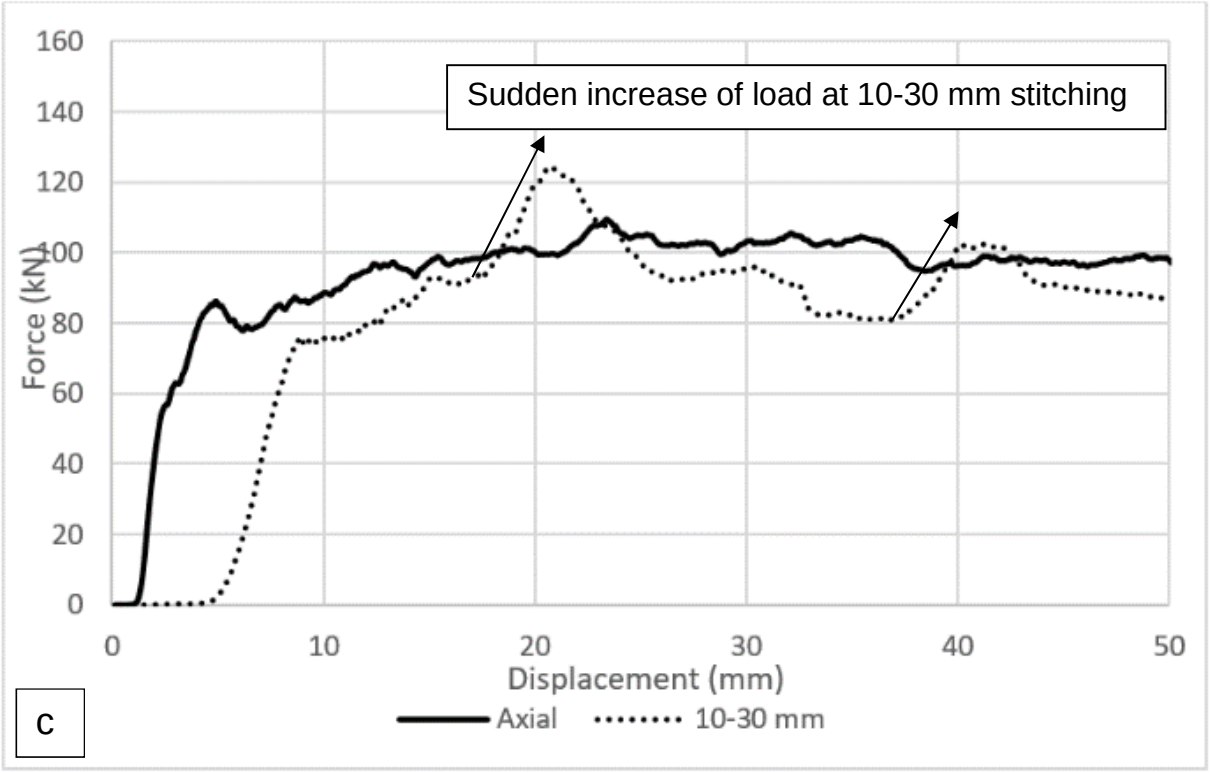

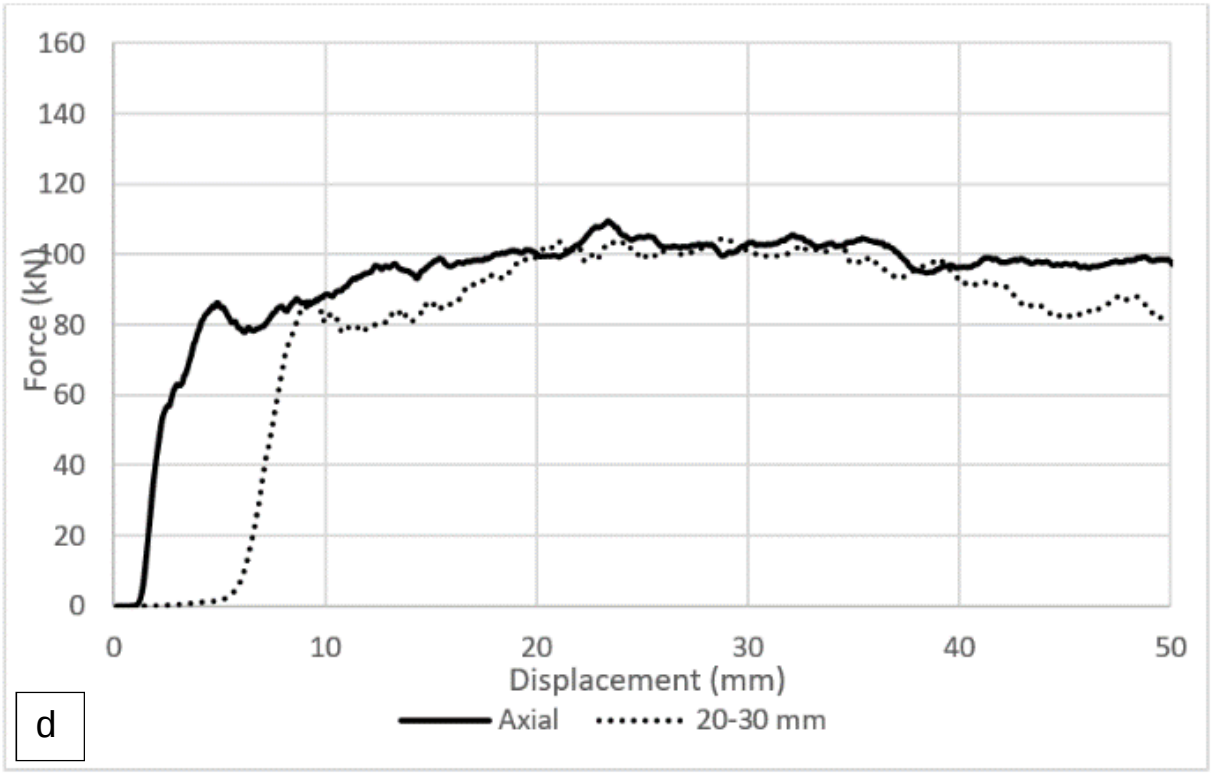

Figure 4-10 Force-displacement curve of multi- stitched composite sections, a) comparison of non-stitched (axial), 10-20 mm, 10-30 mm and 20-30 mm, b) non-stitched (axial) and 10-20 mm, c) non-stitched (axial) and 10-30 mm, d) non-stitched (axial) and 20-30 mm

4.4.3 Crushing of patterned-stitched tubes

In design of 10-20-30 mm and 10-15-20-25-30-35 mm pattern-stitched composite sections, the behaviour is clearly highlighted and showed several increases of load during the crushing process. Various stages of the crushing process of pattern-stitched composite sections is shown in Figure 4-11.

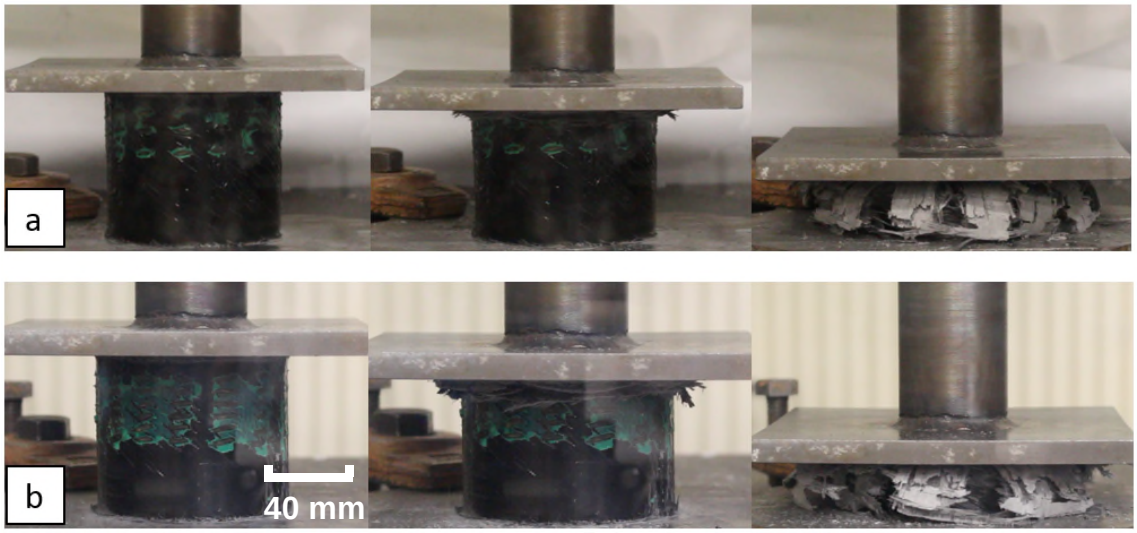

Figure 4-11 various crushing stages of pattern-stitched composite sections, a) 10-20-30 mm, b) 10-15-20-25-30-35 mm.

The crushed morphology comparison of pattern-stitched composite sections and non-stitched specimen is shown in Figure 4-12. It can be noted from these morphologies that, similarly to single and multi-stitched, there is no significant differences in failure mechanisms, apart from Mode-I and Mode-II, fragmentation failure, bundle fracture and axial cracks which only occur due to higher interlaminar fracture toughness resistance caused by the stitching which increases friction and bending and improves SEA value. This axial crack, increases by increasing the number of stitching points, this phenomenon can be clearly seen in Figure 4-12 a and b. The failure mechanism of non-stitch specimen is through laminar bending whereas pattern-stitched design of 10-15-20-25-30-35 mm is through brittle fracture mechanism which consequently leads to higher energy absorption capability. Brittle fracture mechanism is a combination of transverse shearing (fragmentation) and laminar bending. In non-stitched specimen and both pattern-stitched specimens, Mode-I and Mode-II

failure mechanisms are present with friction, crack growth, fronds bending, and fibre and matrix fracture energy absorption mechanisms. However, utilising stitching increased fibre and matrix fracture as well as Mode-II fracture and the main energy absorption mechanism was fracturing of lamina bundles and caused brittle fracture characteristics of pattern-stitched composite sections. Introducing stitching can increase interlaminar fracture toughness, as a result, delamination crack growth resistance in Mode-I improved, bending and friction becomes higher and contribute to SEA value and other failure mechanism such as bending, friction and bundle fracture mechanism contribute to dissipating the energy absorption. Many other intralaminar fracture mechanism such as fibre and matrix debonding, fibre breakage and matrix cracking also contribute in dissipating the crushing energy.

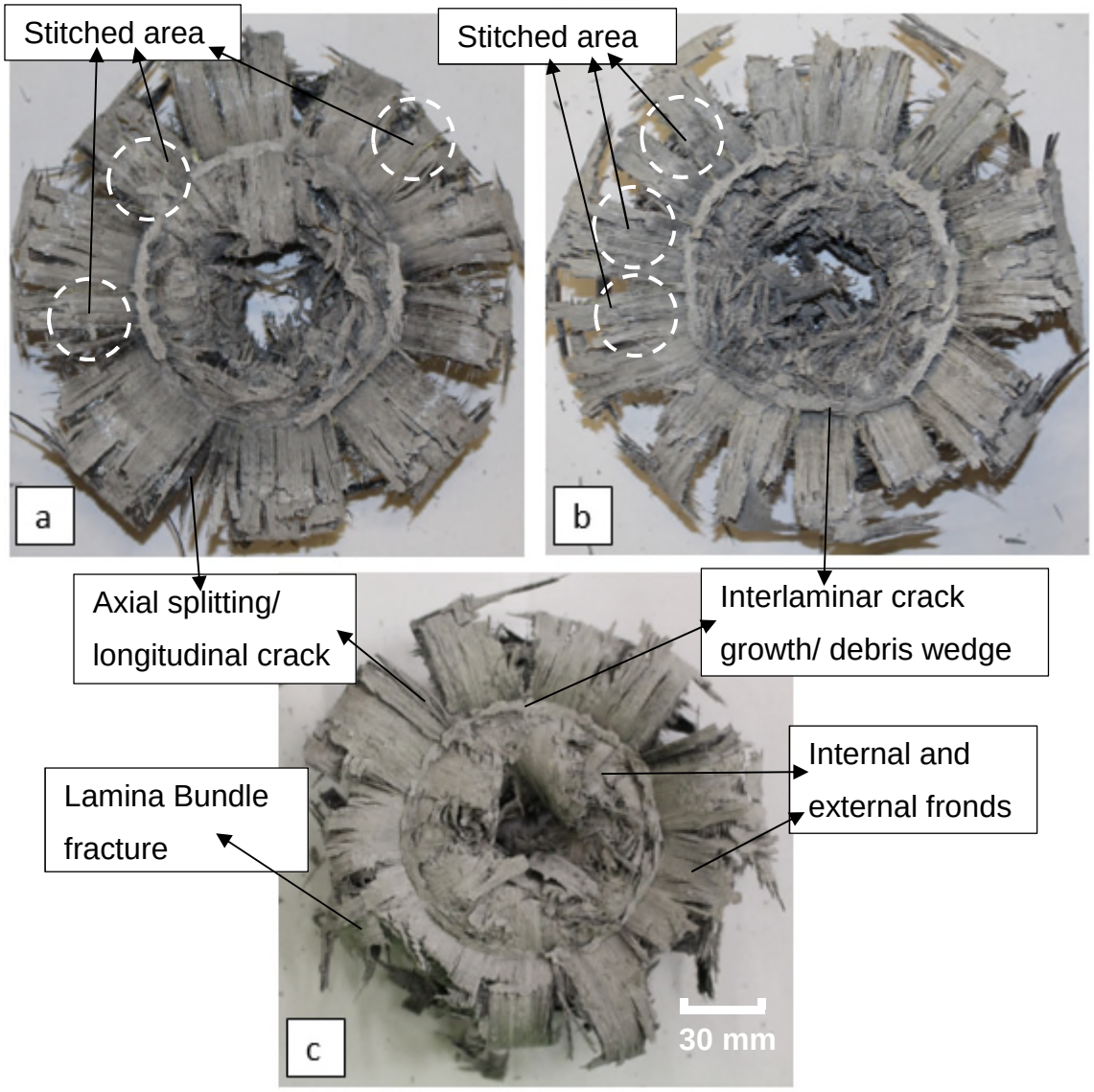

Figure 4-12 plane view of crushed pattern-stitched composite sections, a) 10-20-30 mm, b) 10-15-20-25-30-35 mm, c) non-stitched

In comparison of the force-displacement diagrams, Figure 4-13 a, shows all cases of pattern-stitched specimens against non-stitched specimen. Figure 4-13 b, represents non-stitched specimen compared with 10-20-30 mm stitched specimen. Three sudden increase in load is observed at the stitching locations, reaching highest peak of 125 kN. The sudden drops are controlled by the next stitching point throughout the crushing process, which consequently increases the mean crush force compared with all multi-stitched cases. The mean crush force was similar to non-stitched specimen. It can be noted that, as the number

of stitching locations increase, the drop in load, which occur after passing the stitching point is better controlled.

Figure 4-13 c, represents non-stitched specimen compared with 10-15-20-25-30-35 mm pattern-stitched specimen. Multi-sudden increase in load is observed followed by controlled drops in load. The highest observed peak value is 139 kN, this is the highest value among all other cases, which shows the closer the stitching points are, the crack propagation is better controlled and consequently increase of energy absorption capability. All peaks and drops are above the non-stitched curve and after passing all stitching locations, the normalisation is also higher than non-stitch curve. This design has shown higher mean crush force than all other designs as well as the non-stitched specimen. The mean crush force has increased by 16.3 kN.

This idea would be expanded to other designs followed by increase of stitched locations and reduction of the distance between them to create a smooth and progressive force history. The behaviour can increase the overall mean crushing force which is the ideal performance of composite absorbers. The presented technique is beneficial in terms of weight saving applications, as unidirectional FRP composites were used with the improved structural integrity.

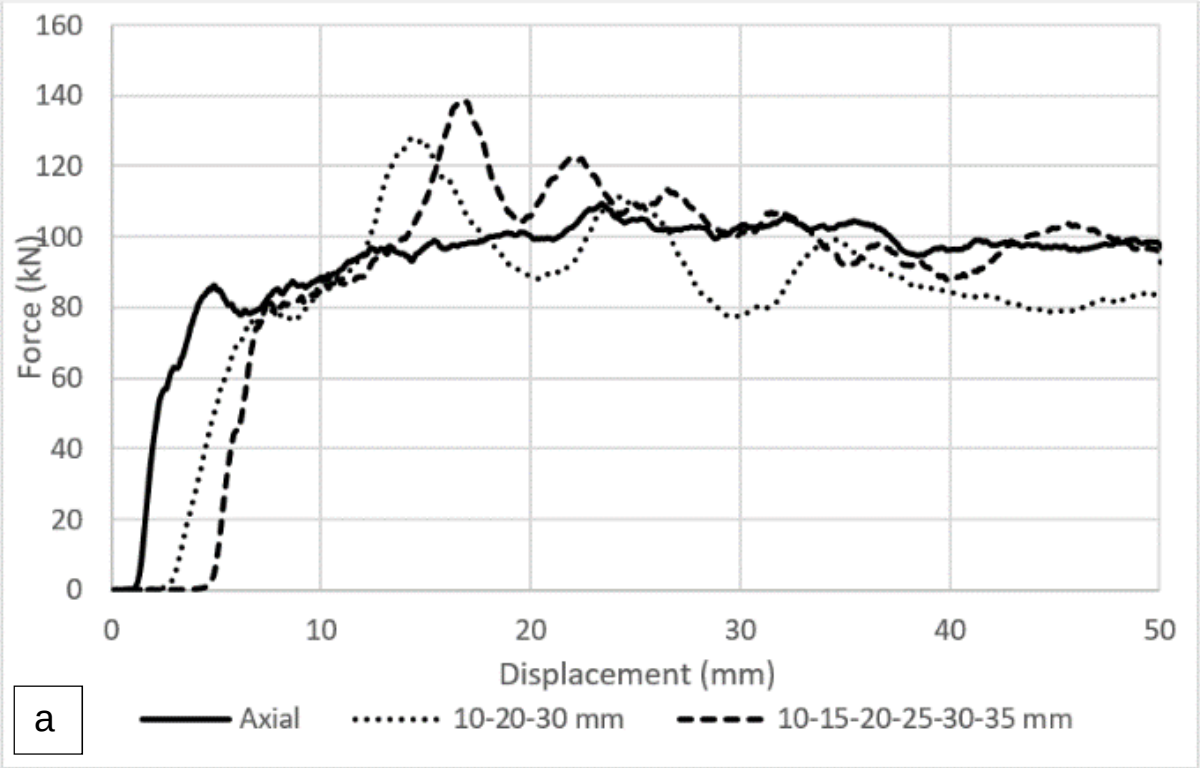
160
140
120
100
80
60
40
20
0
Force (kN)
0
10
20
30
40
50
Displacement (mm)
a
Axial
10-20-30 mm
10-15-20-25-30-35 mm

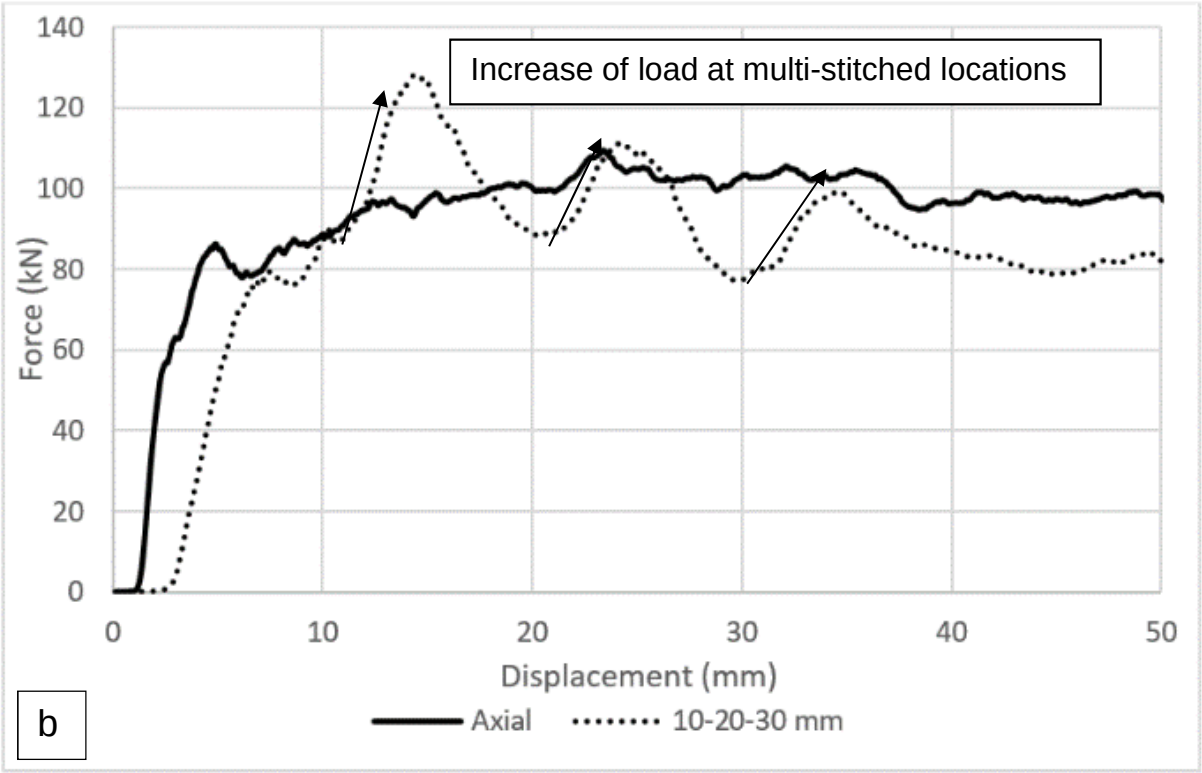
Increase of load at multi-stitched locations
140
120
100
80
60
40
20
0
Force (kN)
0
10
20
30
40
50
Displacement (mm)
b
Axial
10-20-30 mm

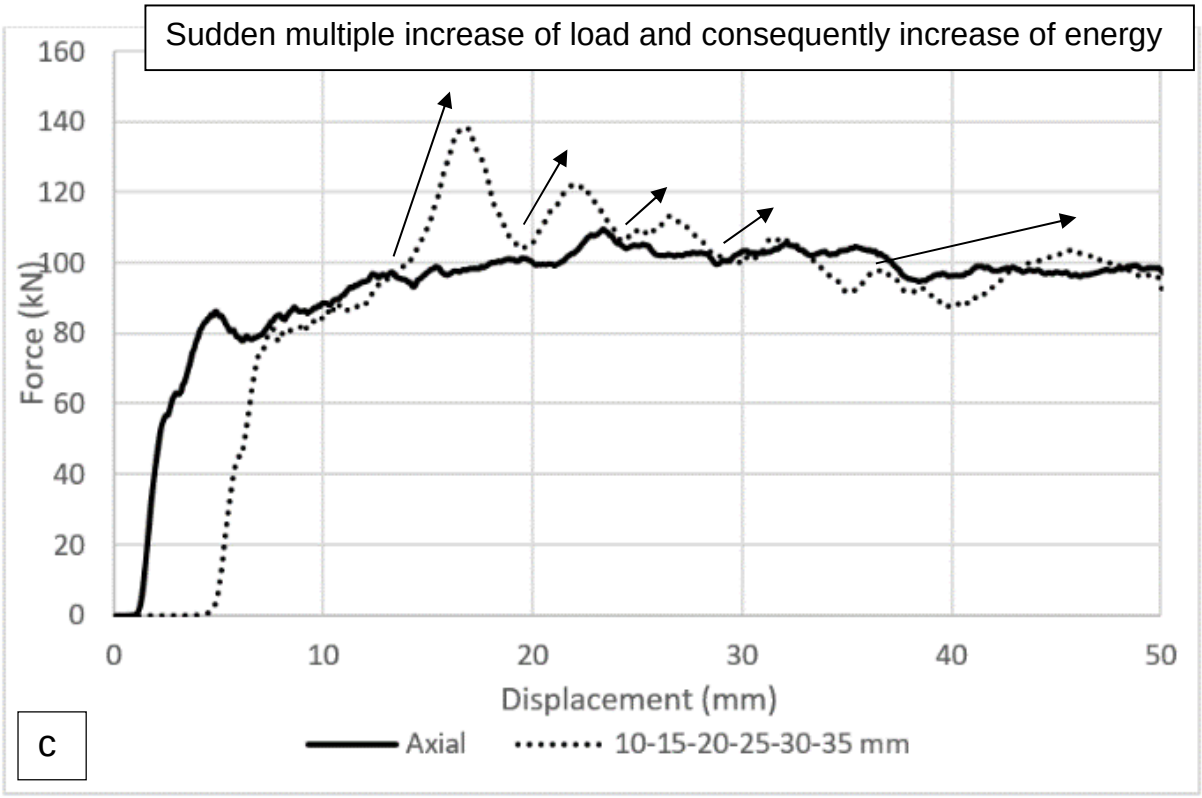

Figure 4-13 Force-displacement curve of pattern- stitched composite sections, a) comparison of non-stitched (axial) with 10-20-30 mm and 10-15-20-25-30-35 mm, b) non-stitched (axial) and 10-20-30 mm, c) non-stitched (axial) and 10-15-20-25-30-35 mm

4.5 Specific energy absorption (SEA) of single-stitched, multi-stitched and pattern-stitched specimens

The specific energy absorption for each case was plotted against non-stitched specimen (see Figure 4-12). The main objective of this chapter was to increase. Non-stitched specimen is the reference SEA with SEA value of 64 kJ/kg. The single stitched specimens at 10 mm, 20 mm and 30 mm had SEA values of rounded up to the nearest number of 58 kJ/kg, 61 kJ/kg and 66 kJ/kg respectively. At single stitched location of 30 mm the SEA has increased significantly. Similarly, the SEA values with stitching at 30 mm were higher in multi-stitched specimens. At multi-stitched locations of 10-20 mm, 10-30 mm and 20-30 mm the SEA values were 55 kJ/kg, 57 kJ/kg and 61 kJ/kg.

The main concentration of this research was to investigate the effect of stitching pattern on SEA and the values were remarkably high compared to non-stitched specimen. At stitching pattern of 10-20-30 mm the SEA value was 63 kJ/kg which is close to the non-stitched specimen, however once minimising the gap between the stitches, it led to higher delamination resistance, friction and bending that contributed to higher SEA value. The SEA value of stitching pattern of 10-15-20-25-30-35 mm was increased to 74.4 kJ/kg. In comparison to non-stitched specimen the final stitching pattern of 10-15-20-25-30-35 mm has increased its SEA value by 15%.

In this research, the focus was oriented on improving specific energy absorption capability by introducing stitching though the thickness and to study the location of single, multi and pattern stitching on specific energy absorption. The SEA has shown 15% improvement with 10-15-20-25-30-35 mm stitching pattern.

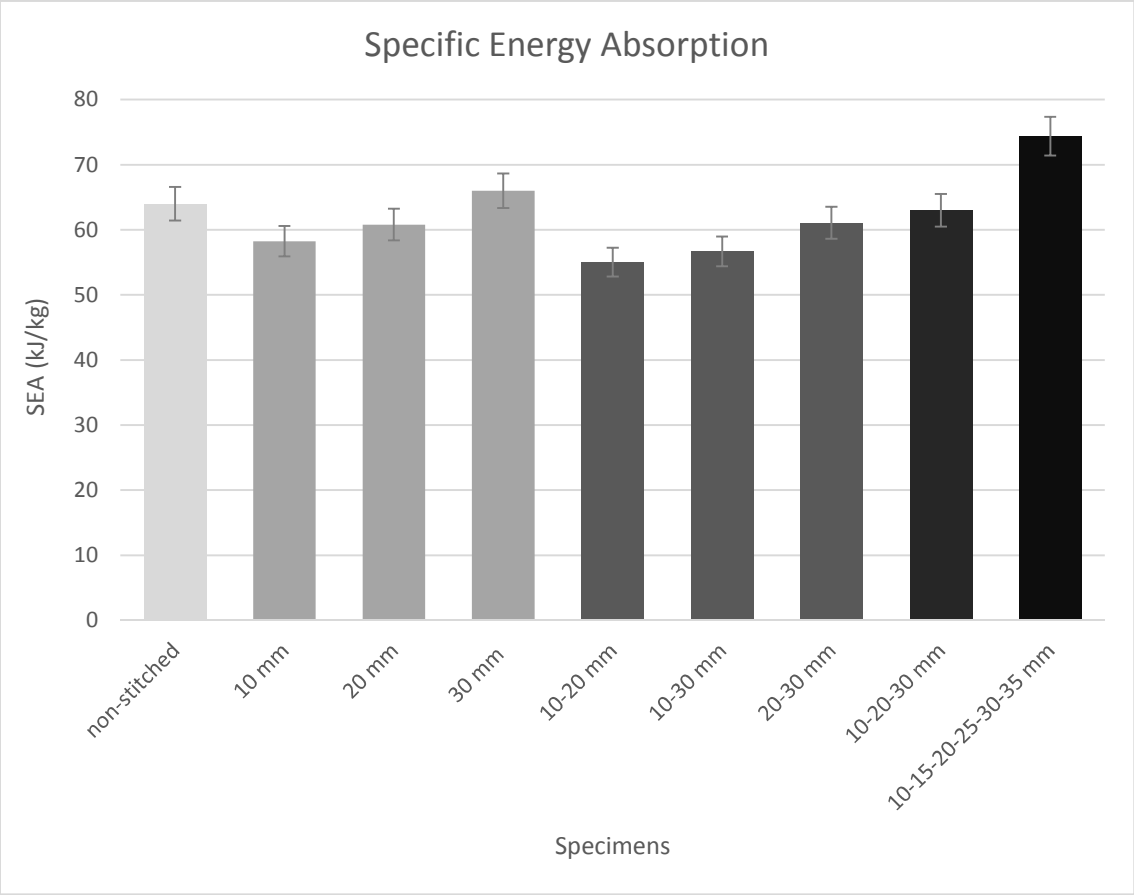

Figure 4-14 Comparison of Specific Energy Absorption (SEA) of single-stitched, multi-stitched and pattern-stitched composite section

4.6 Conclusions

In this study, the crushing behaviour and energy absorption capability of composite tubes under crushing rate of 2 mm/sec have been studied. In axial crushing, Kevlar yarn stitching through the thickness at different locations was introduced and illustrated a steady mean crush load which was obtained for the stitched specimens. Progressive crushing behaviour was observed for all stitched specimens. Single stitched locations showed high peaks followed by a sudden drop specially at 10 mm stitching location and at 30 mm the drop in load was significantly lower, which showed better normalisation after passing the stitching point. In multi-stitched locations, the behaviour was different, the sudden drops were better controlled specially where the stitching points were 5 mm apart. This also reflected on the mean crush force, and higher values were obtained once the stitching points were closer. Further the stitching points were, the lower the mean crush force was. This scenario was also clearly observed in pattern-stitched specimens, in 10-20-30 mm design, three high peaks were observed followed by controlled drop in load, although the mean crush force was similar to non-stitched specimen with minimal differences. However, in 10-15-20-25-30-35 mm pattern-stitch, the initial peak was higher than all other cases due to higher resistance towards crack propagation. Multiple peaks were observed with controlled drops in load, and all fluctuations were higher than non-stitched specimen. The normalisation of the curve was also higher than the non-stitched specimen. It can also be noted that by increasing the number of stitching points, the axial cracks, bundle fracture and fragmentation failure mechanism also increased, due to increase in fracture toughness capability that influence this delamination resistance and improving friction and bending between the plies and consequently increase in local and global mean crush force that causes higher specific energy absorption capability due to brittle failure mechanism which is a combination of fragmentation and laminar bending modes. Pattern-stitching through thickness reinforcement has shown enormous improvement in Mode-I delamination resistance with higher friction and bending that contributed towards higher SEA value than non-stitched specimen. The specific energy absorption of the final design compared with non-stitched specimen is 15% higher.

In summary, stitching at a right position can provide increase in specific energy absorption values than the standard non-stitched composite absorbers; this is an important factor to consider achieving better specific energy absorption in composite structures (see Figure 4-14). Stitching at locations of 30 mm, multi-stitched locations of 10-20-30 mm and 10-15-20-25-30-35 mm, can provide the highest energy absorption capabilities with increase of mean crush load tolerance which indicates a stable crashworthy behaviour respectively.

The present study has established sufficient information on the effect of single and multi-location stitching on high speed crushing of composite tubes, and the positive effects of stitching through thickness was found both on local and mean crushing load. The results of this research have also been compared to previous similar work [145] which was carried out on single stitched composite box structures. These results clearly show that cylindrical tubular structures have significantly absorbed higher energy in comparison with box absorbers (see Figure 4-7). The difference in non-stitched mean crush force is 23 kN and stitched mean crush force is 19 kN. In both studies Kevlar fibre yarn was used for reinforcing the structure.

5 Experimental Studies of Pattern-Stitched Composite Sections under Quasi-Static and Impact Loading

5.1 Introduction

Extensive experimental investigation was carried out on the effect of stitching pattern on energy absorption capability of composite tubular structures under quasi-static and impact loading. In the previous chapter the effect of single, multi and pattern stitching was experimentally investigated. The designed pattern stitching of 10-15-20-25-30-35 mm performed outstandingly regarding specific energy absorption with 15% improvement compared with non-stitched specimen. Hence in this chapter, the main concentration is the effect of through the thickness stitching pattern on energy absorption capabilities and improvement of mean crushing load using the developed pattern. CFRP and GFRP composite absorbers are subjected to the developed stitch pattern and both materials are subjected to quasi-static and impact loading. This enables to study the effect of the developed stitch pattern on specific energy absorption when subjected to impact loading and to study the energy absorption capability of these composite absorbers. The force-displacement history and crushed morphologies are studied and compared with non-stitched specimens. The stitching pattern on both materials showed significant improvement under quasi-static and impact loading conditions. The CFRP and GFRP stitched specimens subjected to quasi-static loading showed increase in SEA percentage values of 14% and 15% respectively. Similarly, the CFRP and GFRP stitched specimens subjected to impact loading showed increase in SEA percentage values of 18% and 17% respectively.

In all previous researches several parameters were investigated to increase interlaminar fracture toughness in composite thin-walled absorbers. The effect of multi-stitched locations and patterns have been previously studied and significant influence was observed on energy absorption capabilities by increasing interlaminar fracture toughness under quasi-static loading whist increasing friction and bending that contribute towards SEA value. However, in real life applications, standard impact test should be carried to investigate the material

behaviour under impact loading. This chapter experimentally aims to improve interlaminar fracture toughness, friction and bending by introducing pattern-stitched locations under quasi-static and impact loading using CFRP and GFRP composite sections. Consequently, this method enables to increase specific energy absorption capabilities.

5.2 Experimental method

5.2.1 Material and specimens

Two different materials were selected to study stitching pattern under quasi-static and impact loading. In previous studies pre-preg GFRP was used to carry out an extensive research on the location of stitching and energy absorption capabilities. Based on previous results, from the top of the specimen 10-15-20-25-30-35 mm stitching pattern when subjected to quasi-static loading significantly improved energy absorption capabilities. The developed stitching pattern was obtained in the last chapter with 15% increase in SEA, this was applied onto CFRP composite sections (see Figure 5-5). CFRP and GFRP composite sections were chosen to study the effect of stitching pattern on the crushing behaviour of composite tubes. Both materials showed different failure mechanisms and absorbed energy in different ways. All dimensions are illustrated in Figure 5-1.

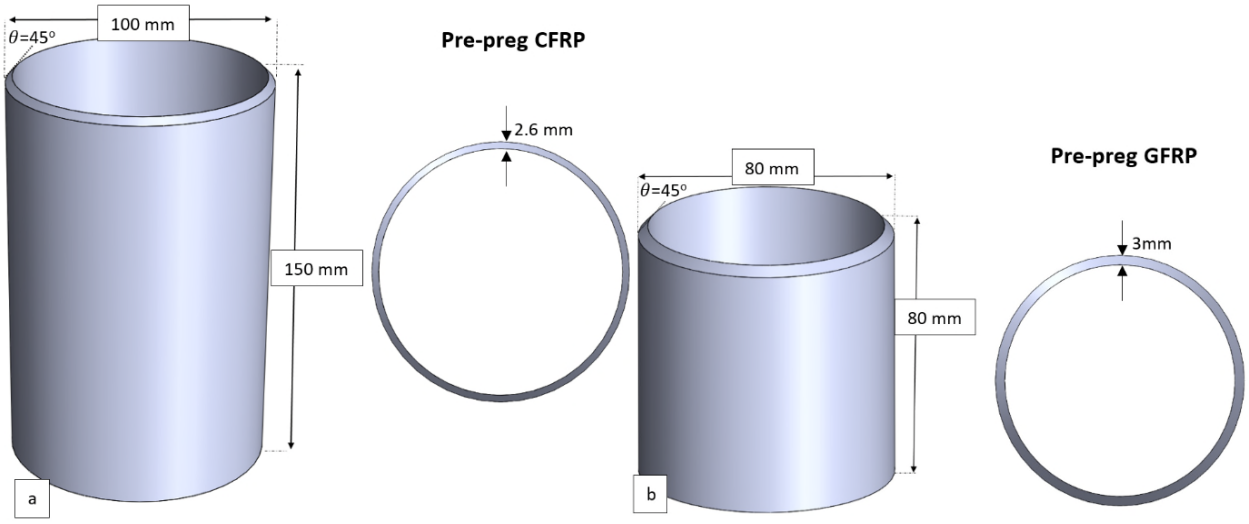

Figure 5-1 Composite absorbers for a) CFRP and b) GFRP geometry configurations

In this study, composite sections were fabricated from glass/epoxy (ρ = 2250 kg/m^3) (TenCate 7781/E772) with laminate design of $[-45/45/0/90/0/90]_S$ to create a symmetric twelve-ply laminate and carbon/epoxy (ρ = 1800 kg/m^3) (Hexcel T300/914C) with laminate design of $[-45/45/-45/45/0/90/0/90/0/90/0]_S$ using hand lay-up techniques. Each GFRP layer has a thickness of 0.25 mm after curing and each CFRP layer has a thickness of 0.118 mm after curing.

The curing process was based on the manufacturer's recommended techniques. The CFRP plies were stacked onto a mandrel, with adding each ply to the laminate, it was subjected to 15 minutes debulking to minimise airgaps between each added layer to the layer beneath. The mandrel was sealed using heat resistant non-stick polymer to eliminate 'resin escape', this method reduces the available room for the resin to escape to. The mandrel and the laminate were then covered with 'breather cloth' to allow air to circulate in the bag for better pressure distribution and sealed in a vacuum bag using heat resistant polymer bag, which is open from two sides. This was fully sealed using a double-sided epoxy tape. Air suction valve is inserted through the sealed bag once sealed, connected to a vacuum pump. Using the breather cloth and vacuum combination enables the maximum pressure to be applied on to the composite laminate to eliminate air gap and delamination with good adhesion between the plies. Following the manufacture's guidance, a pressure gauge was inserted via a second valve to monitor the correct pressure in the bag. This can also be beneficial to check if the bag in fully sealed or pressure drop once the vacuum is switched off. Four to six specimens were tested in each case of study to find the mean deviation of the experimental results. Force displacement curve was the main concentration of this research to study the energy absorption capability and load carrying capability of each case of study against their SEA value to carry-out a comparison between stitched and non-stitched specimens.

The progressive crushing in all specimens were initiated with 45^o bevelled trigger mechanism. All parameters that effected energy absorption capabilities were kept constant in fabrications and testing conditions of GFRP and CFRP composite tubes. These parameters include, geometry, lay-up, strain rate and loading to

concentrate on the effect of stitching-through the thickness. The objective of this research, is to isolate the effect of stitching through the thickness on energy absorption capability, and to improve specific energy absorption capability.

5.2.2 Quasi-static experimental setup

Quasi-static testing was conducted using a hydraulic press with load cell capacity of 500 kN with loading rate of 2 mm/second. All specimens were placed at the centre of the stroke for equal load distributions. The stroke displacement for all specimens was 50 mm. The profile of load-displacement consists of load cell and stroke displacement.

5.2.3 Impact experimental setup

Impact testing was conducted by using a spring loaded drop tower with impactor mass of 108.4 kg and drop height of 2.0 m with initial velocity of 7.022 m/s for all specimens. The configuration of spring and predetermined drop height enables to achieve higher velocity. In this case, the drop tower was set up for maximum output energy. The machine recorded a kinetic energy of 2672 Joules being applied to the specimens which is the maximum output energy of the drop tower. The hammerhead was released from a pre-determined height to initiate and record the load against time until it reaches the specimen and penetrates through the specimen, at this stage the impactor is decelerating and once the impact energy of 2672 J is absorbed by the specimen the impactor stops and the hammer then is pulled up by the machine. The tube leading edge impacted the dynamic load cell to record the force history during the event. An Accelerometer is also used to record the data from the load cell in addition, sampling at 200,000 Hz by dynamic data acquisition system. Displacement is obtained through double integration of acceleration traces, and load cells gave the load values which is calculated based on the displacement equation. A high-speed video camera with full HD resolutions (2,000 frames per second) was used to capture the crushing event.

5.3 Experimental results and discussion

5.3.1 Crushing morphology of multi-stitched tubes

5.3.1.1 CFRP and GFRP under quasi-static loading

Figure 5-2, represents the post-crushing plane morphologies in quasi-static loading in both GFRP and CFRP specimens. The aim of introducing stitching through the thickness was to improve the interlaminar fracture toughness and consequently improving energy absorption capabilities. Figures 5-2 a and 5-2 c are non-stitched specimens and 5-2 b and 5-2 d are the stitched ones. CFRP specimens showed failure mechanisms of fragmentation with fibre fracture. A number of bundle fractures were also observed for CFRP specimens. This mode changed in GFRP specimen, to shape continuous internal and external fronds through a combination of brittle fracture and lamina bending fracture mechanisms.

By introducing stitching through the thickness, brittle failure mechanism appeared in GFRP specimen. This was the prevailing failure mechanism in GFRP stitched specimen (d), followed by lamina bending unlike non-stitched specimen. In CFRP stitched (b) bundle fracture increased through external frond formation. The dominant failure mechanism in CFRP section both stitched and non-stitched was through fragmentation failure mode.

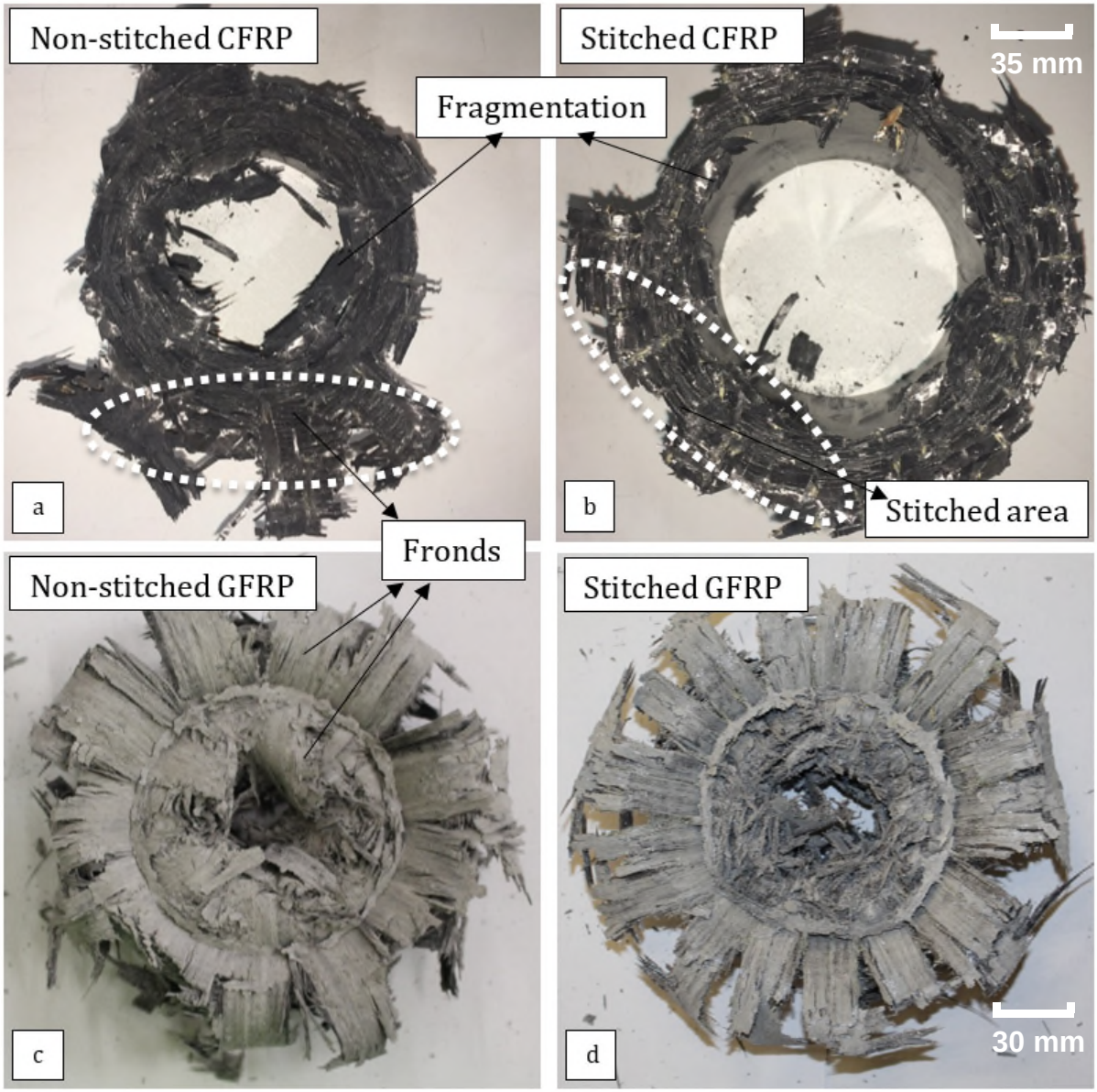

Figure 5-2 CFRP and GFRP plane morphology under quasi-Static loading

5.3.1.2 CFRP and GFRP under impact loading

Various stages of impact testing of CFRP and GFRP is shown in Figure 5-3. It was observed that the failure mechanisms in Figure 5-4 a and 5-4 b (CFRP) are fragmentations, with multiple short interlaminar and axial cracks. In Figure 5-4 c and 5-4 d, representing GFRP tubes, the failure mechanisms are a combination of lamina bending and transverse shearing mode, which is brittle fracture mode. Bundle fractures and lamina bending were observed with multiple short interlaminar and axial cracks. The difference between quasi-static and impact

testing plane morphologies is the transverse shearing mode with multiple short interlaminar cracks in addition to brittle fracture and lamina bending fracture mechanisms.

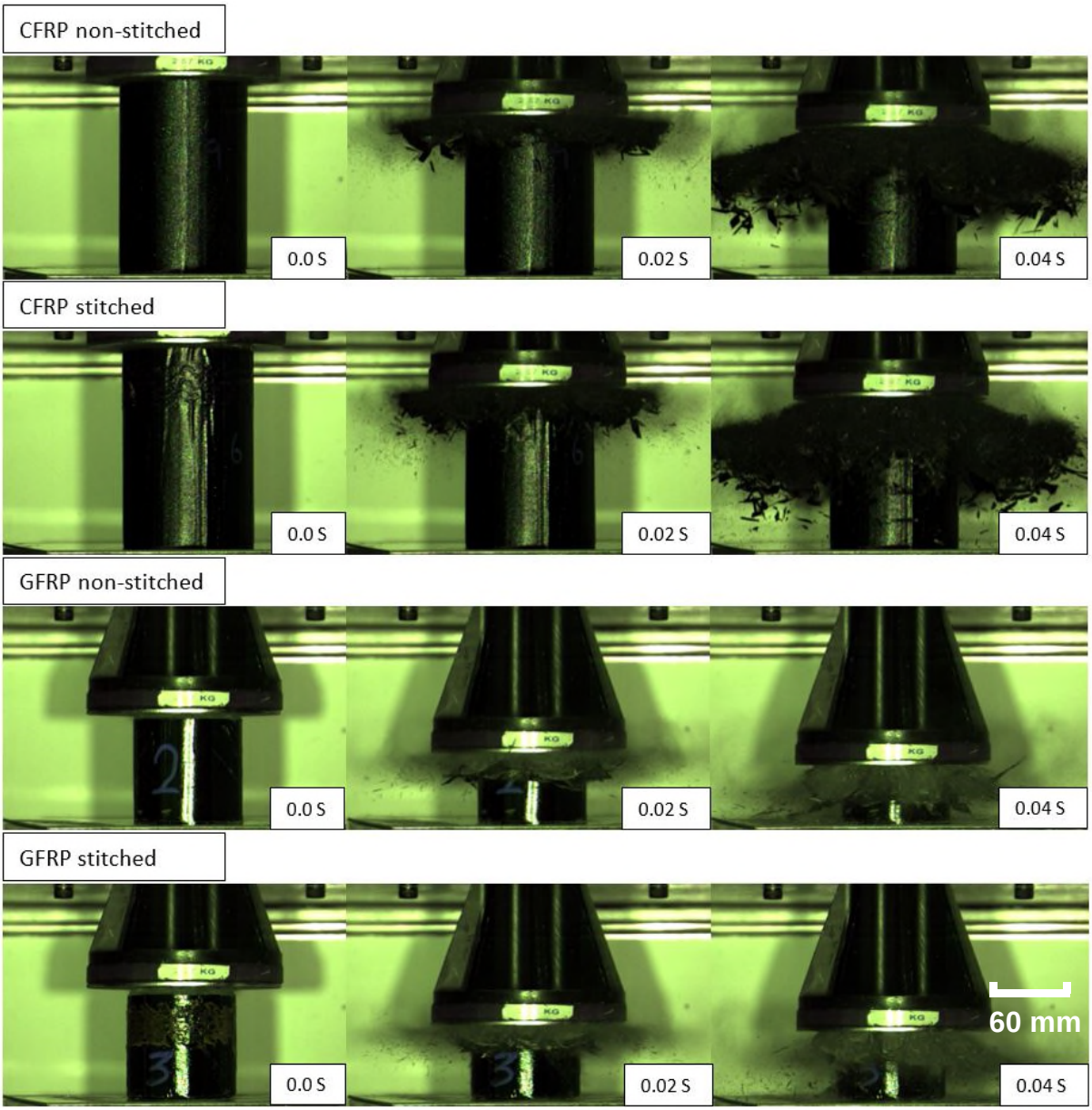

Figure 5-3 Process stages of impact testing at 0, 0.02 and 0.04 seconds, a) non-stitched CFRP b) Stitched CFRP c) non-stitched GFRP d) Stitched GFRP

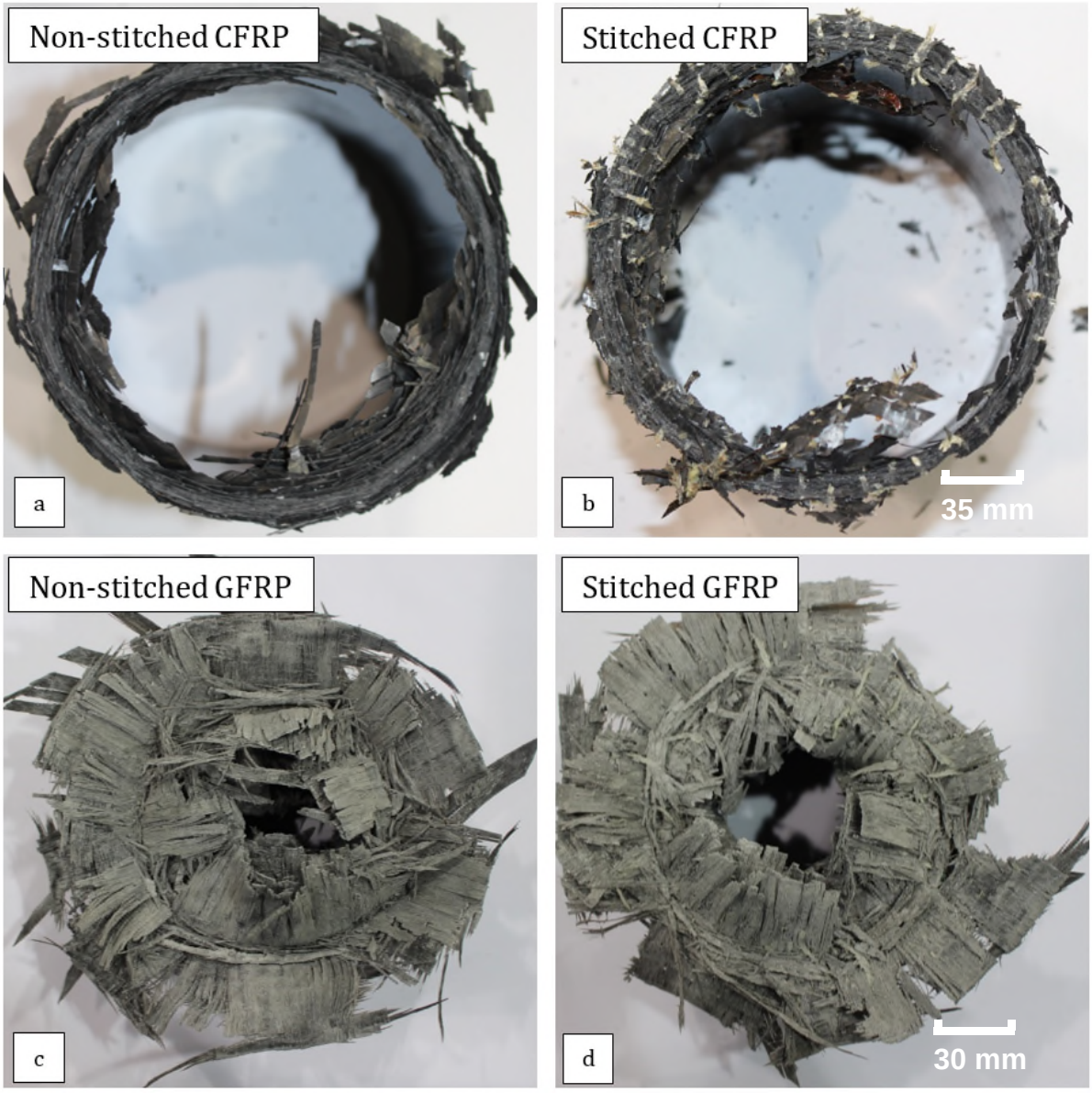

Figure 5-4 Impacted CFRP and GFRP plane morphology a) non-stitched CFRP b) stitched CFRP c) non-stitched GFRP d) stitched GFRP

5.3.2 Force-displacement profile of multi-stitched tubes

5.3.2.1 CFRP and GFRP under quasi-static loading

GFRP and CFRP specimens were tested and plotted against stitched and non-stitched specimens. The stitching pattern which was used to increase interlaminar fracture toughness in composite sections is shown in Figure 5-5.

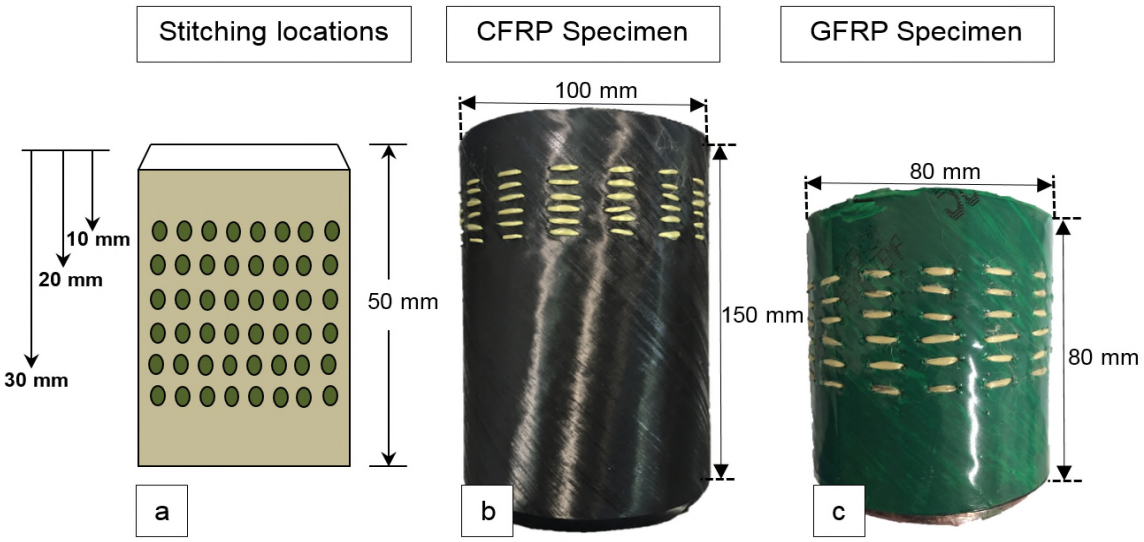

Figure 5-5 a) Multi-Stitched locations at 10-15-20-25-30-35mm and b) uncured CFRP multi-stitched specimen

As expected, tubes with the stitching pattern have shown better energy absorption capability than non-stitched specimens in both CFRP and GFRP specimens. Introducing stitching pattern, caused a sudden increase in load and consequently an increase in energy absorption capabilities indicating a significant increase in crashworthiness behaviour. Four to six specimens were tested in each case of study to find the mean deviation of the experimental results. Figure 5-6 shows five GFRP multi-stitched tested specimens under quasi-static loading, and the mean deviation is plotted.

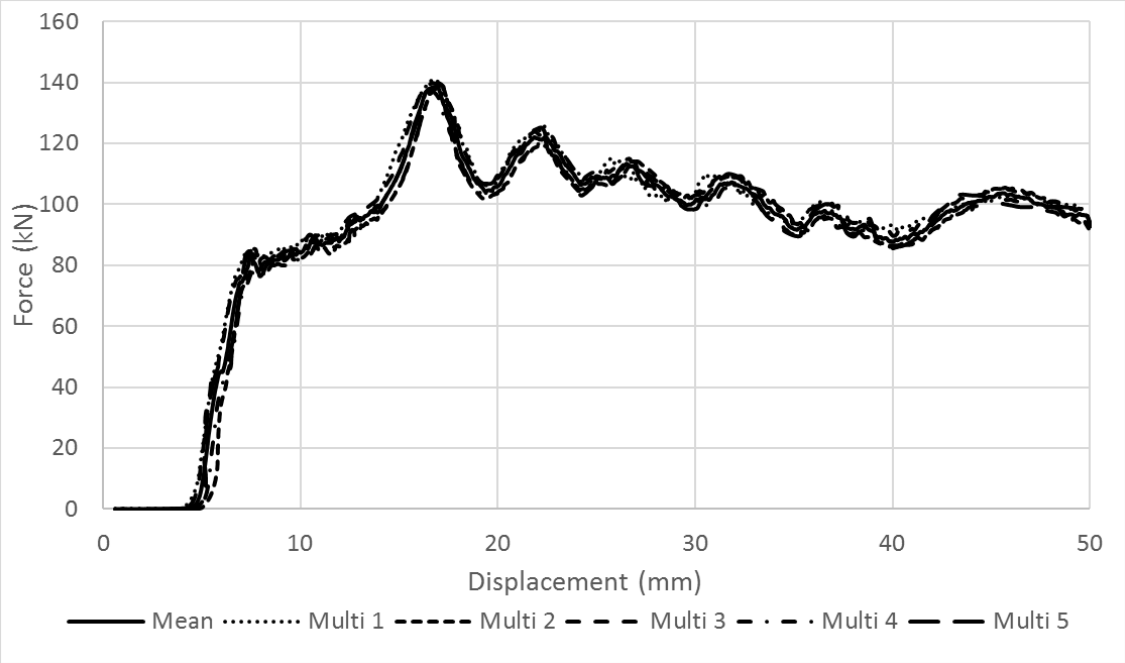

Figure 5-6 Five multi-stitched GFRP specimen repeat tests with mean deviation

All absorbers had progressive crushing behaviour with extensive microcracking collapse and rapid sudden increase in load in the stitched locations. Crushing behaviour of GFRP initiates progressively until it reaches the stitched area (see Figure 5-7). At this point, a sudden increase in load is observed and consequent increase of SEA value. In CFRP specimens, a similar trend is observed (see Figure 5-8). The energy absorption capability has increased significantly until it passes the stitched locations that a normalisation with higher value than non-stitched specimen is observed. The overall performance of both GFRP and CFRP cases show a significant increase in energy absorption capabilities without additional weight to the structure, which indicates significant increase in crashworthiness behaviour and specific energy absorption capability.

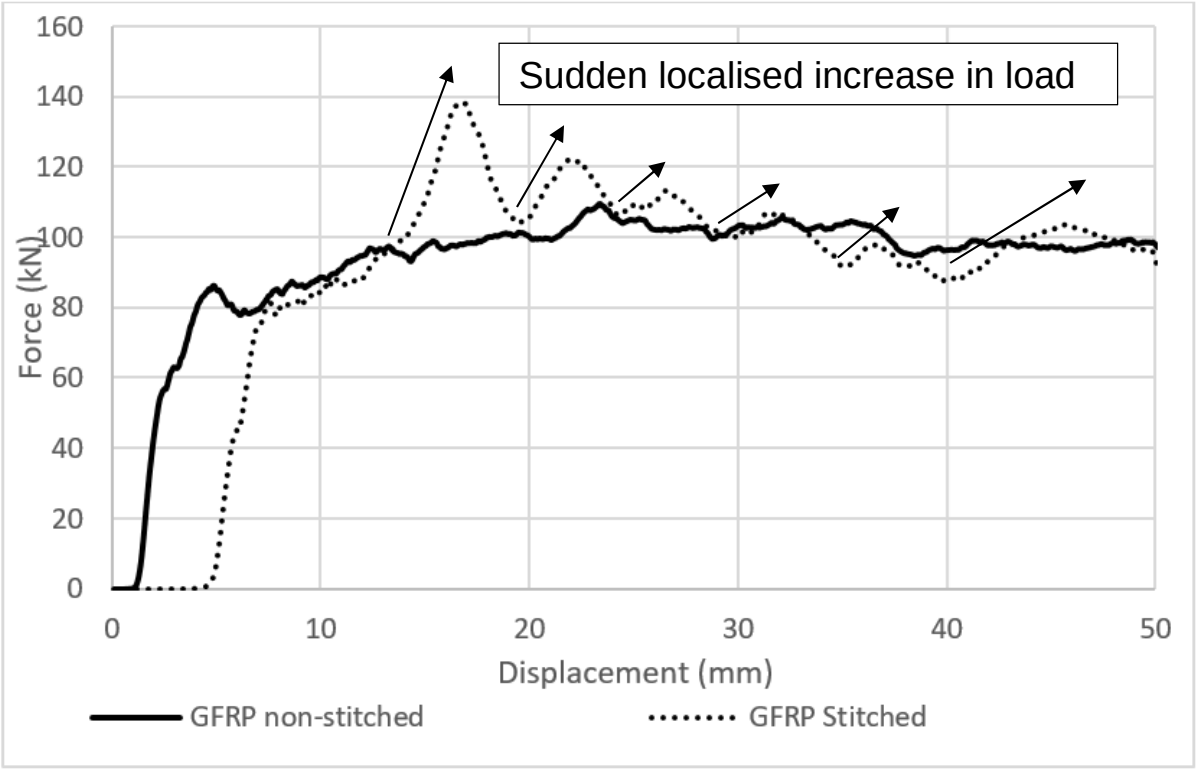

Figure 5-7 Force-displacement of GFRP stitched and non-stitched under Quasi-static loading

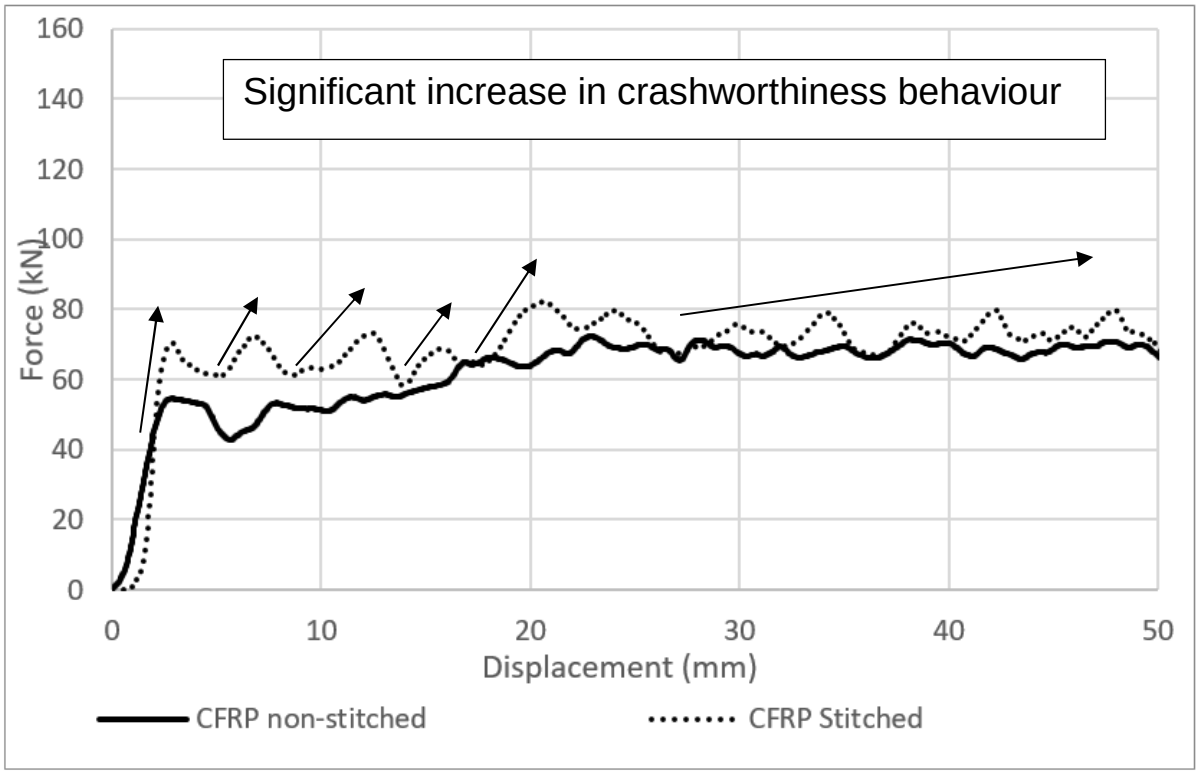

Figure 5-8 Force-displacement of CFRP stitched and non-stitched under Quasi-static loading

5.3.2.2 CFRP and GFRP under impact loading

Figure 5-9 compares the load-displacement curves of GFRP stitched and non-stitched specimens under impact loading. Similarly, Figure 5-10 compares the load-displacement curve of CFRP stitched and non-stitched specimens under impact loading. The results clearly show a significant increase in load and energy absorption capability. The crashworthiness behaviour of stitched GFRP has increased significantly, indicated by a reduction of stroke displacement. Stitched GFRP section performed outstandingly by reducing the stroke displacement by 10 mm (25% improvement/recovery) and absorbing the same amount of energy as non-stitched specimen which was 2672 Joules. By reducing the penetration distance and absorbing the same amount of energy the composite section has shown better crashworthy behaviour. This displacement reduction, indicates that having the same displacement as the non-stitched specimen, stitched specimen is able to absorb more energy than the non-stitched one.

Stitched CFRP specimen showed a similar characteristic, as it was able to absorb the applied energy within a shorter stroke displacement (4.5 mm).

The aim of introducing stitching through the thickness was to increase interlaminar fracture toughness, friction and bending that consequently increases energy absorption capability and this has been achieved in both cases. The force-displacement diagrams do not start from zero as the sensors were off by 2 millimetres from the top of the specimen, from a predetermined setup. The gap between the striker and the tube is determine before the test and the margin was misread, hence the graphs, initiated after the crushing process took place, although the material stiffness and behaviour is unaffected.

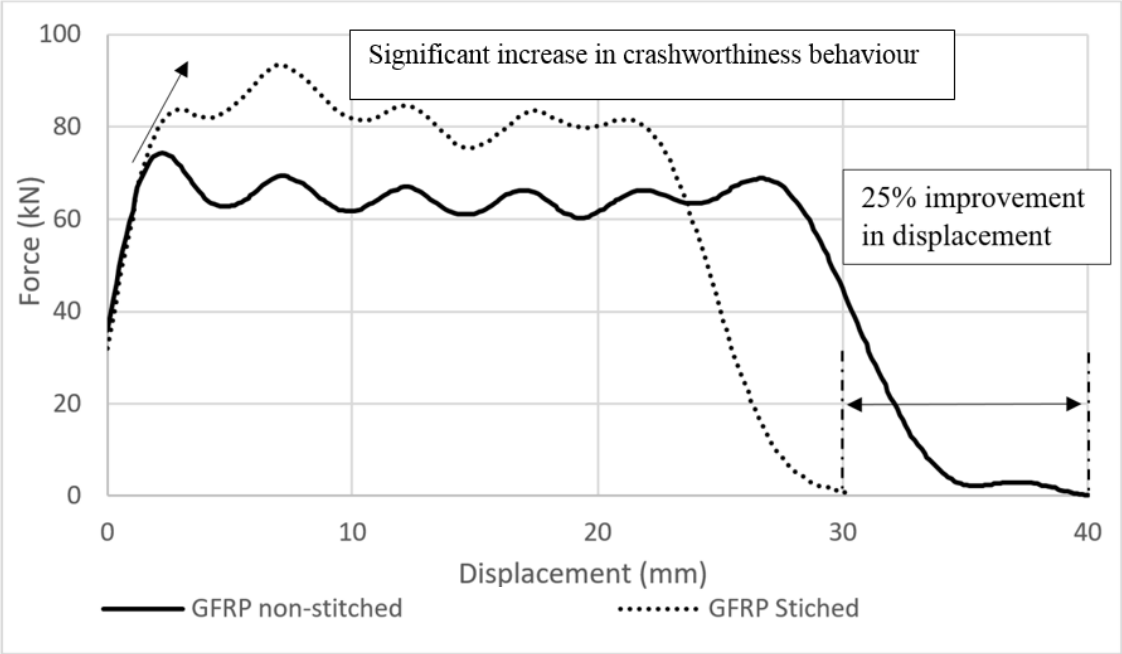

Figure 5-9 Force-displacement of GFRP stitched and non-stitched under impact loading

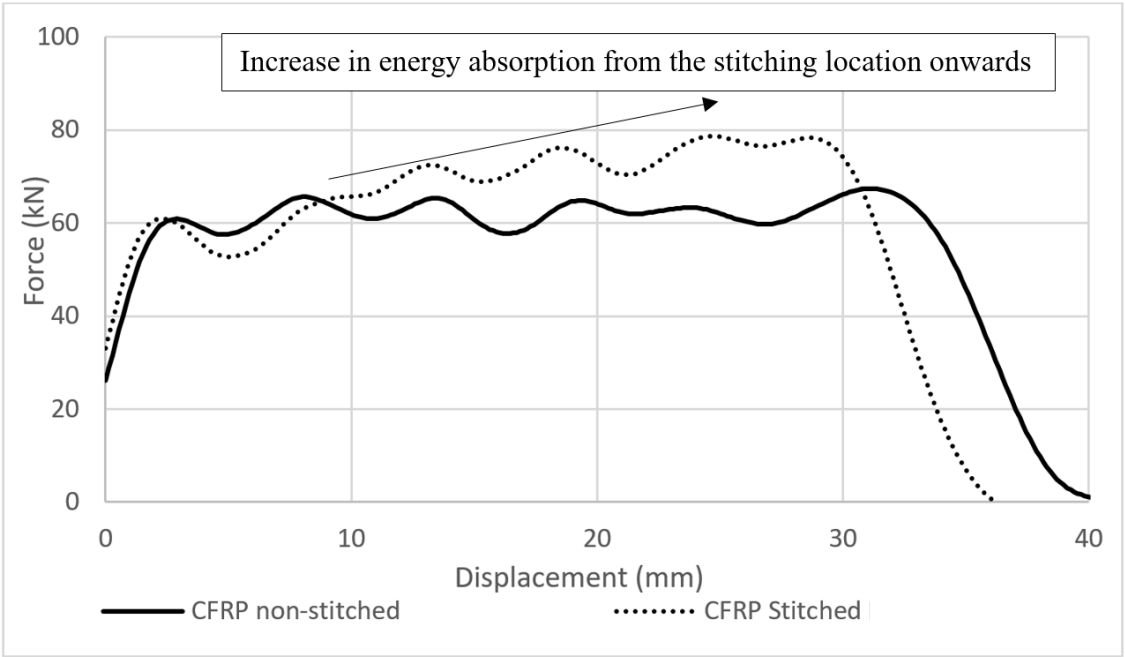

Figure 5-10 Force-displacement of CFRP stitched and non-stitched under impact loading

5.3.2.3 Re-stitching of CFRP specimen to improve SEA

The CFRP specimen has shown some improvements in energy absorption capability, however, further investigation on the crushed morphologies has indicated that the fibres were partially bonded with matrix (see Figure 5-11). This has affected the potential energy absorption capability of the specimen. To be fully cured, a fibre yarn that bonds well with 914 epoxy resin must therefore be used. In this case the Kevlar yarn has shown some bonding capability with the resin. GFRP and CFRP yarns are used on a laminate fabricated from UD CFRP with resin 914 to observe their bonding capability (see Figure 5-12).

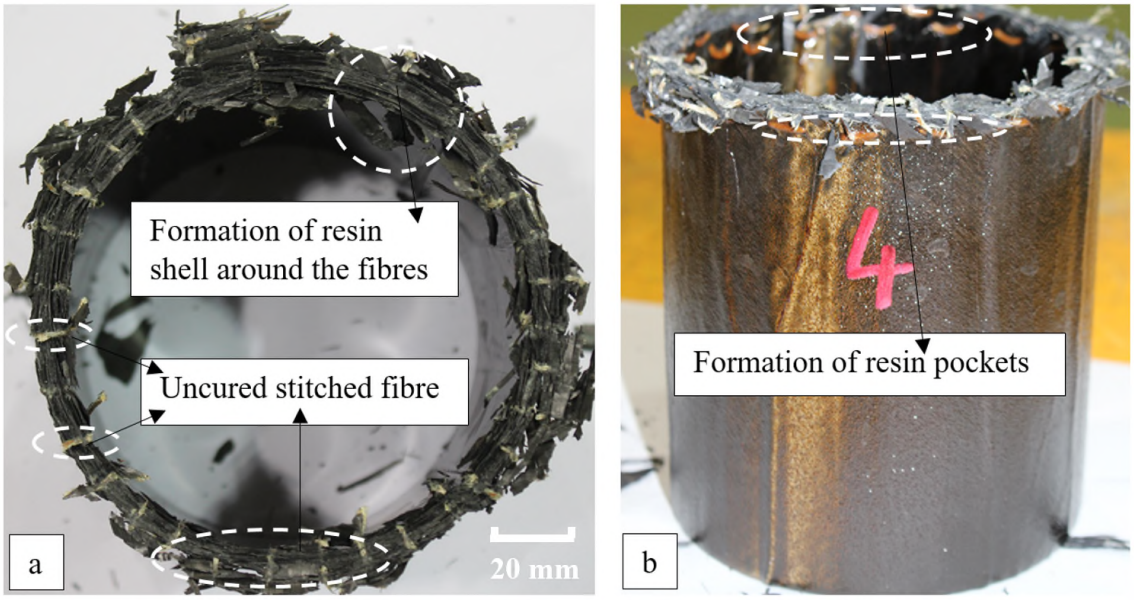

Figure 5-11 a) Formation of resin shell and uncured fibres b) formation of resin pockets

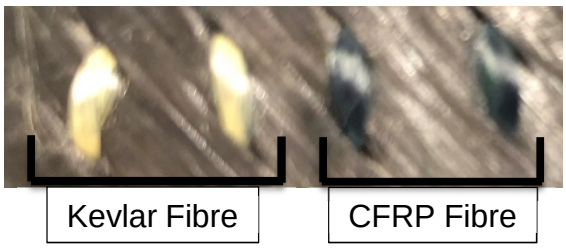

Figure 5-12 GFRP and CFRP stitched on uncured Laminate

The CFRP fibre yarn have fully bonded within the structure after curing process. This was used to construct and fabricate another sets of tubes with CFRP fibre yarn pattern-stitching to compare the fully cured specimen and its effect on energy absorption to partially cured specimen. Using the same fabrication techniques and testing setup (see Chapter 5.2.1 and 5.2.3), the following force-displacement was obtained (see Figure 5-13). Figure 5-13, shows the effect of fully cured CFRP specimen against partially cured specimen. The initial peak has increased to 70 kN and the mean crushing force is 77 kN with reduced displacement to 33 mm. The performance of the fully cured specimen has improved greatly influenced by stitching through the thickness. The fully cured specimen showed higher peak values and mean crushing force has significantly improved. This crashworthiness behaviour compared with non-stitched specimen shows higher specific energy absorption capability with similar penetration distance reduction as GFRP specimen.

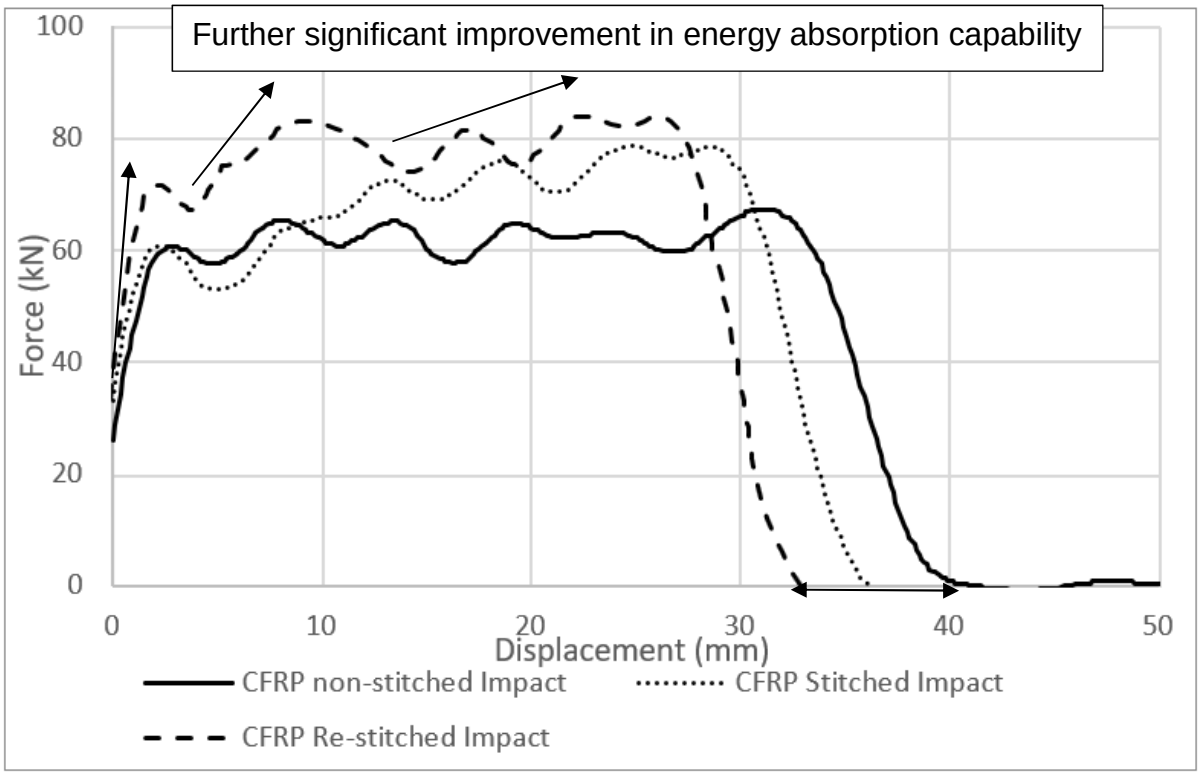

Figure 5-13 Force-displacement curve of fully cured specimen and partially cured specimen

5.3.3 Quasi-static versus impact loading

In this work, the effect of stitching pattern on energy absorption capability was studied. In both cases, CFRP and GFRP have shown increase in load and energy absorption capability by introducing stitching through the thickness. In quasi-static loading, the crushing rate is constant, this enables to investigate the energy absorption capability of the material being tested and set a reference line for material performance. The constant value is set to control the displacement which is in this case set to 2 mm/sec, and the load is plotted against the stroke displacement on the force-displacement diagram.

Impact load is a suddenly applied load, therefore, the applied energy is set to be absorbed by the specimen, the hammer head penetrates through the specimen until the applied energy is fully absorbed. This simulates a real-world scenario in a crashing event. Under quasi-static loading higher energy absorption is observed. This is due to failure mechanisms differences between the two. In impact loading of GFRP (see Figure 5-14), the most dominant failure is through Mode-I, laminar bending with multiple-short interlaminar crack propagation and bundle fracture, transverse shearing is also observed with short interlaminar and longitudinal cracks. In quasi-static, the dominate failure was through Mode-I where the main central crack in the mid-section of the tubes were an indication of Mode-I interlaminar crack propagation along with laminar bending. The combination of fragmentation and laminar bending modes is brittle fracture mode that gives the highest energy absorption capability. In impacted GFRP specimen, the fragmentation is less observed, and the laminar bending failure mode compared with the specimen subjected to quasi-static testing is dominating which led to lower energy absorption. Both specimens subjected to quasi-static and impact loading had brittle fracture failure modes with different combinations of laminar bending and transverse shearing mode, hence the lower energy absorption capability. In both stitched specimens subjected to quasi-static and impact loading, increased longitudinal cracks within the petals are prevailing. In CFRP (see Figure 5-15), the failure mechanism obtained from both impact and quasi-static tests were through fragmentation, due to this, the curve is similar with minimal failure mechanism differences.

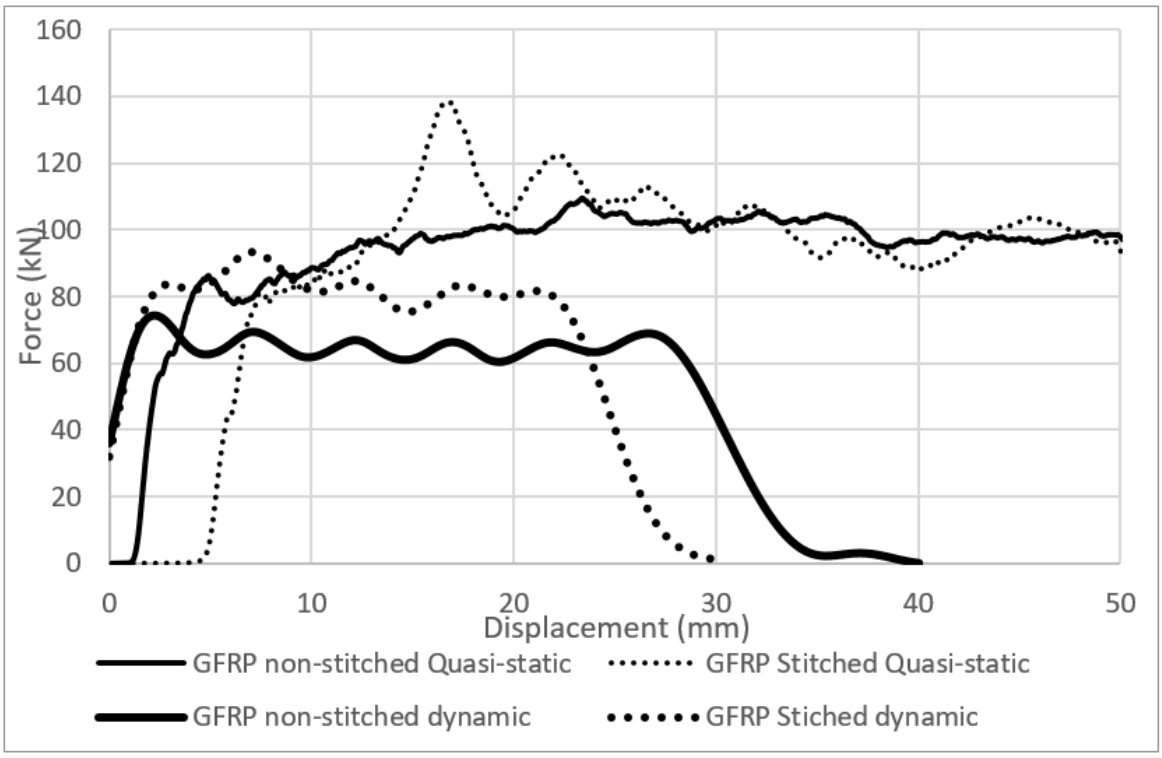

Figure 5-14 Force-displacement curve of GFRP quasi-static loading versus dynamic loading

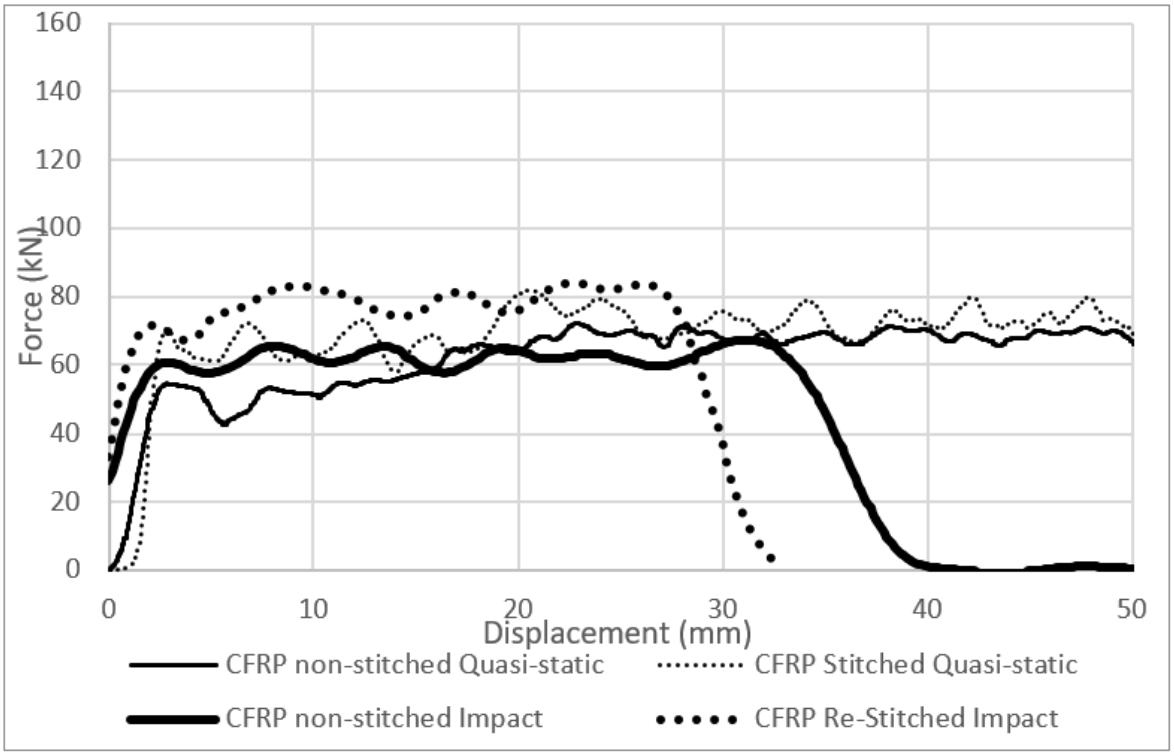

Figure 5-15 Force-displacement curve of CFRP quasi-static loading versus dynamic loading

5.4 Specific energy absorption of multi-stitched CFRP and GFRP subjected to quasi-static and impact loading

Figure 5-16 a, represents the stitched and non-stitched, CFRP and GFRP specimens under quasi-static loading. Stitched GFRP showed the highest SEA with SEA value of about 74.4 kJ/kg with 15% higher value in comparison with non-stitched specimens with SEA value of about 64 kJ/kg. The stitched CFRP reached higher SEA value in comparison with non-stitched specimens with the total SEA value of 62.5 kJ/kg (14% difference).

Figure 5-16 b represents the stitched and non-stitched, CFRP and GFRP specimens under impact loading. SEA value of the non-stitched GFRP which was about 46 kJ/kg and stitched GFRP with SEA value of 54.8 kJ/kg under impact loading showed a difference of 17% improvement. The SEA value of CFRP stitched specimens was 58.33 kJ/kg, this was found out to be not fully cured and further investigation led to using a different stitching fibre yarn, using CFRP that reacted well with the resin. Fabricating the specimen and undergoing the impact loading test, the SEA value was improved to 62.9 kJ/kg and compared to the non-stitched specimens with SEA value of 52 kJ/kg, the improvement was 18%. It is concluded that stitching in all cases, increased SEA which indicates better crashworthiness behaviour.

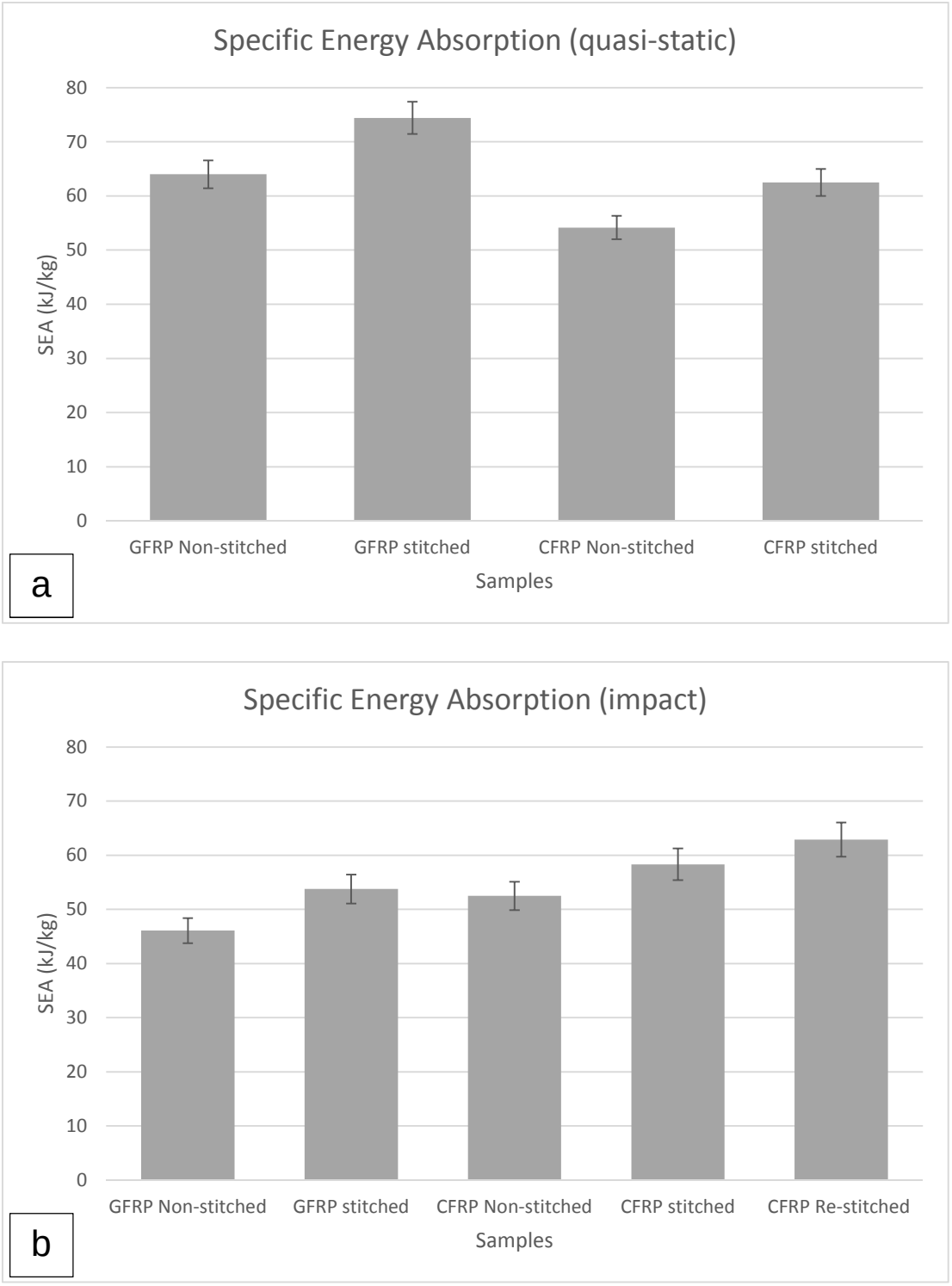

Figure 5-16 Specific energy absorption (SEA) a) quasi-static loading and b) impact loading

5.5 Conclusion

In this study, the effect of through thickness multi-stitching on energy absorption capability of composite absorbers under quasi-static and impact loading was studied. The failure mechanisms were circumferential delamination, axial cracks, laminar bending, and bundle fractures modes. In both GFRP stitched specimens subjected to quasi-static and impact loading, increased longitudinal cracks within the petals are prevailing compared with non-stitched specimen. Stitching through the thickness was introduced into CFRP and GFRP composite sections under quasi-static and impact loading. In both materials, stitched specimens had higher energy absorption capability compared to non-stitched specimens. This significantly increased crashworthiness behaviour of composite absorbers subjected to quasi-static and impact loading and consequently improved energy absorption capability without increasing of structural weight, which indicates, improvement in SEA value. The CFRP and GFRP stitched specimens subjected to quasi-static loading showed increase in SEA percentage values of 14% and 15% respectively. Similarly, the CFRP and GFRP stitched specimens subjected to impact loading showed increase in SEA percentage values of 18% and 17% respectively. This shows the significant influence of through thickness stitching on specific energy absorption.

In Figure 5-17, the energy vs time graphs are represented. In part a, the GFRP stitched and non-stitched specimens are shown. The stitched specimen illustrates a faster energy dissipation than non-stitched specimen, this indicates better energy absorption capability than non-stitched specimen. In CFRP specimen (part b), the curve has improved indicating better energy dissipation. Although because, in CFRP specimens, the fibre yarn used did not fully bond, because Kevlar fibre yarn absorbs moisture, and it partially bonded, (see Figure 5-12) however, this method has shown significant increase in energy absorption which comes from the formation of resin pockets and formation of resin shell around the fibres as well as the fibre yarn being partially bonded. However, by introducing a different fibre yarn on a laminate it was shown better bonding by CFRP fibre yarn. After fabricating the specimens with stitching pattern and using CFRP stitching yarns, the stitched specimen showed significant improvement.

The SEA value increased from 11%, which was the partially bonded specimen to 18% compared with non-stitched specimen.

The present study has established sufficient information on the effect of stitching through the thickness both on localised and mean crushing load under quasi-static and impact loading. This enables the control of the force-crush distance curve to behave at a certain standard regarding crashworthiness and weight saving applications such as automotive and aerospace industry, where increase of energy absorption capabilities without increase of weight of the structure is one of the critical considerations.

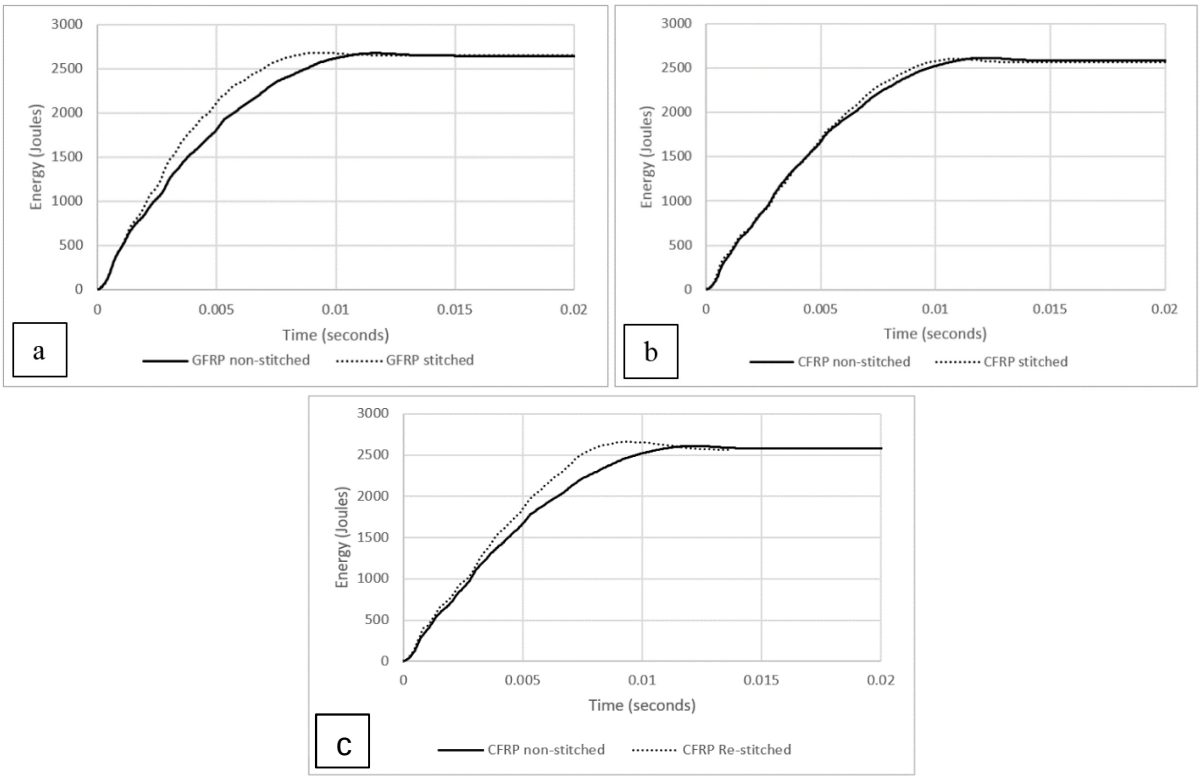

Figure 5-17 Energy vs time a) GFRP stitched and non-stitched b) CFRP stitched partially cured and non-stitched c) CFRP fully cured and non-stitched specimen

6 Numerical Modelling Approach of Composites Structures under Progressive Failure

Finite element models were developed to simulate the crushing behaviour of glass/epoxy tubes with different material models, mesh sizes, failure trigger mechanisms, element formulation, contact definitions, single and various number of shells and delamination modelling. Six different modelling approaches, namely, a single-layer approach and a multi-layer approach, were employed with 2, 3, 4, 6, and 12 number of shells. In experimental studies 12 plies were used to fabricate a 3 mm wall thickness GFRP specimen, and the numerical results were compared with experimental data. By carefully calibrating the values of certain parameters used in defining the above parameters to predict the behaviour and energy absorption response of the FEM model against initial failure peak load (stiffness) and the mean crushing force. In each case, the results were compared with each other, experimental and computational costs. The decision was taken from an engineering point of view, which means compromising accuracy for computational efficiency. The aim was to develop a FEM that can predict energy absorption capability with high accuracy (around 5% error) compared with the experimental results.

6.1 Introduction

In this chapter, the study of composite models in Ls-Dyna and effects of the parameters influencing energy absorption capability has been carried out in detail. Of all the crashworthy composite structures, fibre/epoxy composite crash absorbers are used very frequently by the researchers, due to its low cost, easy fabrication and its energy absorption efficiency.

Accurate prediction of deformed fibre architecture of the final component is vital in respect to energy absorption capability if a virtual design process is used to optimise composite components, that is considered a necessary process if the time taken for the design and costs are to be industrially acceptable. The current study consists of multi-shell configuration, and delamination modelling to capture an accurate enough model to predict energy absorption capability. In many

studies this is eliminated and replaced by friction between each shell acting as the delamination between the plies [56-57]. In one study [158] the dynamic coefficient of friction was set to 0.65, and the author states that the coefficient of friction measured on bulk epoxy sliding against either stainless steel or alumina is around 0.65, whereas the coefficient of friction measured on epoxy reinforced with carbon fibres is significantly lower, namely down to 0.11. It was found that sliding with a stainless steel ball in a direction parallel to the fibre orientation results in a lower coefficient of friction than sliding in anti-parallel direction.

Although different contact definitions can be used to predict the delamination effect. Most cases reviewed in this study captured an acceptable load-displacement curve, energy absorption capability and SEA, which is the main concentration of this study. However, to minimise modelling costs and experimental costs, a model should be developed to capture an acceptable load-displacement curve. A summary of the reviewed numerical studies from chapter 2 is illustrated in the following section.

6.2 LS-DYNA

One of the most frequently used software for crashworthiness application by industry and academics is Ls-Dyna, developed by LSTC and is suited for highly nonlinear transient dynamic finite element analysis.

Ls-dyna within the past decade has added many new features such as new material types, contact algorithms, element formulation, etc. LSTC has gradually expanded to develop a universal tool for most implicit and widely used explicit coding for aerospace, automotive, military and construction. Ls-Dyna has own pre-processor called LS-Prepost.

6.2.1 Material models

New material models are developed and added to Ls-Dyna regularly. Approximately 200 material models are implemented in the software. For unidirectional composite materials these material models narrow down to the following [192].

1. Material model – 22: Composite Damage
2. Material model – 54 and 55: Enhanced Composite Damage
3. Material model – 58: Laminated Composite Fabric
4. Material model – 59: Shell/Solid Composite Failure Model

Material properties such as Shear modulus, Elastic modulus, and Poisson's ratio are essential parameters for a material model. Strength properties for failure analysis are also essential to predict material behaviour. These properties are, transverse compressive strengths, longitudinal compressive strength, transverse tensile strength and shear strength. The mentioned material models, specifically deal with orthotropic materials. Every model has an option to determine the material axes such as local and global orthotropic material axes. For a given geometry and load, the process of calculation is in three steps,

1. Stress and strain distributions, around the stress concentrated areas, are calculated
2. Failure (maximum) load is predicted,
3. Mode of failure is determined.

Analysis consists of two major parts: Stress analysis and Failure analysis. Most often used material models are described with parametric studies to compare the differences.

6.2.1.1 MAT_022: Composite damage model

This is the first composite failure material model implemented in LS-Dyna which was proposed by Chang-Chang [193,194]. Keyword for this model is *MAT_COMPOSITE_DAMAGE or *MAT_022. This model can be used in solid and shell elements. By using the user defined integration rule, the constitutive constants vary through the thickness of the shell.

Corresponding relationships for Chang-Chang composite failure model are as follows [192]. When any corresponding failure criteria exceed 1, it is considered that this element is failed for this mode.

MAT-022 uses three criteria defined by Chang-Chang and five material parameters to define failure modes.

The three failure criteria used are:

1. Tensile fibre mode
2. Tensile matrix mode
3. Compressive matrix mode

The five material parameters are:

1. Shear Strength, S_c
2. Transverse tensile strength, Y_t
3. Transverse compressive strength, Y_c
4. Longitudinal tensile strength, X_t
5. Nonlinear shear stress parameter, α

The matrix cracking failure mode is determined from equation 6-1 and 6-2,

$$F_{matrix} = \left(\frac{\sigma_2}{Y_t}\right)^2 + \bar{\tau} \quad \textbf{(6-1)}$$

$$\bar{\tau} = \frac{\frac{\tau_{12}^2}{2G_{12}} + \frac{3}{4}\alpha\tau_{12}^4}{\frac{S_c^2}{2G_{12}} + \frac{3}{4}\alpha\tau_{12}^4} \quad \textbf{(6-2)}$$

where, σ_2 is stress in matrix direction, $\bar{\tau}$ is fibre and matrix shearing term, τ_{12} is in-plane shear stress, and G_{12} is the shear modulus. The failure is assumed when $\sigma_2 > 0$, then E_2, G_{12}, ν_1 and ν_2 are set to zero.

The compression failure is determined from equation 6-3. Failure is assumed when $\sigma_2 < 0$ and E_2, ν_1 and ν_2 are set to zero.

$$F_{comp} = \left(\frac{\sigma_2}{2S_C}\right)^2 + \left[\left(\frac{Y_C}{2S_C}\right)^2 - 1\right]\frac{\sigma_2}{Y_C} + \bar{\tau} \quad \textbf{(6-3)}$$

The fibre breakage failure mode is determined from equation 6-4. Failure is assumed when $\sigma_1 > 0$, then E_1, E_2, G_{12}, ν_1 and ν_2 are set to zero.

$$F_{fibre} = \left(\frac{\sigma_1}{X_t}\right)^2 + \bar{\tau} \quad \textbf{(6-4)}$$

Where, σ_2 is stress in fibre direction, E_1 and E_2 are the longitudinal and transverse elastic moduli respectively, ν_1 and ν_2 are the in-plane Poisson's ratios.

6.2.1.2 MAT_54-55: Enhanced composite damage model

These material models are improved versions of Chang-Chang composite damage model. Keyword for this model is *MAT_ENHANCED_COMPOSITE_DAMAGE or *MAT_054 or *MAT_055. This model is used for thin shells only. When the model is undamaged, the material is assumed to be orthotropic and linear elastic and when the damage occurs nonlinearity is introduced into the material. Material 54 is suggested by Chang which is called Chang matrix failure criterion and material 55 is suggested by Tsai-Wu which is called Tsai-Wu matrix failure criterion and these two models have very similar formulation.

Material 54 is the same as material 22 but with added compressive fibre failure mode and it also includes compressive and tensile fibre failure and compressive and tensile matrix failure.

Any corresponding failure criteria in the following, if the value is ≥ 0 then it means failure and if the value is < 0 it means elastic.

The Chang- Chang criterion (MAT_54) is given below,

Tensile fibre mode (Failure is assumed when $\sigma_1 > 0$),

$$\left(\frac{\sigma_{11}}{X_t}\right)^2 + \beta\left(\frac{\sigma_{12}}{S_C}\right) - 1 \qquad \textbf{(6-5)}$$

All moduli and Poisson's ratios are set to zero when the tensile fibre failure criteria is met, that is $E_1 = E_2 = G_{12} = \nu_{12} = \nu_{21} = 0$. All the stresses in the elements are reduced to zero and the element layer is failed. Where E_1 and E_2 are the longitudinal and transverse elastic moduli respectively, G_{12} is the shear modulus, ν_{12} and ν_{21} are the in-plane Poisson's ratios, and, β is weight factor for the ratio of the shear stress to shear strength.

Compressive fibre mode (Failure is assumed when $\sigma_{11} < 0$),

$$\left(\frac{\sigma_{11}}{X_C}\right)^2 - 1 \quad \textbf{(6-6)}$$

Where, X_C is the longitudinal compressive strength. For this mode, $E_1 = \nu_{12} = \nu_{21} = 0$

Tensile matrix mode (Failure is assumed when ($\sigma_{22} > 0$),

$$\left(\frac{\sigma_{22}}{Y_t}\right)^2 + \left(\frac{\sigma_{12}}{S_C}\right)^2 - 1 \quad \textbf{(6-7)}$$

For this mode, $E_2 = G_{12} = \nu_{21} = 0$

Compressive matrix mode (Failure is assumed when $\sigma_{22} < 0$),

$$\left(\frac{\sigma_{22}}{2S_C}\right)^2 + \left[\left(\frac{Y_c}{2S_C}\right)^2 - 1\right]\frac{\sigma_{22}}{Y_C} + \left(\frac{\sigma_{12}}{S_C}\right)^2 - 1 \quad \textbf{(6-8)}$$

For this mode, $E_2 = G_{12} = \nu_{12} = \nu_{21} = 0$. For brittle material, when the failure criterion is met, a reduction factor is applied to reduce compressive fibre strength and a softening factor is used to reduce tensile fibre strength.

When the nonlinear shear stress parameter is set to 0, then all the above failure criteria reduces to the original failure criteria of Hashin [194].

Material model 55 formulation is very close to the material model 54. It uses Tsai-Wu failure criteria [195] for compressive and tensile matrix failure modes which are given as single expression as follow:

$$\frac{\sigma_{22}^2}{Y_c Y_t} + \left(\frac{\sigma_{12}}{S_C}\right)^2 + \frac{(Y_c - Y_t)\sigma_{22}}{Y_c Y_t} - 1 \quad \textbf{(6-9)}$$

This material model (Mat_055) is like Chang-Chang failure model except the compressive and tensile matrix failure mode is replaced with the above expression and transverse shear is not considered in this material model.

In the material input, additional parameters such as effective failure strain and maximum strains are required besides strengths. When the strains values are

reached, then the element is deleted. The element is removed when failure occurs in all the composite layers, these layers are defined through shell thickness integration points.

Elements having the same nodes with the deleted elements become “Crashfront” elements. By using a softening reduction factor, the strengths can be reduced and moduli of the crashfront elements, this results in a stable crushing process and sudden release of stress concentration is compensated. To understand the strain parameters, consider an example, shown in Figure 6-1, a 4-noded single shell element undergoes a tensile load in the direction of the fibre. The material and strength properties are taken from [196]. SOFT takes into account the softening strength, using the crashfront elements by scaling down the initial input strength.

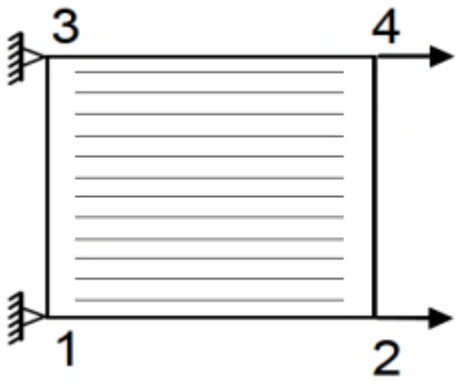

Figure 6-1 Single 4-noded shell element under tension [196]

Initially the element is loaded at a constant strain rate of 1/s in the fibre direction. The stress in the element increases linearly in the fibre direction up to the maximum value, and all elastic properties and stresses are reduced to zero in 100-time steps as shown in Figure 6-2. The maximum strain for fibre tension is set as default value 0.

Then, all the elastic properties and stresses are kept constant except the maximum strain for fibre tension, which is set to 0.02. After the value of maximum stress is reached, the elastic constants and the stresses remain constant until the maximum strain value is reached, then the element is deleted immediately resulting in the stress being reduced to zero, shown in Figure 6-3.

Stresses are kept constant when compressive matrix and fibre criteria are met. In material model 54 and 55, ultimate failure can occur in any four different ways:

1. Chang-Chang failure criterion is satisfied in tensile fibre mode
2. Maximum fibre tensile strain is met
3. Maximum effective failure strain is met
4. Minimum time step is met

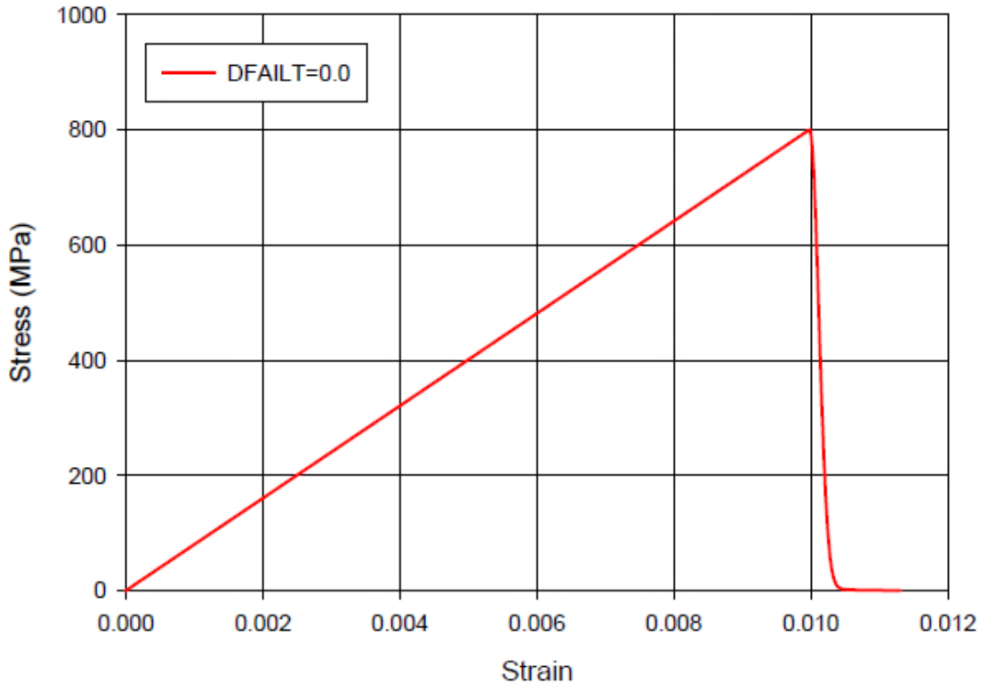

Figure 6-2 Stress-strain curve in fibre direction under tension, DFAILT=0.0 [196]

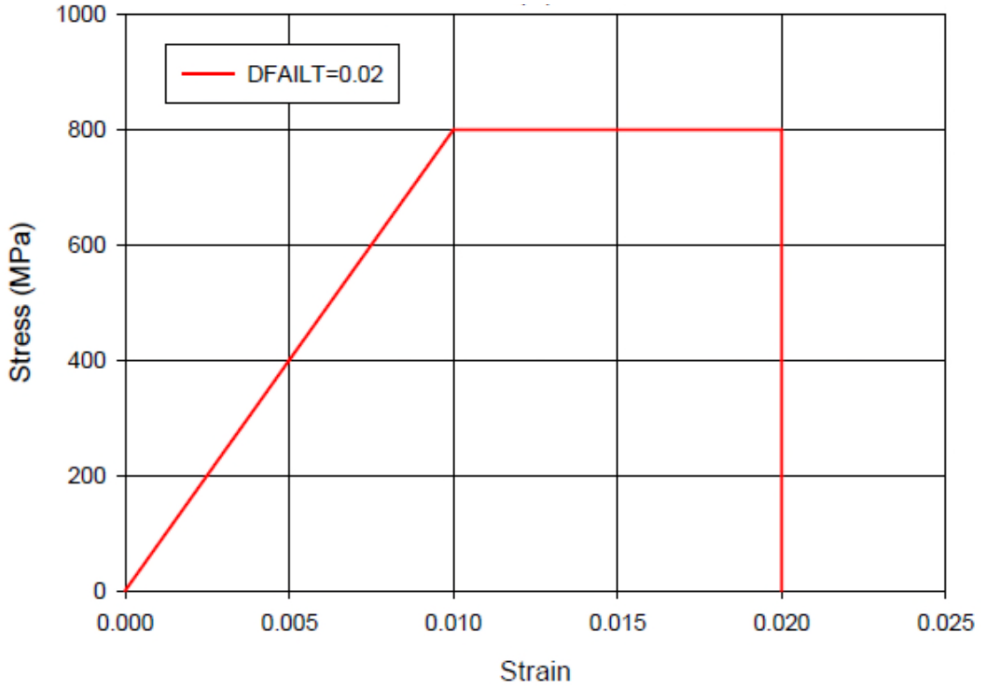

Figure 6-3 Stress-strain curve in fibre direction under tension, DFAILT=0.02 [196]

6.2.1.2.1 Softening reduction factor (SOFT)

A crashfront parameter is the softening reduction factor for the element material strength that share nodes of the crushed element. By default, this value is set to 1, this means that element contains 100% of their strength and when this value drops to 0.5, and it indicates that the row of elements that share the same nodes of crashfront elements have only 50% of its original strength.

In numerical parameters SOFT is considered one of the influential parameter that could amend the shape of the force-displacement curve to match with the experimental results. For every geometric structure this parameter value needs to be amended through trial and error to obtain a good agreement with the numerical and experimental force-displacement results. SOFT parameter can be found in material 54, 55, 58 and 59. This parameter can be activated by giving a positive value for TFAIL in material 54 and 55, which is the time step size for element deletion, and by giving a positive value for TSIZE in material 58 and 59, which is time step for element deletion. When this time step is reached, the element is deleted. When the degree of curvature of the structure is higher, then that structure is more efficient in crushing by fragmentation. For lower value, the structure gives frond formation. These large fronds are accompanied by long

delamination which results in creating an effective damage length that are inefficient for energy absorption. Francesco Deleo, Wade, Paolo Feraboli [159] simulated the model using material 54 in LS-Dyna and noted that by using SOFT parameter, the damage length can be changed by this parameter to reduce material strength of the row of elements which are ahead of the crashfront. Sivarama Kirshnamoorthy [201] showed that crashfront parameter influence the mean crushing force in force-displacement curve. Therefore, it can be concluded that the SOFT parameter significantly influences the amount of energy absorption. As the value of SOFT increases, the energy absorbed is more by the composite structure due to higher strength of the structure.

6.2.1.2.2 MAT_54-55 input parameter definitions

Variable	Definition	Suggested Value
MID	Material identification number	Any arbitrary integer
RO	Mass per unit volume*	ρ from material properties*
EA	Young's modulus in longitudinal direction.	E_1, from material properties
EB	Young's modulus in transverse direction.	E_2, from material properties
EC	Young's modulus through the thickness	Not used
PRBA	Minor Poisson's ratio, $\nu_{ba} = \nu_{21}$	Calculated using ν_{12} , E_1 and E_2
PRCA	Minor Poisson's ratio, $\nu_{ca} = \nu_{31}$	Not used
PRCB	Minor Poisson's ratio, $\nu_{cb} = \nu_{32}$	Not used
GAB	Shear modulus, G_{ab}	G_{12}, from material properties
GBC	Shear modulus, G_{bc}	Assumed equal to G_{ab}
GCA	Shear modulus, G_{ca}	Assumed equal to G_{ab}
KF	Bulk modulus of material	Not used
AOPT	Material axes option parameter	AOPT = 0
XP YP ZP	Material axes coordinates for AOPT = 1	Not used
A1 A2 A3 D1 D2 D3	Material axes coordinates for AOPT = 2	Not used
MANGLE	Material angle in degrees used when AOPT = 3	Not used
V1 V2 V3	Material axes coordinates for AOPT = 3	Not used
DFAILT	Max strain for fiber tension	DFAILT = (F_1^{tu} / E_1) [DFAILT > 0]
DFAILC	Max strain for fiber compression	DFAILC = (F_1^{cu} / E_1) [DFAILC < 0]
DFAILM	Max strain for matrix straining in tension and compression	DFAILM ≥ *max*[(YT/EB) , (YC/EB)]
DFAILS	Max shear strain	0 < DFAILS ≤ 0.1
EFS	Effective failure strain	EFS = 0
TFAIL	Time step size criteria for element deletion	0 < TFAIL < (Δt/10)
ALPH	Shear stress non-linear term	1E-3 ≤ ALPH ≤ 1
SOFT	Crush front strength reducing parameter	Must be calibrated for crush simulations
FBRT	Softening factor for fiber tensile strength after matrix failure	0 ≤ FBRT ≤ 1
YCFAC	Softening factor for fiber compressive strength after matrix failure	0 ≤ YCFAC ≤ (XC/YC)
BETA	Weighing factor for shear term in tensile fiber mode	0 ≤ BETA ≤ 1
XC	Longitudinal compressive strength	$\lvert F_1^{cu} \rvert$, from material properties
XT	Longitudinal tensile strength	F_1^{tu}, from material properties
YC	Transverse compressive strength	$\lvert F_2^{cu} \rvert$, from material properties
YT	Transverse tensile strength	F_2^{tu}, from material properties
SC	Shear strength	F_{12}^{tu}, from material properties
CRIT	Failure criterion used (MAT54 Chang-Chang, MAT55 Tsai-Wu)	Assign value of 54 or 55
*For English units, must be divided by a gravity factor to convert from pound-weight to pound-mass.		

Figure 6-4 MAT_54-55 input parameter definitions [192]

6.2.1.3 MAT_58: Laminated composite fabric failure model

Based on the strain-based failure surface, this model can be used for modelling of composite materials which have unidirectional layers, woven fibres and laminates. Keyword for this model is *MAT_LAMINATED_COMPOSITE_FABRIC or *MAT_058. This model is used for shell elements only. This model is implemented in LS-Dyna by Matzenmiller, Lubliner and Taylor [197], which is also called as MLT composite model and is based on plane stress continuum damage mechanic model.

In material 58, Hashin failure criteria [194] is used with changes for different types of composites. The maximum effective strain is applicable for element layer failure for any different types of composites.

6.2.1.4 MAT_59: Composite failure model

This material model is also called the elastic-plastic material model, which is an enhanced version of Mat_022. It works on the basis of failure surfaces which are: Faceted failure surface and Ellipsoidal failure surface. It will be able to model the material progressive failure due to many failure criteria which includes longitudinal and transverse directions in tension and compression respectively, through-thickness direction in compression and shear.

6.2.2 Delamination models

Delamination modelling has several approaches in Ls-Dyna, Tiebreak contacts have been vastly used and is proven to be robust contact algorithm and relatively simple. Depending on the model of study different contacts can be employed to achieve better prediction.

Two tiebreak formulation mostly used in laminated composite tubes under impact or quasi-static loading, which are namely, tiebreaks with bilinear traction-separation law and a tiebreak with cohesive zone implemented formulation known as option 8 and 11 in LS-DYNA, respectively [188]. Option 8 contact card requires a critical distance to interface failure, interlaminar normal strength and shear strength as input parameters. Option 11 contact card uses a similar formulation as cohesive zone elements, that requires fracture toughness under

pure Mode-I and Mode-II loading, interlaminar normal and shear strength, interfacial stiffness for normal and shear modes and B-K law which is power-law or the Benzeggagh-Kenane law that describes crack propagation [188]. This contact card has been used to model delamination in laminated composites under ballistic impact, however, it has not been used for crushing simulations.

6.2.2.1 CONTACT _ONE_WAY_SURFACE_TO_SURFACE_TIEBREAK Option 8

One-way contact types allow for compression loads to be transferred between the slave nodes and the master segments. Tangential loads are also transmitted if relative sliding occurs when contact friction is active. A Coulomb friction formulation is used to transition from static to dynamic friction. This transition requires that the static friction coefficient be larger than the dynamic friction coefficient and a decay coefficient be defined. The *one-way* term in one-way contact is used to indicate that only the user-specified slave nodes are checked for penetration of the master segments.

The algorithm ties nodes that are initially in contact by creating a linear spring and the debonding of the surface initiates when the maximum stress criterion is met which leads to scaling down of the stress by a linear damage curve until the critical separation is reached and the spring is removed [192].

$$\left(\frac{\sigma_n^2}{NFLS}\right)^2 + \left(\frac{\sigma_s^2}{SFLS}\right)^2 = 1 \qquad \textbf{(6-10)}$$

In which σ_n and σ_s are the normal and shear stresses acting at the interface, and NFLS, SFLS and PARAM are the normal and shear strength of the tie and critical distance, respectively. Once the damage has initiated, the two surfaces begin to separate, and the interfacial stresses are then scaled down as a linear function of the separation distance. PARAM which is the critical distance at which the failure occurs (i.e. deletion of tiebreak and advancing of delamination) [192].

$$PARAM = \frac{2 \times E_{tie}}{S} \qquad \textbf{(6-11)}$$

Where:

$$S = \sqrt{\max\ (\sigma_n, 0)^2 + (\sigma_s^2)^2} \quad \textbf{(6-12)}$$

Due to the failure of the tiebreak interface, E_{tie} is the energy released. With trial and error procedures a sensitivity study was conducted of Mode-I and Mode-II to determine their relative effect(s) on the tiebreak failure process. It can be noted that for composite crushing simulations, Mode-I fracture is dominate mode of failure during tie-break failure process. Thus, to simply the simulations, a pure Mode-I delamination was assumed.

$$G_{IC} = \frac{1}{2}\,\sigma_n\,PARAM \quad \textbf{(6-13)}$$

In this equation (6-13), the critical normal separation of the surface is determined, named as PARAM, based on the energy release rate in Mode-I (G_{IC}) and the critical normal stress.

Since the laminate of the open cross-sections was modelled as multi-shell configurations of shell elements with each layer representing various number of plies. In section 6.5.7, the effect of number of plies in each shell was investigated based on energy absorption capability. Hence, the tiebreak was adopted for each case of study and the tiebreak contact was defined only between these shell layers, rather than between individual plies. However, delamination could occur along any of the plies, if not all, ply interfaces during specimen crushing, as it was observed experimentally [Chapters 3-5]. To account for the energy dissipated by these additional delamination interfaces, PARAM was scaled by the ratio of the number of ply interfaces $n_{delamination}$ to the number of tiebreak interfaces n_{tie} defined as:

$$PARAM' = PARAM \times \frac{n_{delamination}}{n_{tie}} \quad \textbf{(6-14)}$$

based on the experimental observations, it was assumed that delamination occurred among all plies. The values used and calculated in Equations (6-13), and (6-14) are listed in Table 6-2 and 6-3.

6.3 Simulation setup

6.3.1 LS-DYNA model

For the simulations, an Explicit FE LS-DYNA code was used with multi-layered shell configuration to reduce numerical costs. Composite tubes were modelled as multi-layers of Belytschko-Tsay circular shell elements with one integration point in the element plane to represent the direction of the stacking sequence. In double-shell configuration, the GFRP innermost shell has six integration points with another six integration points being assigned to outermost shell to represent all twelve UD-layers. In GFRP tube each individual layer has a thickness of 0.25 mm. The total thickness of both shell is 3 mm. Each fibre orientation was assigned with insertion of an integration point in respect to the stacking sequence used with its associated thickness. The material properties are obtained from [143,144 and 200, 203 and 204] see Table 6-1.

Table 6-1 Material properties of GFRP (TenCate 7781/E772)

GFRP (TenCate 7781/E772)							
E_1 (GPa)	E_2 (GPa)	G_{12} (GPa)	v_{12}	$\sigma_u\ 0^o$ (MPa)	$\sigma_u\ 90^o$ (MPa)	τ_s (MPa)	V_f (%)
39 ± 3	11.8 ± 1	3.2 ± 0.5	0.29	836 ± 20	29 ± 2	97 ± 4	58

In shell theory the thickness of the shell is considered as mid-plane. In double shell configuration, two Shells with radiuses of 37.75 mm and 39.25 mm to represent the inner and outer shells with lengths of 80 mm and 77.5 mm were modelled respectively using LS-PrePost representing the GFRP tube geometry. Each shell was glued together so that the triggering at the top of the shell would not detach during the crushing process, as a separate shell was used. In this triggering approach, two shells were used, one with 2.5 mm in height acting as the trigger (one element size), and the other depending on being inner or outer shell had its representative height assigned. Therefore, the top shell at each FEA case study represents the trigger. Quadrilateral Shell element was used with each element size of 2.5 mm x 2.5 mm. The trigger mechanism was modelled by

reducing first row thickness of the shell elements to represent the bevel trigger, from 1.5 mm to 0.05 mm in each shell. A solid element rigid block was modelled to represent the striker. LS-DYNA Material model of Enhanced_composite_damage (Mat_54-55), which is an orthotropic material with failure criterion of Chang-Chang was used. This failure criterion is a modification of Hashin's failure criterion for assessing lamina failure. The hourglass was set at 10% [154-158,188, 198].

Modelling interlaminar separation or delamination failure (Mode-I) requires either detailed experimental investigation for cohesive zone or three-dimensional representation that both result into increase of computational and experimental costs. Delamination failure causes energy absorption and this can be modelled with multi-layered shell configuration with a contact card that is capable of G_{IC} implemented energy release rate [185-188]. Defining One_Way_Surface_To_Surface_Tiebreak contact between the two shells with inner tube being master and outer being slave.

The tiebreak option enables the detachment of the contact surfaces after reaching a maximum normal stress (NFLS) or shear stress (SFLS). Does the failure parameter, driven by occurring normal and shear stresses, become 1, the contact forces soften linearly until contact distance PARAM is reached and the interface failure is completed. Based on the interlaminar utilisation of the contact, the parameters are determined by the mechanical properties of the matrix material. Consequently, shell layers detach when the interlaminar stress exceeds the matrix properties, which are mainly responsible for interlaminar strength. Maximum normal and shear contact stresses for the tiebreak contact are based upon the mechanical properties of the epoxy resin. The critical normal separation of the surface is set to 0.15 mm and 0.32 mm for non-stitched and stitched specimen. Automatic_Node_To_Surface contact was defined for the striker and inner shell with striker being master and inner shell being slave. Automatic_Single_Surface contact algorithm was utilised. This prevents penetration of the crushing tube by its own nodes.

All bottommost nodes of all shell element layers are constrained in their translational degrees of freedom. The impactor is modelled as rigid with a mass of 108.4kg and velocity of 7.022 m/s. Gravity is modelled with an acceleration factor of 9.81 m/s^2. All simulation results are smoothed using SAE 300 Hz filter [188].

6.4 FE modelling

6.4.1 Delamination interface

Many researchers have used friction to simulate delamination, e.g. [143,144]. Friction influences the energy absorption capability, however, using friction influences SEA value, increasing friction between the shells, causes higher SEA value (see chapter 6.5.3) and this compared with experimental data cannot be considered as a correct FEM. Due to this, a different approach was considered. Tiebreak option 8 was utilised instead of friction to model delamination as this contact card can define Mode-I and Mode-II energy release rate which simulates delamination.

The tiebreak contact definition implemented in LS-DYNA allows for the simulation of delamination at the interface between adjacent shell element layers. Tiebreak Option 8 formulations was investigated for this study; namely, tiebreaks with a bilinear traction-separation law. This requires interlaminar normal and shear strengths and a critical distance to interface failure as input parameters, has been used to model delamination in crush simulations e.g. [161]. However, the optimal critical failure distance parameter selection has not been thoroughly studied in open literature. The formulation of required input parameters such as interlaminar normal and shear strengths, fracture toughness under pure Mode-I and Mode-II loading, interfacial stiffness for normal and shear modes; a description of the model setup using each formulation is explain in 6.3.2.1. To determine the energy rate of Mode-I and Mode-II, DCB and 3ENF test was carried out respectively and the test results were obtained from [203] and [204] respectively.

DCB test determines Mode-I energy release rate (G_{IC}) and 3 End-notched Flexure test determines Mode-II energy release rate (G_{IC}) for delamination growth. Table

The input parameters of Tiebreak contact option 8 are shown in Table 6-2 and Table 6-3 for stitched and non-stitched obtained from [203] and [204].

Table 6-2 Tiebreak input parameters (non-stitched) [203,204]

E_1 (GPa)	E_2 (GPa)	G_{IC} (kJ/m^2)	G_{IIC} (kJ/m^2)	NFLS (MPa)	SFLS (MPa)	PARAM (mm)	*PARAM'* (mm) (2 shells)
39 ± 3	11.8 ± 1	0.33	1.2	26.5	57.3	0.025	0.15

Table 6-3 Tiebreak input parameters (stitched) [203,204]

E_1 (GPa)	E_2 (GPa)	G_{IC} (kJ/m^2)	G_{IIC} (kJ/m^2)	NFLS (MPa)	SFLS (MPa)	PARAM (mm)	*PARAM'* (mm) (2 shells)
39 ± 3	11.8 ± 1	0.69	1.2	26.5	57.3	0.052	0.32

6.4.2 Boundary conditions and contact definitions

The loading striker was modelled as rigid body. The tubes were placed in Z-direction upright and loading striker at the chamfered end of the tube. The interaction between the loading striker and the tube was modelled using a node-to-surface contact definition (contact automatic node to surface). The tiebreak contact definition between the shell layers not only facilitates the simulation of delamination, but also prevents layers from penetrating each other after the tiebreak has failed, as the contact definition would remain in effect. In summary, Automatic_Node_To_Surface contact was defined for the striker and inner shell with striker being master and inner shell being slave. Automatic_Single_Surface contact algorithm was utilised. This prevents penetration of the crushing tube by

its own nodes, this is due to the striker's nodes might cause disturbance to the model and inner shell penetrating its own nodes and elements.

6.4.3 Material model

Material model Mat_022, Mat_054-055, Mat_058 and Mat_059 were used to capture an ideal initial peak and mean crushing force against computational costs. These parameters determine the reliability and the ability of these material model in cylindrical composite structures. The initial peak illustrates the stiffness of the material, and the mean crushing force shows the progressive crushing behaviour. In this section the computational cost is one of the main parameters of case consideration. The time taken for the simulation to converge against the extracted results can be compromised to ideally have a model that converges within a reasonable timeframe and its effect on the extracted results. All bottommost nodes of all shell element layers are constrained in their translational degrees of freedom.

6.4.3.1 Material modelling of Mat-045-055

This model allows the user to create a local material coordinate system to specify the orientation of each ply. There are 21 parameters in Mat_54 that need to be specified; 15 of which are physical parameters and six are numerical parameters [192]. From the 15 physical parameters, 10 parameters are material constants the values of which were obtained from [143,144, 200, 203 and 204] as shown in Table 6-1. The remaining five physical parameters are the tensile and compressive failure strains (element deletion strains) in the fibre direction (DFAILT and DFAILC), the matrix and shear failure strains (DFAILM and DFAILS), and the effective failure strain (EFS). The six numerical parameters can be adjusted to yield desired material behaviour. Based on an extensive parametric study, it was concluded that of these six parameters, the crash front element softening parameter (SOFT) is of key importance to this study. This parameter reduces the strength of elements surrounding a damaged or deleted element.

As mentioned, there are five physical parameters (failure strains) and six numerical parameters in MAT54 whose values need to be determined numerically. A comprehensive parametric study was performed to investigate the effect of these parameters on the simulated load-displacement behaviour. It was determined that the physical parameter DFAILC (fibre compression failure strain) had the greatest effect on the value of initial peak load while the numerical parameter SOFT (crash-front element softening parameter) had the greatest effect on the value of sustained crush load, which determined the value of SEA.

Parameters DFAILT, DFAILM and DFAILS (shear failure strains) were found to have a marginal effect on the results and were kept constant at arbitrarily selected values of 0.02, 0.02 and 0.03, respectively. However, increasing DFAILM value, increased computational cost unreasonably (see chapter 6.6.1). It was found that simulations with DFAILC = -0.004 and SOFT = 0.75 yielded the mean crushing force value and displacement behaviour for chamfered tubes that matched very well with experimental data, as shown in Table 6-4 and Table 6-5.

Table 6-4 The parametric study showing the effect of DFAILC in MAT54 on the peak load, crush and SEA of the circular tube.

DFAILC	Peak Load (Num/Exp %)	Crush Load (Num/Exp %	SEA (Num/Exp %)
-0.0100	157.9%	159.2%	166.1%
-0.007	67.2%	86.9%	87.2%
-0.006	80.3%	86.9%	87.2%
-0.005	106.2%	86.9%	87.2%
-0.004	102.2%	86.9%	87.2%
-0.003	94.1%	86.9%	87.2%

Table 6-5 The parametric study showing the effect of SOFT in MAT54 on the peak load, crush and SEA of the circular tube.

SOFT	Peak Load (Num/Exp %)	Crush Load (Num/Exp %	SEA (Num/Exp %)
0.75	102.2%	103.4%	101.1%
0.80	102.2%	116.2%	125.8%
0.85	102.2%	137.6%	138.8%
0.90	102.2%	153.8%	159.4%

A parametric study was conducted to determine the optimal values of the unknown parameters for the multi-layer modelling approach. The resultant values are presented in the above tables. This developed FEM, with SOFT parameter set to 0.75 (75%) and when DFAILC is set to -0.004 can produce accurate prediction of experimental result. DFAILC value is negative due to compression.

6.4.3.2 Material model results

Figure 6-5 shows a comparison with the mentioned material models. MAT-022 has an initial peak of 141 kN with mean crush force of 13 kN, the displacement reaches 70 mm with computational cost of 14 hours, in comparison with the experimental data, and this material model is not sufficiently accurate to predict the experimental material behaviour. MAT_054-055 on the other hand illustrates an ideal prediction of material prediction, with initial peak value of 80 kN, mean Cushing force of 67 kN, displacement of 33 mm and computational cost of 28 hours. In comparison with the experimental data, which was an initial peak of 78 kN and mean crush force of 69 kN, Mat_054-055 was on average 5% off. Mat_058 illustrated that it over predicts the mean crushing force by 7 kN, although the initial peak value has been improved to 79 kN compared with Mat_054-055. The displacement is reduced to 31 mm and the computational cost has increased to 36 hours. The difference between the two material models lays in the mean crushing force, and Mat_058 over predicts and this results in a reduction in displacement value, resulting into greater difference with experimental data, with

7.5% overall differences. Mat_059 which is a modified version of Mat_022, has shown greater improvement in prediction of crushing behaviour in composites. However, the initial peak is 10 kN off and the mean crushing force value is under predicted by 11 kN, and the displacement value is 36 mm. The overall difference is 9%. The computational cost value is 45 hours.

By taking account for all four reviewed parameters, Mat_054-055 can predict the material behaviour in respect to energy absorption capability and having a reasonable computational cost compared with the extracted results as predicted by [143,144,154-158,188, 198].

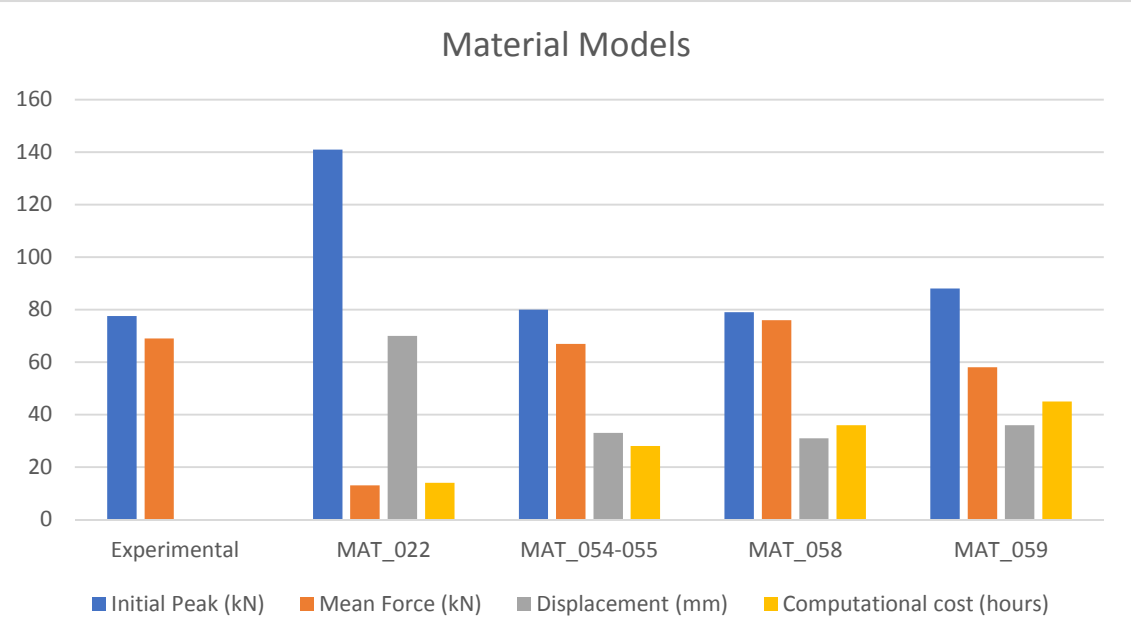

Figure 6-5 Material model comparison

6.4.4 Element formulation

The possibility of using under-integrated elements results in a reduction of computational cost with compromising accuracy of the prediction. To compare the performances, several relevant element formulations were employed, and the results have been discussed. The relevant chosen element formulations are, Hughes-Liu, S-R Hughes-Liu, S-R co-rotational Hughes-Liu, Fully Integrated and Belytschko-Tsay (default). In consideration of this test, since energy absorption capability is the main concern, the parameters chosen are the initial peak, mean

crush force and displacement, however in numerical studies the computational cost plays a major role, therefore this parameter is also considered.

Figure 6-6 shows the differences between the chosen element formulations against the reference parameter of experimental data. The result of Hughes-Liu element formulation showed an initial peak of 82 kN, mean crush force value of 90 kN with displacement of 27 mm, the computational cost was 105 hours. The total difference in performance value was 13% compared with experimental data. The extracted result from S-R Hughes-Liu showed an initial peak of 81 kN, mean crush force of 65 kN and displacement of 34 mm, the computational cost was 115 hours. The mean difference from experimental data was 7%.

Both element formulations have staggering computational cost with around 4 to 5 days to converge each of the simulations. The results obtained from S-R co-rotational Hughes-Liu showed an initial peak value of 80 kN, mean crush force of 66 kN, displacement of 33 mm and computational cost of 128 hours. Fully Integrated element formulation on the other hand was off by 24 kN and 7 kN in initial peak value and mean crush force respectively. Although the computational cost is much lower compared with mentioned element formulations. Both element formulations were off by 6% and 12% respectively.

The Belytschko-Tsay element formulation which is the default parameter in Ls-Dyna was rather close to experimental data with computational cost of 28 hours. The initial peak value was 80 kN, mean force value was 67 kN, and the displacement was 33 mm, with total mean difference of 5%.

By taking account for all four reviewed parameters, Belytschko-Tsay element formulation is the cheapest computational cost compared with other element formulations, as supported by other researchers [143,144,154-158,188, 198], which leads to use of this type of element formulation hereafter.

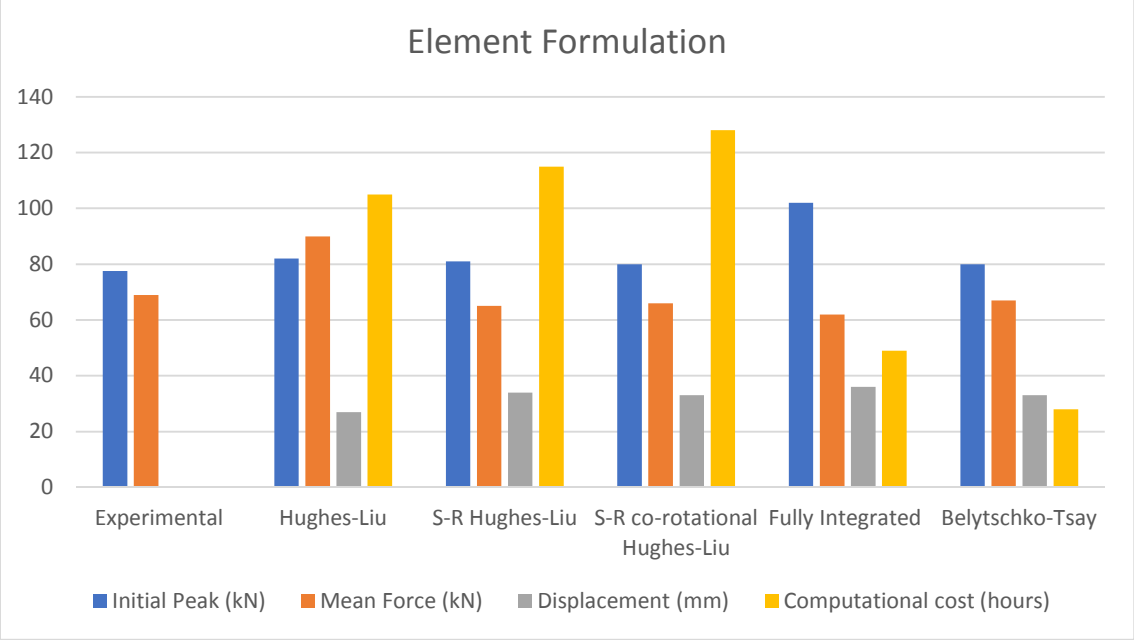

Figure 6-6 Element formulation comparison

6.4.5 Mesh size

In numerical modelling one of the influential parameter is the mesh size, the mesh sensitivity test is beneficial to establish a mesh size regarding a specific model to obtain an acceptable accuracy. In numerical study, compromising accuracy for computable costs is also relatively important. Six different element sizes were modelled with 5.5 mm, 4.5 mm, 3.5 mm, 2.5 mm, 1.5 mm, 0.5 mm quad elements (see Figure 6-7).

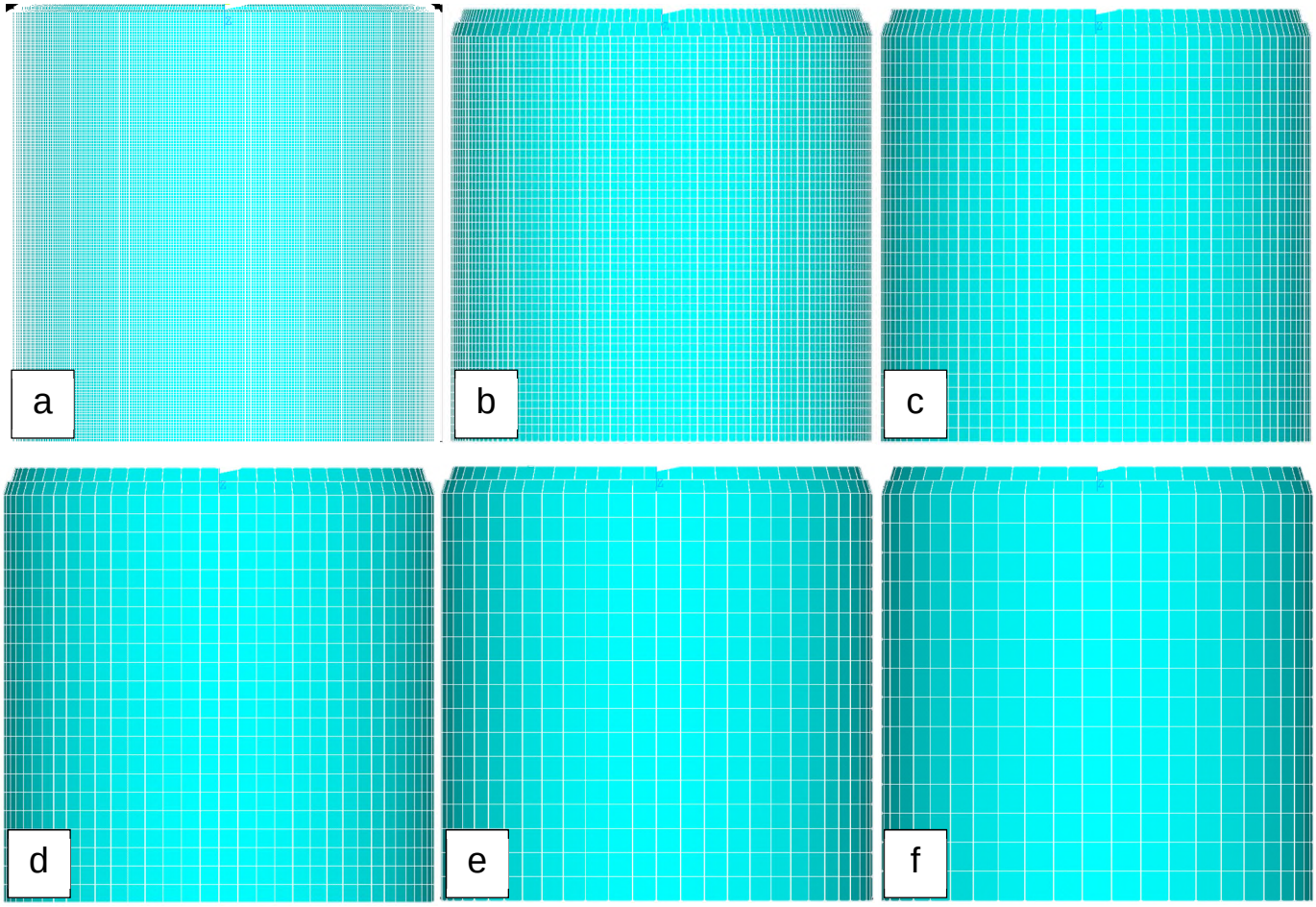

Figure 6-7 Mesh sensitivity models. a) 0.5 mm, b) 1.5 mm, c) 2.5 mm, d) 3.5 mm, e) 4.5 mm, f) 5.5 mm

From a design point of view, the aim is to achieve the cheapest model in terms of computational cost and being able to predict energy absorption capability with an acceptable accuracy. The finer the mesh sizing becomes; the computational cost increases dramatically, and relatively higher accuracy is achieved. A balance of the two needs to be chosen that the energy absorption capability of the model is within an acceptable range and the computational cost is within an acceptable range.

The Figure 6-8, shows the mesh sensitivity comparison of the modelled mesh sizes mentioned in Figure 6-7. The results illustrate a noticeable fact that the mesh 5.5 mm size is too coarse with very high peak forces and low mean crushing force with 86 kN difference between the two. This mesh size has the lowest

computational cost however, the result is nearly 40% off from the experimental data. As the mesh size becomes smaller the accuracy improves. At 4.5 mm the results improved from 5.5 mm case study, although the difference is 29% and at 3.5 mm, the difference is 18%. The peak is higher than experimental by 8 kN and the mean crushing force is lower by 7 kN.

At mesh size of 2.5 mm, the result is in line with experimental data. The difference is 5% and the computational cost is lower than the case 1.5 mm and 0.5 mm by 170% and 280% respectively. Although the accuracy is 1.5% for both cases. The balanced case to accurately calculate and predict energy absorption is 2.5 mm which is supported by many researches [143,144,188, 198].

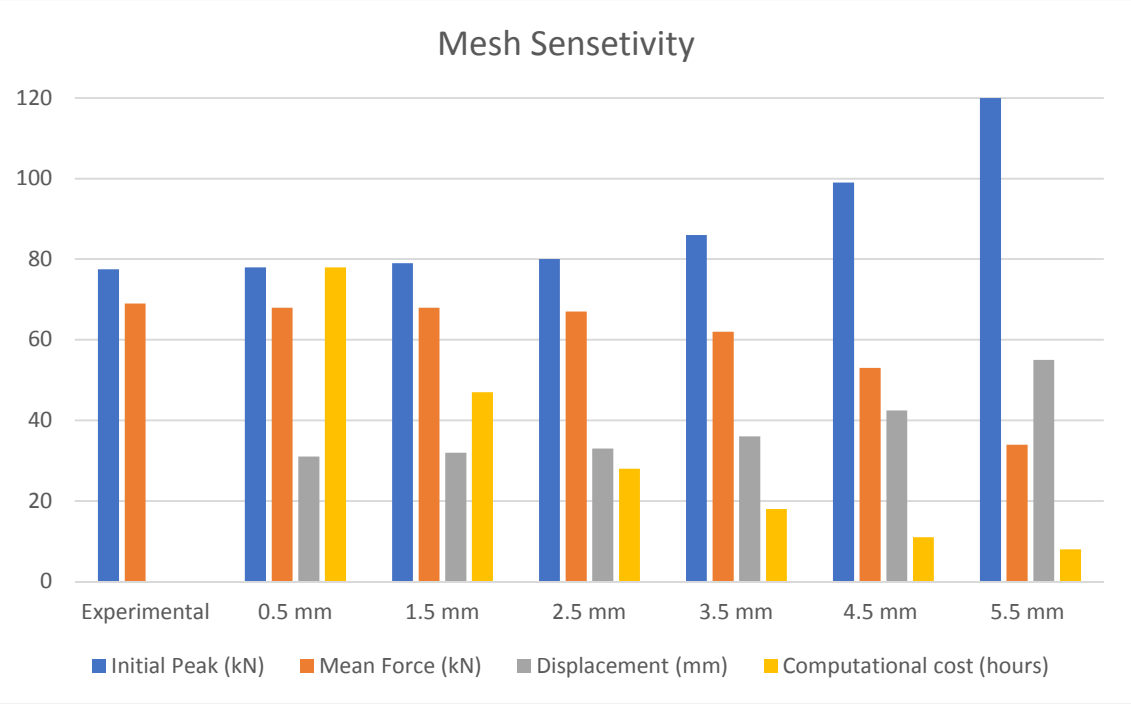

Figure 6-8 Mesh Sensitivity comparison

6.4.6 Trigger modelling

In experimental studies 45^{o} bevelled trigger mechanism was utilised and similarly in numerical studies a suitable trigger mechanism is needed to initiate the progressive failure that matches the experimental studies. The maximum crush force in an FEA model tends to be overestimated significantly [161, 199]. Few approaches were raised to study the effect of different trigger mechanisms on initial peak value of the load and mean crushing force (see Figure 6-9). These case studies are, a) single shell with no trigger, b) single shell inward-chamfer, c) single shell outward-chamfer, d) double shell level size inward-chamfer, e) double shell with 2.5 mm shell size difference inward-chamfer, f) double shell with 2.5 mm shell size difference outward-chamfer, g) double shell with 2.5 mm shell size difference inward-chamfer with different reduced element sizes, h) double shell with 5 mm shell size difference inward-chamfer, i) double shell with 2.5 mm shell size difference inward and outward-chamfer.

The results from the case studies are compared on Figures 6-10 and 6-11. The aim of this research is to find the optimum finite element modelling case to obtain a prediction of the initial peak force value.

Single shell configuration with trigger mechanism has shown better peaks and mean crushing force prediction (case b and c) than without trigger mechanism (case a). However, the double shell configuration has led to better prediction with less than 5% error compared with experimental data. Outward-chamfer in all cases lead to increase in computational costs with lower mean crushing force. Case e and f has shown better prediction of initial peak value of 80 kN and 78 kN. The configuration of the two are similar in sectioning ad positioning of the shells with outer shell being 2.5 mm (one element size) shorter than the inner shell. However, the difference lays in the computational costs, that outward-chamfer as shown in all cases increases by 5-15 hours. Also, the trigger mechanism effects progressive crushing behaviour. The mean crushing force in case f has lower value than case e.

Case g is based on case e, the configuration of the trigger is the same. In this trigger mechanism, the element size is reduced to a smaller size and this acts as

the trigger mechanism, this technique is supported by [143,144,188, 198]. In Figure 6-11, the reduced element sizes are compared against their initial peak value and mean crushing force and computational costs. It can be concluded that as the element size becomes thicker, the peak value increases and from 0.05 mm onwards, this reduction of element size has no effect on initial peak value.

The prevailing case that matches experimental results are 2.5 mm sectioned double shell configuration with inward-chamfering trigger mechanism with reduced element size of 0.05 mm.

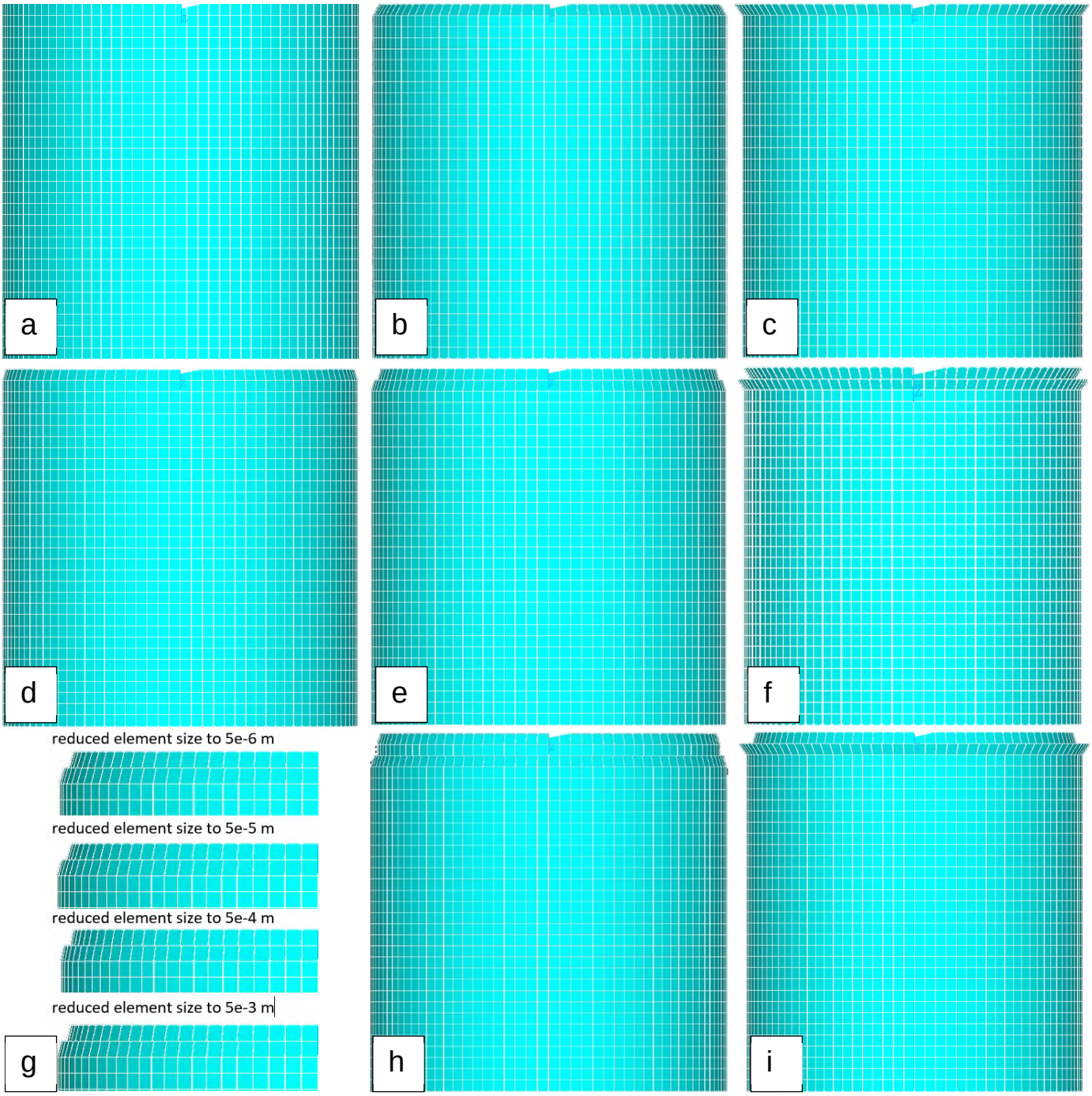

Figure 6-9 Trigger mechanism modelling cases, a) single shell no trigger, b) single shell inward-chamfer, c) single shell Outward-chamfer, d) double shell level size inward-chamfer, e) double shell 2.5 mm shell size difference inward-chamfer, f) double shell 2.5 mm shell size difference outward-chamfer, g) double shell 2.5 mm shell size difference inward-chamfer different reduced element sizes, h) double shell with 5 mm shell size difference inward-chamfer, i) double shell 2.5 mm shell size difference inward and outward-chamfer

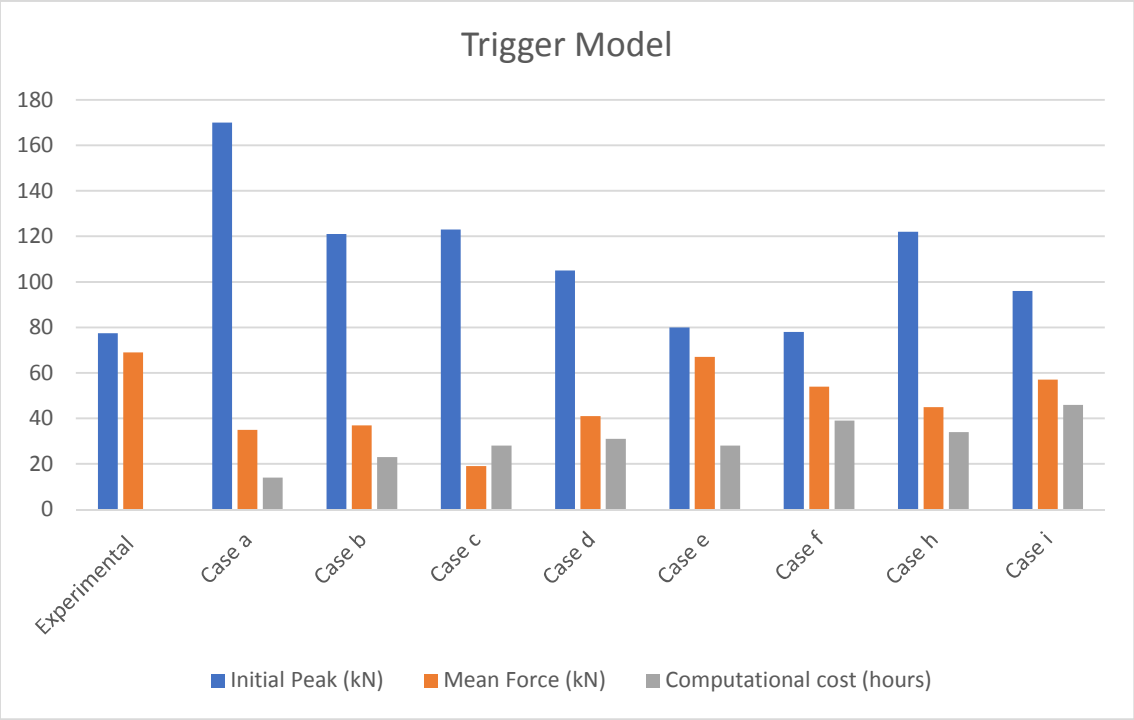

Figure 6-10 Trigger model comparison

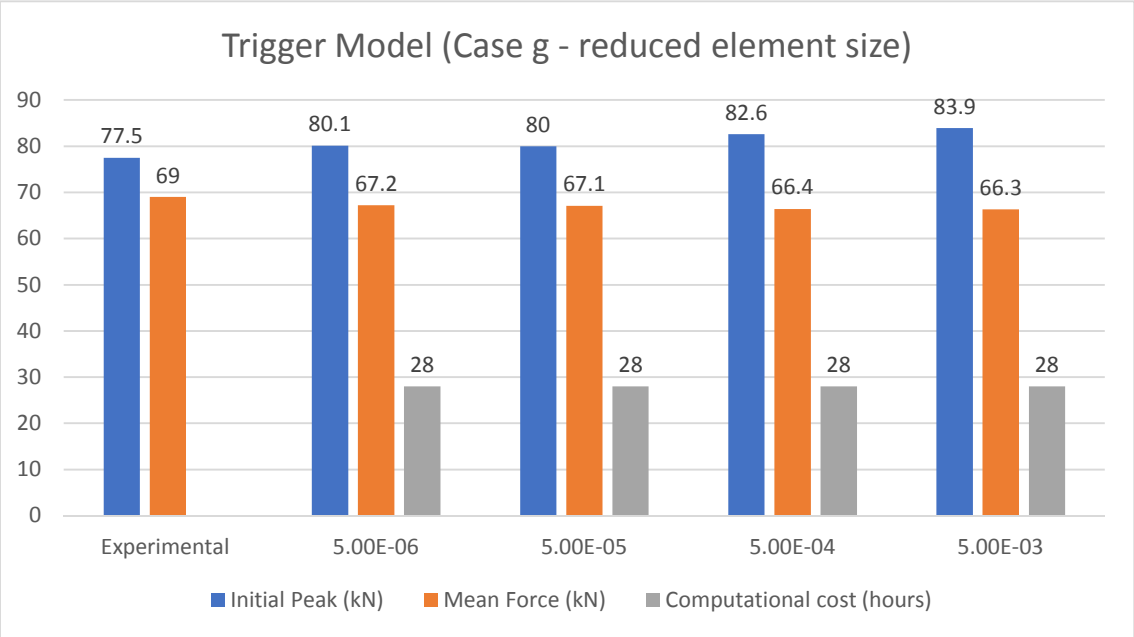

Figure 6-11 Trigger model case g comparison

6.4.7 Number of shell(s) configuration

The effect of number of shells on the energy absorption prediction of FEM is investigated. The studied cases are, 1 shell, 2 shells, 3 shells, 4 shells, 6 shells, and 12 shells (see Figure 6-12).

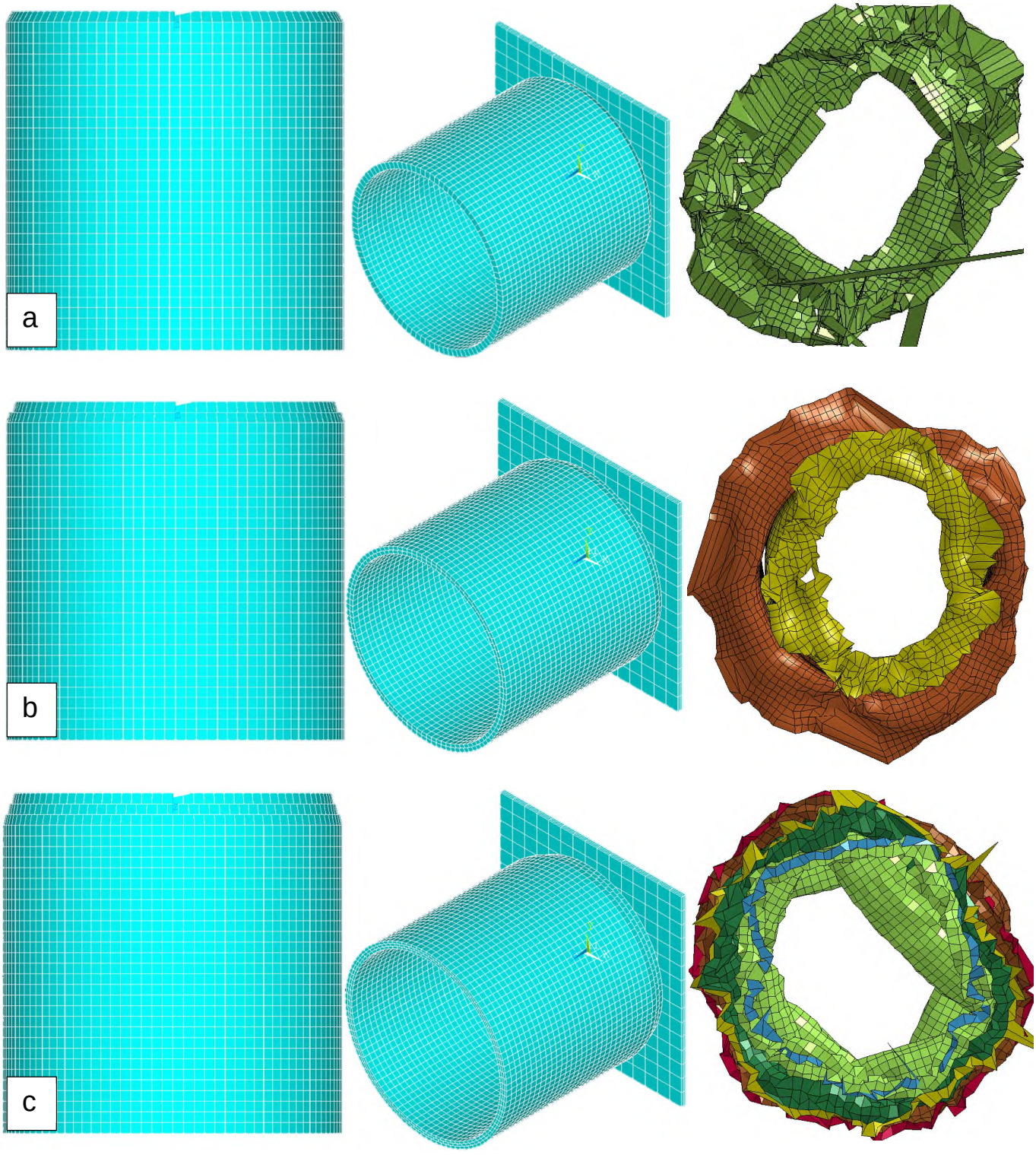
a
b
c

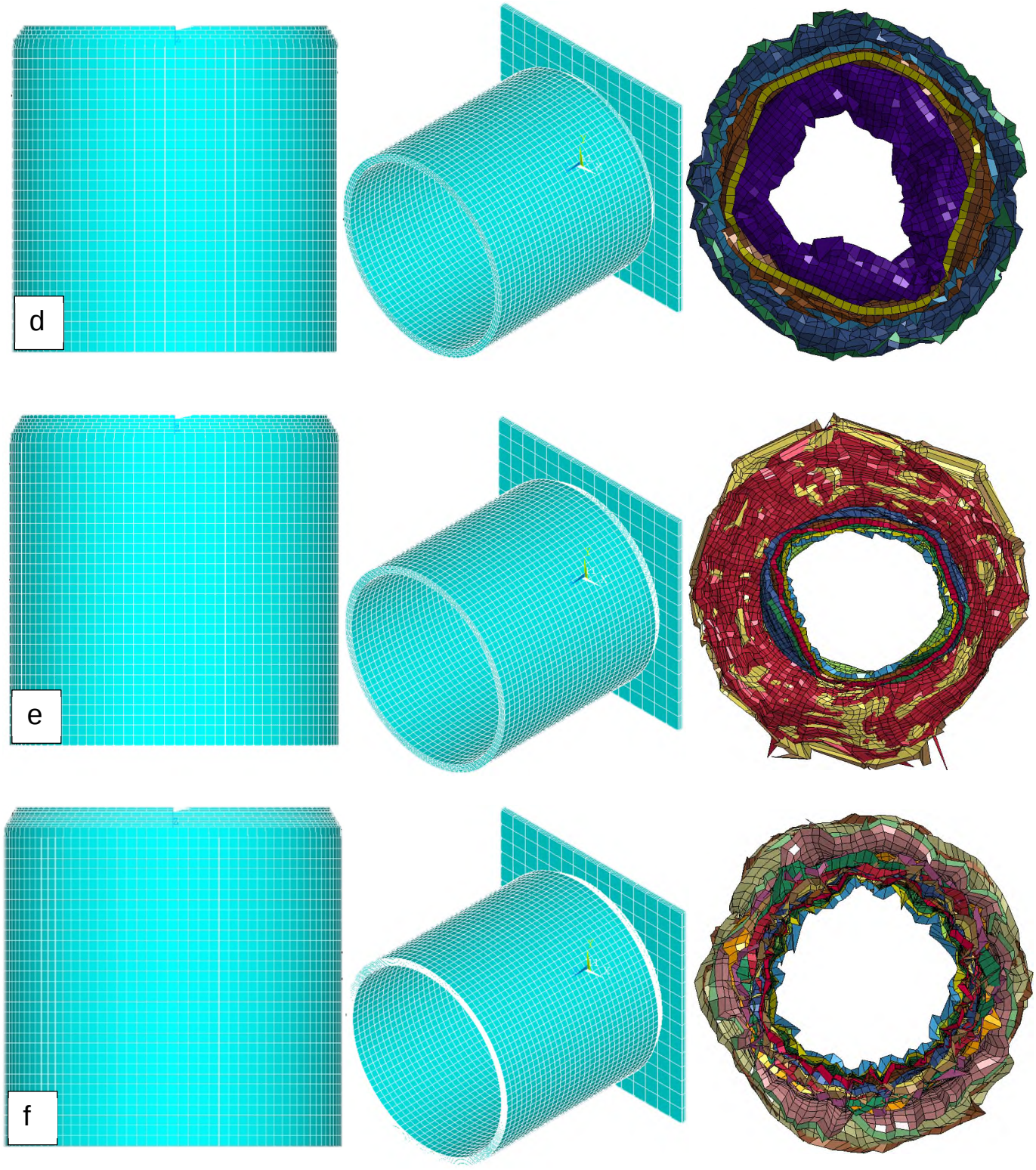

Figure 6-12 Number of shell configuration, a) 1 shell, b) 2 shells, c) 3 shells, d) 4 shells, e) 6 shells, f) 12 shells.

In this study, since the crushed morphology is also one of the factors that is greatly influenced, hence is implemented in Figure 6-12. From the crushed

morphology point of view, it can be concluded that, as the number of shells increase, the symmetricity and predication of crushing behaviour improves. Since 12 plies were used in experimental studies, six case study were considered. All cases were subjected to the same trigger mechanism and applied energy.

In Figure 6-13, the shell configurations are compared. In single shell configuration, the initial peak and mean crushing force is off by 45%. However, in double shell configuration, this improves to 5% difference. The initial peak value is 80 kN with crushing force of 67 kN. Hereafter, the computational cost is the deciding parameter. Since the crushing behaviour slightly or minimally improves by adding more shells. This improvement is in both initial peak value and mean crushing force value. However, the computational cost increases rapidly by adding more shells to the model. Using 12 shells configuration compared with experimental data, it has 1.5% difference and using double shell configuration has 5% difference. As an engineering point of view, this compromising 3.5% results into solving the problem in 4.5 times less computational costs, one takes 28 hours to converge and the other 123 hours.

At this stage since the main concentration is energy absorption capability, the reliable and cheaper computational cost of double shell configuration is considered in this study, and also supported by [143,144,188, 198].

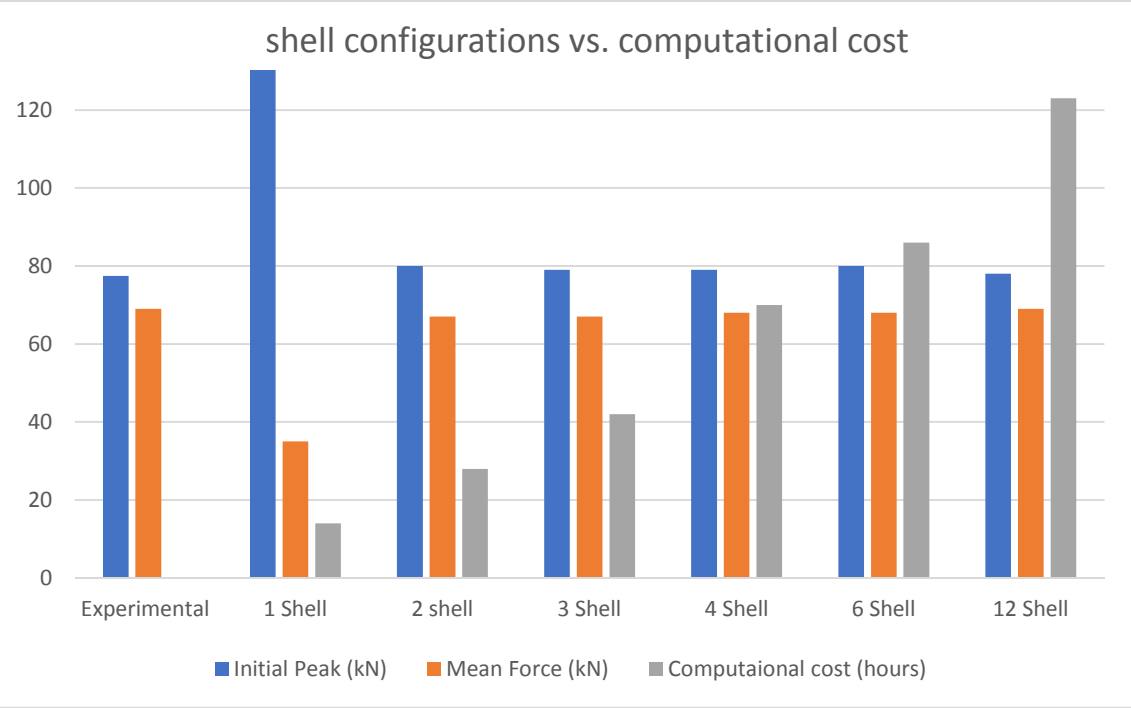

Figure 6-13 Shell configuration comparison

6.5 Model sensitivity to physical parameters

A robust finite element model needs to tolerate small variations in modelling parameters and be able to capture the differences. The aim of this section is to carry out a study of stability and sensitivity with respect to the material parameters, delamination, friction and impact loading. The reference model is the one developed earlier in this chapter and with tweaking the parameters by $\pm$ 10%.

6.5.1 Material model

The following parameters from Mat_54-55 in Ls-Dyna (see chapter 6.4.3.1), have been studied, stiffness, compressive strength, strain to failure in compression and strain to failure in tension. The stiffness and strength have an influence in fibre and matrix arrangements, and the strain to failure is a parameter that influences the experimental energy absorbed per unit of crushed volume/mass. The developed model needs to be compared with the experimental data. SEA value from the experimental data and numerical should be around the error percentage, which is 5%. When energy absorption capability is the main concern, SEA value,

which indicates the absorbed energy per crushed mass should be resembled in both to have a reliable FEM that predicts energy absorption capability.

6.5.1.1 Laminate stiffness

In Figure 6-14, the comparison of laminate stiffness is shown with stiffness increase and reduction of ± 10%. The SEA, initial peak and average crushing force is the main concentration of this study compared with reference FEM. It is noticeable that the computational cost remained the same with minimal change in all cases. The influence of stiffness on crushing behaviour is illustrated in the results. 10% increase, resulted into increase of initial peak value by 3 kN, mean crushing force increased to 71 kN, the SEA value increased by 4 kJ/kg. The displacement value was affected by a drop of 2 mm. 10% decease, resulted into reduction of initial peak value by 2.2 kN, mean crushing force decreased to 63 kN, the SEA value dropped by 12 kJ/kg. The displacement value was affected by an increase of 6 mm.

The results showed that increase in laminate stiffness caused higher initial peak value and mean crushing force value. Vice versa, the reduction of laminate stiffness caused reduction of these values, which shows the model is responsive toward small changes in the parameters.

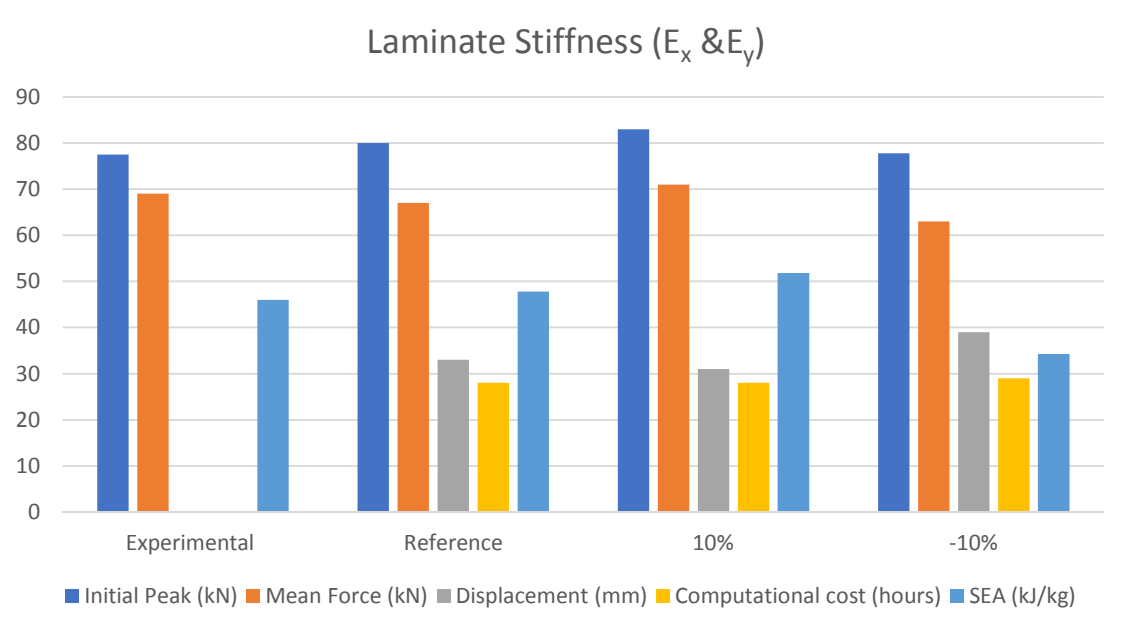

Figure 6-14 Laminate stiffness comparison

6.5.1.2 Compressive strength

Regarding energy absorption capability in Mat_54-55 card, compressive strength play an important role. Figure 6-15, shows the comparison between compressive strength with increase and reduction of $\pm$ 10%. The SEA, initial peak and average crushing force are the main concentration of this study compared with reference FEM. The computational cost remained the same with minimal changes in all cases. Increasing compressive strength, it results into increase of initial peak value by 6.5 kN, increase of mean crush force by 4 kN, reduction of displacement by 3 mm and increase in SEA value by 2 kJ/kg. Reduction of compressive strength by 10% results into, reduction of initial peak force value by 3 kN, reduction of mean crushing force by 1 kN, increase of displacement by 1 mm, and reduction of SEA value by 3 kJ/kg.

The results showed that reduction of compressive strength, caused the mean crushing force value to drop along with the initial peak value.

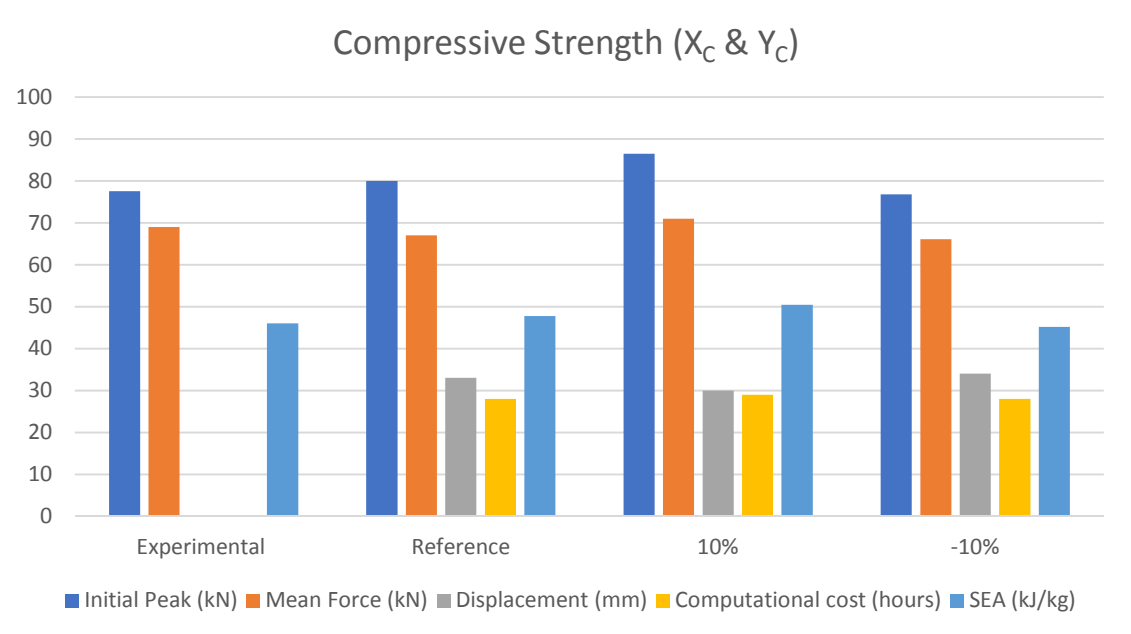

Figure 6-15 Compressive strength comparison

6.5.1.3 Strain to failure

The strain determines the elements deletion, which is an important parameter to adjust the model with experimental results. The Mat_54-55, allows defining different failure strains for shear and tension/compression. The model response is governed by the deletion of elements as previously mentioned. The failure of the elements is mainly affected by the strain to failure in compression (DFAILC) and failure in tension (DFAILT) that have been analysed by increase and reduction of ± 10% of these parameters.

6.5.1.3.1 Strain to failure in compression

In Figure 6-16, an important influence of the failure strain in compression with increase and reduction of ± 10% on the crushing efficiency is shown. The effect of 10% increase in DFAILC, results into increase in mean crush force by 6 kN, the initial peak was not affected, the displacement decreased by 4 mm and the SEA value increased to 53.7 kJ/kg with 6 kJ/kg difference in comparison to the reference model. The effect of 10% drop in DFAILC, results into a drop in mean crushing force value by 5 kN, increase in displacement by 7 mm, and 10 kJ/kg drop in SEA value.

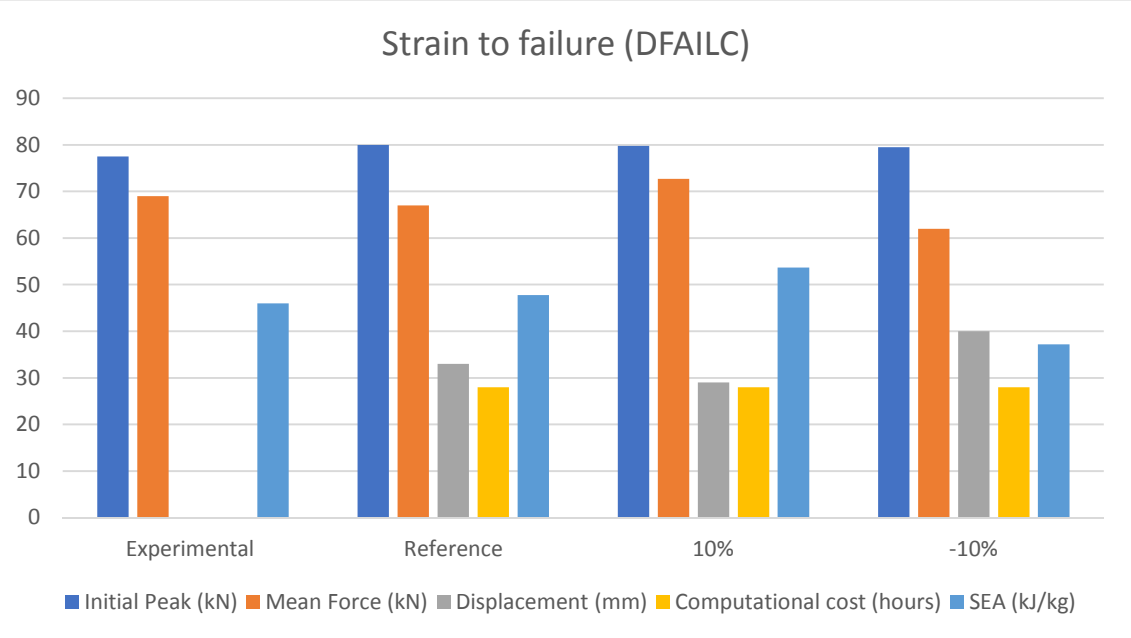

Figure 6-16 Strain to failure in compression (DFAILC)

6.5.1.3.2 Strain to failure in tension

In Figure 6-17, an important influence of the failure strain in tension with increase and reduction of ± 10% on the crushing efficiency is shown. The effect of 10% increase in DFAILT, results into increase in mean crush force by 5 kN, the initial peak increased by 2 kN, the displacement decreased by 2 mm and the SEA value increased to 55 kJ/kg with 7 kJ/kg difference in comparison to the reference model. The effect of 10% drop in DFAILT, results into drop in mean crushing force value by 2 kN, increase in initial peak value by 5 kN, increase in displacement by 2 mm, and 3 kJ/kg drop in SEA value.

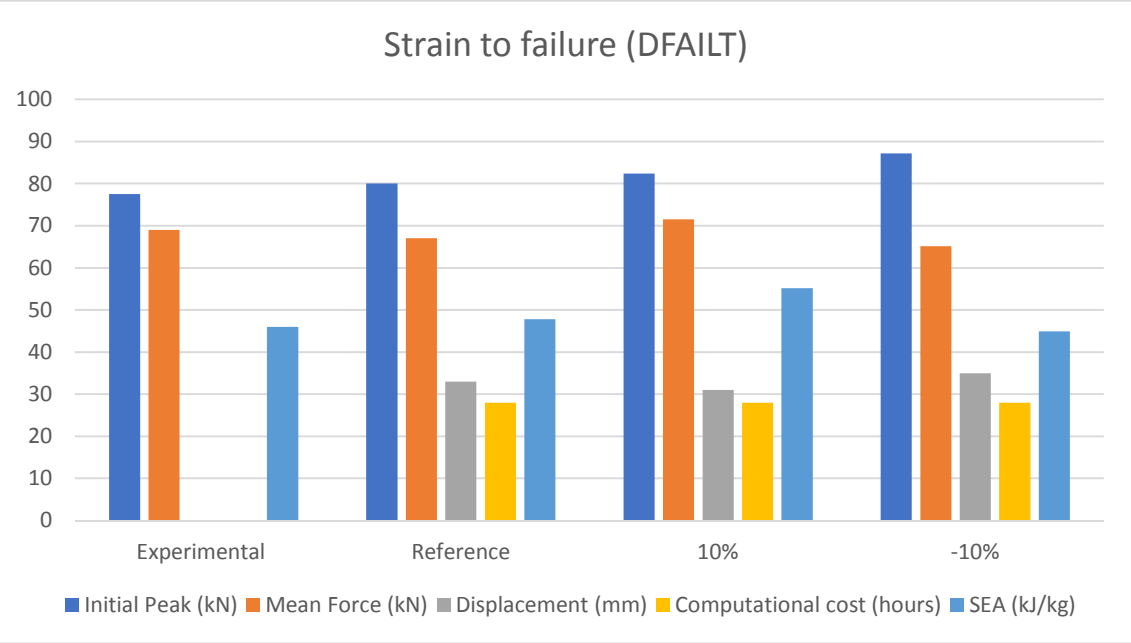

Figure 6-17 Strain to failure in tension (DFAILT)

6.5.2 Delamination model

The delamination between the shell was modelled with tiebreak option 8 described in section 6.3.2 and 6.5.1 in details. The current study in this section is to determine the element size and the sensitivity of the delamination algorithms according to Table 6-2. To ensure the mesh is fine enough to avoid premature failure of the interface and instability. The model sensitivity towards energy release rate would be analysed.

6.5.2.1 Tiebreak contact element size sensitivity

To capture the debonding of the plies, a simple model was created to simulate a DCB test for Mode-I delamination test. Different mesh sizes were considered 1.5 mm x 1.5 mm, 2.5 mm x 2.5 mm and 3.5 mm x 3.5 mm (see Figure 6-18). The relevant results were plotted against experimental studies [203] (see Figure 6-19).

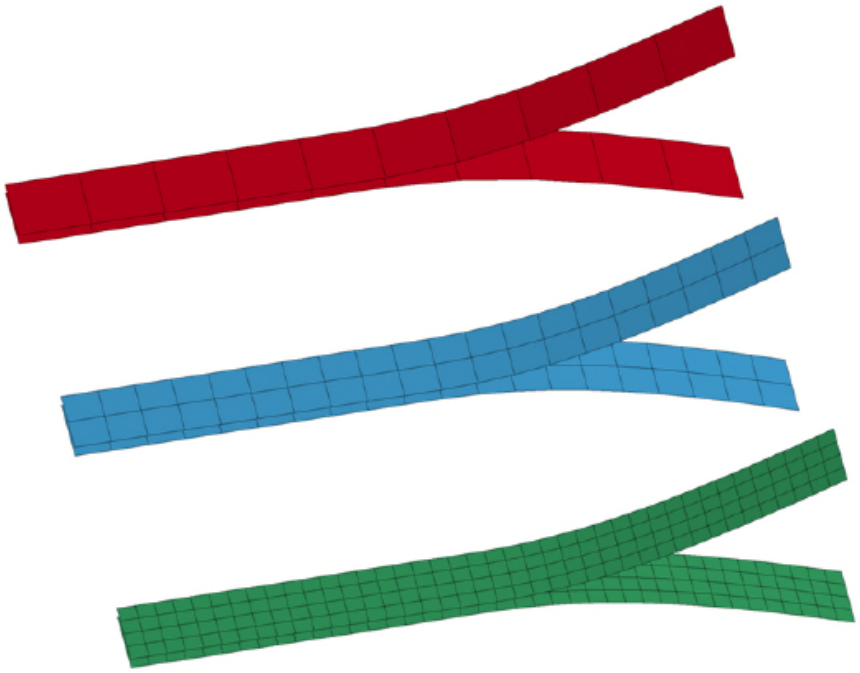

Figure 6-18 Tiebreak contact element size test

To assure the obtained results would be relevant towards experimental data, the FE results were compared with the experimental data. In Figure 6-19, all cases have captured the experimental curve, however, the 1.5x1.5 mm and 2.5x2.5 mm element sizes have closer values with minimal differences. The element size 3.5x3.5 mm overestimated the results throughout, and 2.5x2.5 mm which is the element size (see chapter 6.4.5) concluded to be both accurate enough and computational cost efficient.

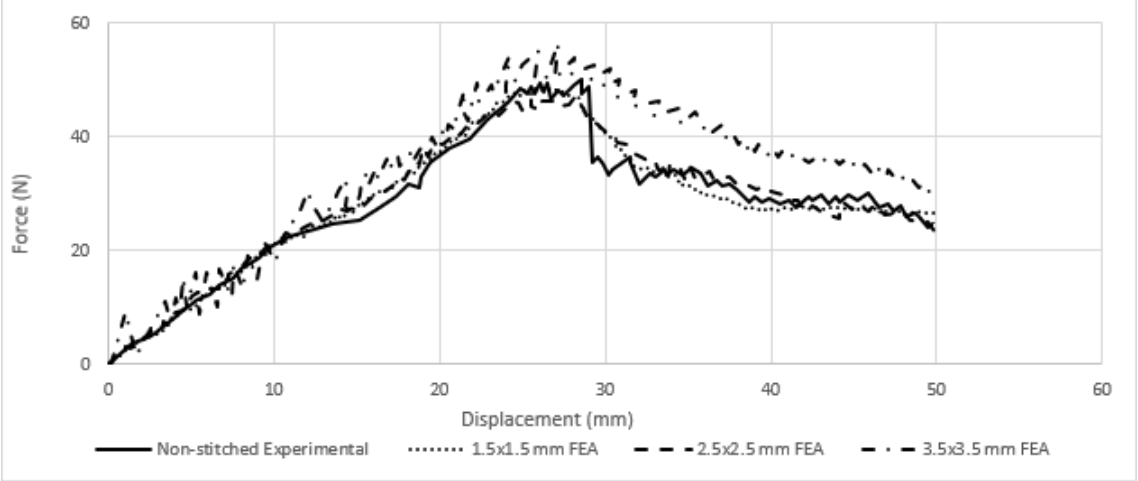

Figure 6-19 Force-distance curve of Mode-I delamination, experimental and FEA comparison

6.5.2.2 Delamination resistance

The aim of this study is to examine the sensitivity and the importance of the effect of tiebreak contact PARAM function on energy absorption capability of the developed FEM. Once the progressive failure has been stablished, the debonding of the plies is ruled purely by normal stress and according to equation 6-13, the G_{IC} is governed by normal stress and PARAM from the contact card. Increase in PARAM, therefore results into increase of G_{IC} proportionally. This effect has been used in this study to analyse its effect on Mode-I delamination resistance.

Figure 6-20 illustrates the effect of this parameter on crushing behaviour and energy absorption capability of the FEM by an increase and reduction of $\pm$ 10%. The effect of 10% increase in G_{IC}, results into increase in mean crush force by 6 kN, no change in initial peak, the displacement decreased by 5 mm and the SEA value increased to 54.5 kJ/kg with 6 kJ/kg difference in comparison to the reference model. The effect of 10% decrease in G_{IC}, results into drop in mean crushing force value by 6 kN, no change in initial peak value, increase in displacement by 7 mm, and 5.5 kJ/kg drop in SEA value.

The result indicate that Mode-I energy release rate has an important influence on the energy absorption capability, mean crushing force value, displacement and SEA value. To conclude this, it can be noted that modelling delamination as Tiebreak option 8, has been established to be sensitive towards capturing and effecting Mode-I delamination. The input parameters have a major effect on delamination resistance. Therefore, it is essential to validate Tiebreak input parameters as it has been carried out in previous sections, (see chapter 6.2.2, 6.4.1 and 6.5.2.1).

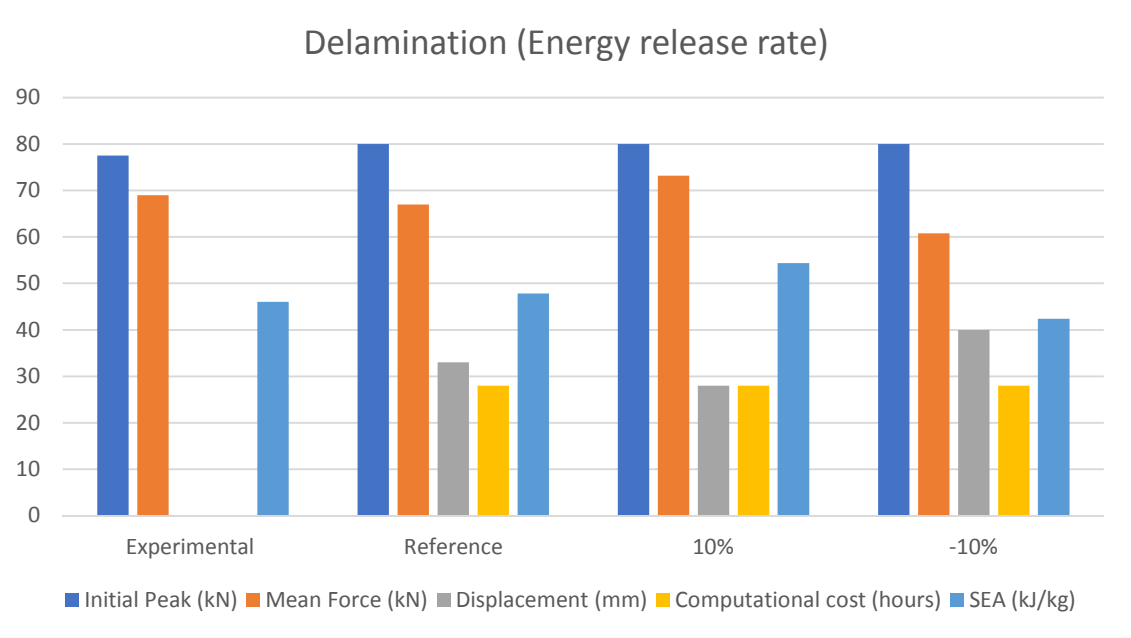

Figure 6-20 Delamination resistance comparison

6.5.3 Friction

Coefficient of friction is one the physical parameters that influences the progression of the simulation. In literature, many values have been stated varying from 0.1 to 0.3 for static and 0.1 to 0.2 for dynamic. The chosen values for static friction coefficient is 0.3 and 0.2 for dynamic friction coefficient [143,144,154-158,188, 198]. Both impactor to inner-shell and inner shell to outer shell friction coefficients are set to 0.3 and 0.2 for static and dynamic respectively. This is based on trial and error and based on previous researchers [143,144,154-158,188, 198]. This combination enables a sensitive crushing performance. In

this study the sensitivity of the FEM to friction is studied. The two scenarios are the friction between the impactor and the inner-shell and the friction between the shells.

6.5.3.1 Impactor to shell

In Figure 6-21, the results from the friction between the impactor and the inner-shell is compared based on an increase and decrease of ± 10%. The influence of coefficient of friction on mean crushing force is 2.5 kN and -3.5 kN. The only parameter that is not influenced by friction is computational cost. The initial peak force increased by 0.5 kN which is minimal and small enough to neglect when increased by 10% and no change with 10% reduction. The main concentration was mean crushing force, displacement and SEA. By 10% increasing the mean crushing force increased by 2.5 kN, the displacement dropped by 2 mm, and SEA value increased by 3 kJ/kg. By decreasing the friction by 10%, the initial peak had no effect, the mean crushing force dropped by 3.5 kN, the displacement increased by 2 mm, and the specific energy absorption decreased to 45.3 kJ/kg, which is around 2.5 kJ/kg. This parameter can influence the energy absorption capability and based on literature the optimum value is 0.3 and 0.2 for static and dynamic respectively [143,144].

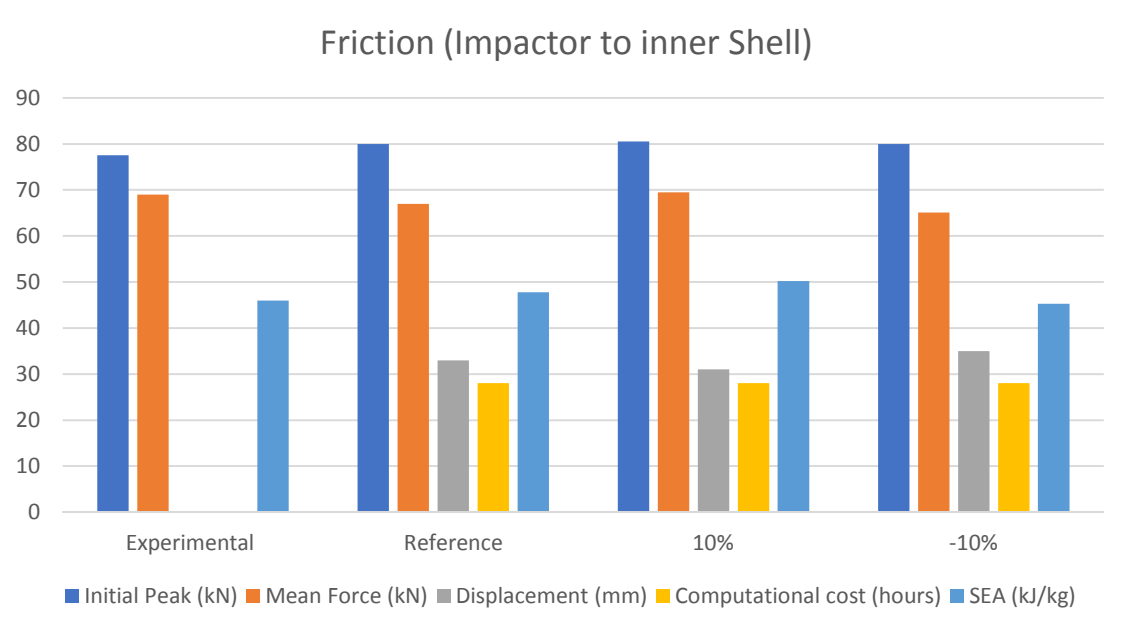

Figure 6-21 Impactor to inner-shell friction coefficient comparison

6.5.3.2 Shell to shell

Many researchers have used friction to simulate delamination, e.g. [143,144]. Friction influences the energy absorption capability of the model and using friction influences the SEA value, for example, increasing friction between the shells, causes higher SEA value. This technique cannot be used, as numerical and experimental results due to the increase in SEA value will be significantly different. Therefore, a different approach was considered. Tiebreak option 8 was utilised instead of friction to model delamination as this contact card can define Mode-I and Mode-II energy release rate which simulates delamination. However, the correct friction between the shells must be implemented. This friction between the plies also exist in real scenarios, and its effect on the energy absorption capability must be addressed.

In Figure 6-22, the results from friction between the inner-shell and the outer-shell is compared based on an increase and decrease of $\pm$ 10%. The influence of coefficient of friction on mean crushing force is 3 kN and -3.5 kN. Throughout the study the computational cost and initial peak force was unaffected. The main concentration was mean crushing force, displacement and SEA. By 10% increasing the mean crushing force increased by 3 kN, the displacement dropped by 1 mm, and SEA value increased by 3.5 kJ/kg. By decreasing the friction by 10%, the initial peak had no effect, the mean crushing force dropped by 3.5 kN, the displacement increased by 3 mm, and the specific energy absorption decreased to 41.8 kJ/kg, which is around 6.5 kJ/kg. This parameter can influence the energy absorption capability and based on literature the optimum value is 0.3 and 0.2 for static and dynamic respectively [143,144].

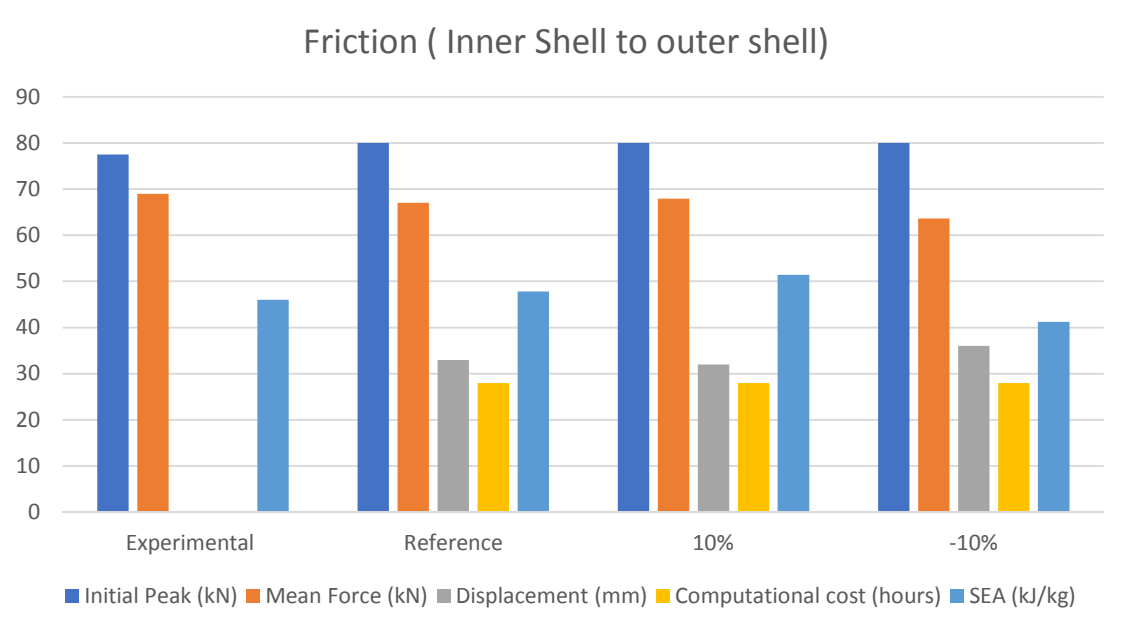

Figure 6-22 Inner-shell to outer-shell friction coefficient comparison

6.5.4 Impact velocity

In this section various impact velocities are raised to study and analyse the developed model against its sensitivity towards capturing the initial peak, mean crush force, displacement (stroke) and specific energy absorption. In this study the experimental data and reference model is compared with different impact velocities and applied kinetic energies. The cases are, 4 m/s (0.84 kJ), 5 m/s (1.31 kJ), 6 m/s (1.89 kJ) and 8 m/s (3.4 kJ). Understanding how robust the model is with respect to the input kinetic energy, would indicate the range of impact conditions the model can predict with certain tolerance.

Figure 6-23 show the extracted results from the simulations. The simulation results illustrate a similar or within 0.4% difference in initial peak value and the specific energy absorption which indicates the energy absorption per crushed mass and is within 4% difference between the reference model. The lower the input kinetic energy the lower the displacement, the displacement values indicate the similar trend. The mean crushing force are slightly affected although the highest difference from the reference model is 3.5%.

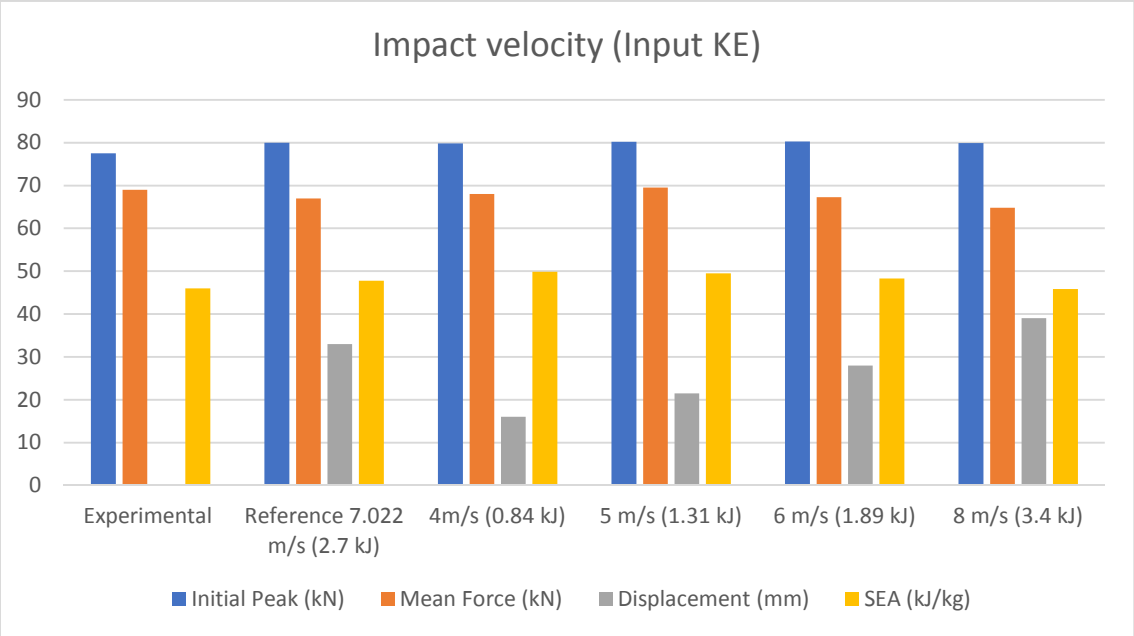

Figure 6-23 Impact velocity or kinetic energy input sensitivity data

6.6 Modelling limitations

Based on the study carried out in section 6.5 where sensitivity towards physical parameters were studied based on the developed model. The FEA results is influenced by many input parameters. To develop a model that is capable of predicting energy absorption in an accurate enough format, few extracted results must also be acceptable. These parameters are computational cost, initial peak force, mean crushing force, displacement and specific energy absorption. A relative simple model approach leads to high efficiency and this was the main concentration of this chapter. There is a balance between computational cost and final results that needs to be within an acceptable range of up to 10% [143].

In Mat_54 some setting parameters have no physical meaning, this limitation might cause the simulation model to be ruled by non-physical process when not near validated crush scenarios are being simulated. Therefore, the applicability of the model to another crush scenario must be carried out with care. A change in geometry and the mechanical properties mean that the model can be adopted to that specific crash scenario with care and some adjustments.

More advanced material cards are being developed with delamination models with solid elements to improve capturing delamination energy, this needs further studies on the mechanical properties of the material and energy release rate in Mode-I and Mode-II. Most importantly using solid elements rapidly increases computational costs compared with shell elements. This technique increases accuracy, although both testing and computational costs increases.

Increasing the material model complexity leads to further test data which is expensive and increases computational costs. Depending on case studies, from an engineering point of view, finite element model with accuracy of up to 10% is acceptable [143-144]. However, the developed model has its limitation to portray or show the fracture and crushed in smaller scale, force-displacement characteristics and debris wedge.

6.6.1 Fracture morphology

Regarding crushed morphologies, to capture axial splits using Mat_54, the DFAILM, which is the failure strain in the matrix direction [192] can be utilised. Adjusting the value of DFAILM enabled matrix splitting to occur (see Figure 6-24), as observed in the experiments (See Chapters 3 to 5). However, this parameter influenced the computational costs to be unreasonably high. Due to this fact and keeping a reasonable experimental efficiency, DFAILM values were retracted to original values. It is worth mentioning that, in this research the main concentration was capturing energy absorption capability. DFAILM had marginal effect on energy absorption capability as mentioned above. In material model Mat_54-55, the stacking sequence plays an important factor on crushed morphologies. In Figure 6-25, the FEM crushed morphologies of $[0]_{12}$ is shown, which resembles the experimental crushed morphologies. However, using $\pm$ 45 leads to inadequate failure modes if DFAILM values exceeds 10% to obtain matrix splitting/separation (see Figure 6-24 b).

Figure 6-26 show the comparison between reference FEM and increase in DFAILM by 10% and 20%. The effect of DFAILM on axial split is shown in Figure 6-24, this improves crushed morphology representation. Although, the results regarding energy absorption capability including SEA values were unaffected by

this parameter. At 10% increase, the axial split occurs in this FEM, this causes 138% increase in computational costs. Increasing DFAILM by 20% causes 176% increase in computational costs.

In consideration of these results, capturing axial split seems rather unreasonable due to its effect on computational costs. Increasing DFAILM value by 10 to 20% had minimal or no effect on the results and below 10% axial split in this FEM does not occur.

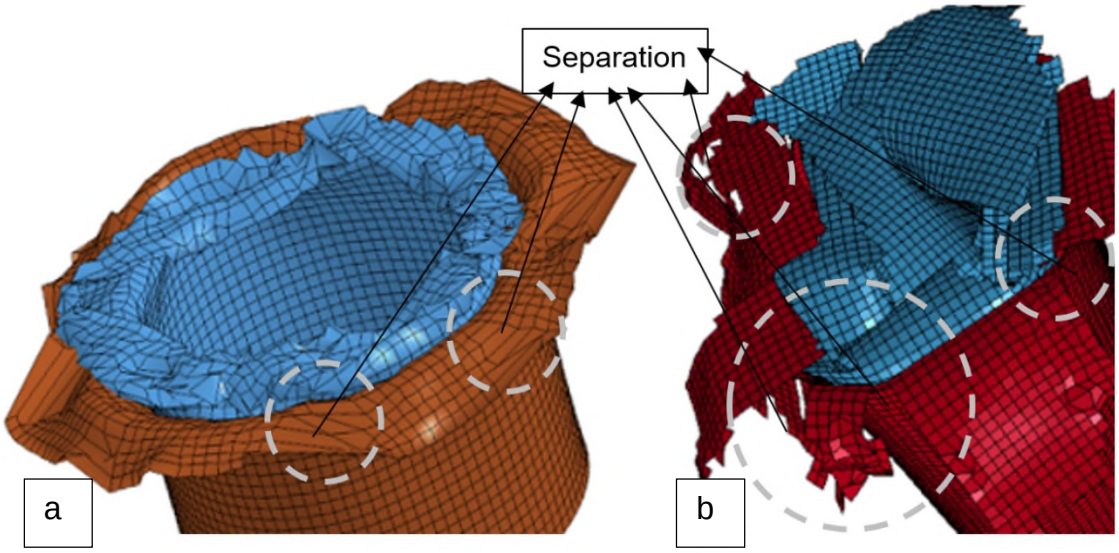

Figure 6-24 Effect of DFAILM on axial split, a) reference model b) 10% increase DFAILM

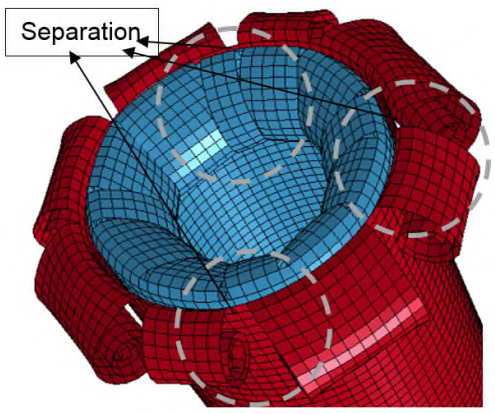

Figure 6-25 Effect of stacking sequence of $[0]_{12}$ configuration on petal formation of FEM crushed morphologies using DFAILM

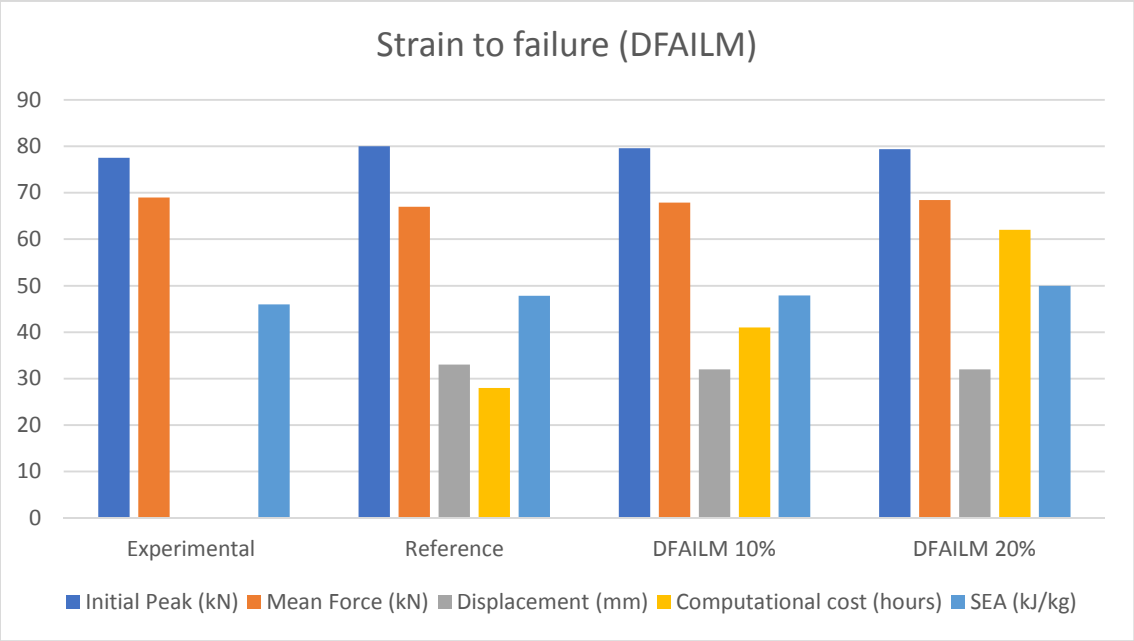

Figure 6-26 Strain to failure in matrix direction (DFAILM)

6.6.2 Force-displacement characteristics

The visual differences in crushed morphologies and crushing process of composite tubes and FEA are captured by the force-displacement curve diagram. Figure 6-27 show the numerical and experimental data and by carrying out a comparison, the model limitations are manifested.

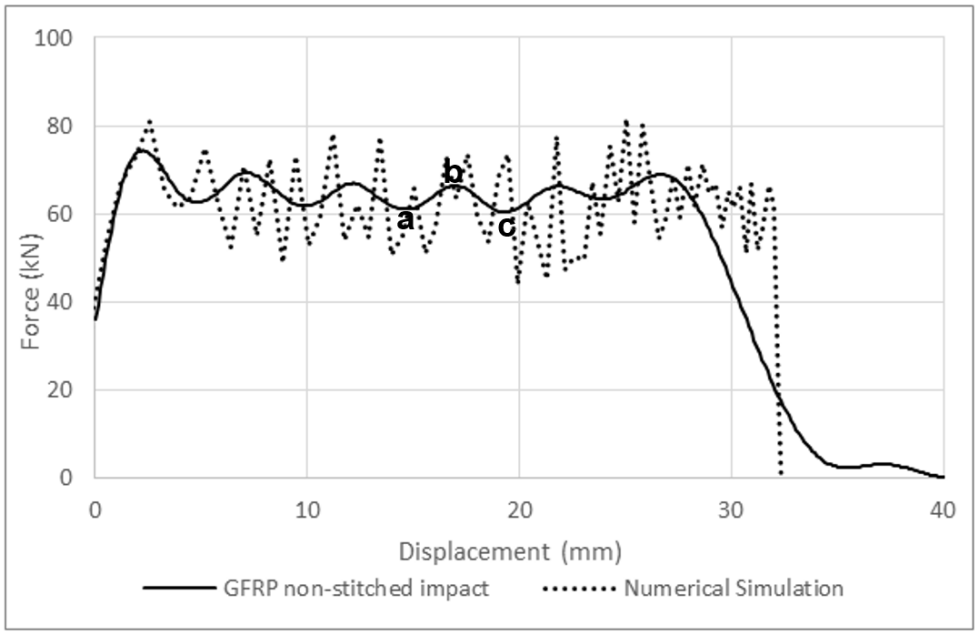

Figure 6-27 force-displacement characteristic experimental and numerical comparison

As described by Hall [17], the experimental (solid black), has a serrated shape where the positive slope segments such as (ab) represent the increase in resistance load due to multiply tracks propagate and initiate until point (b) is reached. Further crushing is initiated causing a negative slope or drop in resistance force.

In finite element (Dotted black), the oscillations are governed by the elements deletion between fronds, and the amplitudes are a function of the strain to failure of the element controlling the tearing and the mode-I delamination resistance.

At any stage of the crushing process, the experimental resistance force is governed by the weakest possible collapse mode(s). The curves from the FEA and the experimental (see Figure 6-27) are different amplitudes and ranges. The amplitudes of the curve and wavelength of FEA is governed by elements deletion as mentioned and the element size effect the wavelengths. Nevertheless, this means that some collapse modes are not captured by the model properly.

6.6.3 Debris wedge

During the crushing process, the fractured material is usually trapped between the main fronds of the tube. This increases the friction and affects the crack growth and delamination resistance.

The FEM is not able to simulate this effect if element deletion takes place and do not interfere any longer with the remaining structure. This issue can be resolve by increasing delamination resistance or increasing friction between the shells if multi-shell configuration is utilised.

Some researchers have tried modelling debris wedge, McGregor [161] used a predefined debris wedge designed as rigid, and Mamalis [155] defined an intermediate layer trying to represent the pulverised material.

6.7 Conclusion

The aim of this chapter was to develop a finite element model using LS-DYNA to simulate the crushing behaviour of composite tubes with chamfer failure trigger mechanism. Various shell configurations were studied and multi-layer shell

element with double-shell configuration produced accurate enough results with difference of less than 5% with minimal computational cost compared with other configurations. This configuration was used to predict energy absorption capability and specific energy absorption, other considerations were deformation and damage progression of the composite tubes. Each shell element or layer can contain either a single ply or multiple plies. The layers were tied using Tiebreak option 8 contact definitions. This contact card has the capability of modelling delamination between the layers through energy-based approach. The material card of Mat_54 was used to represent each ply and few parameters in the material cards were studied to find the optimum configurations to match the experimental studies. SOFT and DFAILC (compression failure strain) were the main parameter that effected energy absorption capability and specific energy absorption was influenced by these parameters. The sensitivity of the model was studied against material model, delamination model, friction and impact velocity. The results show that the model is sensitive towards minimal input change. The simulation results showed that the failure peak load, mean crushing force, SEA, all compared very well with the experimental results.

In conclusion, the developed model in this study was shown to be capable of accurately capturing crushing behaviour of the tubes with minimal differences whilst being computational cost efficient. The numerical and experimental studies are in good agreement.

7 Numerical Study of Axial, Off-Axis, Stitched and Non-Stitched Sections under Quasi-Static and Impact Loading

7.1 Introduction

This chapter presents numerical studies on the effect of off axis and multi-stitching pattern on the energy absorption capability of composite tubular structures under quasi-static and impact loading. A new multi-stitching pattern was developed to study the increase of specific energy absorption capabilities in GFRP and CFRP tube absorbers (chapter 4 and 5). The stitching pattern on both specimens showed a significant increase in specific energy absorption capabilities under quasi-static and impact loading. A multi-shell finite element model was constructed to predict the axial and off-axis crushing behaviour and energy absorption capability of composite structures under quasi-static and impact loading. The method is based on surface contact modelling technique definition in the stitched area to represent the functionality of the stitched area during an impact event. This energy-based approach was used to determine the input parameters for the tiebreak formulations to accurately simulate delamination between the plies. Tiebreak option 8 was utilised to model delamination as this contact card can define Mode-I and Mode-II energy release rate which simulates delamination. A scaling factor was introduced to account for ply interfaces that were not represented by a tiebreak definition. The contact card, tiebreak option 8 was then defined between the shells in respect to the parameters obtained experimentally for stitched and non-stitched specimens. In the stitched area the PARAM' was increased according to the experimental data and validation, and in the non-stitched area normal PARAM' was used. This increases G_{IC} energy release rate within the stitched area and demonstrated similar behaviour as the experimental stitched specimen. The developed numerical approach is efficient in terms of accuracy and simplicity in comparison with the existing methods for multi-layered composites structures.

In all previous studies, several FE modelling was introduced with unique techniques to achieve ideal force/displacement curves focusing on different

parameters including contact definition and crack propagation modelling. The aim of this chapter is to fulfil demands for a crushing finite element model, that can be used in axial and off-axis under quasi-static and impact loading using multi-shell configuration using LS-DYNA software, based on chapter 6. This chapter also focuses on developing a technique to model stitching through thickness to locally increase energy absorption capability that consequently increases overall energy absorption representing experimental studies.

7.2 Experimental testing of circular tubes

7.2.1 Material and tube geometry

In this study, composite sections were fabricated from CFRP and GFRP unidirectional pre-pregs. Glass/epoxy (ρ = 2250 kg/m^3) tubes consists of twelve individual unidirectional (UD) pre-impregnated layers with inner diameter of 74 mm, outer dimeter of 80 mm and length of 80 mm with laminate design of $[-45/45/0/90/0/90]_S$. The integrated sequence of $[-55/35/-10/80/-10/80]_S$ was adopted and used to cancel the 10^o off axis effect. Carbon/epoxy (ρ = 1800 kg/m^3) tubes consists of twenty two individual unidirectional (UD) pre-impregnated layers with inner diameter of 97.4 mm, outer dimeter of 100 mm and length of 150 mm with laminate design of $[-45/45/-45/45/0/90/0/90/0/90/0]_S$ using hand lay-up technique. The specimens subjected to stitching through the thickness, a novel stitching pattern of 10-15-20-25-30-35 mm utilised from the 45^o chamfered end using Kevlar.

Each case study was modelled regarding the experimental setup and all parameters that effected energy absorption capabilities were kept constant, including strain rate, loading rate, lay-up and geometry. The concentration of this study is to find energy absorption capabilities at different conditions of axial, off axis loading, stitched and non-stitched under quasi-static or impact loading.

The material properties were based on experimental studies of [143,144,155,158,182,200,203,204].

Table 7-1 Material properties of CFRP and GFRP [143,144,155,158,182,200,203,204]

GFRP (TenCate 7781/E772)							
E_1 (GPa)	E_2 (GPa)	G_{12} (GPa)	v_{12}	$\sigma_u\ 0^o$ (MPa)	$\sigma_u\ 90^o$ (MPa)	τ_s (MPa)	V_f (%)
39±3	11.8±1	3.2±0.5	0.29	836±20	29±2	97±4	58
CFRP (Hexcel T300/914C)							
E_1 (GPa)	E_2 (GPa)	G_{12} (GPa)	v_{12}	$\sigma_u\ 0^o$ (MPa)	$\sigma_u\ 90^o$ (MPa)	τ_s (MPa)	V_f (%)
67±5	9.8±1	4.8±1	0.32	296±10	27±3	115.5±2	42.5

7.2.2 Experimental setup

In quasi-static testing, a 500 kN load cell capacity hydraulic press was used with 2 mm/second loading rate. All specimens were allocated in respect to the centre of the stroke for equal load distributions. The stroke displacement for all specimens was kept at 50 mm. The profile of load-displacement consists of load cell and stroke displacement.

In impact testing, a drop tower with impactor mass of 108.4 kg was used at 2.0 m height and 7.022 m/s velocity, a total energy of 2672 J was applied to each specimen. The mass is dropped from a pre-determined height of 2.0 m to initiate and record the load against time once it reaches the specimen. It will only stop when the applied energy of 2672 J is absorbed by the specimen. The hammer is then pulled back up by the machine. The impactor once hitting the tube leading edge, the load cell records the force history. A high speed full HD video camera with resolutions of 2,000 frames per second was used to capture the crushing event.

7.3 Finite element modelling

7.3.1 Basic consideration

For the simulations, an Explicit FE LS-DYNA code was used with multi-layered shell configuration to reduce numerical cost. Composite tubes were modelled as double layers of Belytschko-Tsay circular shell elements with one integration point in the element plane to represent the direction of the stacking sequence. The GFRP innermost shell has six integration points with another six integration points being assigned to the outermost shell to represent all twelve UD-layers. In GFRP tube each individual layer has a thickness of 0.25 mm. The total thickness of both shells is 3 mm. In CFRP the innermost shell has eleven integration point with another eleven integration points being assigned to the outermost shell to represent all 22 UD-layers with a thickness of each individual layer being 0.118 mm. The total thickness of both shells is 2.6 mm. Each fibre orientation is assigned with insertion of an integration point in respect to the stacking sequence used with its associated thickness.

7.3.2 FE model setup

In shell theory the thickness of the shell is considered as mid-plane. The outer radius of the GFRP tube was 40 mm with a thickness of 3 mm. Two Shells with radiuses of 37.75 mm and 39.25 mm to represent the inner and outer shells with lengths of 80 mm and 77.5 mm were modelled respectively using LS-PrePost representing the GFRP tube geometry (see Figure 7-1). Each shell was glued together so that the triggering at the top of the shell would not detach during the crushing process. In this triggering approach, two shells were used, one with 2.5 mm in height acting as the trigger, and the other depending on being inner or outer shell had its representative height assigned. Therefore, the top shell at each FEA case study represents the trigger. Similarly, the CFRP tubes were modelled as double shells with radiuses of 48.05 mm and 49.35 mm representing the inner and outer shells with length of 150 mm and 147.5 mm respectively.

Quadrilateral shell elements were used with each element size of 2.5 mm x 2.5 mm. The trigger mechanism was modelled by reducing first row thickness of the

shell elements to represent the bevel trigger, from 1.5 mm to 0.05 mm in each shell. A solid element rigid block was modelled to represent the striker. LS-DYNA Material model of Enhanced_composite_damage (Mat_54-55), which is an orthotropic material with failure criterion of Chang-Chang was used. This failure criterion is a modification of Hashin's failure criterion for assessing lamina failure. The hourglass was set at 10% [154-158,188, 198].

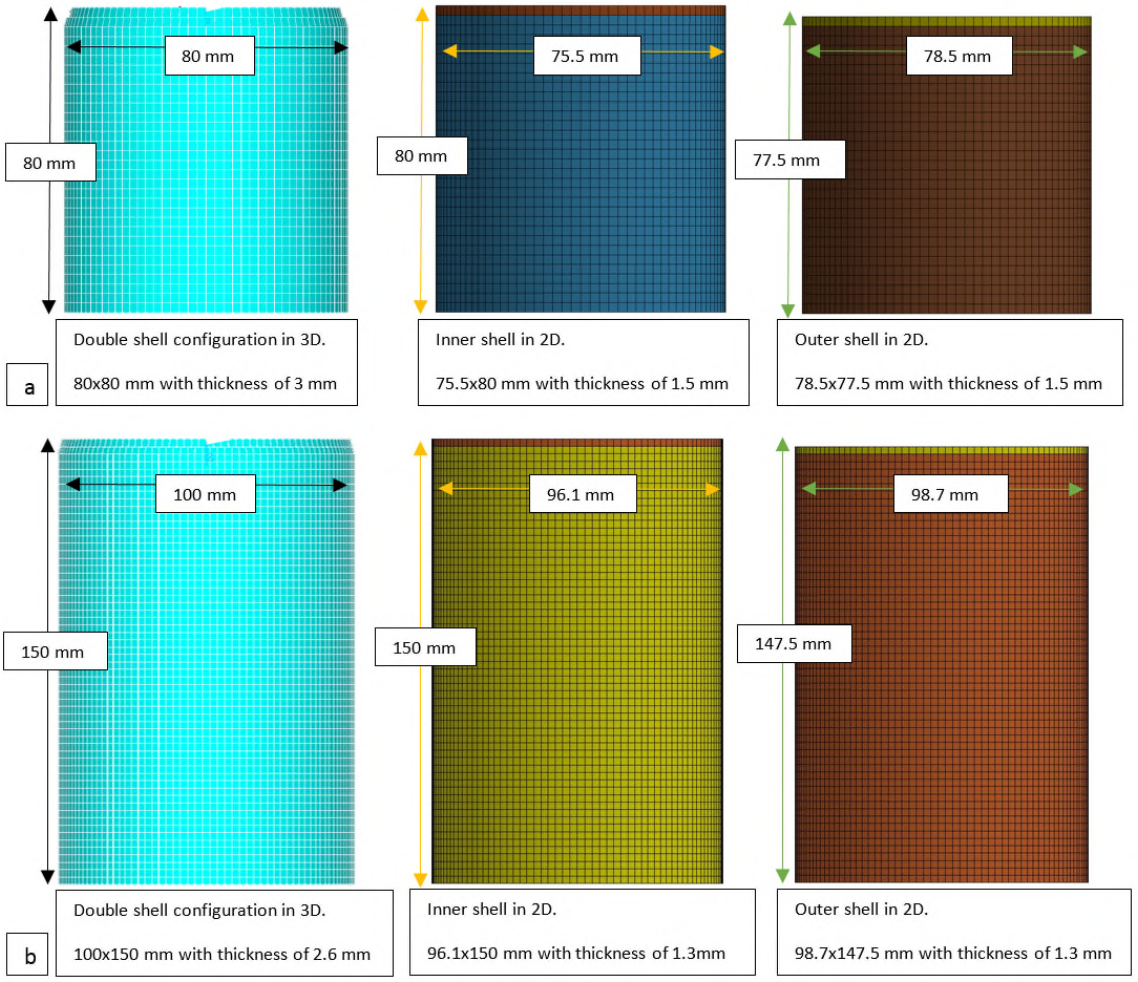

Figure 7-1 shell geometry configuration. a) GFRP shell configuration b) CFRP shell configuration

Modelling interlaminar separation or delamination failure (Mode-I) requires either detailed experimental investigation for cohesive zone or three-dimensional representation that both result into increase of computational and experimental costs. Delamination failure causes energy absorption and this can be modelled with multi-layered shell configuration with a contact card that is capable of G_{IC}

implemented energy release rate [185-188]. Defining One_Way_Surface_To_Surface_Tiebreak contact between the two shells with inner tube being master and outer being slave.

The tiebreak option enables the detachment of the contact surfaces after reaching a maximum normal stress (NFLS) or shear stress (SFLS). If the failure parameter, driven by occurring normal and shear stresses, become 1, the contact forces soften linearly until contact distance PARAM is reached and the interface failure is completed. Based on the interlaminar utilisation of the contact, the parameters are determined by the mechanical properties of the matrix material. Consequently, shell layers detach when the interlaminar stress exceeds the matrix properties, which are mainly responsible for interlaminar strength. Maximum normal and shear contact stresses for the tiebreak contact are based upon the mechanical properties of the epoxy resin. The critical normal separation of the surface is set to 0.15 mm and 0.32 mm for non-stitched and stitched specimen. Automatic_Node_To_Surface contact was defined for the striker and inner shell with striker being master and inner shell being slave. Automatic_Single_Surface contact algorithm was utilised. This prevents penetration of the crushing tube by its own nodes. In the calibration procedure, parameters DFAILT, DFAILM and DFAILS (shear failure strains) were found to have a marginal effect on the results and were kept constant at arbitrarily selected values of 0.02, 0.02 and 0.03, respectively. However, increasing DFAILM value, increased computational cost unreasonably, and produced unrealistic crushed morphologies, this is due the stacking sequence, when ± 45 are used the matrix split becomes unpredictable (see Figure 6-24). utilising a stacking sequence of $[0]_{12}$ has shown effective with realistic axial splits and petal formations (see Figure 6-25). It was found that simulations with DFAILC = -0.004 and SOFT = 0.75 yielded the mean crushing force value and displacement behaviour for chamfered tubes that matched very well with experimental data.

To satisfy quasi-static conditions, it is important that the load is applied in a manner that would yield a minimal inertial effect on the results and the ratio of the kinetic energy to the internal energy must be reasonably small. Time-scaling was

utilised to apply the load in higher rate to reduce total simulation time. A constant loading rate of 0.65 m/s was applied and the kinetic energy to the internal energy were less than 10% upon initial contact and less than 5% throughout the remaining of the crushing process.

All bottommost nodes of all shell element layers are constrained in their translational degrees of freedom. The impactor is modelled as rigid with a mass of 108.4kg and velocity of 7.022 m/s. Gravity is modelled with an acceleration factor of 9.81 m/s^2. All simulation results are smoothed using SAE 300 Hz filter [188].

7.3.3 Stitch modelling

In simple non-stitched specimen, three different components were defined, inner shell, outer shell and the striker. The contact definition for inner shell and out shell was One_Way_Surface_To_Surface_Tiebreak option 8 with static and dynamic coefficient of frictions of 0.3 and 0.2 respectively. To model stitching between the shells, different approaches were taken place, it is worth mentioning that the stitching improves Mode-I interlaminar fracture toughness, therefore the crack propagation resistance improves, to implicate this in finite element, an energy-based contact card was used. Since contacts are defined for components in LS-DYNA explicit, five components were defined, inner shell, stitching of inner shell, outer shell, stitching of outer shell and the striker. The construction of either inner shell or outer shell consists of 14 shells, all these shells were glued together to perform as one shell. This enables defining different components on a shell. This method is used to define the trigger mechanism, defining two contact card for the stitched models. Fourteen shells were used as mentioned, one for the trigger, 6 for the stitching, and 7 shells for the main body, this process was used for both inner and outer shells (see Figure 7-2) and the stitch area on both shells align. The double contact definition technique consists of Tiebreak (option 8) contact with static and dynamic coefficient of frictions of 0.3 and 0.2 respectively were assigned to inner and outer shells. In stitched delamination, the Mode-I crack propagation resistance increases, hence in the modelling of stitching, G_{IC} is increased. Therefore, in non-stitched regions the contact has the parameters

mentioned in table 6-2, and in stitched regions the contact has the parameters mentioned in table 6-3. The critical normal separation of the surface is considered in this contact card, known as PARAM, based on the energy release rate in Mode-I (G_{IC}) and the critical normal stress. In the stitched region, the Mode-I energy release rate (G_I) for delamination growth increases according to table 6-3, which is based on experimental studies and in non-stitched region these parameters are set for normal Mode-I energy release rate (G_I) for delamination growth according to table 6-2.

This method increases the Mode-I delamination crack growth resistance during the crushing process within the stitched area and consequently simulates the stitched area similar to experimental data (see Figure 7-3). The setup and the contact definitions used in the non-stitched and stitched finite element model are shown in Figure 7-3.

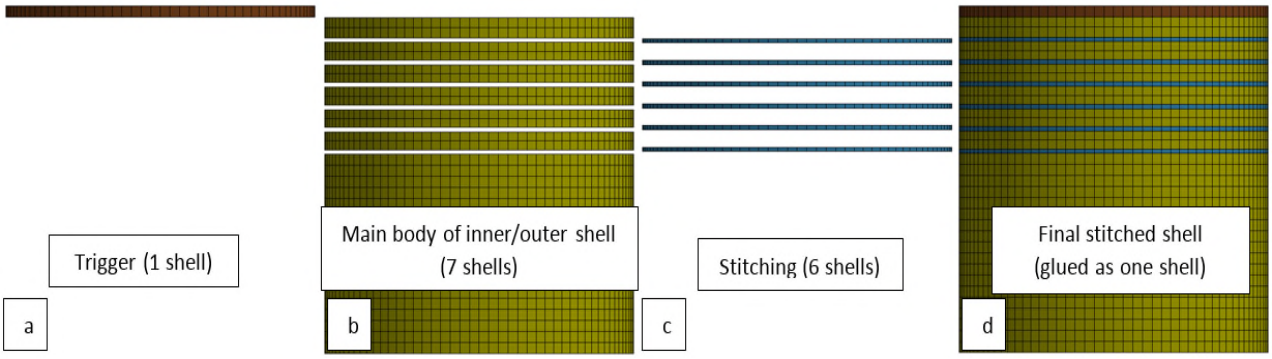

Figure 7-2 construction of either inner or outer stitched shell. a) trigger mechanism (1 shell), b) main body of the inner/outer shell (7 shells), c) stitching (6 shells), d) final stitched shell, glued as one shell

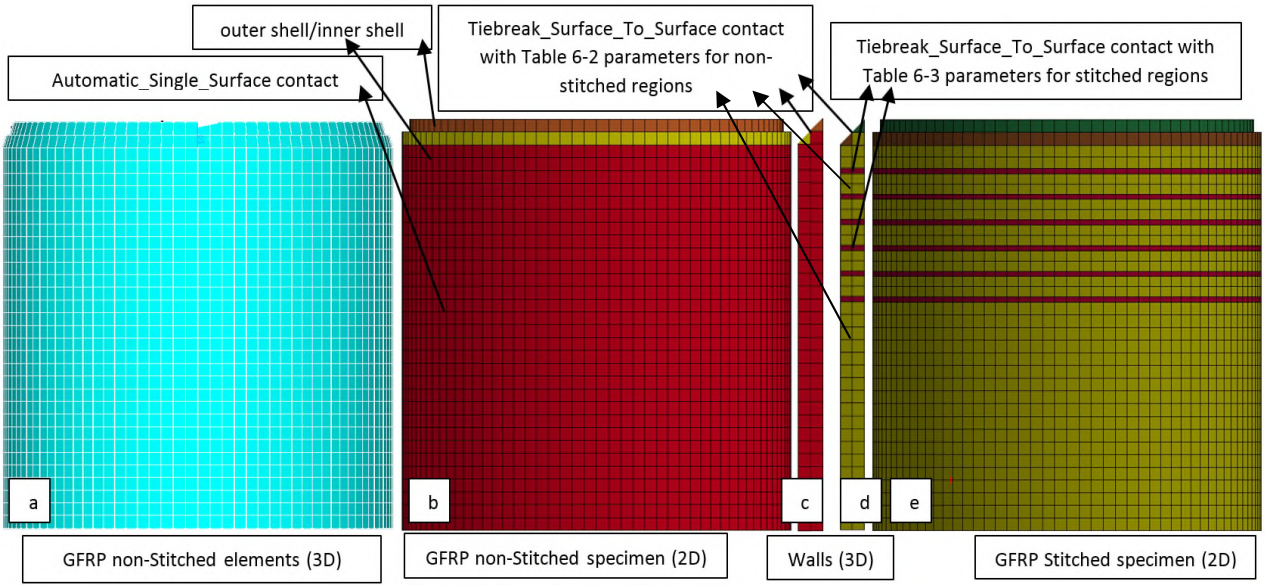

Figure 7-3 FEA contact definition of double shell stitched and non-stitched. a) GFRP non-stitched elements with thickness (3D), b) GFRP non-stitched without thickness (2D), c) GFRP intrawall non-stitched with thickness (3D), d) GFRP intrawall stitched with thickness (3D), GFRP stitched without thickness (2D)

Stitching was modelled using Table 6-2 and 6-3 values with One_Way_Surface_To_Surface_Tiebreak contact card. This technique has led to capture both stitched and non-stitched crack growth behaviour through FEA. Figure 7-4, a) the comparison of stitched and non-stitched DCB tests for mid-plane interface is shown. The stitched specimen has increase Mode-I resistance and delayed crack initiation. Stitching through the thickness has increased crack propagation force by 40 kN. Figure 7-4, b) the FEA analysis for DCB tests for mid-plane interface for stitched and non-stitched specimen has been investigated to establish the effect of the contact definition to increase Mode-I delamination resistance. The combination of this effect on the stitched tubes (see Figure 7-2 and 7-3) can simulate the stitching effect.

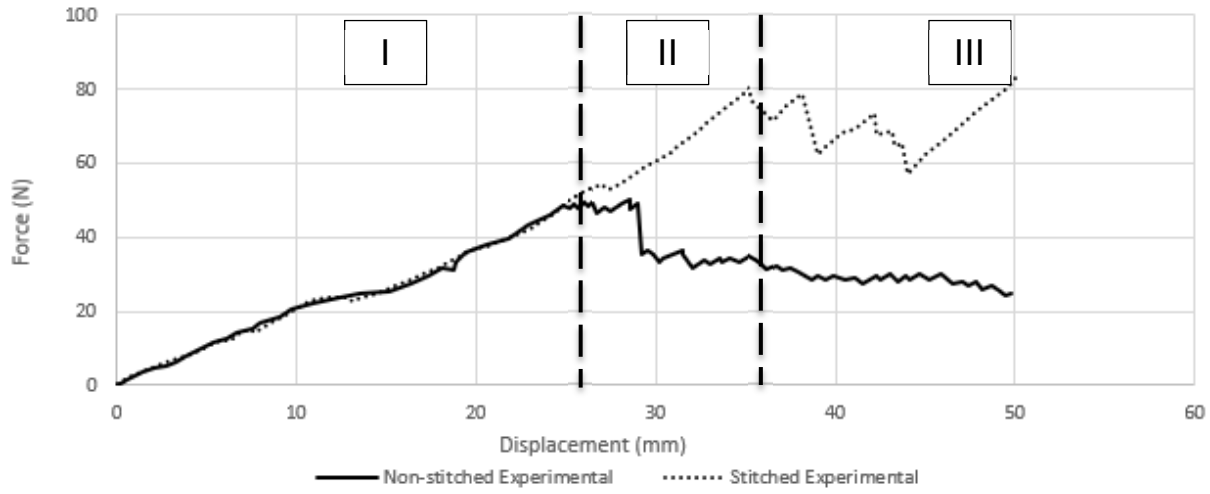

I = Elastic deformation, II = Crack initiation, II = Crack propagation

a

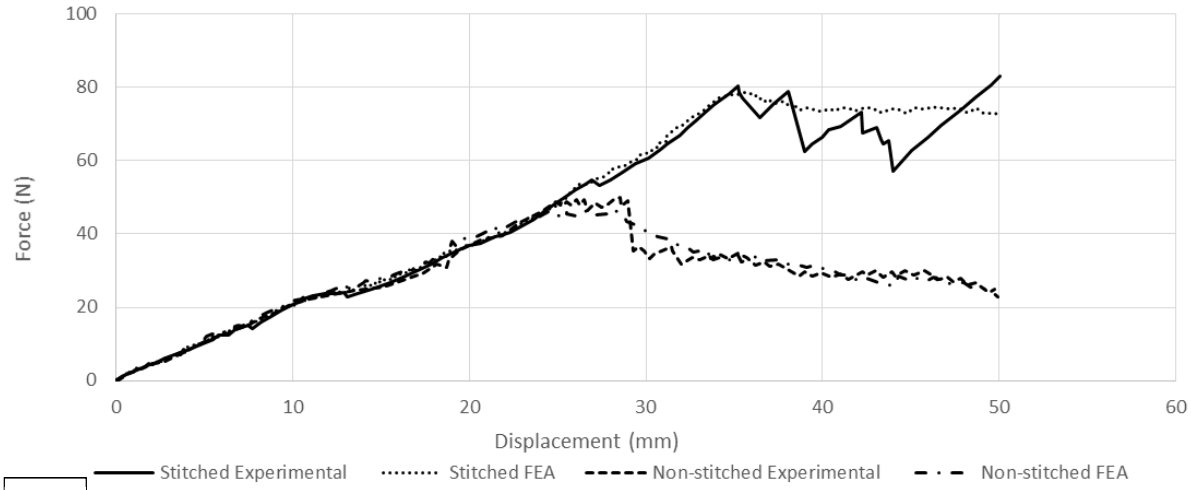

b

Figure 7-4 a) force- displacement (crack growth) comparison of stitched and non-stitched DCB tests for mid-plane interface [203]. b) FEA and experimental comparison of stitched and non-stitched DCB tests for mid-plane interface

To summarise, Stitch modelling was the main concentration of this section. The approach was through Tiebreak option 8, to model delamination as this contact card can define Mode-I and Mode-II energy release rate which simulates

delamination. An energy-based approach was used to determine the input parameters for the tiebreak formulations to accurately simulate delamination between the plies. A scaling factor was introduced to account for ply interfaces that were not represented by a tiebreak definition. Using PARAM function to increase G_{IC} energy release rate based on experimental studies.

CFRP and GFRP specimens were both modelled using the technique mentioned. Since contacts are defined for components in LS-DYNA explicit, 14 shells were used in total, 6 of which represent the stitching area. A total of 5 components were defined. Using multiple shells to represent the trigger, main body and 6 rows of stitching on each shell. The shell was then glued and meshed. This enables the shell to be recognised as one shell. The contact card, tiebreak option 8 was then defined between the shells in respect to the parameters obtained experimentally for stitched and non-stitched specimens. The current tiebreak formulations require a fixed set of input parameters that include, or can be calculated from, the Mode I and Mode II interlaminar fracture toughness values. In the stitched area the PARAM' was increased according to the experimental data and non-stitched area normal PARAM' was used. This increases G_{IC} energy release rate within the stitched area and replicates the stitched specimen.

7.4 Results and discussion

7.4.1 Axial and off-axis crushing under quasi-static loading

This study experimentally and numerically investigates the structural integrity of GFRP composite tubes against axial and off axis loading under quasi-static loading. Off-axis loading angles of 5^o, 10^o, 20^o and 30^o were selected for the study. The results indicated that as the lateral incline angle increases the mean crush force and energy absorption decreases. Axial loading compared with off-axis loading had better energy absorption capability with mean crush force of 100 kN. The experimental (see Figures 7-6 and 7-7) morphologies of axial and off-axis angle 5^o illustrated bundle fracture and close to brittle failure mechanism which is a combination of lamina bending and transverse shearing modes. Off-

axis angle 10^{o} showed transverse shearing mode characterised by wedge-shaped laminate cross section with multiple short interlaminar fractures and axial cracks. Off-axis angle 20^{o} and 30^{o} showed catastrophic failure mechanism with unsymmetrical damage. This results into minimal energy absorption capability.

Figure 7-5 represents the various stages of the axial and off-axis loading conditions. Both experiment and FEA in all cases demonstrate a similar crushing behaviour. In respect to morphologies of the crushed tubes (see Figure 7-6), the effect of off-axis and unsymmetrical crushing behaviour shown in Figure 7-7 d is observed with inner and outer fronds formation.

The main concentration of this study was based on energy absorption capability on each case. The failure mechanism is a factor of how the energy was absorbed and force-displacement curve indicates the amount of energy absorbed in each case. To compare FEA and experimental, the mean crush force values are compared. Figure 7-8 a, shows the five experimental studies at axial and off-axis with angles of 5^{o}, 10^{o}, 20^{o} and 30^{o}. It can be concluded from the graph that as the lateral incline angle increases the energy absorption decreases. Figure 7-8 b represents force-displacement of GFRP axial crushing. The axial experiment data has a mean crush force of 100 kN with FEA being 98 kN. The mean crush force values of experimental and FEA is very close in all cases. In off-axis 5^{o} (see Figure 7-8 c) the experimental data has a mean crushing force of 82 kN and FEA is 80 kN. The experiment and FEA difference in mean crush force at 10^{o} (see Figure 7-8 d) is 2 kN, 61 kN and 59 kN respectively, followed by 3 kN at 20^{o} (see Figure 7-8 e) with mean crush force of 39 kN and FEA 36 kN respectively. At 30^{o} (see Figure 7-8 f) the experimental mean crush force is 25 kN and FEA is 22 kN. The experimental and FE analysis are in good agreement and showed similar trending curves with FEA sensitivity towards lateral inclined angles.

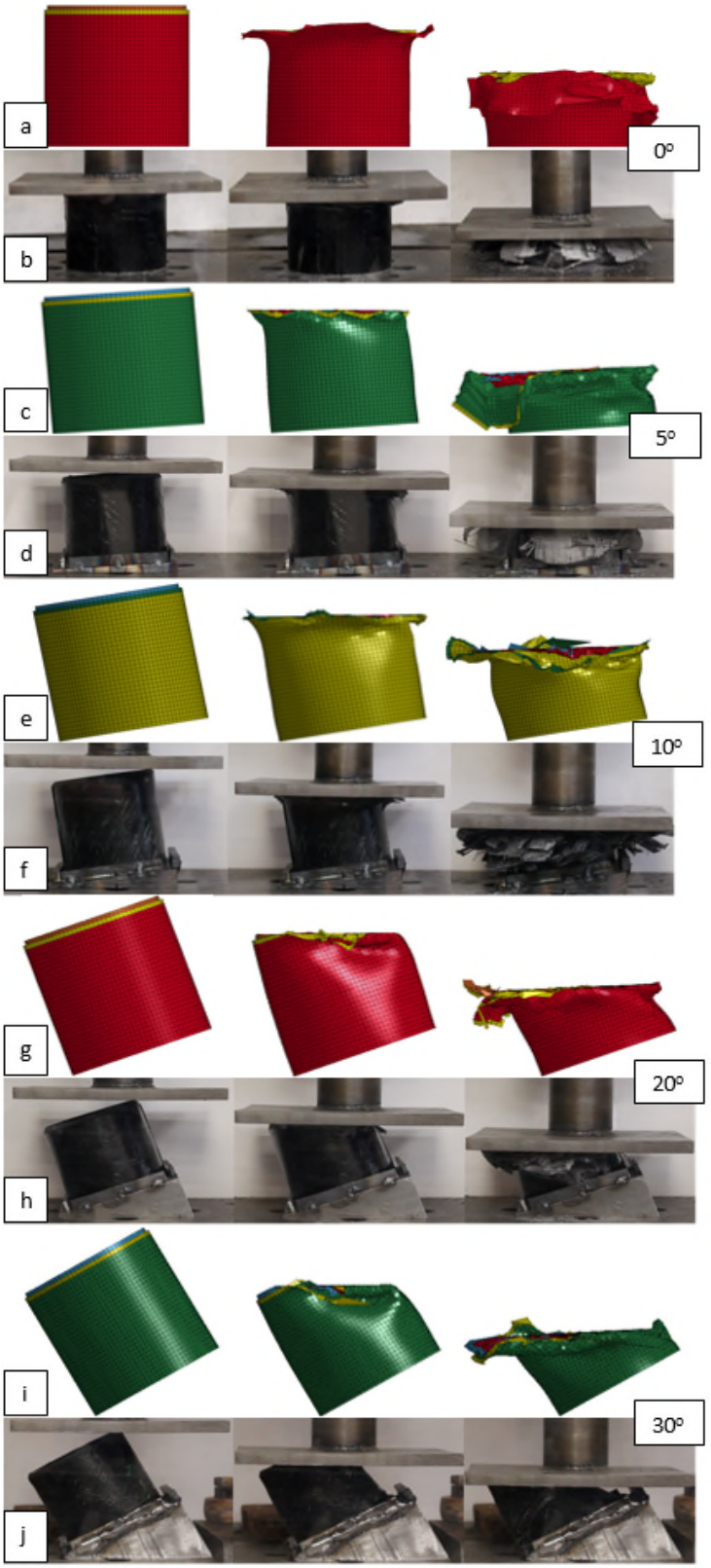

Figure 7-5 Various stages of axial and off-axis crushing a) axial FEA b) axial experiment c) 5° FEA d) 5° experiment e) 10° FEA f) 10° experiment g) 20° FEA h) 20° experiment i) 30° FEA j) 30° experiment

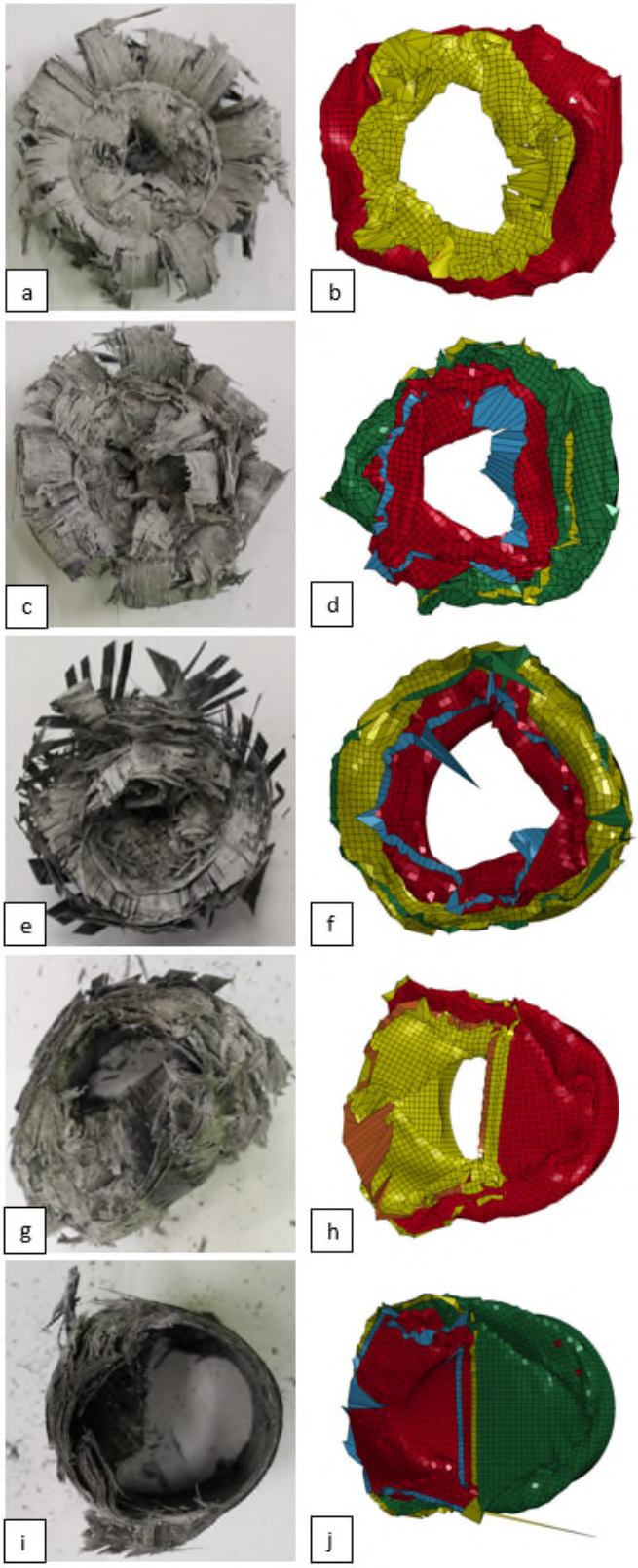

Figure 7-6 Plane view of crushed axial and off-axis specimens a) axial experiment b) axial FEA c) 5º experiment d) 5º FEA e) 10º experiment f) 10º FEA g) 20º experiment h) 20º FEA i) 30º experiment j) 30º FEA

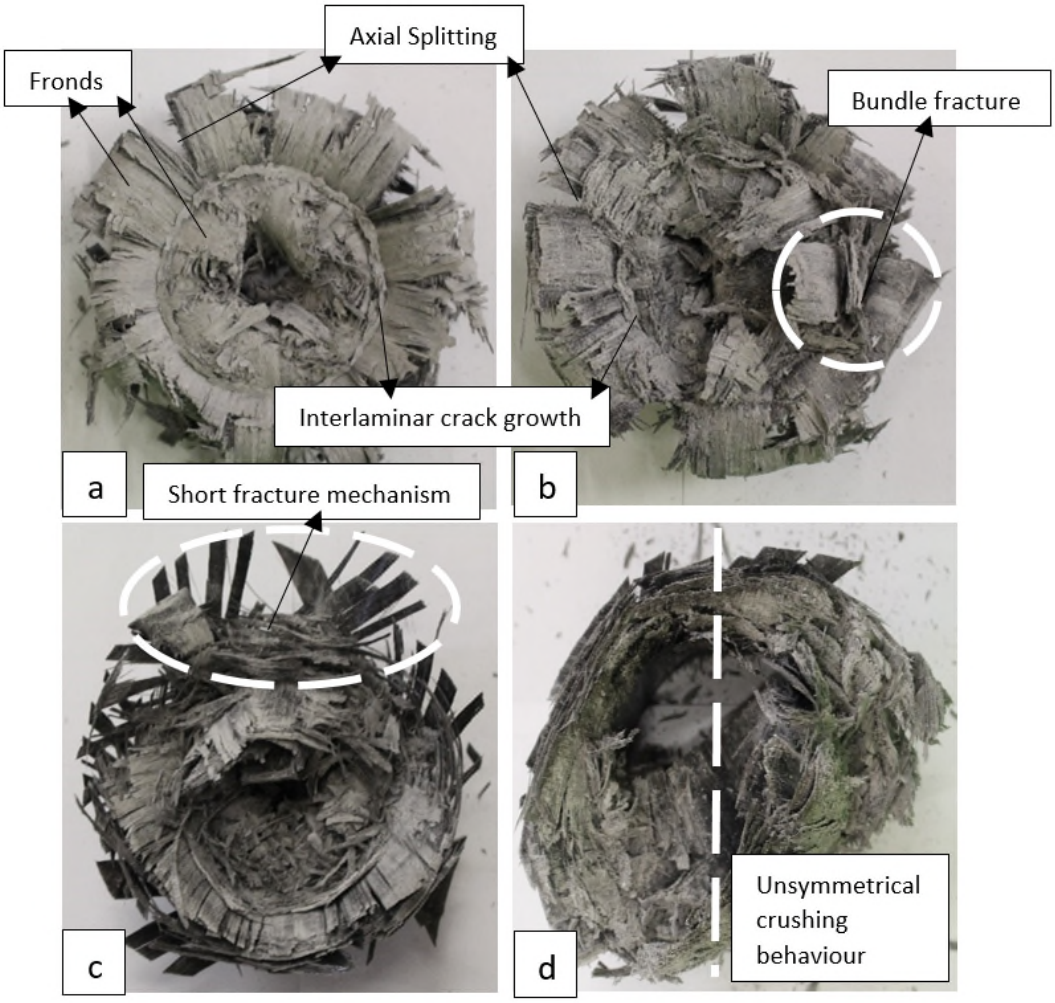

Figure 7-7 Plane view of crushed axial and off-axis specimens a) axial with brittle fracture crushing mode, b) 5º with brittle fracture mode c)10º with transverse shearing mode d) catastrophic failure

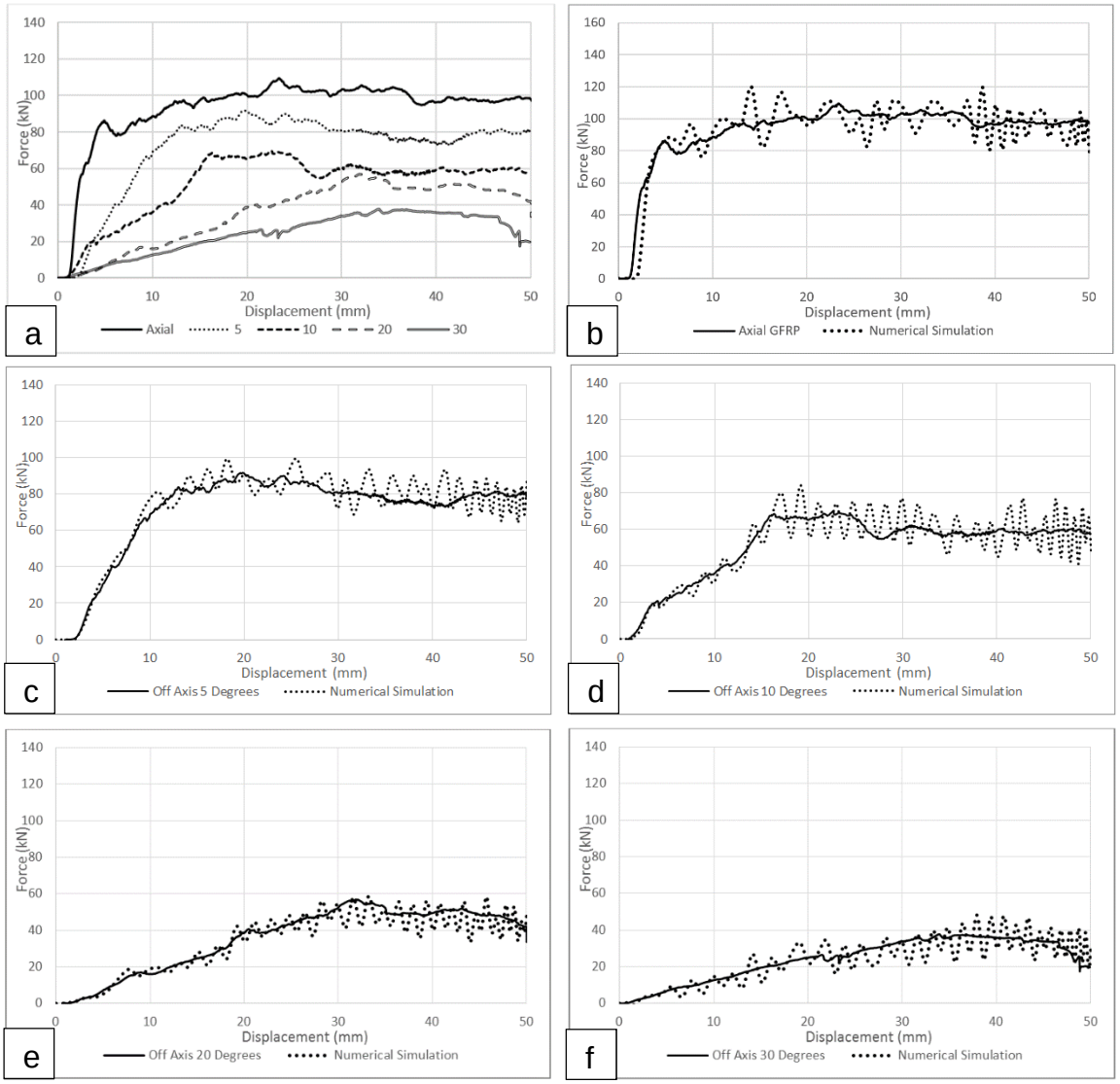

Figure 7-8 Force-displacement of axial and off-axis a) axial and off-axis experimental comparison b) axial experimental and FEA c) 5º experimental and FEA d) 10º experimental and FEA e) 20º experimental and FEA f) 30º experimental and FEA

7.4.2 Axial crushing and improvement of off-axis loading

In this section, the integrated off-axis at 10º is modelled and simulated. This configuration cancels the off-axis effect and improves energy absorption capability. Various crushing stages of the specimens at off-axis loading is shown in Figure 7-9 where the experiment and numerical stages are compared. According to the morphologies of crushed tubes (see Figure 7-10), the effect of ply-orientation and trigger mechanism were modelled to increase energy

absorption capability. By observing both experimental and numerical results, it can be concluded that by altering and tailoring the stacking sequence in respect to composite tube axis and altering the trigger mechanism, the energy absorption can be significantly improved. Figure 7-11 represents the force-displacement history of GFRP integrated specimen and its comparison with the related experimental data. The experimental data has a mean crush force value of 100 kN while the value of the FEA result is 98 kN which shows similar trending curves and high sensitivity towards stacking sequence and trigger mechanism.

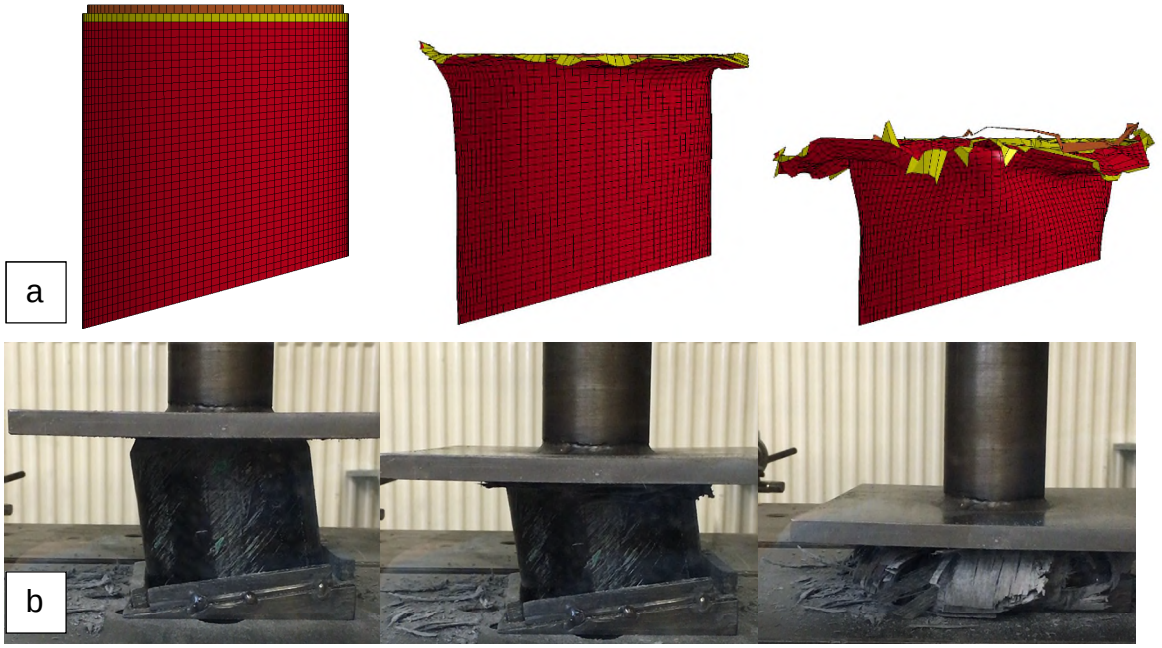

Figure 7-9 Various stages of integrated off-axis at 10^{o} crushing of specimens a) FEA and b) experiment

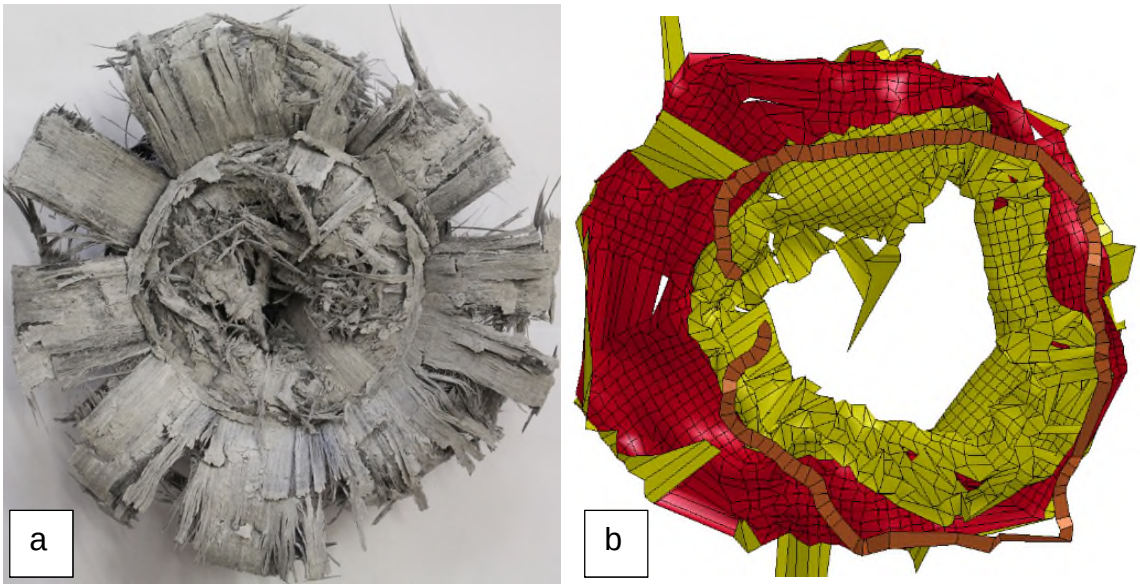

Figure 7-10 Plane view of crushed integrated off-axis at 10º specimen a) experiment b) FEA

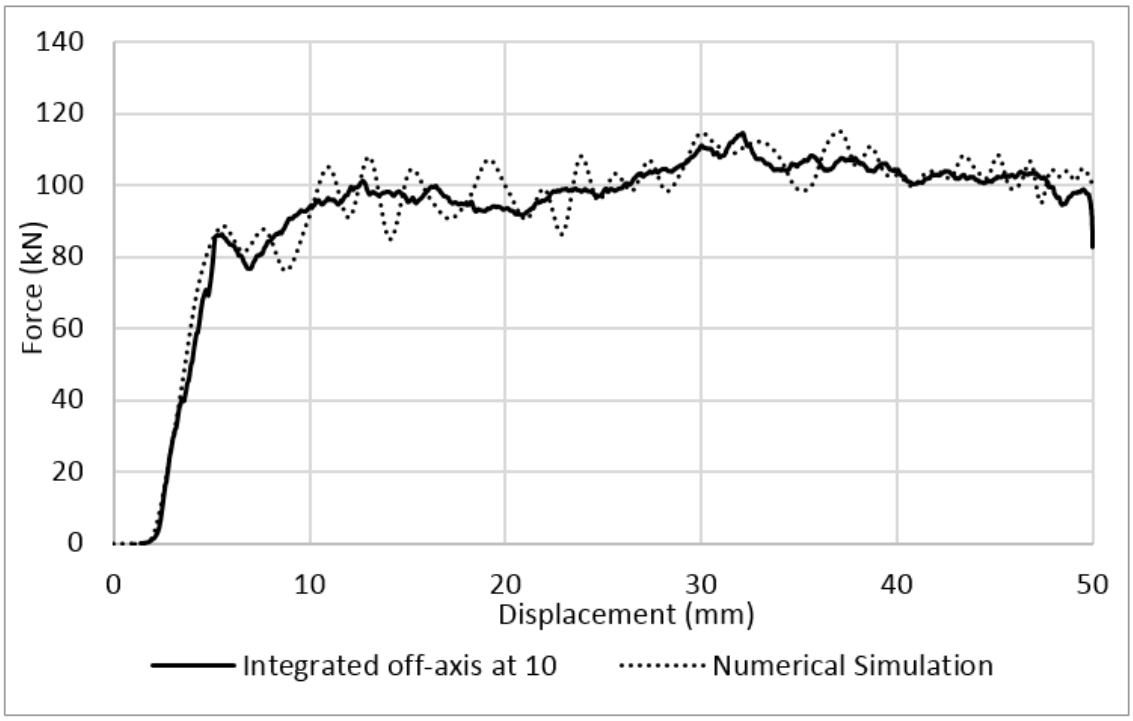

Figure 7-11 Force-displacement comparison of experimental and numerical results of integrated off-axis at 10º

7.4.3 GFRP and CFRP stitched crushing under quasi-static loading

The developed stitching pattern utilised based on previous chapter 4 study, this technique has shown to increase local and global energy absorption capability by increasing interlaminar fracture toughness, friction and bending. Figure 7-12 a and 7-12 e, illustrate the experiment morphologies of stitched specimens followed by FE analysis in Figure 7-12 b and 7-12 f, for GFRP and CFRP respectively. CFRP non-stitched specimen (figure 7-12 c) showed fragmentation with fibre fracture through brittle fracture failure mechanism along with bundle fracture. Whereas in CFRP stitched specimen Figure 7-9 e, the bundle fracture increased, forming external fronds. Figure 7-7 a, shows GFRP non-stitched sample with failure mechanism of continuous internal and external fronds through brittle fracture and lamina fracture combination. Compared with GFRP stitched specimen Figure 7-12 a, it dominates brittle failure mechanism with increased fragmentation failure mechanism and axial cracks.

Introducing stitching through the thickness, the fracture toughness is increased, consequently increasing local and global energy absorption capabilities indicating better crashworthiness behaviour. All the specimens showed progressive crushing behaviour with sudden increase in localised stitched locations (Figure 7-13 a and 7-13 b). Both CFRP and GFRP specimens subjected to stitching through the thickness has shown better energy absorption capabilities. FEA and experimental data are in close agreement. In Figure 7-13 c the GFRP stitched specimen has an experimental mean crush force of 116.3 kN and FEA of 115 kN. Figure 7-13 d shows the CFRP specimen with mean crush force of 65 kN for experimental and 64 kN for FEA. Figure 7-13 e shows the CFRP stitched specimen with mean crush force of 75 kN for experimental and 77 kN for FEA.

Figure 7-12 Plane view of GFRP and CFRP a) GFRP quasi-static Stitched experiment b) GFRP quasi-static stitched FEA c) CFRP quasi-static non-stitched experiment d) CFRP quasi-static non-stitched FEA e) CFRP quasi-static stitched experiment f) CFRP quasi-static stitched FEA

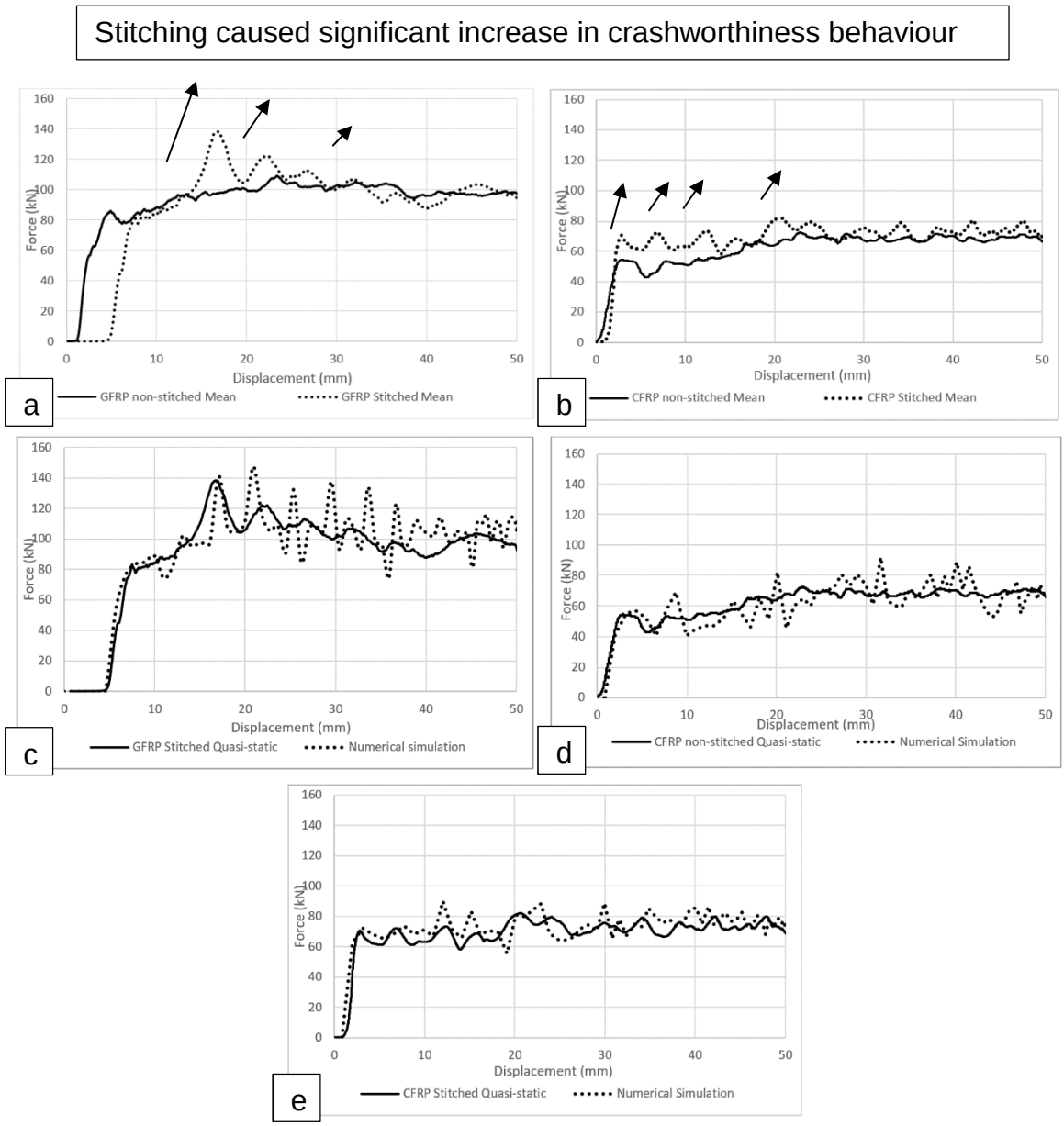

Figure 7-13 Force-displacement of GFRP and CFRP quasi-static Stitched experiment a) GFRP quasi-static stitched and non-stitched b) CFRP quasi-static stitched and non-stitched c) GFRP stitched FEA and experimental d) CFRP non-stitched FEA and experimental e) CFRP stitched FEA and experimental

7.4.4 Stitched GFRP and CFRP crushing under impact loading

Tubes utilising the stitching pattern under quasi-static has shown better energy absorption than non-stitched specimen in both GFRP and CFRP. Similarly, the crashworthiness of the composite tubes subjected to stitching through the thickness has significantly increased. Figure 7-14 shows different stages of experimental test and numerical simulation under impact loading, which are in good agreement. The failure mechanisms are different than quasi-static in GFRP. The difference between the two are transverse shearing mode with multiple short interlaminar cracks in addition to brittle and lamina bending mechanism. However, the dominant failure mechanism is a combination of lamina bending and transverse shearing mode with observation of axial cracks and bundle fracture (see Figure 7-15 a and 7-15 c). In CFRP (see Figure 7-15 e and 7-15 g) morphologies, the failure mechanisms is dominated by transverse mode with multiple short interlaminar fracture and axial cracks.

Utilising stitching through the thickness has significantly influenced the crashworthiness capability of the composite tubes (see Figure 7-16 a and 7-16 b). GFRP stitched specimen managed to absorb the same amount of energy as non-stitched specimen with 25% penetration reduction indicating better crashworthiness behaviour. The aim of introducing stitching through the thickness was to increase fracture toughness and consequently increase energy absorption capability which has been achieved in both materials.

Figure 7-16 c represents GFRP non-stitched experimental and numerical results. The mean crush force is 69 kN for experimental and 68 kN for numerical. Figure 7-16 d represents CFRP non-stitched and it has a mean crush force of 63 kN and 62 kN for experimental and numerical respectively. GFRP stitched (see Figure 7-16 e) has a mean crush force of 84 kN and 82 kN for experimental and numerical respectively. In figure 16 f, CFRP stitched specimen has a mean crush force of 75.5 kN and 77 kN for experimental and numerical respectively.

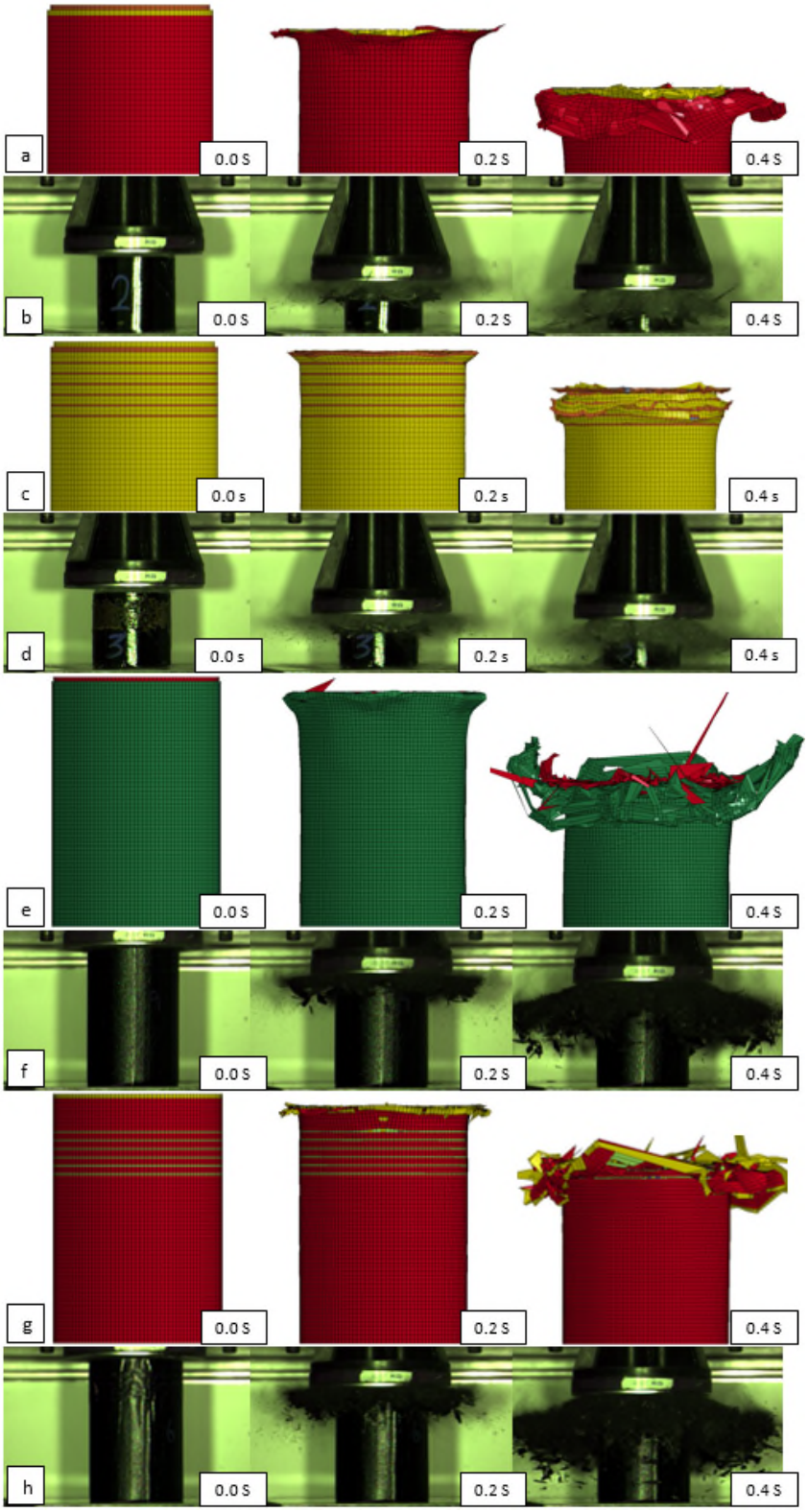

Figure 7-14 Various stages of GFRP and CFRP subjected to impact loading a) GFRP non-stitched FEA b) GFRP non-stitched experimental c) GFRP stitched FEA d) GFRP stitched experimental e) CFRP non-stitched FEA f) CFRP non-stitched experimental g) CFRP stitched FEA h) CFRP stitched experimental

Figure 7-15 Plane view of GFRP and CFRP under impact loading a) GFRP non-stitched FEA b) GFRP non-stitched experimental c) GFRP stitched FEA d) GFRP stitched experimental e) CFRP non-stitched FEA f) CFRP non-stitched experimental g) CFRP stitched FEA h) CFRP stitched experimental

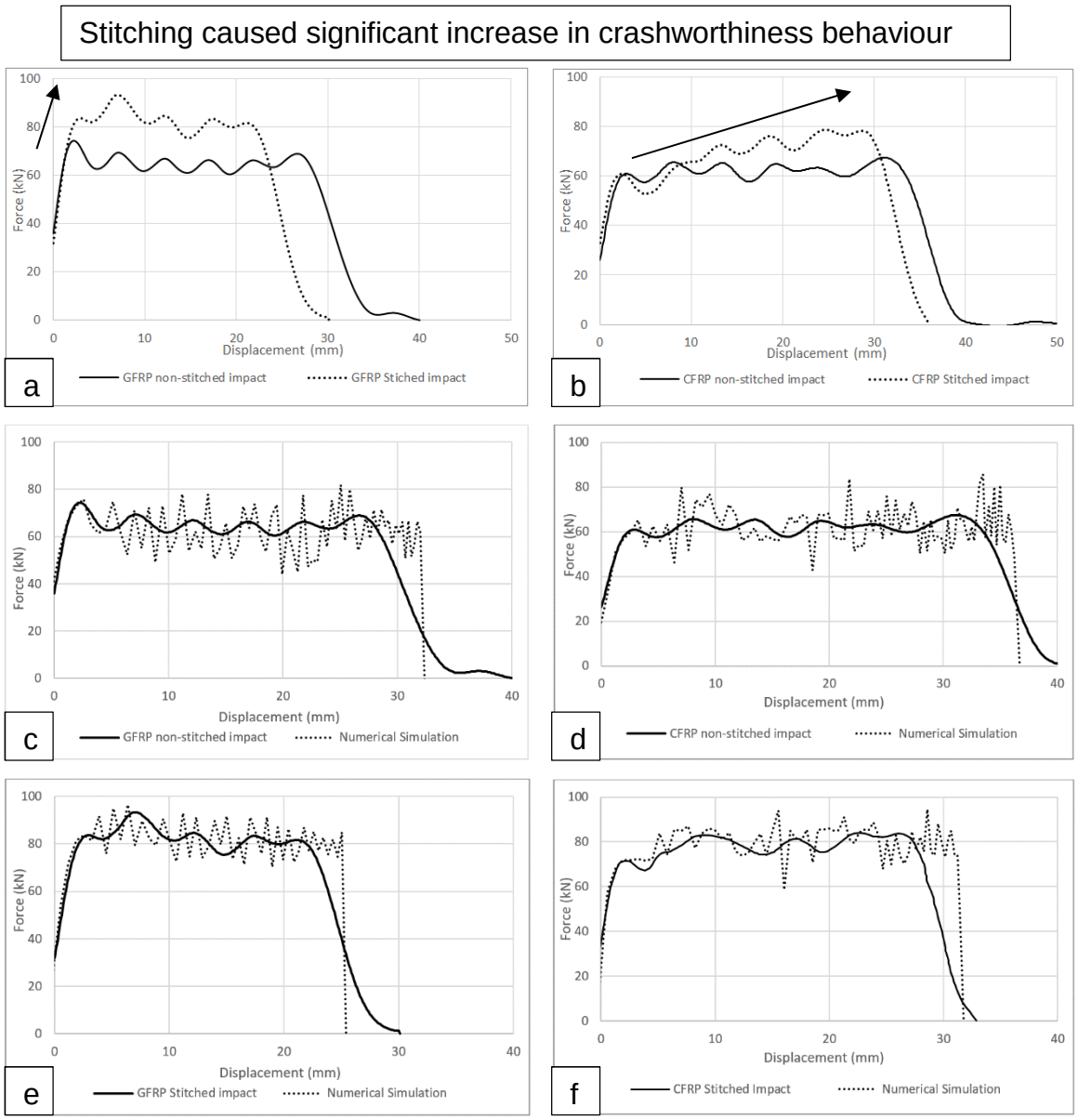

Figure 7-16 Force-displacement of GFRP and CFRP under impact loading a) GFRP stitched and non-stitched b) CFRP stitched and non-stitched c) GFRP stitched FEA and experimental d) CFRP non-stitched FEA and experimental e) GFRP stitched FEA and experimental f) CFRP re-stitched FEA and experimental

7.4.5 Specific energy absorption comparison of FEA and experiment results

The SEA value comparison in this section is to determine the energy absorption capability of finite element model compared with experimental studies. In this section, the differences of numerical and experimental studies are compared. In Figure 7-17, part a, compares the SEA values of stitched and non-stitched CFRP and GFRP FEA and experimental under impact loading. The GFRP non-stitched has 3.8% difference, GFRP stitched has 2% difference. CFRP non-stitched has 2.3% difference, and CFRP stitched has 1.6% difference. In Figure 7-17, part b, compares the SEA values of stitched and non-stitched CFRP and GFRP FEA and experimental under quasi-static loading. The GFRP non-stitched has 2.8% difference, GFRP stitched has 2.6% difference. CFRP non-stitched has 3% difference, and CFRP stitched has 1.9% difference.

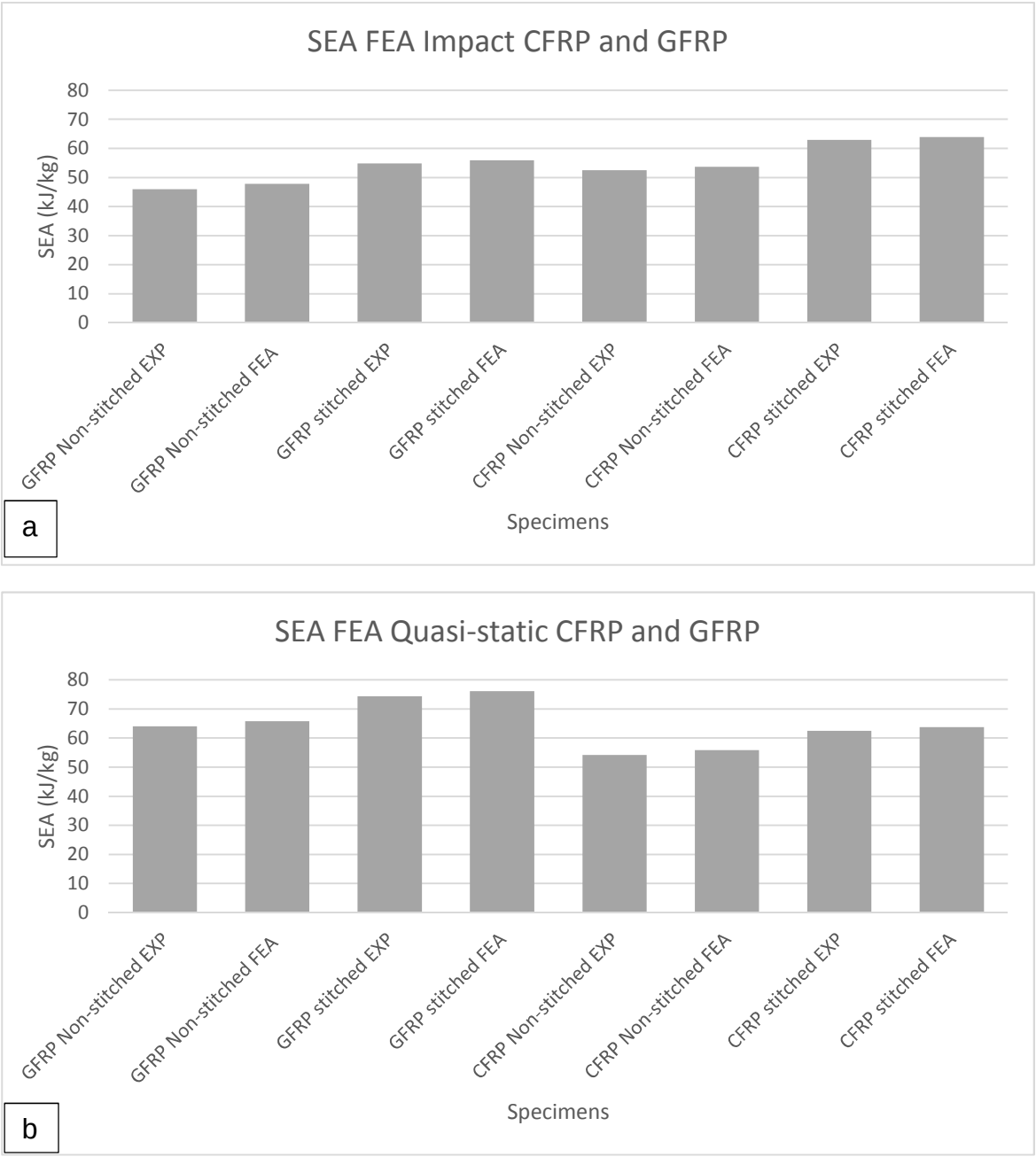

Figure 7-17 SEA comparison of experimental and numerical a) impact loading b) quasi-static loading

7.5 Conclusion

In the present study, the crashworthiness and numerical simulation of circular GFRP and CFRP composite absorbers under axial and off axis, quasi-static and impact loading have been investigated. Axial compared to off-axis loading had better crashworthiness behaviour with mean crush force of 100 kN. It can be concluded that as the lateral inclined angle increased the energy absorption decreased.

Stitching through the thickness has shown significant lightweight potential. This method increases crashworthiness behaviour without increasing the structural weight. The impact loading specific energy absorption of GFRP and CFRP are 17% and 18% higher than non-stitched sections respectively.

Stitch modelling was the main concentration of this section. The approach was through Tiebreak option 8, to model delamination as this contact card can define Mode-I and Mode-II energy release rate which simulates delamination. An energy-based approach was used to determine the input parameters for the tiebreak formulations to accurately simulate delamination between the plies. A scaling factor was introduced to account for ply interfaces that were not represented by a tiebreak definition. The PARAM function was used to increase G_{IC} energy release rate based on experimental studies.

CFRP and GFRP specimens were both modelled using the technique mentioned. Since contacts are defined for components in LS-DYNA explicit, 14 shells were used in total, 6 of which represent the stitching area. A total of 5 components were defined. Using multiple shells to represent the trigger, main body and 6 rows of stitching on each shell. The shell was then glued and meshed. This enables the shell to be recognised as one shell. The contact card, tiebreak option 8 was then defined between the shells in respect to the parameters obtained experimentally for stitched and non-stitched specimens. The current tiebreak formulations require a fixed set of input parameters that include, or can be calculated from, the Mode I and Mode II interlaminar fracture toughness values. In the stitched area the PARAM' was increased according to the experimental data and non-stitched area normal PARAM' was used. This increases G_{IC} energy

release rate within the stitched area and demonstrates the experimental stitched specimen behaviour under various loadings.

The multi-layer shell configuration has shown reliable to predict energy absorption of GFRP and CFRP composite tubes. The method used in different loading conditions has shown sensitivity towards axial and off-axis loading and quasi-static and impact loading conditions. The experimental results and numerical results are in good agreement. Utilising stitching increases interlaminar fracture toughness, the stitch modelling approach took this into consideration and used contact definition to increase crack propagation resistance. This method uses double contact definitions and increases the crack propagation resistance in the stitched area. Each shell was constructed from 14 shells, which were glued as one, therefore in double shell configuration, a total of 28 shells were modelled and used. This method increases local and global energy absorption capability. Simulations of FRP-crushing is possible with a commercial material model along with stitch modelling. The modelling technique approach led to equally good results when the material and geometry of the specimens were changed. Utilising multi-shell configuration with the used contact definitions, the modelling technique were effective in simulations of axial and off-axis loading composite structure under quasi-static and impact loading. Stitching through the thickness enables an efficient design for composite structures and this numerical approach is efficient for multi-layered composites structures.

Finite element models were developed for CFRP and GFRP specimens as mentioned above with and without stitching. Figure 7-18 shows the intrawall failure mechanisms comparison between experimental results and FEA results, and it can be noted that, a double shell configuration can represent the axial and off-axis crushing behaviour. These models were subjected to quasi-static and impact loading. In all cases the FEMs were within 2-4% different from experimental SEA values. The force-displacement curves were compared along with the crushed morphologies and crushing process. In all cases the numerical results were found to be in good agreement with the experiments.

Figure 7-18 Crack Propagation at central intrawall a) axial failure mechanism b) axial FEA zoomed in c) Axial experimental d) axial FEA e) 5º experiment f) 5º FEA g) 10º experiment h) 10º FEA i) 20º experiment j) 20º FEA

8 Conclusions and Recommendations

8.1 Conclusions

In this thesis, the aim was to improve specific energy absorption capability of unidirectional composite crash absorbers. This requires the sustained crush load to be increased. The axial and off-axis crushing behaviour of GFRP composite crash absorbers was studied. The Various angles of 5^o, 10^o, 20^o and 30^o degrees were selected for the study of off-axis loading. The results indicate that by increasing the lateral inclination angle the mean crushing force and consequently energy absorption capability of all tested sections decreased. The fracture mechanism and crushing process were studied to determine the failure mechanism. From a design perspective, it is necessary to investigate the parameters affecting the energy absorption capability of composite tubes at off-axis loading. The effect of lay-up sequence and flat trimming at one end of the composite tube was investigated and tested under quasi-static loading. 10^o off-axis angle was chosen as mentioned in chapter 3. The effect of lay-up sequence and flat trimming improved energy absorption capability with similar mean crushing force as axially tested specimens.

To improve specific energy absorption, stitching through the thickness was utilised. This method improves friction, fronds bending and main central crack propagation resistance. The through-thickness reinforcements were applied into locations of 10 mm, 20 mm, 30 mm, 10-20 mm, 10-30 mm, 20-30 mm, 10-20-30 mm and 10-15-20-25-30-35 mm from top of the composite crash absorbers and tested under quasi-static loading conditions. It is shown that multi-stitched locations can cause multiple increases in crushing load and consequently increase in energy absorption capability of composite crash absorbers. In single stitching at 30 mm a significant improvement was observed. In most cases of single stitching and double stitching caused lower specific energy absorption. However, pattern-stitching of 10-15-20-25-30-35 has shown significant improvement in Mode-I delamination resistance with higher friction and fronds bending that contributed to achieving higher SEA value than the non-stitched

specimen. The pattern-stitched design has shown a 15% increase in specific energy absorption than the non-stitched specimen.

Multi-stitching on GFRP crash absorbers showed significant improvement in specific energy absorption under quasi-static loading. Crashworthiness of multi-stitched crash absorbers under impact loading was studied. To determine the effect of the designed pattern stitching, a material with a different fibre and matrix was chosen (T300/914) with a different geometry. The force-displacement history and crushed morphologies were studied and compared with non-stitched specimens. The stitching pattern on both materials showed significant improvement under quasi-static and impact loading conditions. This technique significantly increased crashworthiness behaviour of composite absorbers subjected to quasi-static and impact loading and consequently improved energy absorption capability without increasing of structural weight, which indicates, improvement in SEA value. The CFRP and GFRP stitched specimens subjected to quasi-static loading showed an increase in SEA percentage values of 14% and 15% respectively. Similarly, the CFRP and GFRP stitched specimens subjected to impact loading showed an increase in SEA percentage values of 18% and 17% respectively. This shows the significant influence of through-thickness stitching on specific energy absorption.

A comprehensive investigation was performed to develop a methodology to model the crushing behaviour of the composite members. This included determining the most effective number of shells, friction, element size, formulation, contact definitions, loading rate, delamination interfaces, trigger mechanism and material model. The aim was to develop a FEM that can predict energy absorption capability with a high accuracy of around 5% error.

Various shell configurations were studied and a multi-layer shell element with double-shell configuration produced accurate results with a difference of less than 5% with minimal computational cost compared with other configurations. This configuration was used to predict energy absorption capability and specific energy absorption, other considerations were deformation and damage progression of the composite tubes. Each shell element or layer can contain

either a single ply or multiple plies. The layers were tied using Tiebreak option 8 contact definitions. This contact card has the capability of modelling delamination between the layers through energy-based approach. The material card of Mat_54 was used to represent each ply and few parameters in the material cards were studied to find the optimum configurations to match the experimental studies. A parametric study was performed in order to obtain the values of the unknown parameters. It was determined that SOFT and DFAILC (compression failure strain) were the main parameters that affected energy absorption capability and specific energy absorption was influenced by these parameters. The sensitivity of the model was studied against the material model, delamination model, friction and impact velocity. The results show that the model is sensitive towards minimal input change. The simulation results showed that the failure peak load, mean crushing force, SEA, all compared very well with the experimental results.

A multi-shell finite element model was constructed to predict the axial and off-axis crushing behaviour and energy absorption capability of composite structures under quasi-static and impact loading. The stitch modelling method is based on surface contact modelling technique definition in the stitched area to represent the functionality of the stitched area during an impact event. Tiebreak option 8 was utilised to model delamination as this contact card can define Mode-I and Mode-II energy release rate which simulates delamination. This energy-based approach was used to determine the input parameters for the tiebreak formulations to accurately simulate delamination between the plies. A scaling factor was introduced to account for all ply delamination that was not represented by a tiebreak definition. The SEA value comparison can determine the energy absorption capability of the finite element model compared with experimental studies. The differences were less than 4% in all cases. in comparison with the existing methods for multi-layered composites structures.

The present study has established sufficient experimental and numerical investigation on the effect of stitching through the thickness on composite tubular structures under quasi-static and impact loading.

8.2 Future work

The different directions of work which could be undertaken for future research are summarised below:

In this project it was concluded that some fibres repel some resins. This has been clearly illustrated in CFRP specimen (chapter 5), when subjected to Kevlar specimen, the SEA improved by 11%, further investigation led to changing the fibre yarn and obtained specimen that fully bonded with the matrix. This led to 18% increase in SEA compared with 11% partially bonded specimen. Therefore, it is recommend that further investigation on fibres that react well and are fully absorbent towards the applied resin for better bonding.

LS-Dyna has been extensively used for crashworthiness of composite structures using shell and cohesive elements. More material models are being added to the its library for better and wider use of the software. Cohesive zone models are used in research for detecting cracks and for better prediction of deformations. Below are some of the recommendations for the future work:

- For better prediction of cracks and deformations and numerical and experimental comparison, a user defined material model can be implemented for the composite tubes based on the material properties and failure criteria to get better results.
- Cohesive zone material models can be used further for detecting delamination(s) in the composite tubes.
- The effect of additional post-failure parameters available for the composite material models in the latest version of LS-Dyna can be studied.
- Other cohesive material models which are available in LS-Dyna library can also be assigned for the composite tubes for better comparison.
- Cohesive material models for modelling delamination and studying different enhanced material models available in LS-DYNA such as Mat_161, Mat_162, Mat_Composite_Msc_Dmg which require solid elements for delamination modelling can be beneficial to produce and develop engineering solutions with reasonable time and resources.

The best position of stitched area in the wall of CFRP and GFRP composite sections can be optimised through an analytical approach. A novel analytical model based on an energy balance approach and multi-objective optimisation problem will be proposed to estimate the optimum position of the stitched area in the wall of composite sections. The optimised position will be maximising the energy absorption capability under axial and off-axis crushing load.

REFERENCES

[1] DiPaolo BP, Tom JG. A study on an axial crush configuration response of thin wall, steel box components: the quasi-static experiments. Int J Solids Struct 2006;43:7752–75.

[2] Santosa S, Wierzbicki T. Crash behaviour of box columns filled with aluminium honeycomb or foam. Compos Struct 1998;68(4):343–67.

[3] Santosa S, Wierzbicki T. Effect of an ultralight metal filler on the bending collapse behaviour of thin walled prismatic columns. Int J Mech Sci 1999;41(8):967–93.

[4] Cheng Q, Altenhof W, Jin SY, Powell C, Harte AM. Energy absorption of aluminium foam filled braided stainless steel tubes under quasi-static tensile loading conditions. Int J Mech Sci 2006;48:1223–33.

[5] Kotzialis C, Derdas C, Kostopoulos V. Blast behaviour of plates with sacrificial cladding. In: 5th GRACM international congress on computational mechanics, June 29–July 1, Limassol, Cyprus; 2005.

[6] Guruprasad S, Mukherjee A. Layered sacrificial claddings under blast loading Part II – experimental studies. Int J Impact Eng 2000;24(9):975–84.

[7] Hanssen AG, Enstock L, Langseth M. Close-range blast loading of aluminium foam panels. Int J Impact Eng 2002;27(6):593–618.

[8] Mosallam, A S. and Nasr, A. (2016) Structural performance of RC shear walls with post-construction openings strengthened with FRP composite laminates. Composite Part B: Engineering, In Press.

[9] James A. Performance comparison of plastic composites with metals for vertical body panel applications. SAE Technical paper; 1999.

[10] Kostopoulos V, Markopoulos YP, Vlachos DE, Galiotis C, Melanitis NE. A heavy duty composite bridge made of glass polyester pultruded box beams. In: Proceedings of RTO applied vehicle technology panel (AVT) specialists' meeting on Low cost composite structures. Loen, Norway; May 7–11, 2001.

[11] Ramakrishna S. Microstructural design of composite materials for crashworthy structural applications. Mater Des 1997;18(3):167–73.

[12] Mamalis AG, Manolakos DE, Ioannidis MB, Papapostolou DP. The static and dynamic and axial collapse of CFRP square tubes: finite element modelling. Compos Struct 2006;74:213–25.

[13] Mamalis AG, Manolakos DE, Ioannidis MB, Papapostolou DP. On the experimental investigation of crack energy absorption in laminate splaying collapse mode of FRP tubular components. Compos Struct 2005;70:413–29.

[14] Ramakrishna S, Hamada H. Energy absorption characteristics of crash worthy structural composite materials. Key Eng Mater 1998;141–143(2):585–619.

[15] Savona CS, Hogg PJ. Effect of fracture toughness properties on the crushing of flat composite plates. Compos Sci Technol 2006;66:2317–28.

[16] Sebaey, T.A. and Mahdi, E. (2017) Filler strengthening of foam-filled energy absorption devices using CFRP beams. Composite Structures, 160, 1-7.

[17] Hull D. A unified approach to progressive crushing of fibre reinforced composite tubes. Compos Sci Technol 1993;35(3/4):231–46.

[18] Abosbaia AAS, Mahdi E, Hamouda AMS, Sahari BB. Quasi-static axial crushing of segmented and non segmented composite tubes. Compos Struct 2003;60:327–43.

[19] Mamalis AG, Manolakos DE, Ioannidis MB, Papapostolou DP. Crashworthy characteristics of axially statically compressed thin-walled square CFRP composite tubes: experimental. Compos Struct 2004;63:347–60.

[20] Farley G. Jones R. Crushing characteristics of continuous fibre reinforced composite tubes. Journal of Composite Materials 1992:26;37–50.

[21] Mamalis A. Manolakos D. Viegelahn G. Crashworthy behaviour of thin-walled tubes of fibreglass composite material subjected to axial loading. Journal of Composite Material 1990:24;72.

[22] Macaulay MA. Introduction to impact engineering. Published by Chapman and Hall, USA, 1987.

[23] Bardi FC, Yun HD, Kyriakides S. On the axisymmetric progressive crushing of circular tubes under axial compression. Int J Solids Struct 2003;40:3137–55.

[24] Lou, H. Yan, Y. Meng, X. and Jin, C. (2016) Progressive failure analysis and energy-absorbing experiment of composite tubes under axial dynamic impact. Composites Part B: Engineering, 87, 1-11.

[25] Fairfull AH, Hull D. Effect of specimen dimensions on the specific energy absorption of fibre composite tubes. In: Proceedings of ICCM-VI; 1987. p. 36–45.

[26] Farely GL. Effect of specimen geometry on the energy absorption of composite materials. J Compos Mater 1986;20:390.

[27] Thornton P.H. The crush behavior of glass fiber reinforced plastic sections, Compos Sci Technol, 1986;27:199-223.

[28] Thornton PH, Harwood JJ, Beardmore P. Fiber reinforced plastic composites for energy absorption purposes. Compos Sci Technol 1985;24:275–98.

[29] Mamalis AG, Manolakos DE, Ioannidis MB, Papapostolou DP. On the response of thin-walled CFRP composite tubular components subjected to static and dynamic axial compressive loading: experimental. Compos Struct 2005;69(4): 407–20.

[30] Mamalis, A.G, Johnson, W (1983) The quasi-static crumpling of thin-walled circular cylinders and frusta under axial compression. International Journal of Mechancal Sciences, 25, 713-732.

[31] Eshkoor, R.A, Oshkovr, S.A, Sulong, A.B, Zulkifili, R. Ariffin, A.K, and Azhari, C.H. (2013) Effect of trigger configuration on the crashworthiness characteristics of natural silk epoxy composite tubes. Composite Part B: Engineering, 55, 5-10.

[32] Mamalis AG, Manolakos DE, Demosthenous GA, Ioannidis MB. Energy absorption capability of fibreglass composite square frusta subjected to

static and dynamic axial collapse. Thin-Walled Struct 1996;25(4):269–95.

[33] Farely GL. Energy absorption of composite materials. J Compos Mater 1983;17:167.

[34] Hamada H, Coppola JC, Hull D, Maekawa Z, Sato H. Comparison of energy ab-sorption of carbon/epoxy and carbon/PEEK composite tubes. Composites 1992;23(4):245–52.

[35] Mamalis AG, Manolakos DE, Ioannidis MB, Papapostolou DP. On the experimental investigation of crash energy absorption in laminate splaying collapse mode of FRP tubular components. Compos Struct 2005;70(4):413–29.

[36] Thornton PH. The crush behavior of pultruded tubes at high strain rates. J Compos Mater 1989;24:22.

[37] Farley GL, Jones RM. Crushing characteristics of composite tubes with ‘‘near elliptical” cross sections. J Compos Mater 1992;26:1252.

[38] Elgalai AM, Mahdi E, Hamouda AMS, Sahari BS. Crushing response of composite corrugated tubes to quasi-static axial loading. Compos Struct 2004;66(1–4):665–71.

[39] Zarei H, Kröger M, Albertsen H. An experimental and numerical crashworthiness investigation of thermoplastic composite crash boxes. Compos Struct 2008;85(3):245–57.

[40] Abdewi EF, Sulaiman S, Hamouda AMS, Mahdi E. Quasi-static axial and lateral crushing of radial corrugated composite tubes. Thin-Walled Struct 2008;46(3):320–32.

[41] Carroll M, Ellyin F, Kujawski D, Chiu AS. The rate-dependent behaviour of ±55° filament-wound glass–fibre/epoxy tubes under biaxial loading. Compos Sci Technol 1995;55:391–403.

[42] Abosbaia AAS, Mahdi E, Hamouda AMS, Sahari BB, Mokhtar AS. Energy absorption capability of laterally loaded segmented composite tubes. Compos Struct 2005;70:356–73.

[43] Mahdi E, Hamouda AMS, Sahari BB, Khalid YA. Effect of hybridisation on crushing behaviour of carbon/glass fibre circular-cylindrical shells. J Mater Proc Technol 2003;132:49–57.

[44] Palanivelu S, Paepegem W, Van Degrieck J, Kakogiannis D, Van Ackeren J, Van Hemelrijck D, et al. Comparative study of the quasi-static energy absorption of small-scale composite tubes with different geometrical shapes for use in sacrificial cladding structures. Polym Test 2010;29:381–96.

[45] Palanivelu S, Van Paepegem W, Degrieck J, Vantomme J, Kakogiannis D, Van Ackeren J, et al. Crushing and energy absorption performance of different geometrical shapes of small-scale glass/polyester composite tubes under quasi-static loading conditions. Compos Struct 2011;93:992–1007.

[46] Farely GL. Effect of fibre and matrix maximum strain rate on the energy absorption of composite materials. J Compos Mater 1986;20:322.

[47] Desjardins SP. et al. Aircraft crash survival design guide. USAA VSCOM TR 89-D-22A-E, Vol I-IV, December 1989.

[48] Thornton PH. and Jeryan RA. Composite structure for automotive energy management. Presented at Autocom'87, 1-4 June 1987, Dearbon, MI.

[49] Beardmore P. and Johnson CF. The potential for composites in structural automotive applications. Journal of Composite Sci. Technol., 1986:26;251-81.

[50] Matthews FL., Davies GAO., Hitchings D., and Soutis C. Finite element modelling of composite materials and structures. Woodhead Published Limited, USA, 2000.

[51] Mahdi E, Hamouda AMS, Sen AC. Quasi-static crushing of hybrid and non-hybrid natural fibre composite solid cones. Compos Struct 2004;66:647–63.

[52] Meidell A. Computer aided material selection for circular tubes designed to resist axial crushing. Thin-Walled Struct 2009;47:962–9.

[53] Jimenez MA, Miravete A, Larrode E, Revuelta D. Effect of trigger geometry on energy absorption in composite profiles. Compos Struct 2000;48:107–11.

[54] Bambach MR. Axial capacity and crushing of thin-walled metal, fibre–epoxy and composite metal–fibre tubes. Thin-Walled Struct 2010;48:440–52.

[55] Mahdi E, Homouda AMS, Mokhtar AS, Majid DL. Many aspects to improve damage tolerance of collapsible composite energy absorber devices. Compos Struct 2005;67:175–87.

[56] Ghasemnejad H, Hadavinia H, Aboutorabi A. Effect of delamination failure in crashworthiness analysis of hybrid composite box structures. Mater Des 2010;31:1105–16.

[57] Hadavinia H, Ghasemnejad H. Effects of Mode-I and Mode-II interlaminar fracture toughness on the energy absorption of CFRP twill/weave composite box sections. Compos Struct 2009;89:303–14.

[58] Farley GL. Energy absorption of composite materials. Composite Materials 1983:17;167.

[59] Thornton PH. Energy absorption in composite structures. Journal of Comp. Mats. 1979:13;247.

[60] Schmueser DW. and Wickliffe LE. Impact energy absorption of continuous fiber composite tubes. Journal of Eng. Mat. Trans. ASME 1987:72;77.

[61] Farley GL. and Jones RM. Crushing characteristics of continuous fibre-reinforced composite tubes. Journal of Composite Materials 1992:26;37.

[62] Thornton PH. and Edwards PJ. Energy absorption in composite tubes. Journal of Composite Materials, 1982:16;521.

[63] PE fibre reinforcement prevents crush. News article in British Plastics and Rubber, January, 1990;10.

[64] Hamada, H. and Ramakrishna, S. (1995) Scaling effects in the energy absorption of carbon-fiber/PEEK composite tubes. Composites Science and Technology, 23, 211-221.

[65] Hamada, H., Ramakrishna, S. Satoh, H. (1995) Crushing mechanism of carbon fibre/PEEK composite tubes. Composites, 26, 749-755

[66] Nilson S. Polyetheretherketone matrix resins and composites. Int. Encyclopaedia of Composites, VCH Publishers Inc, 1991:6;282.

[67] Mamalis AG., Manolakos DE., Demosthenous GA. and Ioannidis MB. The static and dynamic axial crumbling of thin-walled fibreglass composite square tubes. Composites Part B, 1997;28(4):439-451.

[68] Naik N.K. and Ganesh V.K. Prediction of On-Axes Elastic Properties of Plain Weave Fabric Composites. Composite Science and Technology, 1992:45;135-152.

[69] Ishikawa T. and Chou T.W. Stiffness and strength of woven fabric composites. Journal of Materials Science, 1982:17;3211-3220.

[70] Yang Y.C. and Harding J. A numerical micromechanics analysis of the mechanical properties of a plain weave composite, Computers and Structures, 1990:36(5);839-844.

[71] Whitcomb J.D. Three-dimensional stress analysis of plain weave composites. Composite Materials and Fracture (3rd Volume), ASTM STP 1110, O'Brien T.K. American Society for Testing and Materials, Philadelphia, USA, 1991:417-438.

[72] Santulli C. Impact damage evaluation in woven composites using acoustic and thermoelastic techniques. PhD Thesis, Liverpool University, 2000.

[73] Riva E. (2005) Mechanics of woven composites. PhD thesis, 97-98, University of Parma.

[74] Farley GL. Effect of specimen geometry on the energy absorption of composite materials. Journal of Composite Mats, 1986:20;390.

[75] Abdewi, E.F. (2016) FRP Composite Tube Subjected to Quasi-Static Axial and Lateral Compression Loadings. Reference Module in Materials Science and Materials Engineering.

[76] Lau, S.T.W. Said, M.R. Yaakob, M.Y. (2012) On the effect of geometrical designs and failure modes in composite axial crushing: A literature review. Composite Structures, 94, 803-812.

[77] E. Mahdi, T.A. Sebaey. An experimental investigation into crushing behavior of radially stiffened GFRP composite tubes. Thin-Walled Structures, (2014); 8–13.

[78] Mahdi E, Hamouda AMS, Sahari BB, Khalid YA. Effect of residual stresses in filament wound laminated conical shell. J Mater Proc Technol 2003;138:291–6.

[79] Alkateb M, Mahdi E, Hamouda AMS, Hamdan MM. On the energy absorption capability of axially crushed composite elliptical cones. Compos Struct 2004;66:495–501.

[80] Libo Yan, Nawawi Chouw. Crashworthiness characteristics of flax fibre reinforced epoxy tubes for energy absorption application. Materials & Design, 2013; 629–640

[81] Elfetori F. Abdewi, S. Sulaiman, A.M.S. Hamouda, E. Mahdi. Effect of geometry on the crushing behaviour of laminated corrugated composite tubes. Journal of Materials Processing Technology (2006); 394–399

[82] Perowansa Paruka, Mohd Kamal Mohd Shah. Influence of Axial and Oblique Impact Loads on Crush Response Properties of Square Tube Structures Made with FRP Pultruded Composites. Procedia Engineering (2013); 572–578

[83] Mahdi E, Hamouda AMS, Sahari BB, Khalid YA. Experimental quasi static crushing of cone–tube–cone composite system. Compos Part: B 2003;34:285–302.

[84] Mahdi E, Sahari BB, Hamouda AMS, Khalid YA. An experimental investigation into crushing behaviour of filament-wound laminated cone–cone intersection composite shell. Compos Struct 2001;51:211–9.

[85] Czaplicki MJ., Robertson RE. and Thorton PH. Comparison of bevel and tulip triggered pultruded tubes for energy absorption. Composites Science and Technology 1991:40;31.

[86] Thuis HGSJ., Metz VH. The influence of trigger configurations and laminate lay-Up on the failure mode of composite crush cylinders. Composite Structures, Vol. 25, pp. 37-43.

[87] Hamada H, Ramakrishna S. Scaling effects in the energy absorption of carbon-fiber/PEEK composite tubes. Compos Sci Technol 1995;55(3):211–21.

[88] Dormegnie D, Coutellier D, Delsart D, Deletombe E. Studies of scale effects for crash on laminated structures. Appl Compos Mater 2003;10:49–61.

[89] Thornton PH. Energy absorption in composite structures. J Compos Mater 1979;13(247).

[90] Othman, A. Abdullah, S. Ariffin, A.K, Mohamed, N.A.N. (2016) Investigating the crushing behavior of quasi-static oblique loading on polymeric foam filled pultruded composite square tubes. Composite Part B: Engineering, 95, 493-514.

[91] Palanivelu S, Van Paepegem W, Degrieck J, Van Ackeren J, Kakogiannis D, Van Hemelrijck D, et al. Experimental study on the axial crushing behaviour of pultruded composite tubes. Polym Test 2010;29:224–34.

[92] Saito H, Chirwa EC, Inai R, Hamada H. Energy absorption of braiding pultrusion process composite rods. Compos Struct 2002;55:407–17.

[93] Farley GL. The effect of crushing speed on the energy-absorption capability of composite tubes. Journal of Composite Mats, 1991:25;1314.

[94] Zhou G. The use of experimentally-determined impact force as a damage measure in impact damage resistance and tolerance of composite structures. Compos Struct 1998;42:375–82.

[95] Cantwell WJ, Morton J. The impact resistance of composite materials-a review. Composites 1991;22(5):347–62.

[96] Abrate S. Impact on laminated composite materials. Appl Mech Rev 1991;44(4):155–90.

[97] Liu D, Malvern LE. Matrix cracking in impacted glass/epoxy plates. J Compos Mater 1987;21:594–609.

[98] Davies GAO, Hitchings D, Zhou G. Impact damage and residual strengths of woven fabric glass/polyester laminates. Compos Part A 1996;27A:1147–56.

[99] Cantwell WJ, Morton J. Comparison of the low and high velocity impact response of CFRP. Composites 1989;20(6):545–51.

[100] Mitrevski T, Marshall IH, Thomson RS, Jones R. Low-velocity impacts on pre-loaded GFRP specimens with various impactor shapes. Compos Struct 2006;76:209–17.

[101] Aktasß M, Atas C, I_çten BM, Karakuzu R. An experimental investigation of the impact response of composite laminates. Compos Struct 2009;87:307–13.

[102] Hosseinzadeh R, Shokrieh MM, Lessard L. Damage behaviour of fiber reinforced composite plates subjected to drop-weight impacts. Compos Sci Technol 2006;66:61–8.

[103] Sutherland LS, Soares CG. Impact on low fibre-volume, glass polyester recangular plates. Compos Struct 2005;68:13–22.

[104] Evci C, Gülgeç M. An experimental investigation on the impact response of composite materials. Int J Impact Eng 2012;43:40–51.

[105] Freitas M, Reis L. Failure mechanisms on composite specimens subjected to compression after impact. Compos Struct 1998;42:365–73.

[106] Evci C, Gülgeç M. Effective damage mechanisms and performance evaluation of ceramic composite armors subjected to impact loading. J Compos Mater 2014;48(26):3215–36.

[107] Sutherland LS, Soares CG. The effects of test parameters on the impact response of glass reinforced plastic using an experimental design approach. Compos Sci Technol 2003;63:1–18.

[108] Mitrevski T, Marshall IH, Thomson R. The influence of impactor shape on the damage to composite laminates. Compos Struct 2006;76:116–22.

[109] Richardson MOW, Wisheart MJ. Review of low velocity impact properties of composite materials. Compos Part A 1996;27A:1123–31.

[110] Shyr TW, Pan YH. Impact resistance and damage characteristics of composite laminates. Compos Struct 2003;62:193–203.

[111] Davies GAO, Zhang X. Impact damage prediction in carbon composite structure. Int J Impact Eng 1994;16(1):149–70.

[112] Belingardi G, Vadori R. Low velocity impact tests of laminate glass-fiber-epoxy matrix composite material plates. Int J Impact Eng 2002;27:213–29.

[113] Schoeppner GA, Abrate S. Delamination threshold loads for low velocity impact on composite laminates. Compos Part A 2000;31:903–15.

[114] Yang FJ, Cantwell WJ. Impact damage initiation in composite materials. Compos Sci Technol 2010;70:336–42.

[115] Liu D. Characterization of impact properties and damage process of glass/ epoxy composite laminates. J Compos Mater 2004;38(16):1425–42.

[116] Quaresimin M, Ricotta M, Martello L, Mian S. Energy absorption in composite laminates under impact loading. Compos Part B 2013;44:133–40.

[117] Zhang L. Engineering plasticity and impact dynamic. Published by World Scientific, 2001.

[118] Abrate S. Impact on composite structures. Cambridge University Press, 1998.

[119] Timoshenko S. Theory of plates and shells. Mc Graw Hill, New York, 1959.

[120] Davies G. and Morton J. (ed.). Structural impact and crashworthiness. 2 volumes, Elsevier, 1984.

[121] Kim KJ. and Yu TX. (ed.). Impact response and dynamic failure of composites and laminate materials. TTP, Trans-Tech Publications, 1998.

[122] Sierakowski RL. and Newaz GM. Damage tolerance in advanced composites. Technomic Publishing Company, 1995.

[123] Wu HY. and Springer GS. Impact induced stresses, strains and delaminations in composite plates. Journal of Composite Materials 1988:22;533-560.

[124] Pang SS., Yang C. and Zhao Y. Impact response of single-lap composite joints. Composites Engineering 1995:5;1011-1027.

[125] Hancox NL. An overview of the impact behaviour of fibre-reinforced composites. in “Impact behaviour of fibre-reinforced composite materials and structures”, Reid SR. and Zhou G., Woodhead publishing Ltd., Cambridge, UK, 2000.

[126] Mamalis AG., Robinson M., Manolakos DE., Demosethenous GA., Ioannidis MB. and Carruthers J. Crashworthy capability of composite material structures. Composite Structures, 1996:13-5;263-8223.

[127] Thornton PH. The Crush of Fiber-Reinforced Plastics. In Handbook of Ceramics and Composites Volume 1: Synthesis and Properties, Cheremisinoff, N. P. ed., Marcel Dekker Inc., New York, 1990;307-337.

[128] Wang, Y. Feng, J. Wu, J. and Hu, D. (2016) Effects of fiber orientation and wall thickness on energy absorption characteristics of carbon-reinforced composite tubes under different loading conditions. Composite Structures, 153, 356-368.

[129] Mittal, G. Rhee, K.Y. Miskovic-Stankovic, V. Hui, D. Reinforcements in multi-scale polymer composites: Processing, properties, and applications, Compo Part B, 2018;138:122-139.

[130] Berthelot JM. Composite materials, mechanical behaviour and structural analysis. ISBN 0-387-98426-7 Spring-Verlag New York, USA, 1999.

[131] Farley GL. and Jones RM. Analogy for the effect of material and geometrical variables on energy absorption capability of composite tubes. Journal of Composite Materials, 1992:26(1);78.

[132] Jacob GC., Fellers JF., Simunivic S. and Starbuck M. energy absorption in polymer composites for automotive crashworthiness. Journal of Composite Materials 2002:36;813.

[133] Mamalis AG., Manolakos DE., Demosthenous GA. and Ioannidis MB. Analysis of failure mechanisms observed in axial collapse of thin-walled circular fibreglass composite tubes. Thin-walled Structures, 1994:26.

[134] Mamalis AG, Manolakos DE, Demosthenous GA and Ioannidis MB. The static and dynamic collapse of fibreglass composite automotive frame rails. Composite Structures, 1996;34:77-90.

[135] Czaplicki MJ, Robertson RE and Thornton PH. Non-axial crushing of E-glass/polyester pultruded tubes. Journal of Composite Materials, 1990;24.

[136] Hong-Wei Song and Xing-Wen Du. Off-axis crushing of GFRP tubes. Compos Sci Technol, 2002;62:2065–2073.

[137] Saito H, Inai R, Yokoyama A, Hamada H. Basic study of progressive crushing mechanism. Key Eng Mater 2000;177–180:321–6.

[138] Warrior NA, Turner TA, Robitaille F, Rudd CD. The effect of interlaminar toughening strategies on the energy absorption of composite tubes. Composites: Part A 2004;35:431-437.

[139] Jacob GC, Fellers JF, Simunovic S. and Starbuck M. Energy absorption in polymer composites for automotive crashworthiness. Journal of Composite Materials 2002;36: 813-50.

[140] Cauchi Savona S, Hogg PJ. Effect of fracture toughness properties on the crushing of flat composite plates. Compos Sci Technol 2006;66:2317-2328.

[141] Solaimurugan S and Velmurugan R. Influence of fibre orientation and stacking sequence on petalling of glass/polyester composite cylindrical shell under axial compression. Int Jnl of Sol and Struc 2007;44:6999-7020.

[142] Solaimurugan S and Velmurugan R. Progressive crushing of stitched glass/polyester composite cylindrical shells. Compos Sci Technol 2007;67:422-437.

[143] Ghasemnejad H, Blackman BRK, Hadavinia H and Sudall B. Experimental studies on fracture characterisation and energy absorption

of GFRP composite box structure. Composite Structures 2008;88(2):253-261.

[144] Ghasemnejad H and Hadavinia H. Off-axis crashworthiness characteristic of woven glass/epoxy composite box structures. J. Reinf Plast Comp. 2010;29(15), 2306-2330.

[145] Ghafari-Namini, N. and Ghasemnejad, H. Effect of natural stitched composites on the crashworthiness of box structures. Materials & design, 2012;39:484-494.

[146] Korkiakoski, S. Haavisto, M. Barouei, M.R. Saarela, O. Experimental compaction characterization of unidirectional stitched noncrimp fabrics in the vacuum infusion process. Polymer composite, 37 (2015), pp. 2692-2704. doi: 10.1002/pc.23464

[147] Dransfield, K. Baillie, C. Mai, YW. Improving the delamination resistance of CFRP by stitching – a review. Compos Sci Technol, 50(3) (1994), pp. 305–17.

[148] Cauchi-Savona S. Zhang C. Hogg P. Optimisation of crush energy absorption of non-crimp fabric laminates by through-thickness stitching. Compos A: Appl Sci Manuf, 42 (7) (2011), pp. 712–722.

[149] Solaimurugan, S. and Velmurugan, R. Progressive crushing of stitched glass/polyester composite cylindrical shells. Compos Sci Technol, 67 (2007), pp. 422-437

[150] Korkiakoski, S. Sarlin, E. Suikonen, R. Saarela, O. Influence of reinforcement positioning on tension-tension fatigue performance of quasi-unidirectional GFRP laminates made of stitched fabrics, Composite Part B, 112 (2017), pp. 38-48

[151] Zhao, N. Rödel, H. Herzberg, C. Gao, S.L. Krzywinski, S. Stitched glass/PP composite. Part I: tensile and impact properties, Composites Part A, 40 (2009), pp. 635-643.

[152] Cook, R.D. Malkus, D.S. Plesha, M.E. Concepts and Applications of Finite Element Analysis. 1989, Wiley Publishing.

[153] Bisagni, C. Pietro, G.P. Fraschini, L. Terletti, D. Progressive crushing of fiber-reinforced composite structural components of a Formula One racing car, Compos Struct, 68 (4) (2005), pp. 491-503.

[154] Huang, J. Wang, X. Numerical and experimental investigations on the axial crushing response of composite tubes, Compos Struct, 91 (2) (2009), pp. 222-228

[155] Mamalis, A.G. Manolakos, D.E. Loannidis, M.B. Papapostolou, D.P. The static and dynamic axial collapse of CFRP square composite tubes: finite element modelling, Compos Struct, 74 (2) (2006), pp. 213-225.

[156] Palanivelu, S. Paepegem, W. Degrieck, J. Kakogiannis, D. Ackeren, J. Hemelrijck, D. Parametric study of crushing parameters and failure patterns of pultruded composite tubes using cohesive elements and seam, Part I: central delamination and triggering modelling, Polym Test, 29 (6) (2010), pp. 729-741.

[157] Palanivelu, S. Paepegem, W. Degrieck, J. Kakogiannis, D. Ackeren, J. Hemelrijck, D. Parametric study of crushing parameters and failure patterns of pultruded composite tubes using cohesive elements and seam, Part II: multiple delaminations and initial geometric imperfections, Polym Test, 29 (7) (2010), pp. 803-814.

[158] Bussadori, B.P. Schuffenhauer, K. Scattina, A. Modelling of CFRP crushing structures in explicit crash analysis, Compos Part B-Eng, 60 (2014), pp. 725-735.

[159] Deleo, F. Wade, B. Feraboli, P. Rassaian, M. Crashworthiness of Composite Structures: Experiment and Simulation. In: Proceedings of 50th AIAA Conference. Palm Springs, CA, May, 2009.

[160] Xiao, X. Botkin, M. Johnson, N.L. Axial crush simulations of braided carbon tubes using MAT58 in LS-DYNA, Thin Wall Struct, 47 (6–7) (2009), pp. 740-749.

[161] McGregor, C. Vaziri, R. Xiao, X. Finite element modelling of the progressive crushing of braided composite tubes under axial impact. Int J Impact Eng 2010;37:662-72.

[162] McGregor, C. Zobeiry, N. Vaziri, R. Poursartip,A. A constitutive model for progressive compressive failure of composites, J Compos Mater, 42 (25) (2008), pp. 2687-2716.

[163] Xiao, X. Modeling energy absorption with a damage mechanics based composite material model, J Compos Mater, 43 (5) (2009), pp. 427-444.

[164] Oshkovr, S.A. Taher, S.T. Oshkour, A.A. Ariffin, A.K. Azhari, C.H. Finite element modeling of axially crushed silk/epoxy composite square tubes, J Compos Struct, 95 (2010), pp. 411-418.

[165] Kim, G.H. Choi, J.H, Kweon, J, H. Manufacture and performance evaluation of the composite hat-stiffened panel, Compo Struct, 2010;92:2276-2286.

[166] Chatiri, M. Gull, T. Matzenmiller, A. An assessment of the new LS-DYNA layered solid element: basics, patch simulation and its potential for thick composite structures analysis. In: Proceedings of the 7th European LS-DYNA conference, Salzburg, 14–15 May, 2009.

[167] Wagner, W. FE – modeling of fiber reinforced polymer structures. In: Proceedings of the 5th world congress on computational mechanics, Vienna, 7–12 July, 2002.

[168] Feraboli, P. Development of a corrugated test specimen for composite material energy absorption. J Compos Mater 2008;42(3):229–56.

[169] Greco, F. Luciano, R. A theoretical and numerical stability analysis for composite micro-structures by using homogenization theory, Compos Part B: Eng, 42 (3) (2011), pp. 382-401.

[170] Sun, H. Di, S. Zhang, N. Pan, N. Wu, C. Micromechanics of braided composites via multivariable FEM, Comput Struct, 81 (20) (2003), pp. 2021-2027.

[171] Tabiei, A. Aminjikarai, B.S. A strain-rate dependent micro-mechanical model with progressive post-failure behavior for predicting impact response of unidirectional composite laminates, Compos Struct, 88 (1) (2009), pp. 65-82.

[172] Crashworthiness Working Group of the CMH-17. Simulation of the quasi-static crushing of a fabric composite plate. Abaqus Technology Brief; 2011.

[173] Feindler, N. Drechsler, K. Doll, J. Test method to analyse the energy absorption of composite material using flat coupon testing. In: Proceedings of the 5th international conference on composites testing and model identification, Lausanne, 14–16 February, 2011.

[174] Borovkov, A. Palmov, V. Banichuk, N. Saurin, V. Barthold, F. Stein, E. Macro-failure criterion for the theory of laminated composite structures with free edge delaminations. Comput Struct 2000;76:195–204.

[175] Johnson, A. Pickett, A. Impact and crash modelling of composite structures: a challenge for damage mechanics. In: Proceedings of the 9th user conference EURO-PAM, Darmstadt, 7–8 Octoberm, 1999.

[176] Greve, L. Andrieux, F. Deformation and failure modelling of high strength adhesives for crash simulation. Int J Fract 2007;143(2):143–60.

[177] Tang, C.Y. Tsui, C.P. Lin, W. Uskokovic, P.S. Wang, Z.W. Multi-level finite element analysis for progressive damage behavior of HA/PEEK composite porous structure. Compos Part B: Eng 2013;55:22–30.

[178] Barut, A. Madenci, E. Tessler, A. Starnes Jr, J.H. A new stiffened shell element for geometrically nonlinear analysis of composite laminates, Comput Struct, 77 (2000), pp. 11-40.

[179] Mohite, P.M. Upadhyay, C.S. Region-by-region modeling of laminated composite plates, Comput Struct, 85 (2007), pp. 1808-1827.

[180] Holzapfel, M. Grundolf, K. Adamski, P. Elsenhans, H. Doll, J. Hambrecht, T. Untersuchungen zur Modellierung von Strukturen aus FKV unter Crashbelastung mit. Hilfe von Mehrschalen modellierungen. In: 7th German LS-DYNA Users Conference, Bamberg, 2008.

[181] Feindler, N. Charakterisierungs und Simulationsmethodik zum Versagensverhalten energieabsorbierender Faserverbundstrukturen (PhD thesis). Munich: Technical University of Munich; 2012. ISBN: 978-3-8439- 1557-1.

[182] Hussain, N.N. Regalla, S.P. Rao, Y.V.D. Comparative Study of Trigger Configuration for Enhancement of Crashworthiness of Automobile Crash Box Subjected to Axial Impact Loading, Procedia Eng, 2017;173:1390-1398

[183] Johnson, A.F. Modelling fabric reinforced composites under impact loads. Compos Appl Sci Manuf, 32 (2001), pp. 1197-1206.

[184] Joosten, M.W. Dutton, S. Kelly, D. Experimental and numerical investigation of the crushing response of an open section composite energy absorbing element. Compos Struct, 93 (2011), pp. 682-689.

[185] Pinho, S.T. Camanho, P.P. De Moura, M.F. Numerical simulation of the crushing process of composite materials. Int J Crashworthiness, 9 (2004), pp. 263-276.

[186] LNS, Ciou. BG, Falzon. R, Boman. Et al. Finite element modelling of composite structures under crushing load. Compos struct 2015;131:215-

[187] Siromani, D. Henderson, G. Mikita, D. Mirarchi, K. Park, R. Smolko, J. Awerbuch, J. Tan, T-M. An Experimental Study on the Effect of Failure Trigger Mechanisms on the Energy Absorption Capability of CFRP Tubes under Axial Compression. Compos Part A, 2014.

[188] Siromani, D. Awerbuch, J. Tan,T.-M. Finite element modeling of the crushing behavior of thin-walled CFRP tubes under axial compression, Compos B Eng, 64 (2014), pp. 50-58.

[189] Easa.europa.eu. (2018). [online] Available at: https://www.easa.europa.eu/system/files/dfu/NPA%202013-20.pdf [Accessed 23 Jan. 2018].

[190] Tong, L. Mouritz, A.P. Bannister, M. 3D fibre reinforced polymer composites. ELSEVIER, ISBN-13 (2002), 978-0-08-043938-9.

[191] Boeing Demonstrates Use of Stitching Machine for Carbon Fiber Fabric, (1997) [online] Availbale at: - http://aviationweek.com/awin/boeing-demonstrates-use-stitching-machine-carbon-fiber-fabric [Accessed 18 Sep. 2016]

[192] Hallquist, J.O. LS-DYNA Theory Manual, Livermore Software Technology Corporation, Livermore, California, 2006.

[193] Chang, F.K and Chang, K.Y. Post-Failure Analysis of Bolted Composite Joints in Tension or Shear-Out Mode Failure, Journal of Composite materials, vol. 21, p. 809, 1987.

[194] Hashin, Z. Failure Criteria for Unidirectional Fiber Composites, Journal of Applied Mechanics, vol. 47, pp. 329-334, 1980.

[195] Tsai, S.W. Wu, E.M. A General Theory of Strength for Anisotropic Materials, Journal of Composite Materials, vol. 5, p. 58, 1971.

[196] Zheng, X. Nonlinear Strain Rate Dependent Composite Model for Explicit Finite Element Analysis, Akron, 2006.

[197] Matzenmiller, A. Lubliner, J. Taylor, R. L. A constitutive model for anisotropic damage in fiber composites, Mechanics of Materials, vol. 20, pp. 125-152, 1995.

[198] Reuter, C. Troster, T. Crashworthiness and numerical simulation of hybrid aluminium-CFRP tubes under axial impact, Thin-Walled. Struct., 117 (2017), pp. 1-9.

[199] Mamalis, A.G. The static and dynamic axial collapse of CFRP square tubes: Finite element modelling, Composites structures. 74(2) (2006), pp. 213-225.

[200] Yousefi, A.K. Buckling and crack propagation analysis of composite laminated structures, Kingston University, Master Thesis, (2016).

[201] Krishnamoorthy, S. K. Hoptner, J. Kopp, G. Friedrich, H.E. Prediction of structural response of FRP composites for conceptual design of vehicles under impact loading, in 8th European LS-DYNA Users Conference, Strasbourg, (2011)

[202] Bela, S. Livemore Software, Tie-break contacts in Ls-Dyna (2010).

[203] Jayasinghe, P.D.N. New Development on Mode-I Delamination Failure of FRP Composites, Published BEng thesis, (2016), Kingston University

[204] Kiani, A. New Development on Mode-II Delamination Failure of FRP Composites, Published BEng thesis, (2016), Kingston University

[205] Arifin, A.A. Sulong, A.B. Quasi-static Energy Absorption of Pultruded Composite Tubes E-Glass/Polyester Under Oblique Loading with

Different Cross-section. Advanced Materials Research 2012, 341-342, p. 843-847.

[206] Reyes, A. Langseth, M., Hopperstad, O.S. Square Aluminum Tubes Subjected to Oblique Loading. International Journal of Impact Engineering 2003, 28, p. 1077-1106.

[207] Zhoua H, Attardb TL, Dhiradhamvitb K, Wangc Y, Erdmanc D. Crashworthiness characteristics of a carbon fibre reinforced dual-phase epoxy–polyurea hybrid matrix composite, Composites Part B: Engineering, 2015:(71);17–27.

[208] Carruthers, J.J. Kettle, A.P. Robinson, A.M. Energy absorption capability and crashworthiness of composite material structures: a review, Appl. Mech. Rev. 51 (1998), pp. 635–649, ISSN 0003-6900.

[209] Zhu, G. Sun, G. Liu, Q. Li, G. Li, Q. On crushing characteristics of different configurations of metal-composites hybrid tubes, Compos. Struct. 175 (2017) pp. 58-69.

[210] McGregor, C. Vaziri, R. Poursartip, A. Xiao, X. Axial crushing of triaxially braided composite tubes at quasi-static and dynamic rates. Compos Struct, 157 (2016), pp. 197–206.

[211] Hu, D. Zhang, X. Ma. Song, B. Effect of fiber orientation on energy absorption characteristics of glass cloth/epoxy composite tubes under axial quasi-static and impact crushing condition. Composites: Part A, 90 (2016), pp. 489-501

[212] Mouritz, AP. Cox, B.N. A mechanistic approach to the properties of stitched laminates. Compos Part A: Appl Sci Manuf, 31 (2000), pp. 1–27.

[213] Esnaola, A. Ulacia, I. Aretxabaleta, L. Aurrekoetxea, J. Gallego, I. Quasi-static crush energy absorption capability of e-glass/polyester and hybrid e-glass basalt/polyester, compos struct. 76 (2015), pp. 18–25, ISSN 0261-3069.

[214] Liu, Q. Xing, H. Ju, Y. Ou, Z. Li, Q. Quasi-static axial crushing and transverse bending of double hat shaped CFRP tubes, Compos. Struct. 117 (2014), pp. 1–11, ISSN 0263-8223.

[215] Bisagni, C. Experimental investigation of the collapse modes and energy absorption characteristics of composite tubes. Int J Crash. 14 (2009), pp. 365–78.

[216] Taher, S.T. Mahdi, E. Mokhtar, A.S. Magid, D.L. Ahmadun, F.R. Arora, P.R. A new composite energy absorbing system for aircraft and helicopter. Compos. Struct. 75 (2006), pp. 14-2

[217] Zeinoddini, M. Harding, J.E. Parke, G.A.R. Contribution of ring resistance in the behaviour of steel tubes subjected to a lateral impact, Int J Mech Sci, 42 (12) (2000), pp. 2303-2320

[218] Ahmad, Z. Thambiratnam, D.P. Tan, A.C.C. Dynamic energy absorption characteristics of foam-filled conical tubes under oblique impact loading, Int J Impact Eng, 37 (5) (2010), pp. 475-488

[219] Nagel, G.M. Thambiratnam, D.P. Dynamic simulation and energy absorption of tapered thin-walled tubes under oblique impact loading, Int J Impact Eng, 32 (10) (2006), pp. 1595-1620

[220] Han, D.C. Park, S.H. Collapse behavior of square thin-walled columns subjected to oblique loads, Thin-Walled Struct, 35 (3) (1999), pp. 167-184

[221] Reyes, A. Langseth, M. Hopperstad, O.S. Crashworthiness of aluminum extrusions subjected to oblique loading: experiments and numerical analyses, Int J Mech Sci, 44 (9) (2002), pp. 1965-1984

[222] Yang, S. Qi, C. Multiobjective optimization for empty and foam-filled square columns under oblique impact loading, Int J Impact Eng, 54 (2013), pp. 177-191

[223] Chen, W.G. Experimental and numerical study on bending collapse of aluminum foam-filled hat profiles, Int J Solids Struct, 38 (2001), pp. 7919-7944

[224] Chen, W. Wierzbicki, T. Santosa, S. Bending collapse of thin-walled beams with ultralight filler: numerical simulation and weight optimization, Acta Mech, 153 (2002), pp. 183-206

[225] Singace, A.A. El-Sobky, H. Uniaxial crushing of constrained tubes, Journal of Reinforced Plastic Composite, (2001), 215(3).

[226] Ghasemnejad,H. Hadavinia,H. Aboutorabi, A. Effect of delamination failure on the crashworthiness of hybrid composite box structures, Materials and Design, (2010), 31:1105-1116.

[227] Greve, L. Pickett, A.K. Payen, F. Experimental testing and phenomenological modelling of the fragmentation process of braided carbon/epoxy composite tubes under axial and oblique impact, Compos B Eng, 39 (7) (2008), pp. 1221-1232

[228] Sun, G. Liu, T. Huang, X. Zheng, G. Li ,Q. Topological configuration analysis and design for foam filled multi-cell tubes, Eng Struct, 155 (2018), pp. 235-250

[229] Song, J. Numerical simulation on windowed tubes subjected to oblique impact loading and a new method for the design of obliquely loaded tubes, Int J Impact Eng, 54 (2013), pp. 192-205

[230] Nia, A.A. Nejad, K.F. Badnava, H. et al. Effect of buckling initiators on mechanical behavior of thin-walled square tubes subjected to oblique loading, Thin-Walled Struct, 59 (2012), pp. 87-96

[231] Zhou, C. Jiang L. Tian, K. et al. Origami crash boxes subjected to dynamic oblique loading, J Appl Mech-T ASME, 84 (9) (2017), Article 091006

[232] Zhou, C. Wang, B. Ma, J. et al. Dynamic axial crushing of origami crash boxes, Int J Mech Sci, 118 (2016), pp. 1-12

[233] Sun, G. Pang, T. Xu, C. Zheng, G. Song, J. Energy absorption mechanics for variable thickness thin-walled structures, Thin-Walled Struct, 118 (2017), pp. 214-228

[234] Li, G. Zhang, Z. Sun, G. et al. Comparison of functionally-graded structures under multiple loading angles, Thin-Walled Struct, 94 (2015), pp. 334-347

[235] Li, G. Xu, F. Sun, G. Li, Q. A comparative study on thin-walled structures with functionally graded thickness (FGT) and tapered tubes withstanding oblique impact loading, Int J Impact Eng, 77 (2015), pp. 68-83

[236] Zarei, H.R. Experimental and numerical crashworthiness investigation of hybrid composite aluminum tubes under dynamic axial and oblique loadings, Int J Auto Eng (2015), pp. 1084-1093

[237] Ghafari-Namini, N. Design of new crash absorbers stitched by natural fibres to improve effective crash growth, (2013), Kingston University. PhD Thesis

[238] Alkbir, M.F.M. Sapuan, S.M. Nuraini, A.A. Ishak, M.R. Fibre properties and crashworthiness parameters of natural fibre-reinforced composite structures: a literature review, Compos Struct, 148 (2016), pp. 59-73